ROTATIONAL BANDS IN ^{176}Re

AND

IBA CALCULATIONS FOR ODD-ODD Re ISOTOPES

By

Wen-Tsae Chou

A DISSERTATION

Submitted to
Michigan State University
in partial fulfillment of the requirements
for the degree of

DOCTOR OF PHILOSOPHY

Department of Chemistry

1989

ABSTRACT

ROTATIONAL BANDS IN ^{176}Re AND IBA CALCULATIONS FOR ODD-ODD Re ISOTOPES

By

Wen-Tsae Chou

Rotational bands in odd-odd ^{176}Re have been studied via the heavy-ion reactions, ^{159}Tb(^{22}Ne,5nγ)^{176}Re at MSU NSCL and ^{165}Ho(^{16}O,5nγ)^{176}Re at SUNY Stony Brook, using in-beam γ-ray spectroscopic techniques. Ge detectors, with anti-Compton shields, were used to take singles, coincidence, delayed-coincidence, and angular-correlation spectra.

Two rotational bands have been characterized. One of the bands is the so-called "doubly-decoupled band" with ΔI=2 E2 intra-band transitions. This band shows backbending at a crossing frequency (≈0.29 MeV) close to that of even-even W but lower than that of ^{177}Re. This suggests that the effects of the odd neutron and odd proton on the crossing frequency seem to cancel each other out in this particular case. The observation of this band supports the mechanism of heavy-ion compound-nucleus reactions forming particle states highly-aligned with rotation, with the subsequent γ-ray cascades feeding down through similar states.

The other band is a regular rotational band connected by ΔI=1 transitions. No linking transitions between these two bands have been identified; therefore, spin could not be assigned uniquely. In general,

our results agree with some previous studies (Santos et al.), but our delayed-coincidence results showed the existence of meta-stable states, which were not mentioned. In addition, they observed a 70.5-keV transition, which we did not. Such ambiguities make assignments difficult. They assigned the band $K^{\pi}=6^{+}$, a coupling of $\pi 5/2^{+}[402\uparrow]$ and $\nu 7/2^{+}[633\uparrow]$; whereas, we favor an assignment of $K^{\pi}=7^{+}$, a coupling of $\pi 9/2^{-}[514\uparrow]$ and $\nu 5/2^{-}[512\uparrow]$.

IBA calculations have proven to be able to give an accurate description of the properties of low-lying collective levels in even-even and odd-mass nuclei. We have extended this model to odd-odd nuclei, applied to the Re isotopes. Our calculations make no restrictions as to orbits because of the particular, very efficient model-space truncation scheme used. The results are compared qualitatively with experimental data, and have achieved remarkably good agreement in what is a very stringent test of the IBA methods.

ACKNOWLEDGEMENTS

I wish to thank Professor Wm. C. McHarris, my research advisor, for his guidance. His suggestions and patience during the preparation of this thesis are greatly appreciated.

Dr. Olaf Scholten deserves my sincerest gratitude for his programs and many helpful discussions.

I also wish to thank Dr. Jerry Nolen for his careful review of this thesis.

Finally, I would like to thank my parents, sisters, and brother for their endless love and support.

TABLE OF CONTENTS

LIST OF TABLES

LIST OF FIGURES

CHAPTER I

INTRODUCTION

In-beam Υ-ray spectroscopy of deformed nuclei is not a relatively new subject; however, most studies have concentrated on even-even and odd-mass nuclei. The reason odd-odd nuclei have received less attention is because of the suspect complexity of their spectra. Also, a fair understanding of the neighboring odd-mass nuclei is needed to interpret the spectra of odd-odd nuclei. But studies have shown them to be less complex than anticipated, especially highly deformed odd-odd nuclei [Sl84], where states come in bands rather than singly. A possible mechanism consistent with this unexpected simplicity invokes a rotational alignment of particles to assist the core in handling the large amount of angular momentum brought into the compound nucleus in heavy-ion reactions. Once such "klokast" states (with large Coriolis matrix elements) are populated, the subsequent Υ decay preferentially feeds into similar states, populating a select subset of lower-lying states.

During recent years, the development of experimental and computational techniques has extended the study of nuclear structure to new dimensions. One of the most extraordinary phenomena was the discovery of the discrete-line superdeformed band in ^{152}Dy [Tw86]. Since then many instances have been found in the light rare-earth region, with the possibility of such bands also in Os and nearby isotopes. It has been found [Ta88] that optimum population of such bands probably requires a relatively cold compound nucleus rather than the highest possible angular momentum consistent with a particular reaction; also, superdeformed bands thus far reported in odd-mass nuclei [Wa88] receive greater population than those in even-even nuclei. If this is generally true, then it is likely that superdeformed bands in

odd-odd nuclei could even receive more population, which makes the study of odd-odd nuclei even more interesting.

Backbending has been a popular subject since it was first observed in even-even nuclei in the early 1970's [Jo71]. It is believe to be related to the pairing correlations in nuclei, where large amounts of angular momentum are known to weaken the pairing. The standard mechanism is that the Coriolis force acts oppositely on the two members of a pair, lifting their degeneracy and ultimately aligning the particle angular momentum as much as possible with the rotation axis. For odd-mass nuclei, depending on the position of the single nucleon, its blocking could weaken the pairing correlation and thus make the backbending occur at lower frequencies, or it could occupy the favorable orbits and delay backbending until higher frequencies. Many nuclei in well-deformed regions show backbending, but only a few odd-odd cases have been reported so far (and not until 1985 [Fo85]). This stimulates our search for backbending in other odd-odd nuclei. Hopefully, we could learn more about how single unpaired nucleons affect the backbending.

There are many other reasons for studying odd-odd nuclei. Among these probably the most important is that odd-odd nuclei offer us a good source for studying proton-neutron residual interactions. Normally these residual interactions are masked by the rest of the nucleus, but if the last odd-odd nucleons are decoupled from the core, then these "doubly-decoupled bands" offer a relatively clean source of information. The first such band was characterized by Kreiner et al. [Kr84] in 1984, and since then several such bands have been discovered, most of them in the Ta-Re-Ir region. From systematics, it is obvious that ^{176}Re is a good candidate for exhibiting a doubly-decoupled band.

It is important to learn the systematic behavior of a series of odd-odd nuclei, and a few heavier odd-odd Re isotopes have been studied. Therefore, we elected to study the more neutron-deficient Re nucleus, $^{176}_{75}Re_{101}$, via in-beam Y-ray spectroscopy. We wished to test the aligned-state mechanism, to look for doubly-decoupled band(s), and also to analyze the continuum Y-ray spectrum for possible superdeformed behavior. We produced ^{176}Re by the ^{159}Tb(^{22}Ne, 5nY) reaction in order to emphasize high-spin states, using 108- and 113-MeV ^{22}Ne beams from the MSU NSCL K500 superconducting cyclotron. Excitation-function and angular-correlation experiment, as well as coincidence experiment, were conducted at SUNY Stony Brook, using a 96.9-MeV ^{16}O beam on a ^{165}Ho target.

Not many theoretical calculations have been done for odd-odd nuclei because of the same reasons that caused experimentists to hesitate. The IBA model has proven to be able to give a rather accurate description of the properties of low-lying collective levels in even-even nuclei. Likewise, its extension to odd-mass nuclei, the IBFA model, is able to reproduce a large variety of properties in phenomenological calculations. Recently, we have developed a computer code with which it is possible to calculate odd-odd nuclei in the framework of the IBA model. We call it the IBFFA model. A series of calculations has been performed for $^{176-184}$Re in order to examine the extension of this model to odd-odd nuclei.

Chapter II of this thesis is a brief discussion of some of the theoretical models used in describing nuclear structure. Chapter III will include some important features in studying nuclear structure via heavy-ion reactions. Detailed experimental set-ups and data analysis

will be covered in Chapter IV. In Chapter V the experimental results and construction of the level scheme will be presented and discussed. Finally, a short outline of the IBA model, results of calculations, and qualitative comparisons with experimental data will be presented in Chapter VI.

CHAPTER II

THEORETICAL CONSIDERATIONS

To understand and correlate the properties of nuclei requires knowing the appropriate laws that govern the interactions among nucleons. The nuclear problem is very complicated because the force between two nucleons is not completely known. Under these circumstances there is no other choice but to make simplifying assumptions, which can provide approximations of the fundamental forces. Many models have been worked out, each adopting its own approximations, which are usually suggested by experimental evidence. Among them are the shell model, the Fermi-gas model, and the collective model.

The shell model starts with the assumption that each nucleon moves in an effective spherically symmetric potential, which is an approximate representation of the interaction of that nucleon with all of the others [Mc68,Se77,Fr81b]. The greatest success of the shell model is the prediction of the magic numbers of closed shells. Much evidence that supports the shell model is associated with these numbers.

The nucleons are distributed with spherical symmetry in space only for nuclei having a complete, filled shells. Any nucleons outside the closed shell tend to deform the nucleus away from the spherical shape, and the potential energy for this deformed nucleus is no longer spherically symmetric. As a consequence of deformation, there are many phenomena for which the shell model fails to explain, here the appropriate model turns out to be the collective model.

Coriolis effects are not very strong or apparent in our daily life, but they are very apparent in the case of rotational nuclei. Sometimes these effects can completely obscure the behavior of rotational bands. To a first-order approximation [St75], the Coriolis effect is proportional to j, the particle orbital angular momentum, so it is

comparatively large for nucleons occupying states with, for example, j=13/2.

$^{176}_{76}Re_{105}$, which has both proton number and neutron number far away from magic numbers, is a well-deformed neutron-deficient nucleus. For the present study, there is no need to review the theory of the shell model, but some of its ideas are useful and will be mentioned at appropriate places. The intrinsic states of an odd-odd nucleus are the coupling of the single-particle states of its odd-mass neighbors [Ga58]. From the level schemes of the odd-mass neighbors of odd-odd Re nuclei, we note that their low-energy states are usually occupied by a single unpaired $i_{13/2}$ (neutron) or $h_{11/2}$ (proton) nucleon. Such states are expected to show large Coriolis effects, and these effects should remain when they are coupled with other states. Thus, we believe there are sizable Coriolis effects in ^{176}Re, making it necessary to look into the Coriolis force a little deeper.

A. COLLECTIVE MODEL

There are different kinds of collective motions in nuclei [Mc68,Se77,Fr81b,Di84]. The most important excitation mode that appears in the energy region we are interested in is rotation. Therefore, we shall restrict our discussion to collective rotation of deformed nuclei.

The earliest experimental evidence for nuclear deformation came from the measurement of odd-mass nuclear quadrupole moments, which are many times larger than those expected for a single odd nucleon moving in the field of a spherical core. It was first suggested by Rainwater

[Ra50] that the motion of an odd nucleon might cause nuclear deformation and all of the nucleons in the nucleus could contribute collectively to the quadrupole moment. Consequently, the deformation might be reinforced by adding more nucleons, and, indeed, strongly deformed nuclei are always found toward the middle of the shells.

Nuclei with nonspherical shapes have distinguishable orientations in space; thus, it is expected that they may exhibit rotational levels, which can be built on each intrinsic state [Bo75]. The shell-model states are no longer valid for deformed nuclei. The angular momentum of the single-particle state is not a constant of the motion anymore, but only its projection, which is labeled by Ω, on the symmetry axis. Most of the degeneracy of the shell-model states will be lifted, and they are now called Nilsson states, usually labeled with the asymptotic quantum numbers $\Omega^{\pi}[N,n_z,\Lambda,\Sigma]$ [Bo75,Fr81b]. Here N is the total number of oscillation quanta as in the shell model, n_z is the number of nodes perpendicular to the symmetry axis, Λ and Σ are the respective projections of the orbital and spin angular momentum on the symmetry axis, $\Omega=\Lambda\pm\Sigma$, and π is the parity. In odd-odd nuclei the intrinsic states consist of the coupling of the single proton state with the single neutron state, producing $\Sigma = \Sigma_p + \Sigma_n$ (triplet) or $\Sigma = \Sigma_p - \Sigma_n$ (singlet) [Ga58]. Generally, the collective rotational band is composed of regularly spaced levels having enhanced intra-band E2 transitions because of the large quadrupole deformation.

The energy levels of a rotational band can be expressed as

$$E = E_0(K) + AI(I+1) + BI^2(I+1)^2. \qquad \text{(II-1)}$$

This equation shows the familiar rotational term plus correction(s) from Coriolis coupling and centrifugal stretching [Bo75]. To derive this equation would immediately lead us into a discussion of the Coriolis force. Therefore, it will be left to the next section.

B. CORIOLIS FORCES

A convenient way to describe a rotating nucleus is by particles coupled to a rotor having a symmetry axis. The coupling scheme [Mc65] and the notation are shown in Figure II-1. The total Hamiltonian for the system can be written as [Mc65,Bo76,Fl76,El81a]

$$\begin{aligned} H &= H_{intr} + \hbar^2/2\mathcal{J}(R^2) \\ &= H_{intr} + H_{rot} + H_c + H_{pn} + H_{irot} , \end{aligned} \tag{II-2}$$

and each term can be expressed as:

$$H_{intr} = H_{sp}(p) + H_{sp}(n) + V_{pn} , \tag{II-3}$$

$$H_{rot} = \hbar^2/2\mathcal{J}\,(I^2 - K^2) , \tag{II-4}$$

$$\begin{aligned} H_c &= -\hbar^2/2\mathcal{J}\,(I_+ j_- + I_- j_+) \\ &= -\hbar^2/2\mathcal{J}\,[(I_+ j_{p-} + I_- j_{p+}) + (I_+ j_{n-} + I_- j_{n+})] , \end{aligned} \tag{II-5}$$

$$H_{pn} = \hbar^2/2\mathcal{J}\,(j_{p+} j_{n-} + j_{p-} j_{n+}) , \tag{II-6}$$

$$\text{and} \quad H_{irot} = \hbar^2/2\mathcal{J}\,[(j_p^2 - \Omega_p^2) + (j_n^2 - \Omega_n^2)] . \tag{II-7}$$

Here we use the relation $\mathcal{J}_1 = \mathcal{J}_2 = \mathcal{J}$, being the moment of inertia, and $K = \Omega = |\Omega_p \pm \Omega_n|$.

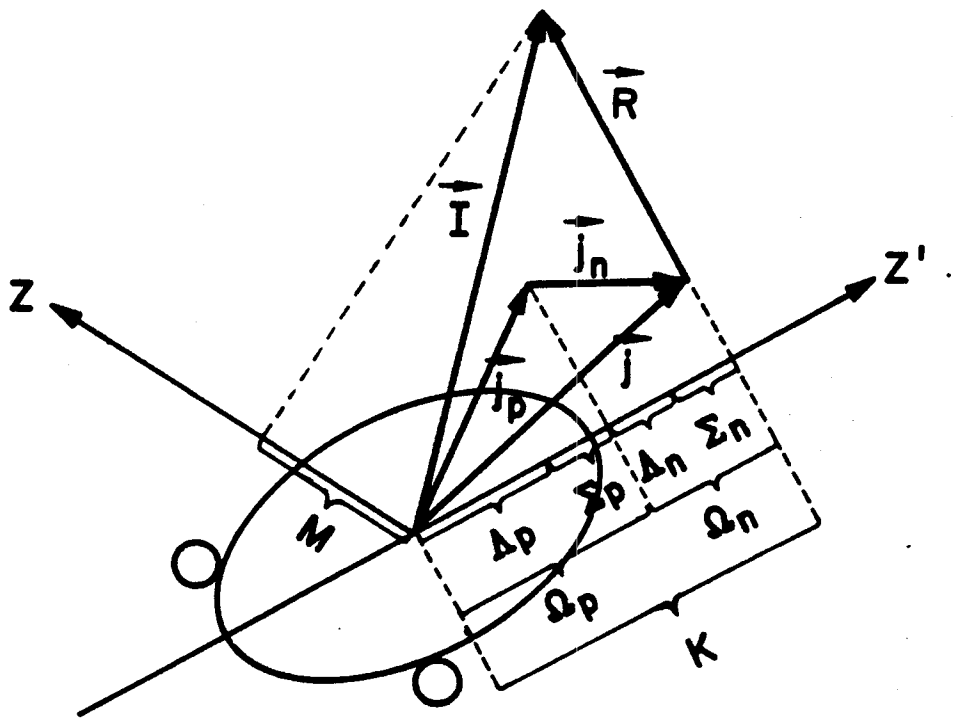

j = angular momentum of proton or neutron
Ω = projection of j on the symmetry axis Z'
J = total angular momentum of particles
R = rotational angular momentum of the system
I = total angular momentum of the system
K = projection of I on the symmetry axis Z'
M = projection of I on a space-fixed axis Z

Figure II-1. The coupling scheme for particles and a rigid rotor. Taken from Reference [Mc65].

The $I_{\pm}$ and $j_{\mp}$ are normal shift operators but operate in different inertial frames. In the nuclear-fixed frame where we normally operate, I_+ becomes a lowing operator and I_- a raising operator. The basis functions are chosen to be the eigenfunctions of $H_{sp}(p) + H_{sp}(n) + H_{rot}$. V_{pn} is the residual proton-neutron interaction, which is the reason for splitting the $K=|\Omega_p \pm \Omega_n|$ doublet. H_{irot} is an intrinsic contribution from the rotational degree of freedom. Since it involves only intrinsic variables, it would not affect the relative position of the members within a band. Thus, it is usually included with V_{pn} as a constant term. There is an contribution from the coupling of particle degrees of freedom through the rotational motion H_{pn}, which can connect proton and neutron states that have Ω's differing by two units. Thus, it can shift the odd and even members of a band with respect to each other, but it can do this only for K=0 bands made up from a coupling of $\Omega_p = \Omega_n = \pm 1/2$. However, this operator may be ignored except in special cases.

The Coriolis force is the force that, when we move something in a rotating system, causes it to be pushed sidewise. In the rotating nuclear system, initially the particles are bound to the core in some way prescribed by the usual forces in the absence of rotation, but as the nucleus rotates, the Coriolis force tries to decouple them from the core and align them along the rotation axis [St72,St75,Di84]. The matrix elements of H_c, the Coriolis coupling term, are single-particle operators and have the form:

$$\langle I, K', j, \Omega'_{p(n)} \mid H_c \mid I, K, j, \Omega_{p(n)} \rangle$$
$$= -\hbar^2/2\mathcal{J}\,[(I(I+1)-K(K\pm1)]^{1/2}[\langle\Omega'_{p(n)}|j_{\pm p(n)}|\Omega_{p(n)}\rangle\langle\Omega'_{p(n)}|\Omega_{p(n)}\rangle]. \qquad \text{(II-8)}$$

This coupling term is larger for high j and small Ω, and it increases with I. There is no cross term in H_c, so for an odd-odd nucleus it is applied to protons and neutrons separately. The selection rule for this coupling is $\Delta K = \pm 1 = \Delta\Omega_{p(n)}$. In odd-mass nuclei, it has a diagonal term only when Ω=1/2 [Bo76], and this term is responsible for the usually staggered K=1/2 bands (and sometimes can even invert the order of the members in the band). For odd-odd nuclei, usually the terms in the second bracket are non-zero for only one of the two single particles. However, for K=0 and K=1 bands [Em73], which come from special couplings, namely, $K = \Omega_p + \Omega_n = 1/2 + 1/2 = 1$ and $K = \Omega_p - \Omega_n = 1/2 - 1/2 = 0$, both terms are non-zero, and this is the situation where Coriolis effects can be large. This is the main reason for the existence of doubly-decoupled bands in the odd-odd nuclei. This will be discussed further in Chapter III.

If the Coriolis force is not large, then it can be treated as a perturbation on rotational energy levels [Bo75]. It would give a negative contribution proportional to the I(I+1) term and a positive contribution proportional to the $I^2(I+1)^2$ term, so we reach the equation for rotational energy:

$$E = E_0(K) + AI(I+1) + BI^2(I+1)^2.$$

For most nuclei, the contribution to A comes from $\hbar^2/2\mathcal{J}$; B is down by about 10^{-3} and is usually a negative value, resulting from centrifugal stretching (which we have not corrected here). However, in some odd-mass or odd-odd nuclei, because of the large Coriolis mixing, the B coefficient becomes positive. We need detailed wave functions and to

take into account all the bands that could be mixed in order to calculate the magnitude of this effect, and this is beyond our scope! However, understanding it qualitatively will help us to interpret the band structure of the nucleus.

As mentioned above, the Coriolis effect is in general larger for high-j and low-Ω orbits and increases with spin I. One of the extreme cases, of special interest to us, is for the K=1/2 bands of odd-mass Re nuclei. Here the Ω_p=1/2 states originate from the $h_{9/2}$ spherical states. The Coriolis effect is so large that it even shifts the unfavored signature band members to much higher energies. It also distorts the spacings of the neutron bands built on states originating with j=13/2 in the odd-mass Os nuclei. The effects in these odd-mass states remain when they are coupled to form states of odd-odd nuclei. All of these will be discussed again in later chapters in light of specific examples.

CHAPTER III

SPECIAL FEATURES OF DEFORMED NUCLEI

A. HEAVY-ION FUSION REACTIONS

Coulomb excitation has been widely used to excite nuclei to high spins and to study rotational behavior of deformed nuclei. Indeed, it was born with the rotational model [Hu53]. However, since Coulomb excitation is only an electromagnetic excitation, i.e., the reaction energy is insufficient to allow the projectiles penetrate close enough to where nuclear forces are involved, this process cannot excite the nucleus all the way up to the highest possible spins, nor can it excite other than collective features. Also, it can only be used to study stable nuclei (at the present!). Fortunately such disadvantages have been overcome by heavy-ion compound-nucleus fusion reactions. With the availability of various heavy-ion beams, nowadays it is possible to study neutron-deficient nuclei via in-beam γ-ray spectroscopy.

The compound nucleus, having both high excitation energy and spin, will decay by particle emission [Di80,Di83,Di84], usually by neutrons since which do not have to cross the Coulomb barrier, until the excitation energy is about one neutron binding energy. Because of the angular momentum barrier, evaporated particles will usually carry away only a small amount of angular momentum. Then, γ-ray emissions take over and de-excite the nucleus, which at the beginning of the γ-ray cascade still retains most of the angular momentum, to its ground state.

There are two basic types of γ-ray transitions [Ri81,Di83,Di84] in the de-excitation process, as shown in Figure III-1. The "statistical" transitions cool the nucleus toward the yrast line (for a given spin, the state with the lowest excitation energy is called the yrast state), but remove little angular momentum. Most of the structure information

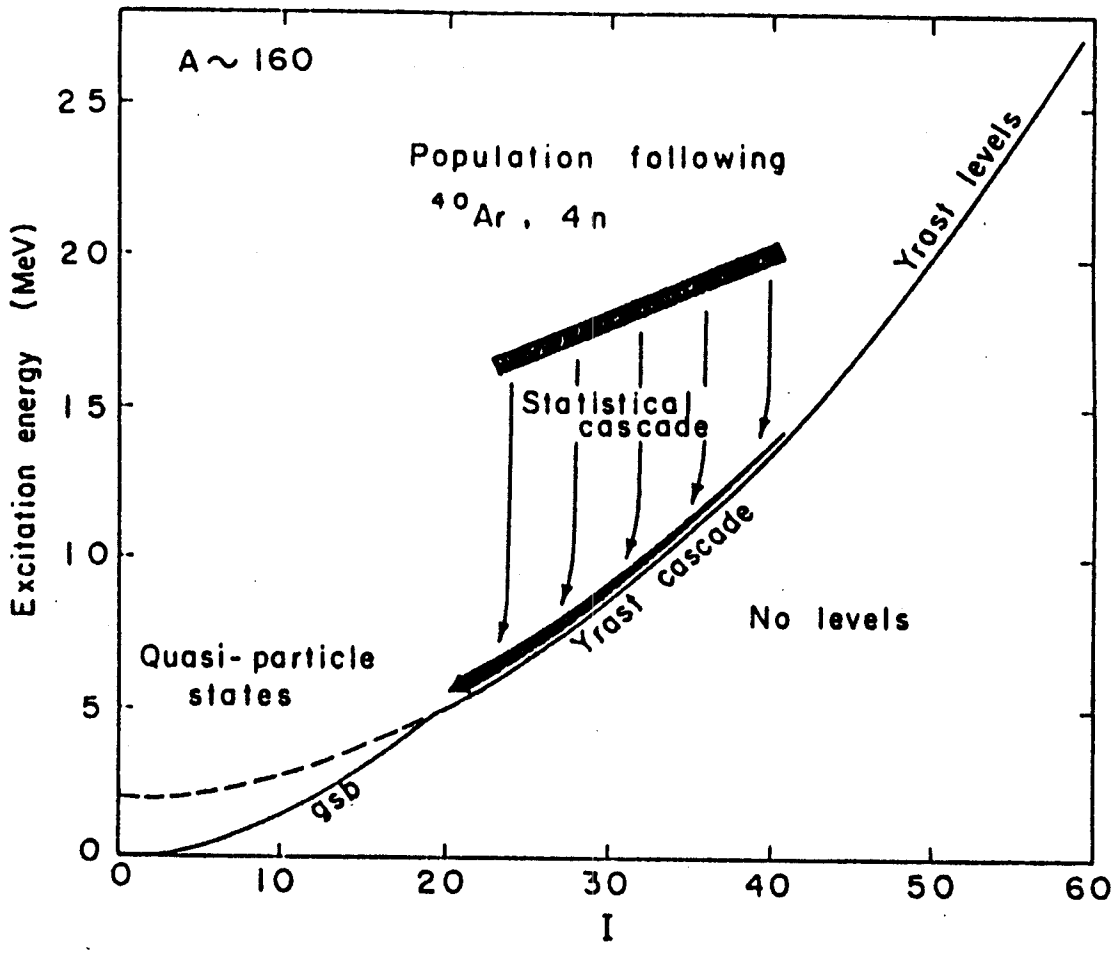

Figure III-1. Excitation energy is plotted against angular momentum in a nucleus (with mass around 160) that is the product of an (^{40}Ar,4n) reaction. The populated energy and angular momentum range is shown, together with the proposed cascade pathway to the ground state. Taken from Reference [st75].

is contained in the "yrast-like" transitions, which decay roughly parallel to the yrast line and remove angular momentum. In the higher-spin region, the level density is so high that transitions can not be resolved, producing a continuum spectrum. In the lower spin region, the transitions can be resolved, producing the discrete spectrum.

Studying the discrete spectrum, one can learn detailed information about the band structure, such as the intrinsic states of the band heads and the spins of the band members. This is the main subject of our present work, and many variations will be discussed.

The study of continuum spectra is focused on extracting the dynamic moment of inertia $\mathcal{J}^{(2)}$ [Di80,Di83,Vo83,Di84], which is defined as

$$\mathcal{J}^{(2)} / \hbar^2 = (d^2E / dI^2)^{-1} = dI / \hbar d\omega . \qquad \text{(III-1)}$$

The idea is that if the nucleus is a perfect rotor, there is a high correlation between energy and spin. One aspect of this correlation is that there are no two Y-rays with the same energy. Thus, in a two-dimensional plot of $E_\gamma^{(1)}$ vs. $E_\gamma^{(2)}$ [De80], no point should be found along the diagonal line, and the pattern is like a series of ridges parallel to the diagonal. The width W of the "valley" along the diagonal is determined by the difference between Y-ray energies and is related to the moment of inertia of the band by

$$W = 2\Delta E = 8(d^2E_\gamma / dI^2) = 8(d\omega / dI) = 8\hbar^2 / \mathcal{J}^{(2)}_{\text{band}} . \qquad \text{(III-2)}$$

This useful piece of information can be obtained without resolving the spectrum, with the requirement that the populated bands have similar

moments of inertia at a given Y-ray energy. Actually, the first indication of superdeformation outside the actinide region came from the study of the continuum spectrum of ^{152}Dy [Ny84]. The $\mathcal{J}^{(2)}_{band}$ was evaluated from the width of the valley between 0.80 and 1.35 MeV, shown in Figure III-2 to be (85 ± 2) $\hbar^2$ MeV^{-1}, which corresponds to a quadrupole deformation of $\varepsilon \approx 0.51$ (ε, the quadrupole deformation which is $\approx \Delta R/R$).

B. SUPERDEFORMED BANDS

Superdeformation was discovered by Polikanov and his colleagues [Po62] in the spontaneously-fissioning isomers in some actinide nuclei, which decay with half-lives orders of magnitude smaller than expected. It was not until 1967 that Strutinski [St67] explained that those nuclei have a secondary minimum in the potential energy surface and are prolate shape isomers with a major to minor axis ratio nearly 2 : 1.

Calculations [Ne75,Ra80,Sc82a] of the high-spin structure of nuclei in the Dy region, with A≈150, have predicted that these nearly spherical, or slightly oblate, shape nuclei will become prolate with a large deformation before they eventually decay by fission. The first indication of such a superdeformed rotational band was in the continuum Y-ray spectrum of ^{152}Dy [Ny84], where a deformation of $\varepsilon > 0.5$ was extracted. With the development of better techniques, multi-detector, Compton-suppressed Ge detector arrays became available. This progress extended the studies of discrete Y-ray spectra to much higher spin and gave birth to the first characterization of the superdeformed band in

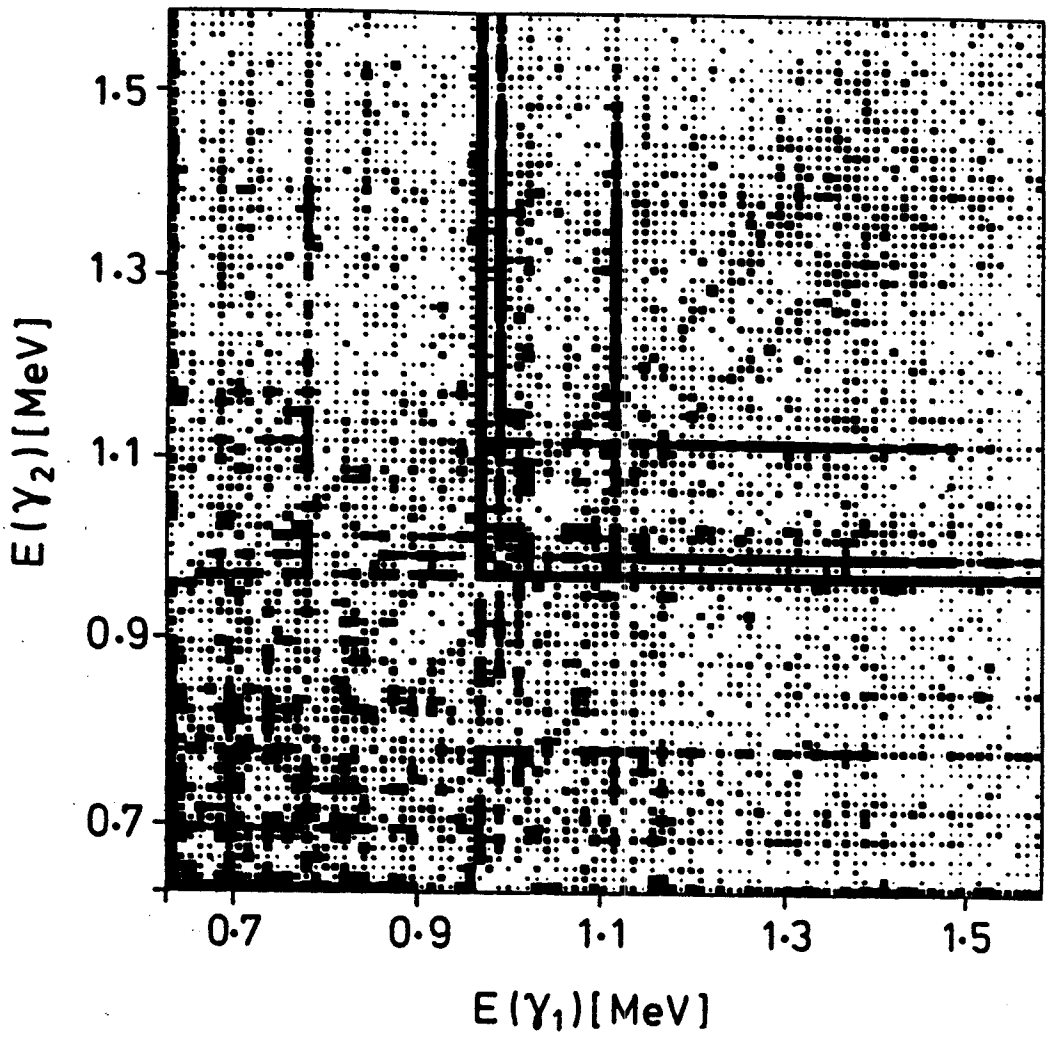

Figure III-2. Correlation spectrum of $E(Y_1)$ vs. $E(Y_2)$ for ^{152}Dy. Vertical and horizontal stripes are due to discrete lines from yrast Y rays below spin 40. The superdeformed prolate structure is identified by the ridges parallel and close to the $E(Y_1)=E(Y_2)$ diagonal for energies between 0.80 and 1.35 MeV. Taken from Reference [Ny84].

^{152}Dy [Tw86], with observed discrete transitions up to spin I ≈ 60. (Actually a band with unusually large deformation was observed in ^{132}Ce by Nolen et al. in 1985 [No85], but it has somewhat smaller deformation, an axis ratio of 3:2.) Since then, about a dozen such discrete superdeformed bands have been identified. They can be grouped into two regions: (1) Gd, Tb, and Dy with mass around 150 [Ha88,De88a,Ja88b, De88b,Rz88]; (2) La, Ce, and Nd with mass around 130 [No85,Be87b,Be87c, Wa87,Lu88].

These two groups have similar properties. States in superdeformed bands are connected by regularly spaced transitions with ΔI=2, strongly enhanced E2 transitions due to the large quadrupole deformation. They behave nearly like rigid rotors, with deformation ε ≈ 0.6 for the mass 150 group and ε ≈ 0.4-0.5 for the other group. The population mechanism for such bands is not yet clear. However, it is believed that it depends on the maximum angular momentum and excitation energy which are brought into the reaction [Ma87]. A recent experiment [Ta88] shows that to populate such a band a relatively cold residual nucleus needs to be formed, but one with angular momentum higher than the spin at where this band becomes yrast. In general, the superdeformed bands receive on the order of 1% of the total population.

How a superdeformed band decays to normal bands is not clear either, because of the weak, scattered intensity of this decay. ^{135}Nd is the only nucleus where the linking transitions to the ground state band have been established [Be87b]. Superdeformed bands have also been studied in other Nd isotopes, $^{133-137}$Nd [Be87c,Wa88]. Experimental evidence shows that bands in the odd-mass Nd nuclei receive more population than in even-even ones (in ^{133}Nd 20%, the current maximum)

and it seems that such bands lie at lower excitation energy in odd-mass Nd. It is hoped that, because of their much larger populations, more linking transitions can be observed in odd-mass nuclei and some of the questions about superdeformed bands can be answered.

Searches for superdeformed bands have also been carried out in ^{178,180}Os [Bu88,Rz88] and ^{184}Pt [Wa88a]. The latter search failed, whereas for Os nuclei, although the analysis is not yet complete, there is strong indication that a superdeformed band might exist.

It is encouraging to learn that such bands could be found in the mass region we are exploring now. Although we do not expect to observe discrete transitions from superdeformed bands, we could still analyze the continuum spectrum. Hopefully, our studies can contribute useful information to the understanding of superdeformed bands.

C. BACKBENDING

A plot [St75] of energy E versus spin I for the ground state band of ^{162}Er (Figure III-3) looks rather ordinary. However, if we plot these data as moment of inertia versus the square of the rotational frequency ω (proportional to the slope of an E vs. I plot), a drastic change is found around $I \approx 16$. This interesting phenomenon is called "backbending", and it was first observed in 1971 by Johnson et al. [Jo71] in the ground-state rotational band of ^{160}Dy.

The ground state of an even-even nucleus, in the collective model, has K=0 with all of the nucleons paired up. However, when the nucleus starts rotating, the Coriolis force acts oppositely on the members of a

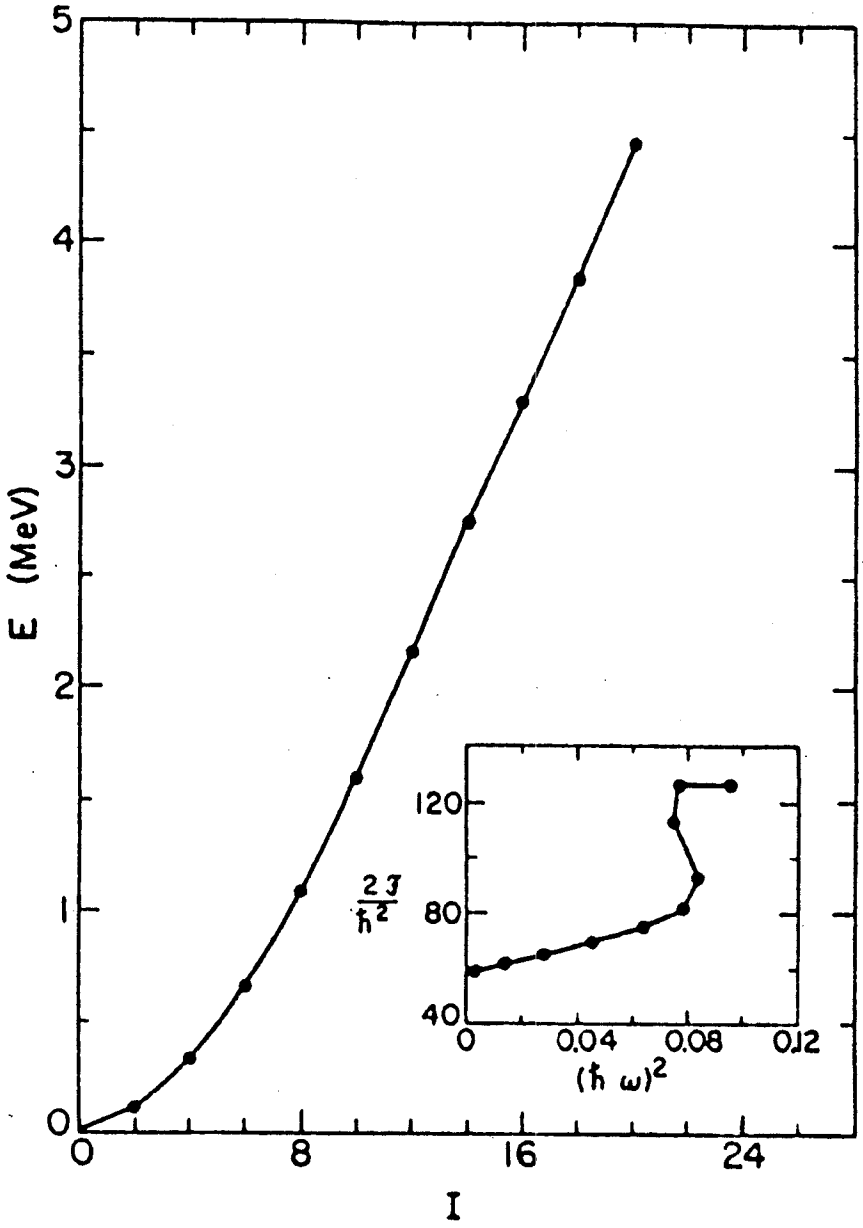

Figure III-3. A plot of energy vs. I for the ground-band rotational levels in ^{162}Er. The insert shown the same data in the type of plot generally used to show backbending behavior. Taken from Reference [St75].

pair of nucleons, breaks the symmetries, and reduces the pairing correlations. This is what causes the gradual increase of the moment of inertia in Figure III-3. Eventually the nucleus will align a pair of high-j particles rather completely along the rotational axis, while still keeping the pairing correlations among the lower-j nucleons [St72,St75,Ma81,Di84,Ga88]. This situation shows up in the $\mathcal{J}$ versus $(\hbar\omega)^2$ plot as a sudden change. This process also corresponds to a band crossing between the completely paired ground state band and a two-quasi-particle[1] band (S-band), the latter having a larger moment of 29inertia so it is energetically more favorable and becomes the yrast band after the crossing.

Earlier observations of backbending were in rare-earth nuclei with mass A≈160. In that region nucleons in the $i_{13/2}$ orbits are the ones with the highest angular momentum j, and they suffer the Coriolis force the most. The experimental proof that backbending is from aligning a pair of $i_{13/2}$ quasi-neutrons comes from blocking experiments. In such experiments the backbending frequencies are compared between an odd-mass nucleus and a corresponding even-even core nucleus. A good example is ^{161}Yb [Ri80a], which has an extra neutron outside the ^{160}Yb core. The band, built on $\nu 3/2^-[521]$ (from the $h_{9/2}$ spherical state), backbends at a similar energy as ^{160}Yb [Ri80b]. On the other hand, a band built on

---

1. Quasi-Particle
Due to the residual interaction between the particles, the picture of a particle occupying a state in the extreme single-particle view becomes partly a particle and partly a hole occupying a state. This combination of particle and hole is known as a quasi-particle.

$\nu 3/2^+[651]$ (from the $i_{13/2}$ spherical state) backbends at much higher energy (0.36 MeV), because the most favorable position was blocked by the odd-neutron. Other examples, such as ^{157,159}Er [Gr73] and ^{165}Yb [Ri74], also showed that this band, which occupies $i_{13/2}$ neutron orbits, delays its backbending until higher energy; on the other hand, odd neutrons in lower-j orbits [Ga80] weaken the pairing force, but the effect, depending on the orientation of the orbits, on the backbending frequency is not so strong. ^{159}Tm, which has one fewer proton than ^{160}Yb, backbends at an energy similar to ^{160}Yb [La81]. It shows that one fewer (or one more) proton does not affect the alignment of the core neutrons. In addition, odd-mass Ho isotopes [Gr74] also backbend at about the same frequencies as their even-even neighbors. The odd-proton has very little effect on the neutron pairs. This is what one would expect [Ga81], since they are in different shells.

Many nuclei, like ^{158}Er [Le77], ^{160}Yb [Be79a,Ri80b], and ^{162}Hf [Ri80c], show a second backbending after the $i_{13/2}$ neutron alignment. Calculations have predicted that this must result from the alignment of $h_{11/2}$ protons [Be81,Fa78,Fr81a], agreeing with the experimentally observed crossing frequency.

Many experiments have been performed studying the nature of backbending. It is clear nowadays that the alignment of $i_{13/2}$ quasi-neutrons, in general, causes the first backbending in heavy rare-earth nuclei, while alignment of $h_{11/2}$ quasi-protons causes it in light rare-earth nuclei. The studies also show that the frequency of band crossing depends strongly on the deformation of the nucleus and the position of the Fermi surface within the high-j subshell [Be88,Ga88]. These are

very essential points when considering blocking effects.

Most of these studies of highly aligned bands were done across the N=90 region. Recent studies in the Pt-Au region [Ka78,La86,Ja88a], also one instance in W isotopes [Ra86], propose an almost simultaneous crossing of $\nu i_{13/2}$ and $\pi h_{9/2}$ quasi-particle pairs. The evidence of this surprising behavior came from comparing i_x^2 and the crossing frequencies of the neighboring three types of nuclei. Why these $\pi h_{9/2}$ quasi-protons align at such a low frequency ($\approx$0.24 MeV) has not yet been fully understood. However, it was proposed that the configurations of the quasi-particle would drive the nuclear shape toward a prefer deformation [Ga82,Ga88], and this deformation effect might be responsible for such low crossing frequencies caused by $\pi h_{9/2}$ quasi-protons.

Although many even-even and odd-mass nuclei exhibit backbending, the first example in odd-odd nuclei, ^{158}Tm, was not reported by Foin et al. [Fo85] until 1985. The band has the configuration,

---

2. Rotational Alignment
I_x is the projection of the total angular momentum I along the rotational axis, and I_m is the mean value of the two angular momenta involved in the transition. Then I_x can be evaluated by [Be79b]

$$I_x(I_m) = [(I_m + 1/2)^2 - K^2]^{1/2}. \qquad \text{(III-3)}$$

Another procedure for deducing I_x was developed [Be80,Fr81a,Pi81] by adopting the Harris formula [Ha65]:

$$i_x = I_x(\omega) - (J_0 + J_1\omega^2)\omega \qquad \text{(III-4)}$$

Here J_0 and J_1 are inertia parameters characterizing the collective motion, and i_x, which is usually called the alignment, the projection of angular momentum j along the rotational axis. When backbending occurs, there will be a sharp increase of i_x. So, nowadays, the most common method to extract the crossing frequency is to plot $\hbar\omega$, which is $\approx E_\gamma/2$, versus i_x. J_0 and J_1 are derived by least-squares fitting of the first few experimental data points.

$[h11/2]_p[i13/2]_n$, and backbending occurs at 0.35 MeV, which is higher than ^{158}Er (the corresponding even-even core) and ^{159}Tm, owing to the blocking argument, but is the same as ^{159}Er, which has similar blocking effect. ^{136}Pm [Be87a], a different case, backbends at a frequency of $\hbar\omega \approx 0.28$ MeV because of the decoupling of a pair of $h_{11/2}$ protons. From these few available examples, we would like to conclude that odd-odd nuclei can backbend readily as other types of nuclei. But, the problem is that there have not yet been extensive studies of odd-odd nuclei, and there are still plenty of cases waiting to be dug out. From the intrinsic states in the odd-mass neighbors of ^{176}Re, we know that neutron $i_{13/2}$ and proton $h_{9/2}$ orbits are available for ^{176}Re. Therefore, there is a good chance that we can observe backbending. Also, the fact that even-even [Dr82] and odd-mass [Dr83,Ne76] Os isotopes, as well as some odd-mass Re isotopes [Ne76,Ya83], do show backbending encourages us.

D. DOUBLY-DECOUPLED BANDS

Way back in the early 1970's, experimentalists were puzzled by the spin assignments for the ground states of ^{184,186}Ir. From the results of radioactive decay studies [Ho73], the spin of the ground state seemed most likely to be 5 for both nuclei; however, finding the proper odd-proton and odd-neutron states to couple and give a spin-5 ground state was difficult. Emery et al. [Em73] investigated this situation and concluded that it was because that the odd-proton orbit involved in the ground-state configuration of ^{184,186}Ir is an Ω=1/2 orbits, which has such a large decoupling constant that the I=K state is not the lowest state of the band. Kreiner et al. [Kr84,Kr85] studied ^{186}Ir later via in-beam γ-ray spectroscopy and observed a ΔI=2 band built on the I=5 ground state, which truns out to have both its odd-proton and odd-neutron occupying Ω=1/2 orbits. After this first characterization of the doubly-decoupled band, many such bands have been observed, most of them in the Ta-Re-Ir region [kr84,Kr85,Kr86,Da86,Kr87a,Kr87b,Kr88a, Kr88b,Sh88].

Since the doubly-decoupled bands are the coupling of $\Omega_p = \Omega_n = 1/2$, to understand the nature of these bands it seems that we should look into the Ω=1/2 orbits in odd-mass nuclei first. In odd-mass nuclei, rotational bands built on a $K = \Omega = 1/2$ orbit always show peculiar behavior. They are famous for having staggered spacings or for being split into two parts distinguished by the signature factor, $(-1)^{I+K}$ (usually only one part is observed experimentally). Sometimes there is even an inversion of the normal spin sequence. This comes about because there is an additional term in the rotational-energy expression, the

diagonal effect of the Coriolis force acting in the rotating system [Em73,Bo75], and this term is proportional to $a(-1)^{I+1/2}(I+1/2)$. How much this term affects the rotational levels depends greatly on the magnitude of a, the decoupling constant (Coriolis matrix element), which can be derived from two consecutive transitions of the same signature. It is clear that this Coriolis term would shift members of one signature up in energy and the members of the other down, thus staggering the band spacings or, in the extreme, splitting the band into two parts.

In an odd-odd nucleus, if both the odd-proton and the odd-neutron occupy $\Omega = \pm 1/2$ orbits, the effects discussed above will certainly be transmitted into the odd-odd nucleus. This special coupling will produce $K = \Omega_p + \Omega_n = 1/2 + 1/2 = 1$ and $K = |\Omega_p - \Omega_n| = 1/2 - 1/2 = 0$ bands. The Coriolis operator can connect these two bands and give a effect which is equivalent to the diagonal effects in odd-mass systems. The magnitude of this effect depends on spin, signature, and the sum of the proton and neutron decoupling constants [Kr85]. If, for example, both a_p and a_n are positive, then odd-spin states will have large couplings and be lowered in energy.

In addition to the Coriolis effects, two other terms also affect the K = 0 bands [Bo73,Kr85]. Recall that in Chapter II, H_{pn} makes a contribution to K = 0 bands coupled by $\Omega_p = \Omega_n = \pm 1/2$. This term is signature and decoupling constant dependent, but not I dependent. Thus, it affects most low spin states and favors even-spin states if a_p and a_n have the same sign. A third term comes from V_{pn}, which also contains an additional term for K = 0 states. However, V_{pn} is not well understood, and this term is also I independent. It should be emphasized again that

we do not try to do any quantitative analysis here, but try only to understand the origins of doubly-decoupled bands qualitatively.

Looking across the nuclear chart, we see that odd-mass $^{177-185}$Re [Br88,Fi84,Fi87,El81b,Le72,Ya83] all have bands built on the $\pi 1/2^-[541]$ states with quite large (>5) decoupling constants. This is able to make the $I = 5/2^-$ instead of the $I = 1/2^-$ the state with the lowest excitation energy. The odd-neutron nuclei, $^{177-185}$Os [Dr83,Br88,Fi84, Fi87,El81], also have a staggered $K = 1/2$ band (in general $a \approx 1.0$) at rather low energies. Since the intrinsic states of an odd-odd nucleus are the coupling of odd-proton and odd-neutron states, it is no wonder that doubly-decoupled bands appear in the odd-odd Re isotopes. We believe that the odd-proton nucleus is the driving force for this doubly-decoupled band, since it has by far the larger decoupling constant.

Since a_p and a_n are both positive, the odd-spin members of the $K = 1$ band are the favored states; indeed, only these states have been observed experimentally so far. The lowest state of this $K = 1$ band is $I = 5$ for ^{186}Ir [Kr85], while it is $I = 3$ for ^{184}Ir [Kr88b] and the Ta isotopes [Kr87a,Kr88a]. It seems that there is a certain relation between the spin of the lowest state of the $K = 1$ band of the odd-odd nucleus and that of the $K = 1/2$ band in odd-proton nucleus. For the heavier odd-mass Ir isotopes, $I = 9/2$ is the lowest state. On the other hand, $I = 5/2$ is the lowest state for the odd-mass Ta isotopes and lighter Ir isotopes. For the Re isotopes, although $I = 5/2$ is found to be the spin of the lowest state [Le72,Si74], the $9/2 \rightarrow 5/2$ transition was not experimentally observed in some isotopes because its energy is so low that it can be easily masked by x-rays, or because it is highly

converted. There have been no 5 → 3 transitions observed yet in the known doubly-decoupled bands of Re nuclei [Da86,Kr87b]. Therefore, the situation is somewhat ambiguous for them. Also, the K = 0 band, which is the singlet coupling, has never been observed so far, probably because of its higher excitation energy.

CHAPTER IV

EXPERIMENTAL APPARATUS AND METHODS

To study the rotational levels of the well-deformed, neutron-deficient, odd-odd ^{176}Re, heavy-ion fusion reactions were chosen to produce it. Experiments have been done both at NSCL, Michigan State University, and at SUNY Stony Brook.

A. EXPERIMENTS AT NSCL

1. Reaction and Detecting System

The reaction ^{159}Tb(^{22}Ne,5nγ)^{176}Re, was used in order to emphasize high-spin states of ^{176}Re. The target was a self-supporting, ≈1mg/cm^2 thick foil of ^{159}Tb (100% abundant). For our first exploration of this barely known nucleus, we used 108-MeV total beam energy. This beam energy was chosen according to the excitation functions, which are shown in Figure IV-1, calculated by the code CASCADE [Pü77]. We could not run an excitation function, because of the difficulty in changing beam energies. Two bare intrinsic Ge detectors were used. They were placed at ±90° or 90-125° with respect to the beam direction. These detectors were 15% efficient, with 2.4-keV FWHM resolution for 1.332-MeV ^{60}Co line. Thin Cu and Cd foils were placed in front of the detectors to minimize the x-rays emitted by the Tb target and compound nucleus.

For our second set of experiments, the beam energy was increased to 113-MeV in order to reduce the probability of producing ^{177}Re. The same two Ge detectors were used, but each had a NaI(Tl) annulus, with sizes 20.3×20.3- and 30.5×30.5-cm, as anti-Compton shields. A photograph of our set-up is shown in Figure IV-2. Besides the Ge detectors, a low-energy photon spectrometer (LEPS), having better resolution for

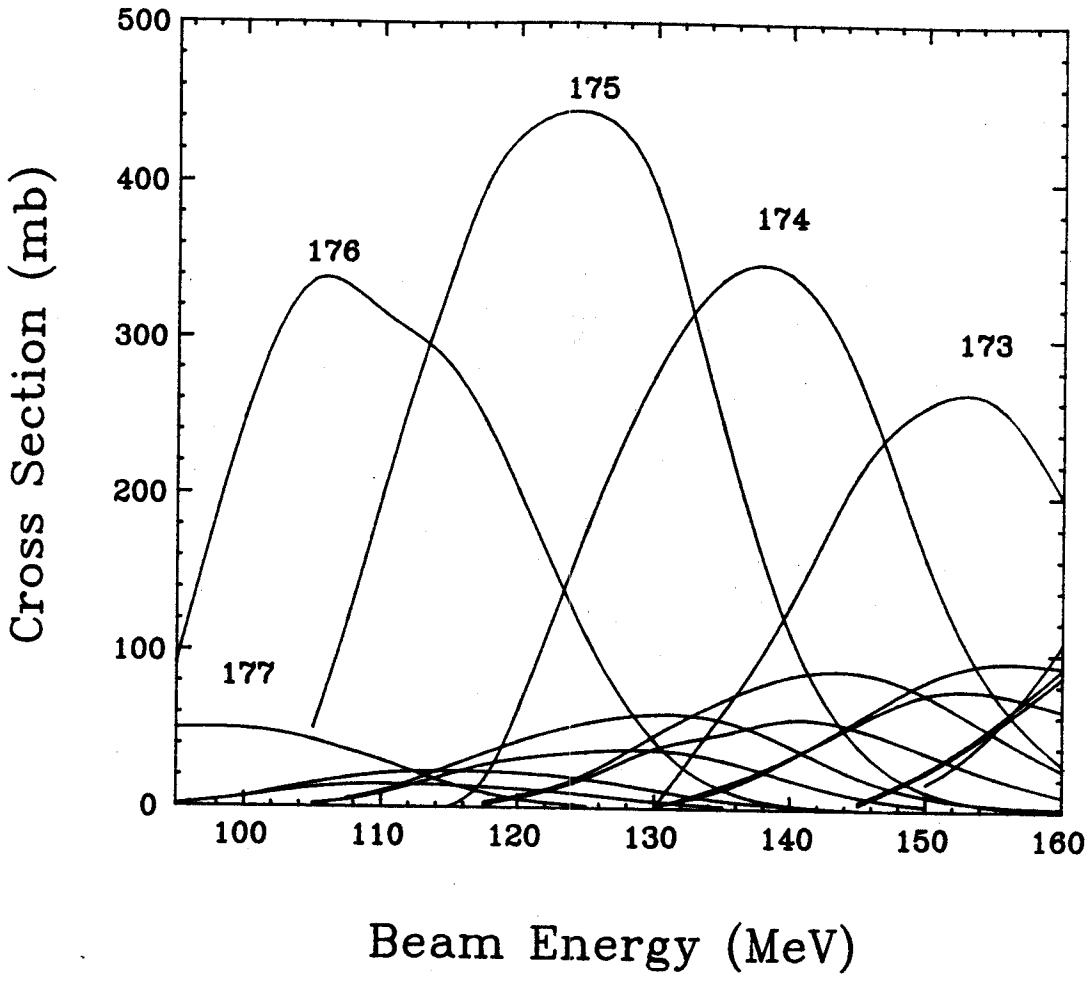

Figure IV-1. Cross sections versus beam energies calculated by CASCADE for a ^{22}Ne beam on a ^{159}Tb target.

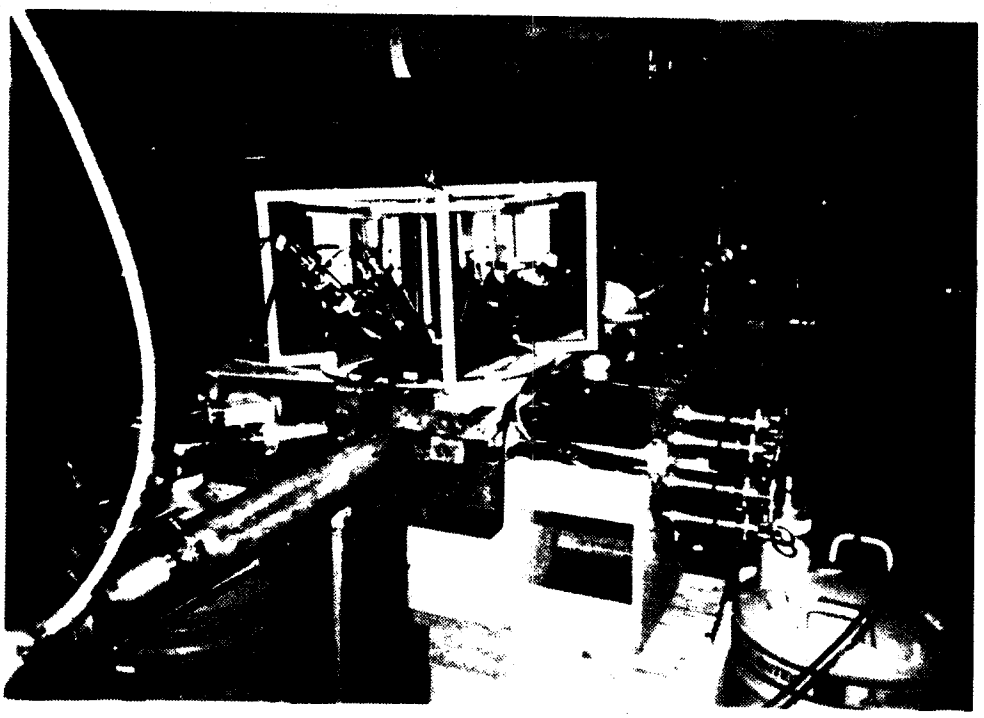

Figure IV-2. A photograph of the set-up at MSU NSCL.

low-energy Y transitions, was positioned at $\approx -150^{\circ}$. It was hoped that the LEPS could resolve the low-energy Y transitions from x-rays. Also, seven 7.6×7.6-cm NaI(Tl) detectors, clustered around the target at various angles and distances, were used as a multiplicity filter. No fold requirement was set on the multiplicity filter during the run, only for off-line sorting.

2. Data Acquisition System and Analysis

The electronics set-up could be divided into two main portions according to their functions: energy signals and logic signals. A block diagram of the electronics is shown in Figure IV-3. The signals from the pre-amp detectors were sent to spectroscopic amplifiers and then to amplitude-to-digital converters (ADC's), which convert analog signals into binary digits that are ready for data acquisition (DAQ) system. This spectroscopic amplifier distorts the steepness of the risetime of incoming pulse, which makes accurate timing measurements more difficult.

The Y-transitions that deexcite the vast majority of nuclear excited states are always related to each other, and they usually occur within one nanosecond. This time interval is shorter than the resolving time of the electronic modules, so these transitions are considered as "prompt coincidence". In order to obtain accurate timing, the pre-amp signals were sent to a timing filter amplifier (TFA) then to a constant fraction discriminator (CFD), which utilizes the property that the time for a peak to reach a set fraction of its maximum value is almost time-invariant. The output signals at this stage are well-timed and can be used for all kinds of logical purposes.

Meta-stable states occur quite often in well-deformed nuclei and

Figure IV-3. A block diagram of the electronics set-up at MSU NSCL.

ADC: Amplitude-to-digital converter.
AMP: Spectroscopic amplifier.
BGO: Bismuth germanate
CFD: Constant fraction discriminator.
COIN: Coincidence unit.
DAQ: Data acquistion system.
DISC: Discriminator.
FI/FO: Fan in/fan out.
GDG: Gate and delay generator.
Ge: Ge detector.
LOGIC: Logic unit.
NaI(Tl): NaI(Tl) detector.
RD: Rate divider.
TAC: Time-to-digital converter.
TFA: Timing filter amplifier.

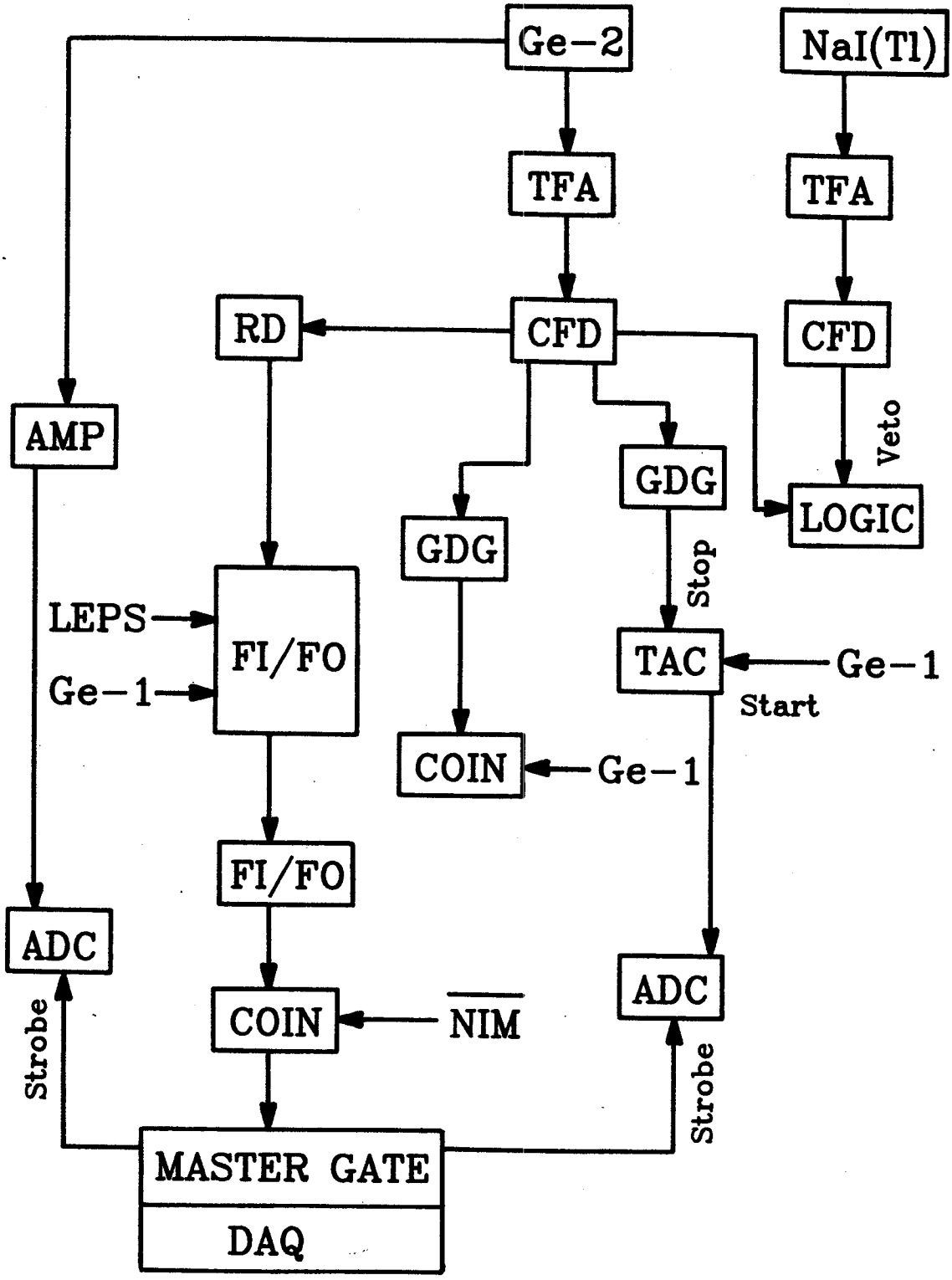
Ge-2
NaI(Tl)
TFA
TFA
RD
CFD
CFD
AMP
Veto
GDG
GDG
LOGIC
Stop
LEPS
FI/FO
TAC
Ge-1
Ge-1
Start
COIN
Ge-1
FI/FO
ADC
ADC
Strobe
COIN
NIM
Strobe
MASTER GATE
DAQ

Figure IV-3.

the life time of these states can be around tens of nanoseconds. In order to catch any of these states, we set the coincidence as an overlap of 250-ns wide logic pulses. Any two of the three Ge detectors fired was taken as a valid coincidence event. Because of the long resolving time set on the coincidence unit, we no longer collected prompt coincidences only. Thus, a time-to-digital converter (TAC) was adopted to give time relation of these coincidence transitions. It used signals from one of the two intrinsic Ge as start and signals from the other one as stop. By gating on different portions of the TAC spectrum, we could acquire various information, such as prompt coincidences and delayed coincidences. This is the so-called three-parameter ($E_\gamma \times E_\gamma \times t$) coincidence.

The data were recorded on magnetic tapes via the NSCL 68000 data-acquisition system. It is capable of handling several thousand events per second without any unendurable dead-time. With the present set-up singles as well as coincidences events could be collected simultaneously. Each kind of events, namely, singles, coincidences, and Compton-suppressed coincidences, has its own bit register, which is the index for off-line sorting. However, after a few hours of data collection, usually the singles collecting rates were scaled down by a factor of the order of ten, so as to enhance the amount of coincidences events within a tape and to reduce the number of tapes that we might end up with.

The data recorded on tapes were filtered off-line by selecting certain bits or setting appropriate gates on histograms using a program FILTER [Sh83]. Afterwards, the filtered data could be sorted into various gated-spectra according to needs using program SARA [Sh83].

3. Calibration

Standard γ-ray sources, such as ^{133}Ba, ^{137}Cs, and ^{152}Eu, were used to calibrate the efficiency and energy of the Ge detectors. The spectra were taken with exactly the same experimental set-up. The spectra were analyzed by fitting the peaks with Gaussian curves and varying exponential tails using program PHAEDRUS [Sc83]. The areas of the peaks then were compared with known intensities, normalized, and plotted versus energies as efficiency calibration curves. For energy calibration, the known energies of the transitions were plotted versus peak positions. Least-squares fit was used for both curves.

B. EXPERIMENTS AT SUNY STONY BROOK

Because the data we collected at NSCL had poor statistics, some of the γ-transitions could not be definitely assigned to ^{176}Re or ^{177}Re. Another experiment seemed to be necessary and for this we run at the Nuclear Structure Laboratory at SUNY Stony Brook with its superconducting LINAC. By using the detector array there, it was possible to gain more statistics in a short time period. In addition, angular correlation information can be obtained and excitation function experiments could also be conducted. A ^{165}Ho target and a ^{16}O beam were chosen.

There were problems in trying to adhere a thin Ho layer to a Pb backing. In the case of using a thin target without backing, the recoiling compound nuclei can leave the target before γ decay, so there will be significant Doppler effects and the resolution can be poor.

Since we needed good resolution in order to distinguish Y-rays coming from ^{176}Re or ^{177}Re, we decided to use a thick target with a thickness of ≈51.7 mg/cm^2.

The detector array is shown in Figure IV-4. It contains six n-type Ge detectors, each surrounded by a bismuth germanate (BGO) anti-Compton shield of the transverse type [Hi86]. The distance from the detectors to the target was 14.2 cm, and they were positioned at angles of 35°, 98°, 165°, -158°, -90°, and -35° (the one at 165° was not working properly and was disassembled from the array), respectively, to the beam direction. The Ge detectors had an efficiency of ≈25% relative to a 7.6×7.6 cm NaI(Tl) detector for 1.3-MeV Y-rays, and the resolutions are 2.3-2.7 keV. There were also fourteen hexagonal BGO's working as a multiplicity filter, covering a solid angle of about 80% of 4π. Seven of them were located above the target chamber and seven were below. The threshold was set at approximately 100 keV for these BGO's. A photograph of this set-up is shown in Figure IV-5.

The principles of the the electronic set-ups were the same as used in NSCL, but there was no time-to-amplitude converter (TAC). A block diagram of the electronics is shown in Figure IV-6. A Y-Y coincidence was defined by the overlap of 50-ns wide logic pulses. The requirement set on the multiplicity filter was 3. So a valid coincidence event was considered as at least two Ge detectors and at least three BGO's fired. This greatly reduced background radiation, x-rays, and Coulomb excitation lines from the target.

The valid coincidence events were stored on magnetic tapes for off-line analysis. About 50 million events were collected during a 48-hour run. Gains were checked and matched for all the detectors and every

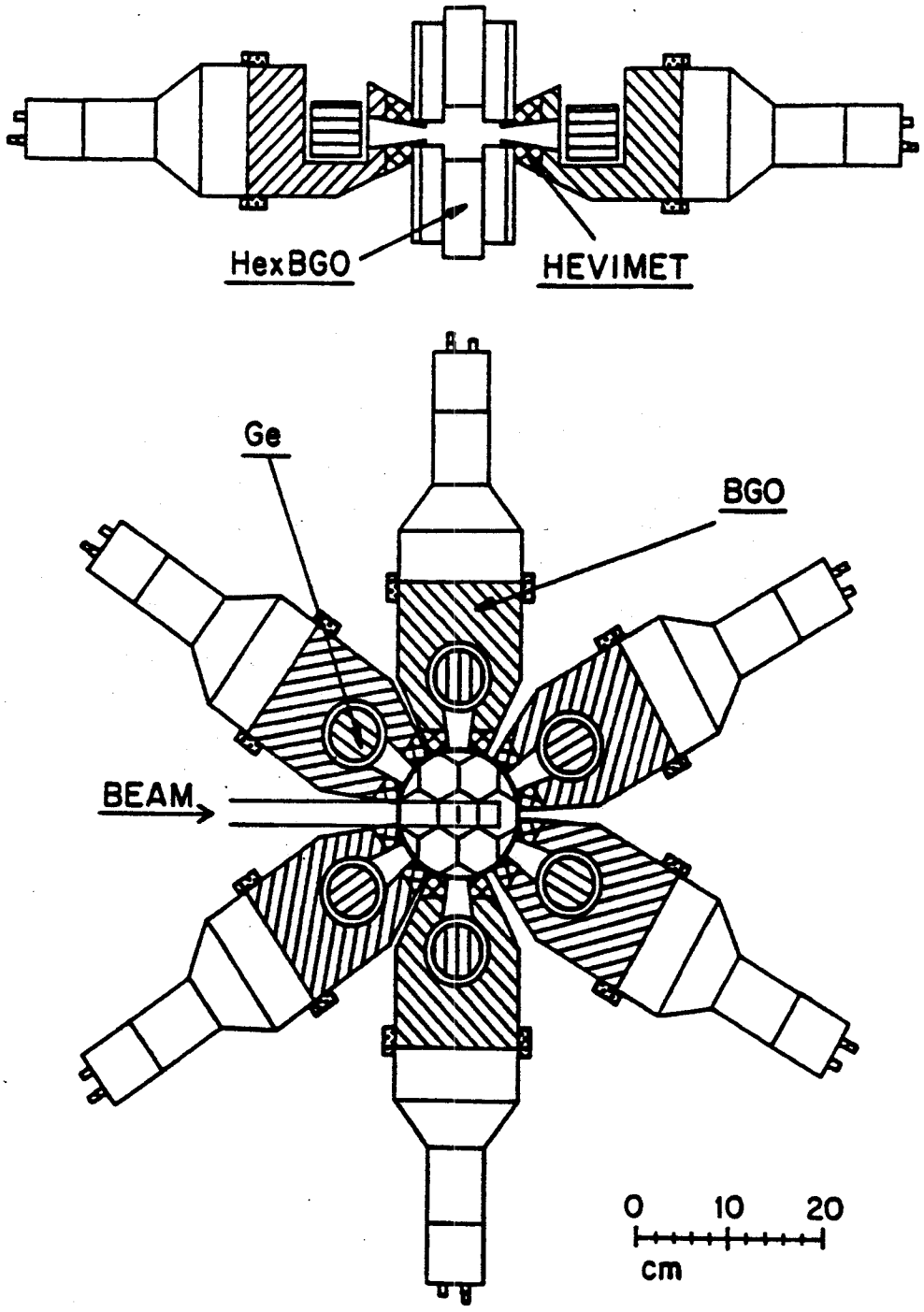

Figure IV-4. The detector array at SUNY Stony Brook.

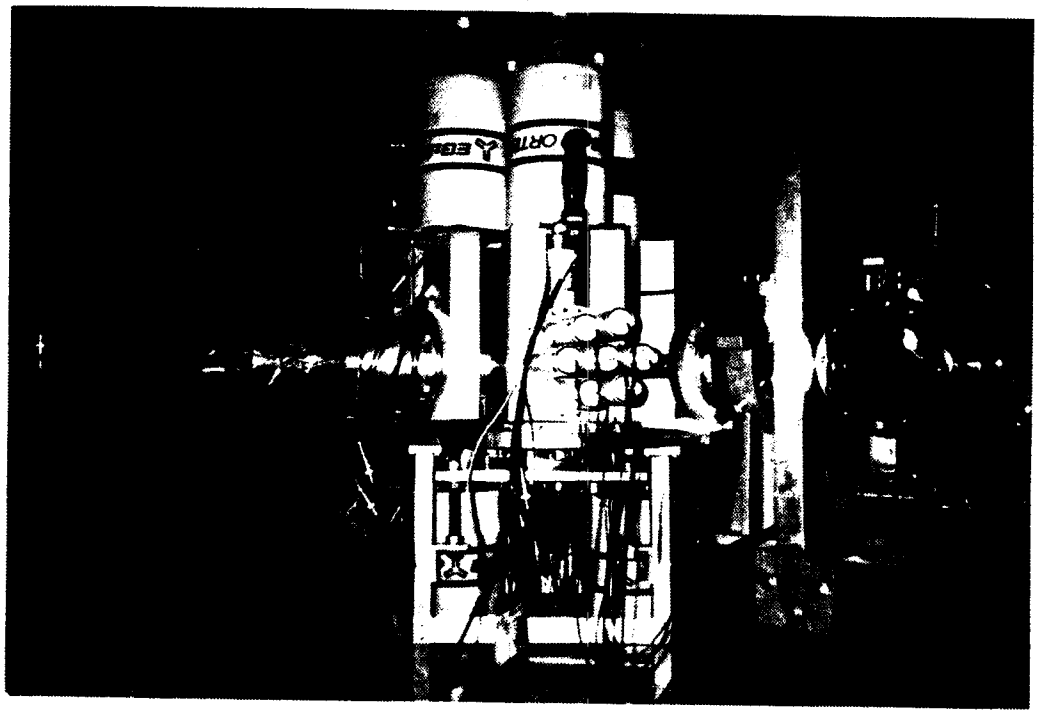

Figure IV-5. A photograph of the set-up at SUNY Stony Brook.

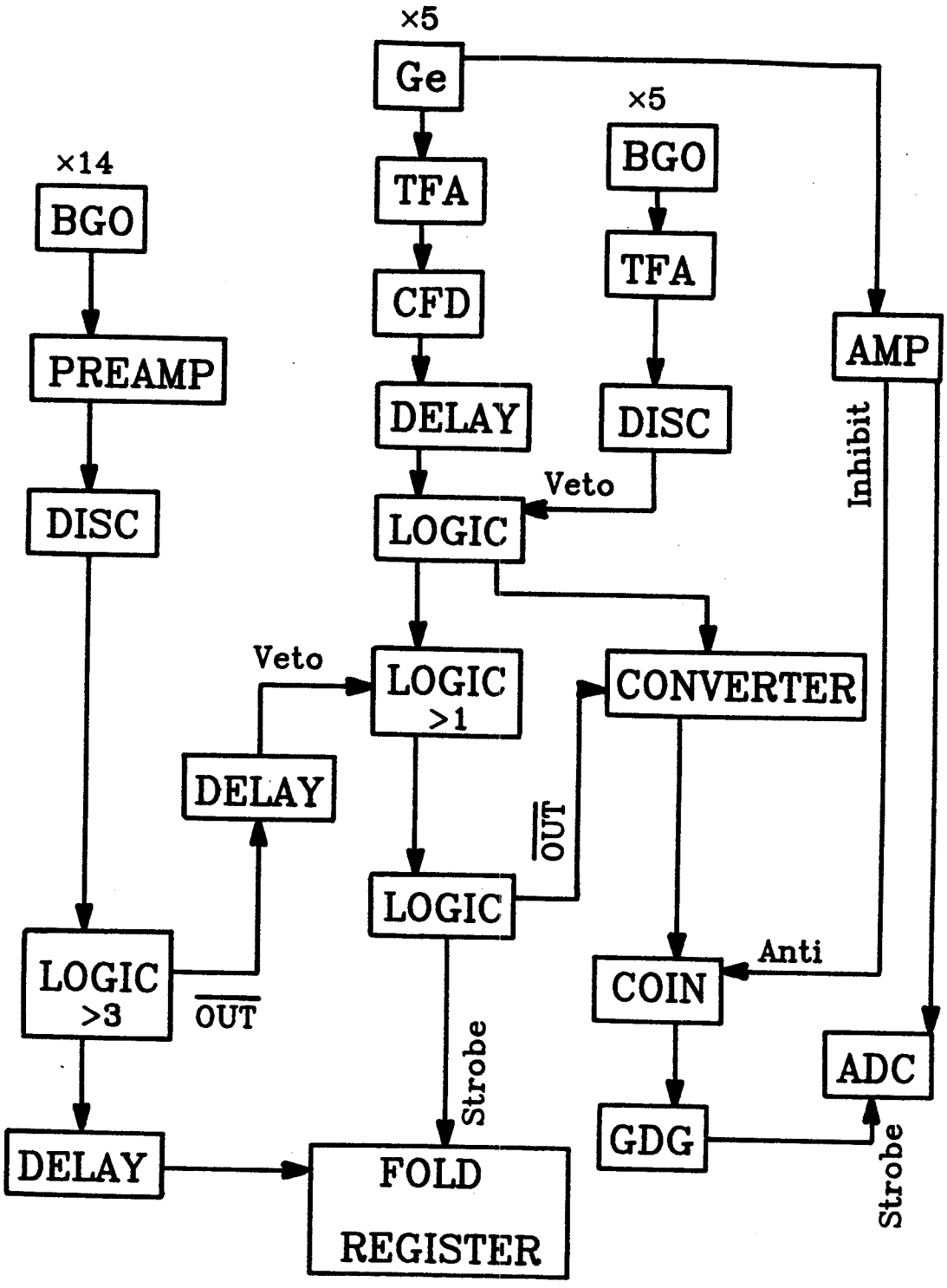

Figure IV-6. A block diagram of the electronics set-up at SUNY Stony Brook.
See Figure IV-3 caption (p.36) for abbreviations.

tape. Coincidences between any two Ge detectors were sorted out and added together to produce a symmetrized array of E_γ versus E_γ. This array was used to generate background-subtracted gated-coincidence spectra and to construct the level scheme.

Angular-correlation information can also be extracted from the coincidence data. The two detectors at 98° and -90° were sorted against the other three detectors to produce a two-dimensional array. Gates then could be set on the known quadrupole transitions of this array at both axis to produce one horizontal and one vertical projection. Average directional-correlation [Kr73] intensity ratios of other transitions could be extracted from these two spectra and used to distinguish whether the transitions were dipoles or quadrupoles.

CHAPTER V

STUDY OF ^{176}Re

A. RESULTS FROM THE REACTION, $^{159}Tb(^{22}Ne,5n\gamma)^{176}Re$

1. With 108-MeV Beam Energy

1.1 Singles

^{176}Re was barely known prior to our study. Only a few transitions from ^{176}Os decay [Ho76] were ever reported. Fortunately, its odd-mass neighbor, ^{177}Re, was well-studied. Figure V-1 shows the singles spectra taken at angles 90° and 125° with respect to the beam direction. γ-transitions from ^{177}Re were observed; however, there are new transitions that could not be assigned to background radiations or radioactivities, and they are believed to come from ^{176}Re. Also, in the radioactivity spectra, which were taken just after the beam was shut off, the two lowest ground-state-band transitions of ^{176}W were observed. (The half-live of ^{176}Re is 5.7 minutes, and it decays to ^{176}W.) This is a proof that ^{176}Re was produced during the reaction.

1.2 Coincidences

This was the first time that the K500 cyclotron had been run on the second-harmonic mode and was able to provide a beam with such a low total energy. The intensity of the beam was only ≈10nA on a Faraday cup placed behind the target. This intensity was so low that not enough statistics could be collected during a 48-hour run. An integral coincidence spectrum is shown in Figure V-2. Also, as can be seen from this spectrum, because only two bare Ge detectors were used, a large portion of the spectrum was from Compton scattering. Although about 3×10^7 events were recorded on magnetic tapes, the "real" events were few.

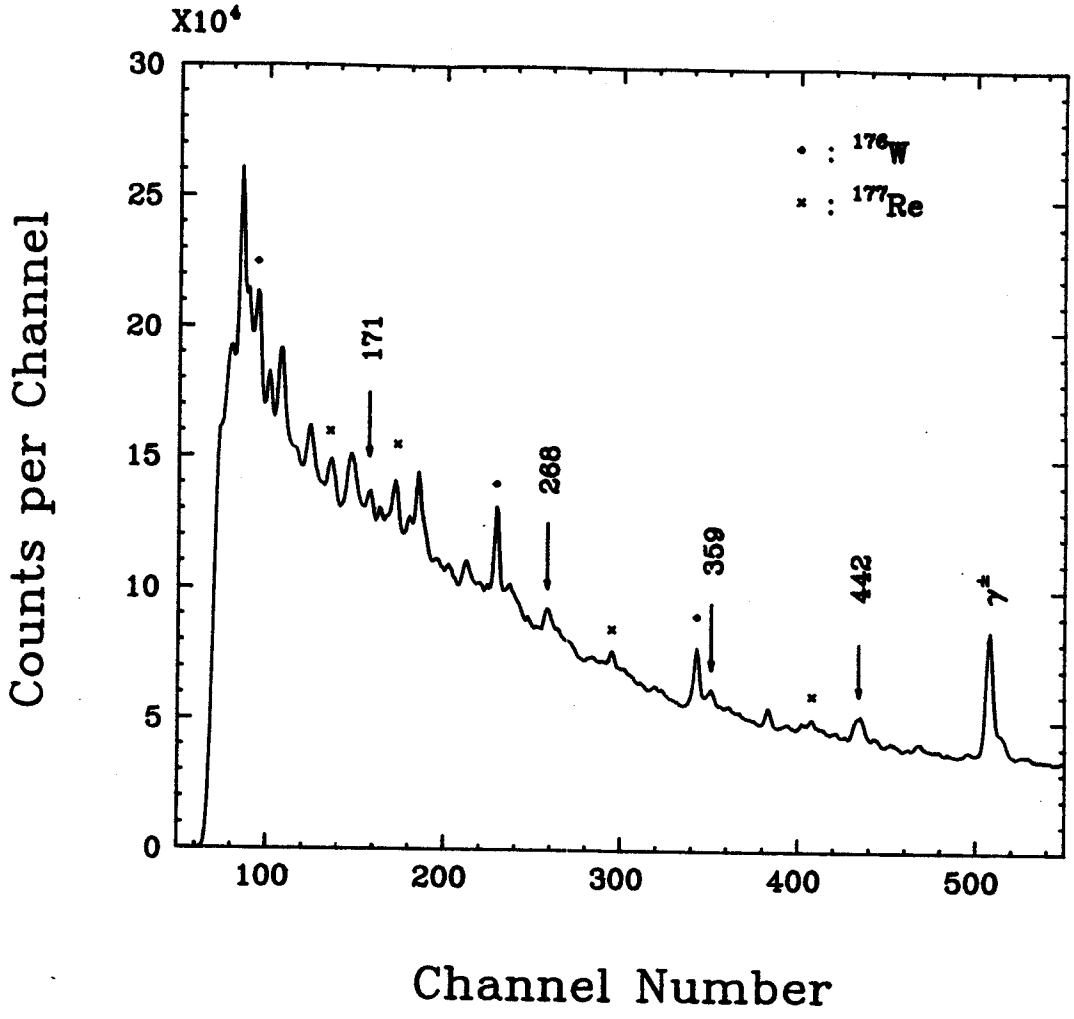

Figure V-1. Singles Y-ray spectra from the $^{159}Tb(^{22}Ne,5nY)^{176}Re$ reaction at a beam energy of 108 MeV. (a) at 90°.

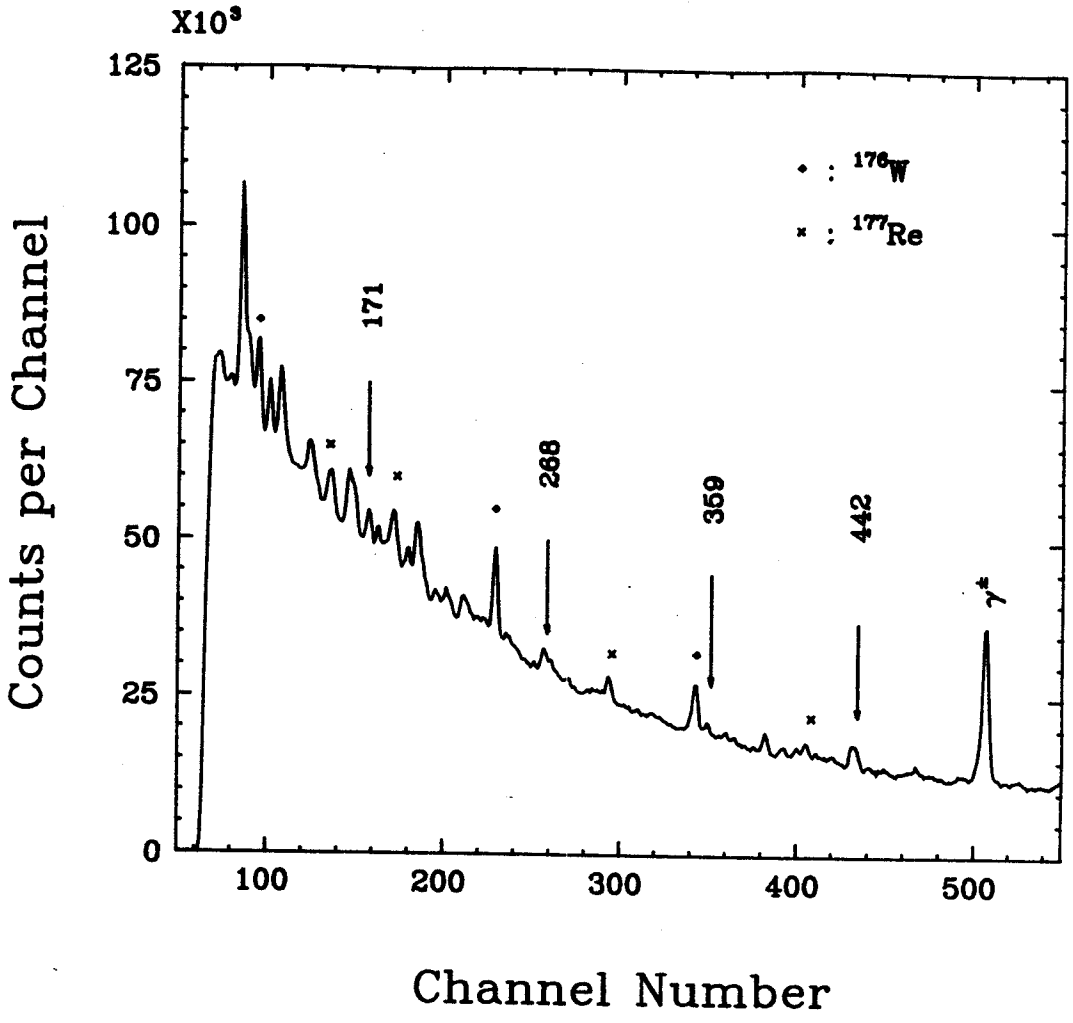

Figure V-1. (cont'd.). (b) at 125°.

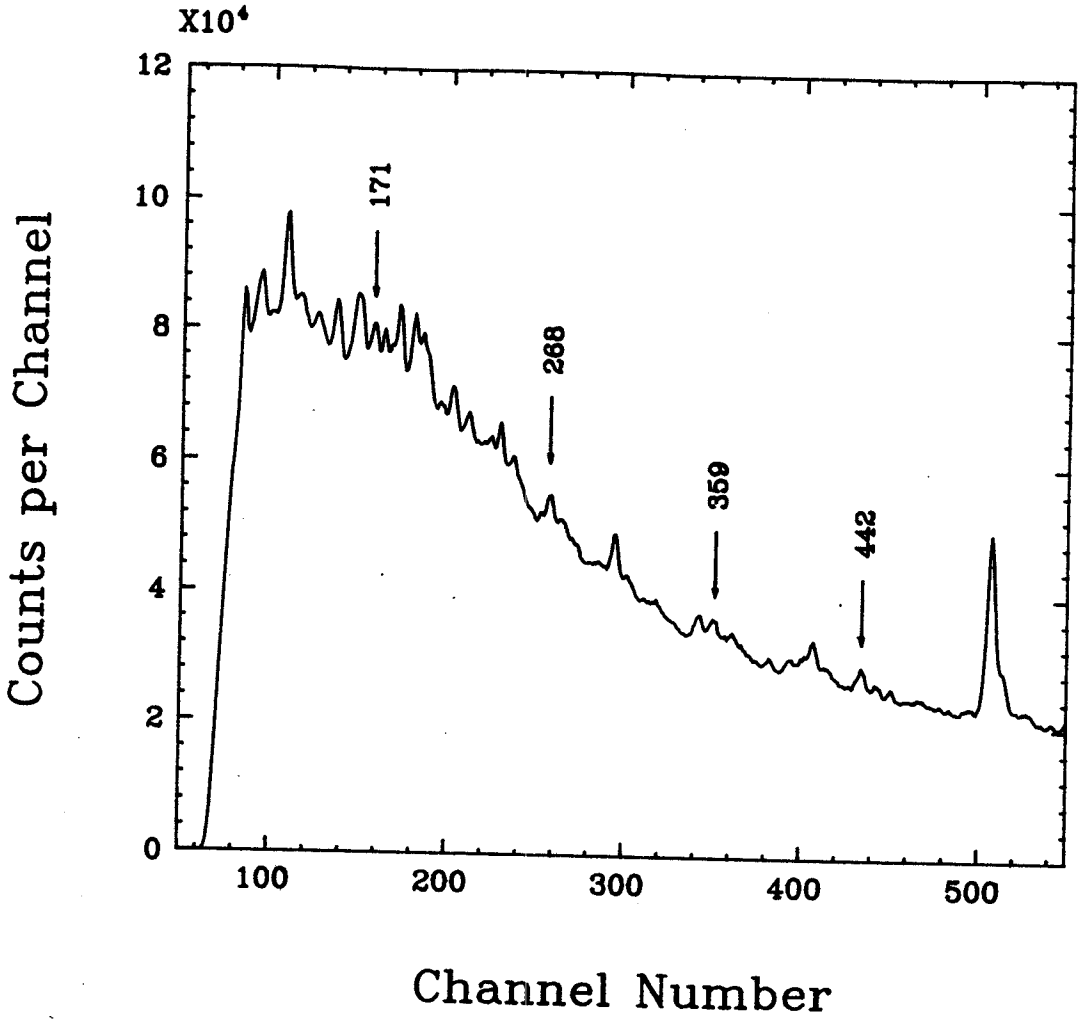

Figure V-2. Integral coincidence spectrum from the reaction $^{159}Tb(^{22}Ne,5nY)^{176}Re$ at a beam energy of 108 MeV.

Coincidence is the "key" for solving relations between γ-rays. In other words, we want to know when one of the detector "sees" a certain transition, what the other one "sees". In order to obtain this sort of information, energy gates have been set on the strong transitions on one of the Ge detectors, and the tapes were sorted event by event to generate spectra of the other detector, using the program SARA [Sh83]. Spectra obtained under such circumstance are called gated-coincidence spectra. Several flat regions, i.e., where there is no apparent peak, across the integral coincidence spectrum have been chosen as background. The background spectra were added together to form a total background spectrum, which then can be subtracted from the gated-coincidence spectra.

Several transitions of the K=1/2 decoupled band of ^{177}Re were observed in these spectra. In addition, there were some other strong transitions in the spectrum with very close energies to those of ^{177}Re. However, in this mass region γ-rays with similar energies are not unusual. Therefore, we could not exclude them simply because of their energies. We analyzed them, but did not reproduce the same kind of coincidence relations as reported [Le72,Ya83] before. Although this is most likely due to the statistics, we hesitate to draw any conclusions at this moment.

Among the new transitions observed, excluding these ambiguous ones, there are only four transitions, namely 171-, 268-, 359-, and 442-keV, that are definitely in coincidence with one another. They are those labeled in the integral coincidence spectrum shown in Figure V-2. Figure V-3 shows selected gated-coincidence spectra for these transitions. Although the standard background subtraction method was

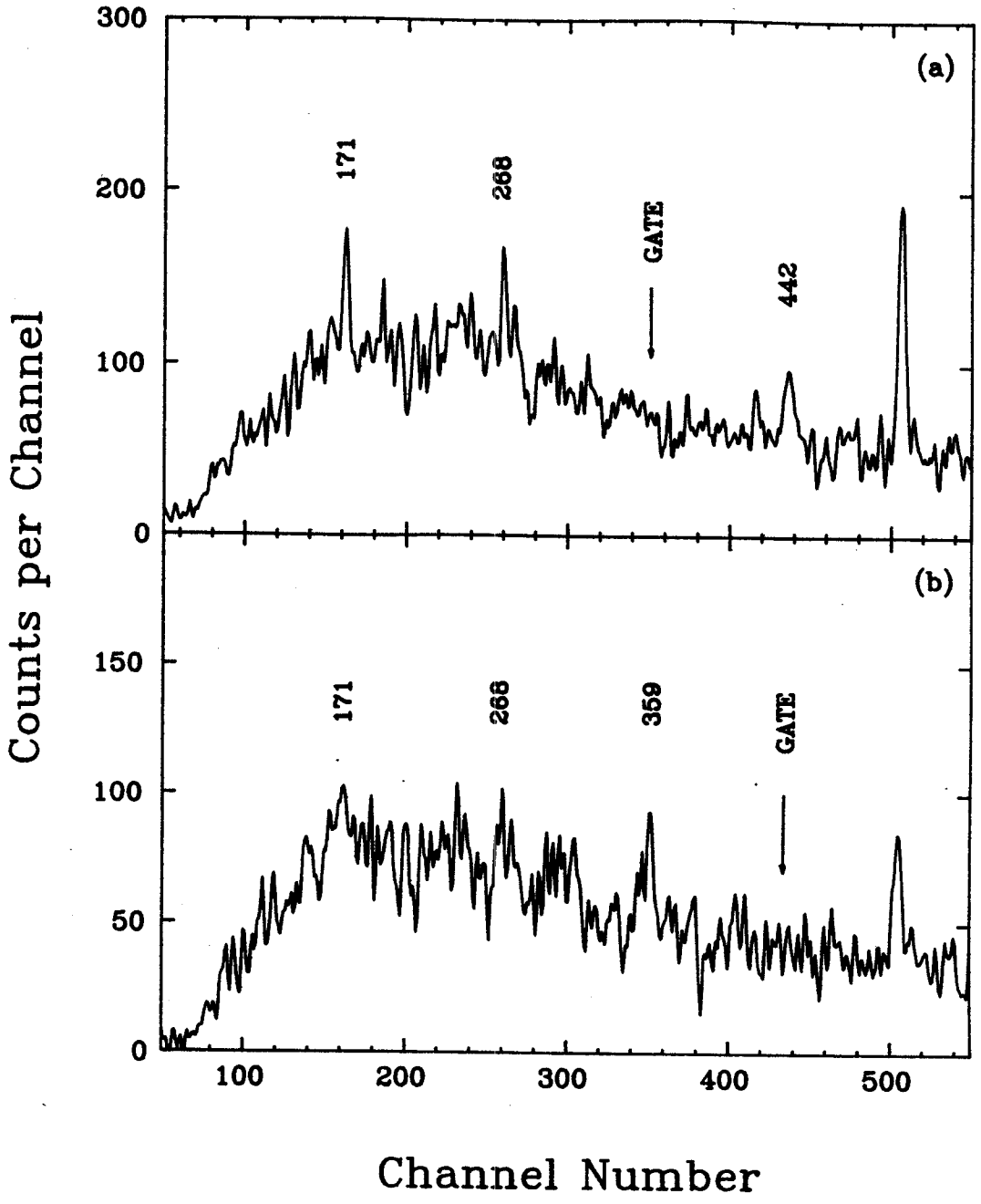

Figure V-3. Two gated-coincidence spectra from the reaction $^{159}Tb(^{22}Ne,5n\gamma)^{176}Re$ with a 108-MeV total beam energy. (a) gated on 359-keV. (b) gated on 442-keV.

used, it was not possible to clean up the gated spectra very well.

2. With 113-MeV Beam Energy

From the results of 108-MeV ^{22}Ne experiment, it was clear that quite a bit of ^{177}Re was produced. Therefore, the beam energy was increased to 113-MeV, trying to emphasize the production of ^{176}Re. Also, the higher the beam energy is, the larger amount of angular momentum can be brought into the compound nucleus in the heavy-ion reactions.

According to the experience from the last experiment, minimizing Compton background is essential. The only devices accessible were the two NaI(Tl) annuli. These NaI(Tl) anti-Compton shields significantly reduce the background and with them we can reach a peak-to-total ratio of roughly 40%. Singles and integral coincidence spectra are shown in Figure V-4 and Figure V-5. By comparing these spectra with the one shown in Figure V-2, the effect of Compton suppression is readily appreciated (note that Figure V-2 and Figure V-5 have about the same energy range, although the channel numbers are different). However, because of the bulky size of the annuli, the distance from the target to the center of the Ge crystal had to be increased. The final effect was improved the quality of the data but at an expense of cutting the open solid angle of the Ge detectors. Although most of the events collected were valid, the only way to improve the statistics was longer counting time. One million suppressed-suppressed coincidence events were collected in 90 hours.

The beam energy was increased by 5 MeV; nevertheless there was still a noticeable amount of ^{177}Re being produced. Again, we tried to

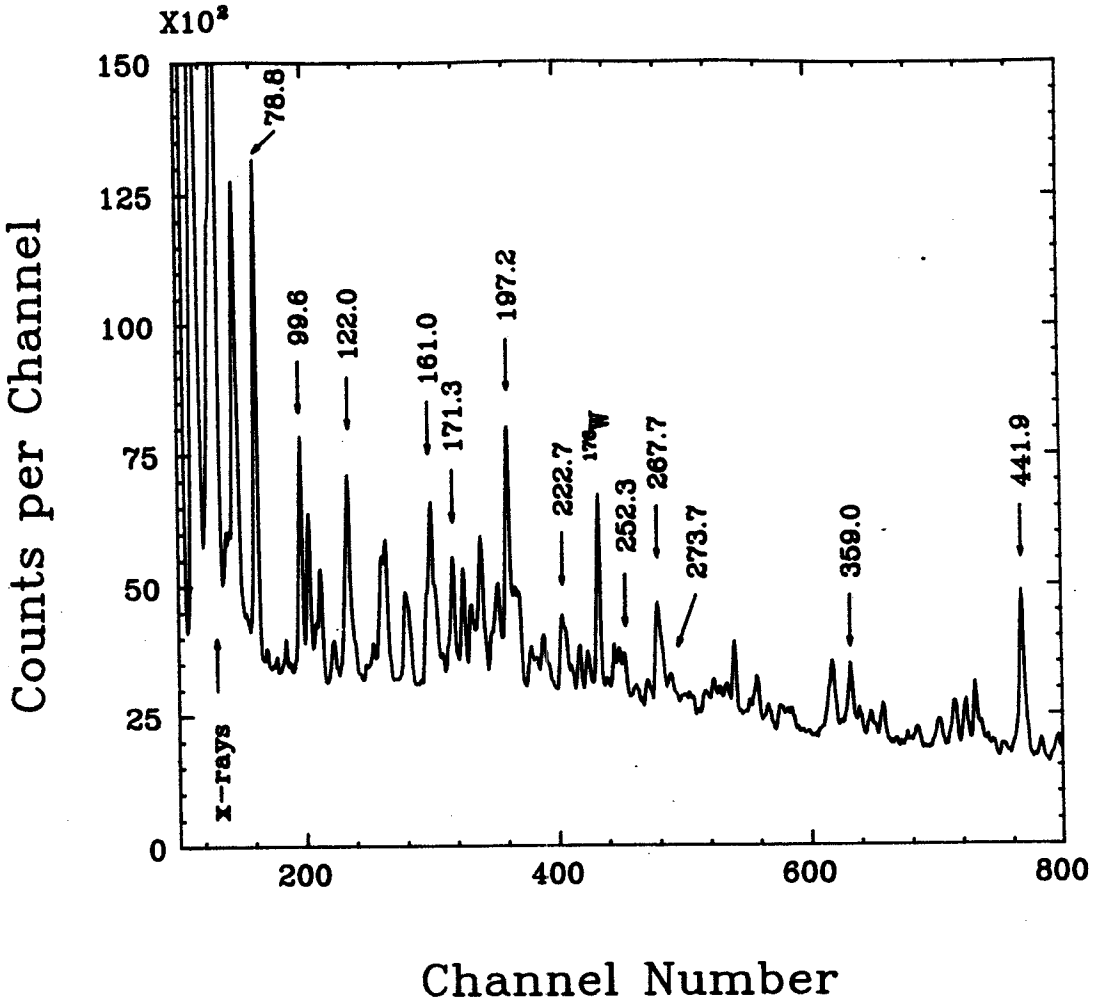

Figure V-4. Singles Y-ray spectra from the $^{159}Tb(^{22}Ne,5n\gamma)^{176}Re$ reaction at a beam energy of 113 MeV.

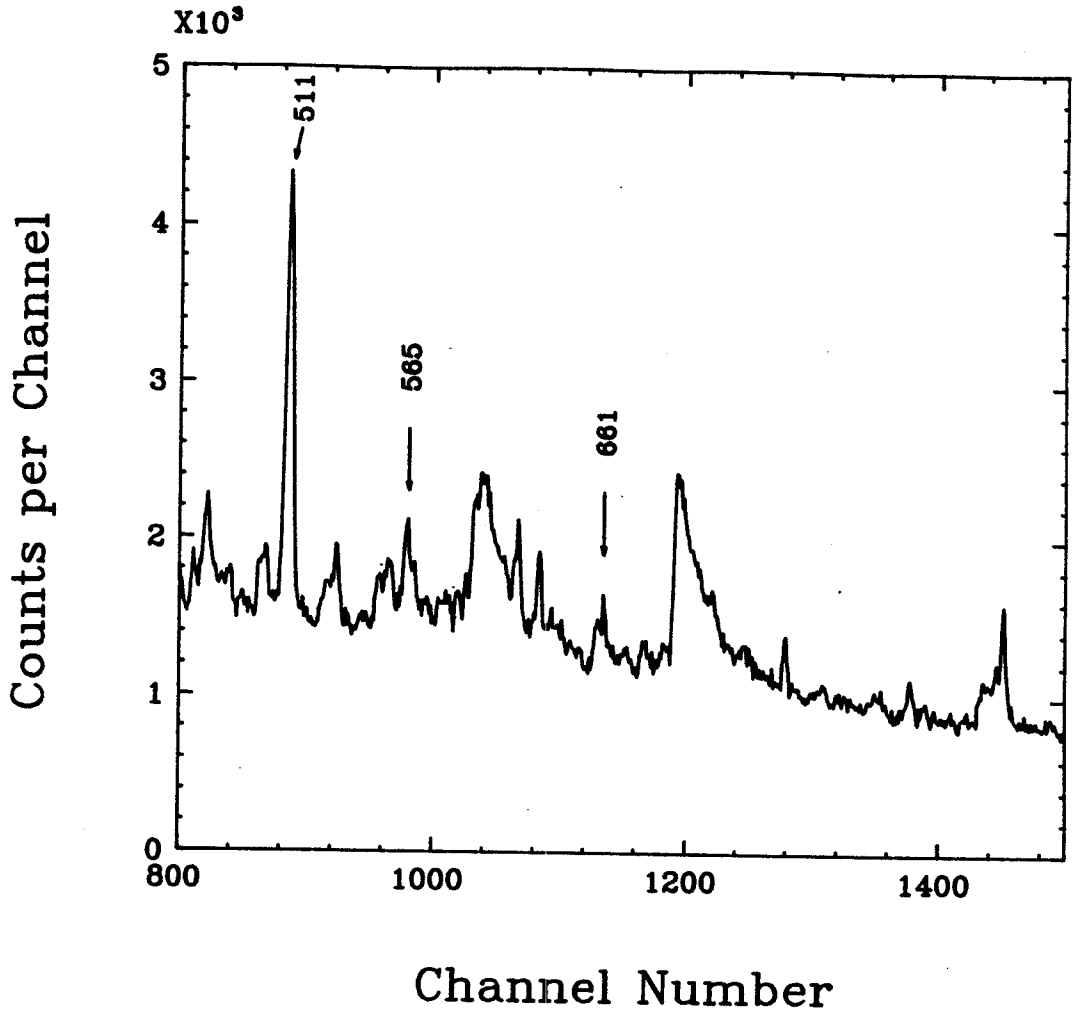

Figure V-4. (cont'd.).

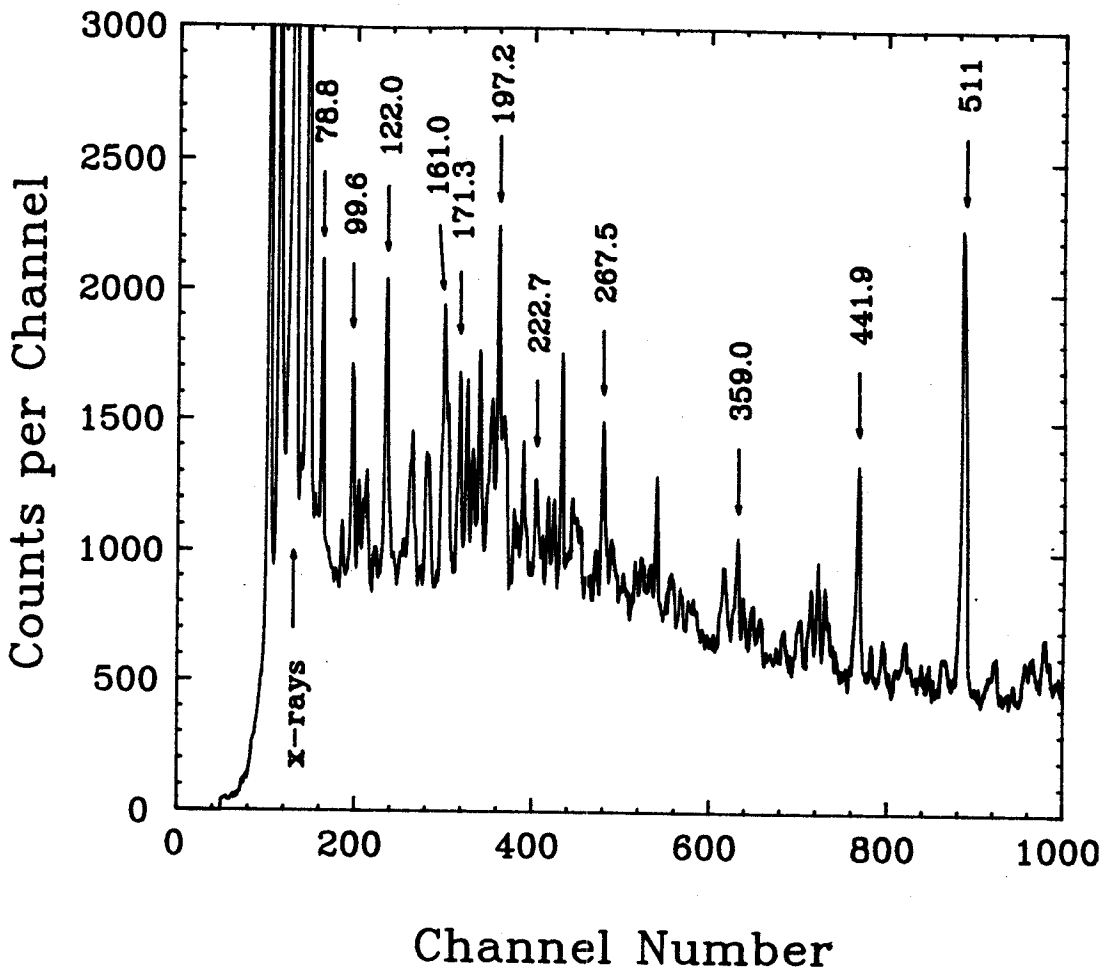

Figure V-5. Integral coincidence spectrum from the reaction $^{159}Tb(^{22}Ne,5nY)^{176}Re$ at a beam energy of 113 MeV.

re-construct the rotational bands that have been reported before. We were able to reproduce the coincidence relations among the lowest several transitions of each band. Although the complete rotational bands could not be constructed from our data, we believe transitions that have been reported for ^{177}Re can be excluded from the spectra, unless some of them are indicated as multiplets.

Table V-1 lists the energies and intensities of the γ-rays observed, excluding transitions from ^{177}Re and other activities. Some of the transitions are part of unresolved multiplets. Their intensities were obtained by fitting the peak with assuming multiplicity based on the width of the multiplets.

2.1 Methods of Analysis

Since in the experimental set-up a coincidence event was defined as the overlap of 250-ns wide logic pulses, all sorts of events, including those having measurable half-lives, were collected. Therefore, in our analysis we shall distinguish events as prompt coincidence, and late or early coincidence. To be specific, the signal of Ge-detector-2 was delayed by 250 ns with respect to that of Ge-1. Thus, if signals occurred at both detectors simultaneously, a signal would appear at the 250-ns position in the TAC spectrum. This is the prompt peak. Coincidence spectra (prompt gated-coincidence spectra) generated with a time gate set on the TAC prompt peak, in addition to an energy gate, gave prompt coincidence information. If a signal occurred later at Ge-2 than at Ge-1, a signal would appear at the right side of the prompt peak. Then with a time gate set on the right side of TAC prompt peak and using Ge-1 as energy gating detector and Ge-2 as the displaying

Table V-1. Energies and Relative Intensities of γ-rays in the Singles Spectrum from the $^{159}Tb(^{22}Ne,5n\gamma)^{176}Re$ Reaction.

E_γ (keV)	I_γ
78.8	100
99.6	41(2)
104.1[1]	28(2)
122.0(0.6)	34(3)
137.4[1]	20(1)
158.9	13(1)
161.0	29(2)
171.3	23(2)
180.3	14(1)
197.2	53(3)
200.3	18(2)
222.7(0.7)	14(1)
252.3	9(1)
267.7(0.6)	28(3)
273.7	4.1(0.4)
315.1	9(1)
359.0(0.6)	19(3)
420.5	8(2)
441.9(0.6)	12(2)

* The uncertainty is ±0.2 keV unless otherwise indicated.
[1] γ-rays from the Coulomb excitation of the ^{159}Tb target.

detector, the spectrum shows whatever occurs later than the gating transition. Following the same procedure but gating on the left side of the TAC spectrum, early coincidence could be obtained.

There were only about 10-15 counts for the strong transitions in the prompt gated-coincidence spectra. Therefore, the tapes were read three times and the resulting spectra were smoothed. By doing this the peaks became much more visible.

The half-life of a delayed transition can also be derived from the TAC spectrum. To do this, we simply set an energy gate of that transition on one of the Ge detectors and displayed the TAC spectrum. Under such conditions, the TAC spectrum no longer gave a symmetrical peak, but a peak having a tail on one side. The slope of the tail corresponds to the half-life of the gating transition according to the following equations:

$$\log(\text{counts}) = c - b \times (\text{time}) \ , \qquad \text{(V-1)}$$

$$t_{1/2} = \log 2 \ / \ b \ , \qquad \text{(V-2)}$$

where b is the slope, c is a constant, and $t_{1/2}$ is the half-life.

2.2 Prompt Coincidences

The prompt coincidence relations among the 171.3-, 267.7-, 359.0-, and 441.9-keV transitions, which have been identified in the previous run, were confirmed. Two gated-coincidence spectra are shown in Figure V-6, and Figure V-7 shows the sum of four gated spectra. The energies of the 267.7-, 359.0-, and 441.9-keV Y-rays can not be determined

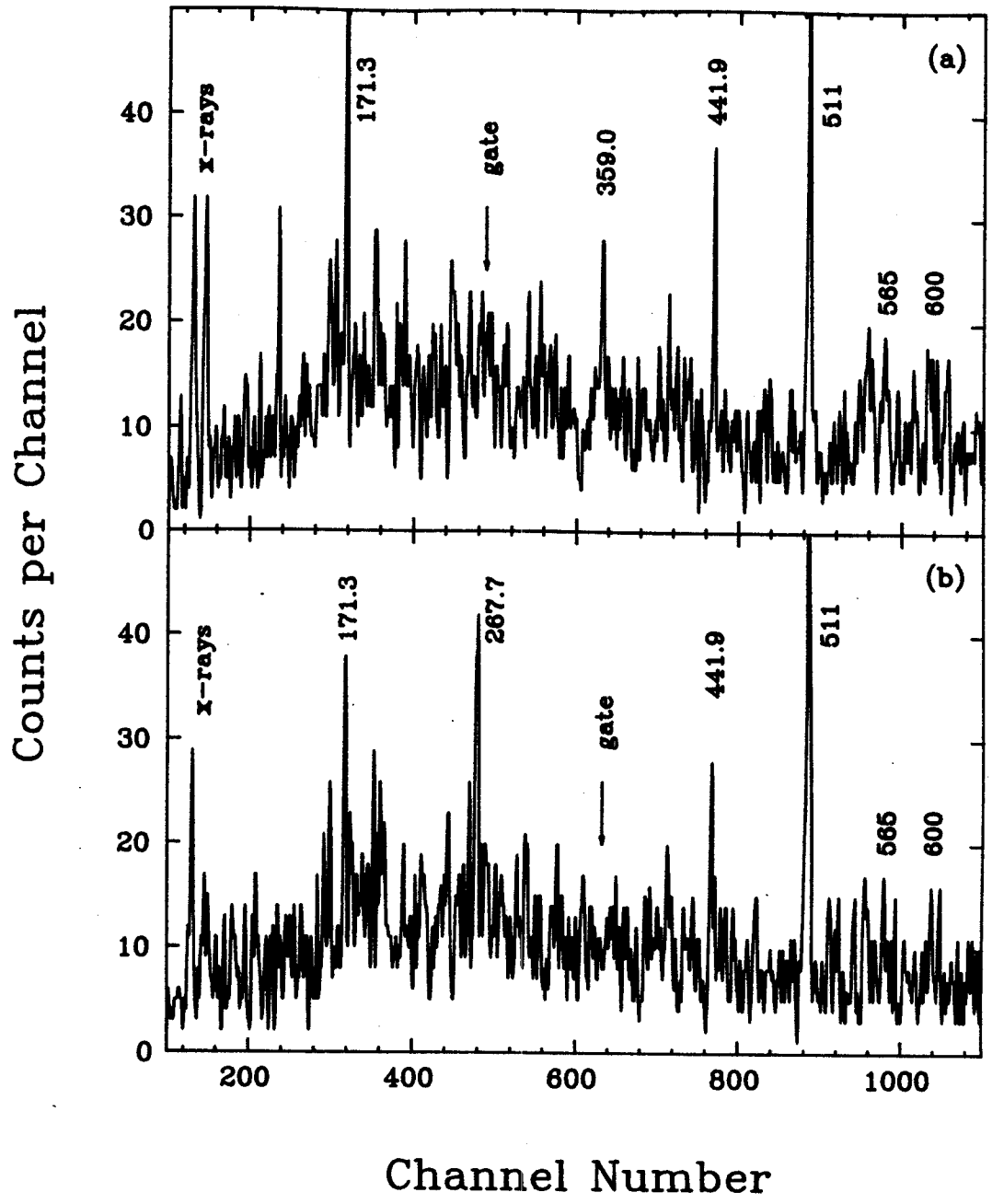

Figure V-6. Two gated-coincidence spectra from the reaction $^{159}Tb(^{22}Ne,5n\gamma)^{176}Re$ with a 113-MeV total beam energy. (a) gated on 267.7-keV. (b) gated on 359.0-keV.

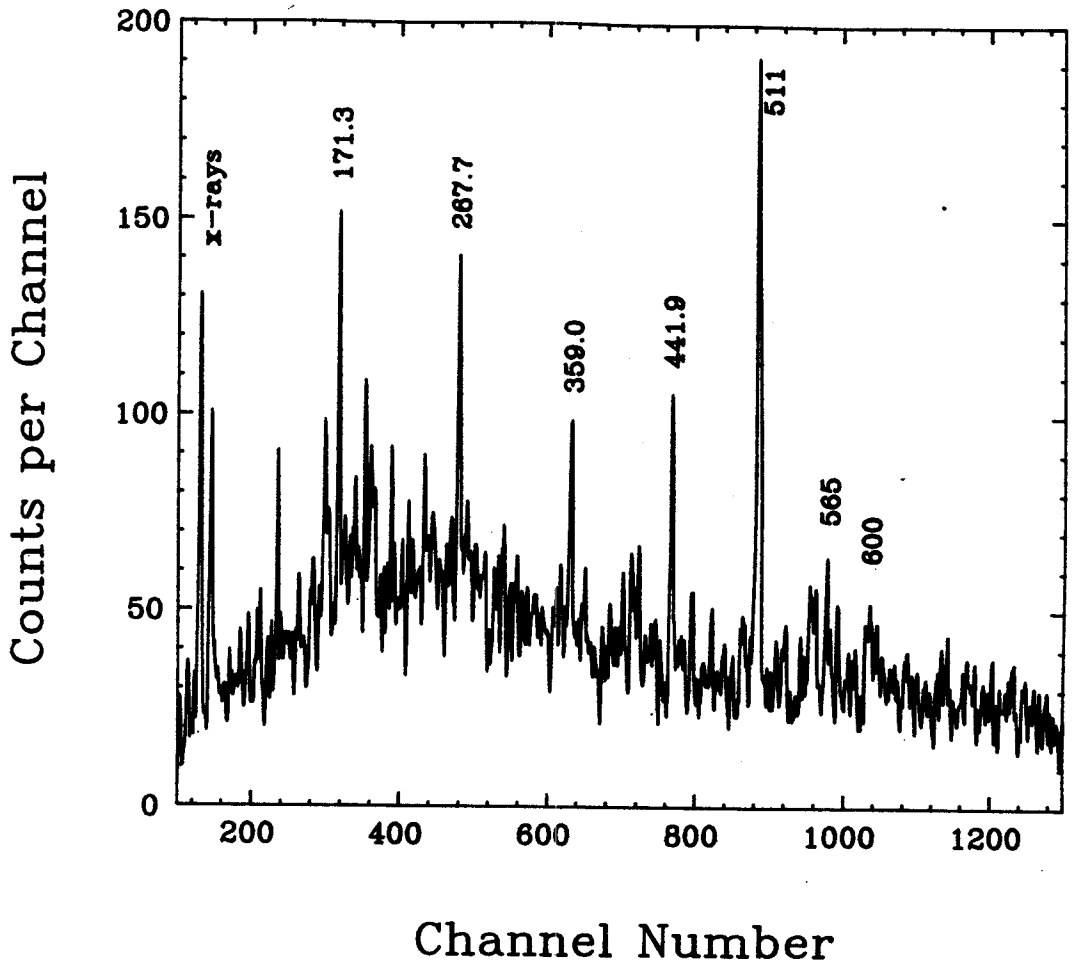

Figure V-7. Sum of four gated-coincidence spectra of the reaction $^{159}Tb(^{22}Ne,5n\gamma)^{176}Re$ with a beam energy of 113 MeV.

precisely from the singles spectrum because of contamination from ^{177}Re, and they have been derived from gated-coincidence spectrum. Because of lack of statistics, these have errors as large as ±0.6 keV. Two more γ-rays, 565- and 600-keV transitions, were also in coincidence with the group mentioned above. Their energies are also derived from coincidence spectra and thus have the larger uncertainty. From the spacings between the levels, it strongly suggested that there should be another transition between the 441.9- and 565-keV transitions. However, there is no good candidate besides the 511-keV peak. It is most likely that there is indeed a transition under the huge 511-keV peak, because its energy is so close to 511 keV that it could not be resolved from the electron-positron annihilation peak. Energy gates have been set on the left and right portion of the 511-keV peak, as well as on the whole peak, to obtain gated-coincidence spectra. But no clear coincidence relation could be derived from these spectra. This is understandable, since 511.0- and 509.7-keV transitions from ^{177}Re are also mixed in.

Transitions at 99.6, 122.0, 161.0, 197.2, and 222.7 keV are in strong coincidence with one another, possibly also with the 252.3- and 273.7-keV transitions. Two selected coincidence spectra and a sum of gated-coincidence spectrum are shown in Figures V-8 and V-9, respectively. The 122.0-, 161.0-, as well as 222.7-keV transitions, are superimposed on transitions from ^{177}Re and their energies were determined from gated coincidence spectra, rather than from singles. The 197.2-keV transition is in coincidence with itself (see Figure V-8). Apparently there are two γ-rays with almost the same energy, because the width of the 197.2-keV peak is not wider than a single-energy peak. One of the two 197.2-keV peaks is in coincidence with the 99.6-keV γ-ray,

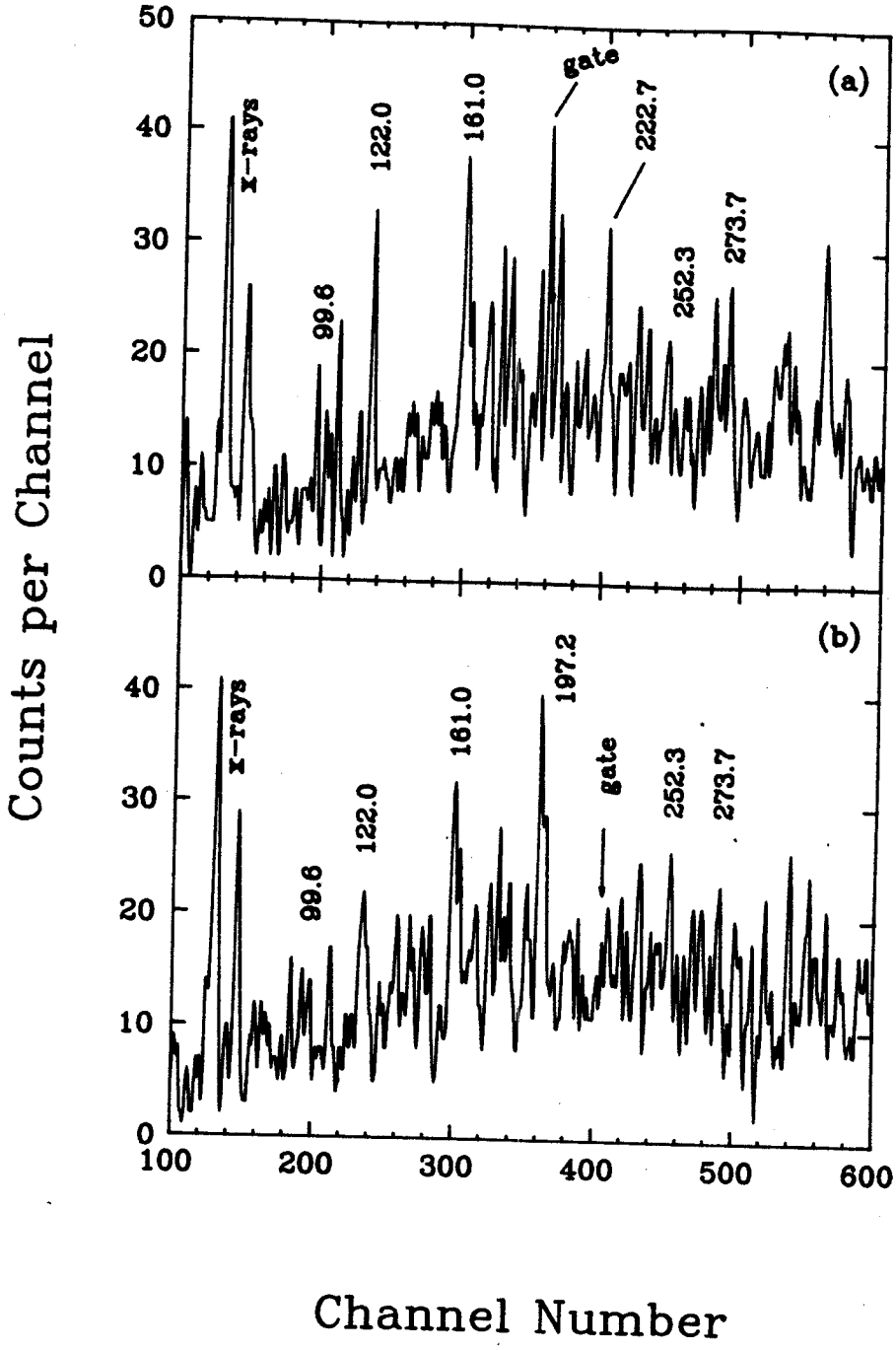

Figure V-8. Two gated-coincidence spectra from the reaction $^{159}Tb(^{22}Ne,5n\gamma)^{176}Re$ with a 113-MeV total beam energy. (a) gated on 197.2-keV. (b) gated on 222.7-keV.

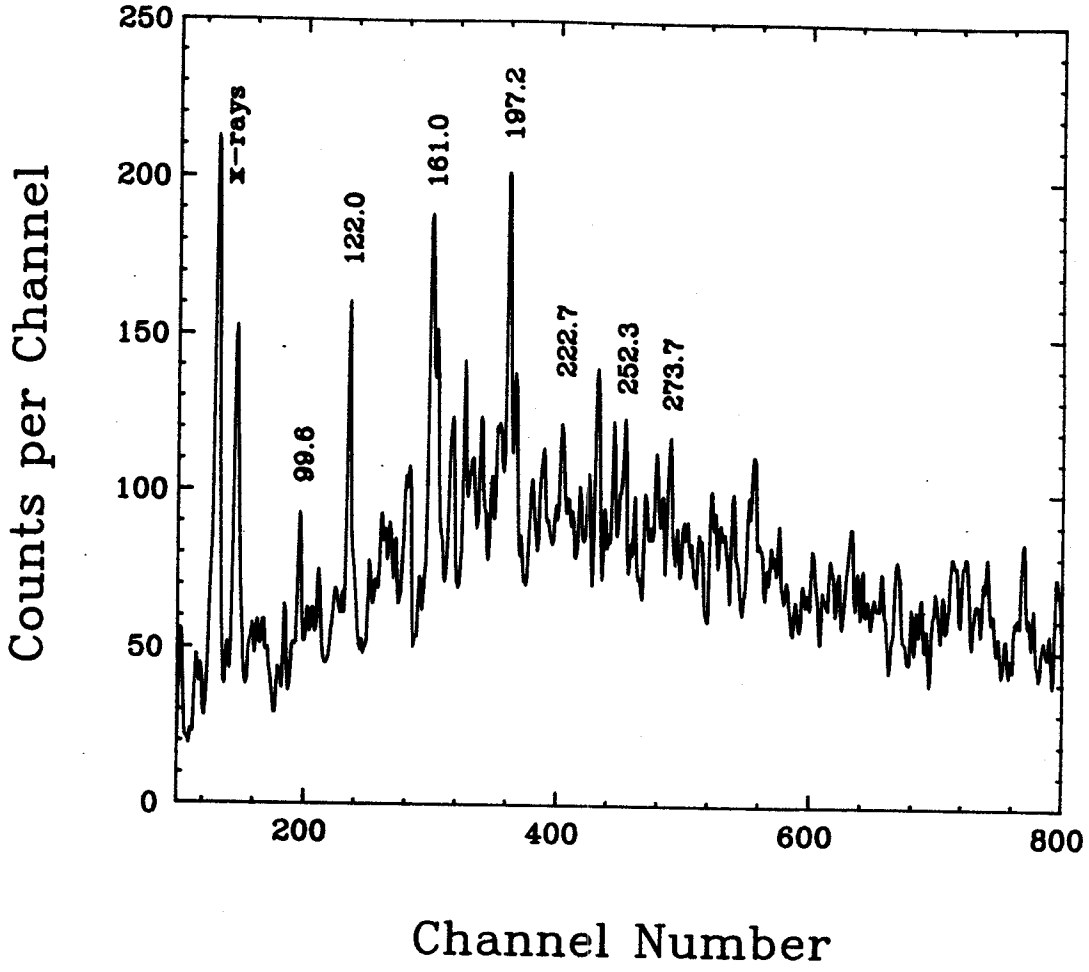

Figure V-9. Sum of five gated-coincidence spectra from the reaction $^{159}Tb(^{22}Ne,5n\gamma)^{176}Re$ with a beam energy of 113 MeV.

etc., and the other is in coincidence with the 315.1- and 420.5-keV γ-rays.

2.3 Delayed Coincidences

By now, almost all the strong transitions in the spectrum have been found to be in prompt coincidence with some other transitions. However, the strongest transition, at 78.8-keV in the singles spectrum, is only weakly in coincidence with the 104.1-keV transition. This results from Coulomb excitation of the ^{159}Tb target [Di63,Se67]. However, from the intensity of the 104.1-keV transition (see Table V-1), Coulomb excitation cannot account for the entire intensity of the 78.8-keV transition. (Remember these M1 transition with energies less than 80-keV have large internal conversion coefficients, and need to be corrected. For example, α is 4.63 [Rö78a] for a 79-keV M1 transition and only 2.12 for a 104-keV transition.) Also, from the 137.4-keV transition, which is the cross-over transition from the same level as 78.8-keV has a ratio to the 78.8-keV transition of 1:6. It also reveals that only 41% of the intensity of 78.8-keV transition comes from Coulomb excitation of the target. Another transition of 79.6-keV from ^{177}Re decay might also contribute to part of the observed intensity. However, checking a related delayed transition (94.9 keV, I_γ=3.6) and considering the multipolarity of these two transitions, the contribution from ^{177}Re decay comes out to be only about 3% of the 78.8-keV intensity. Since nothing else was found in prompt coincidence with it, this transition might be in delayed coincidence with other transitions.

A total prompt coincidence spectrum, obtained with a time gate set on the TAC prompt peak but no energy gate is shown in Figure V-10.

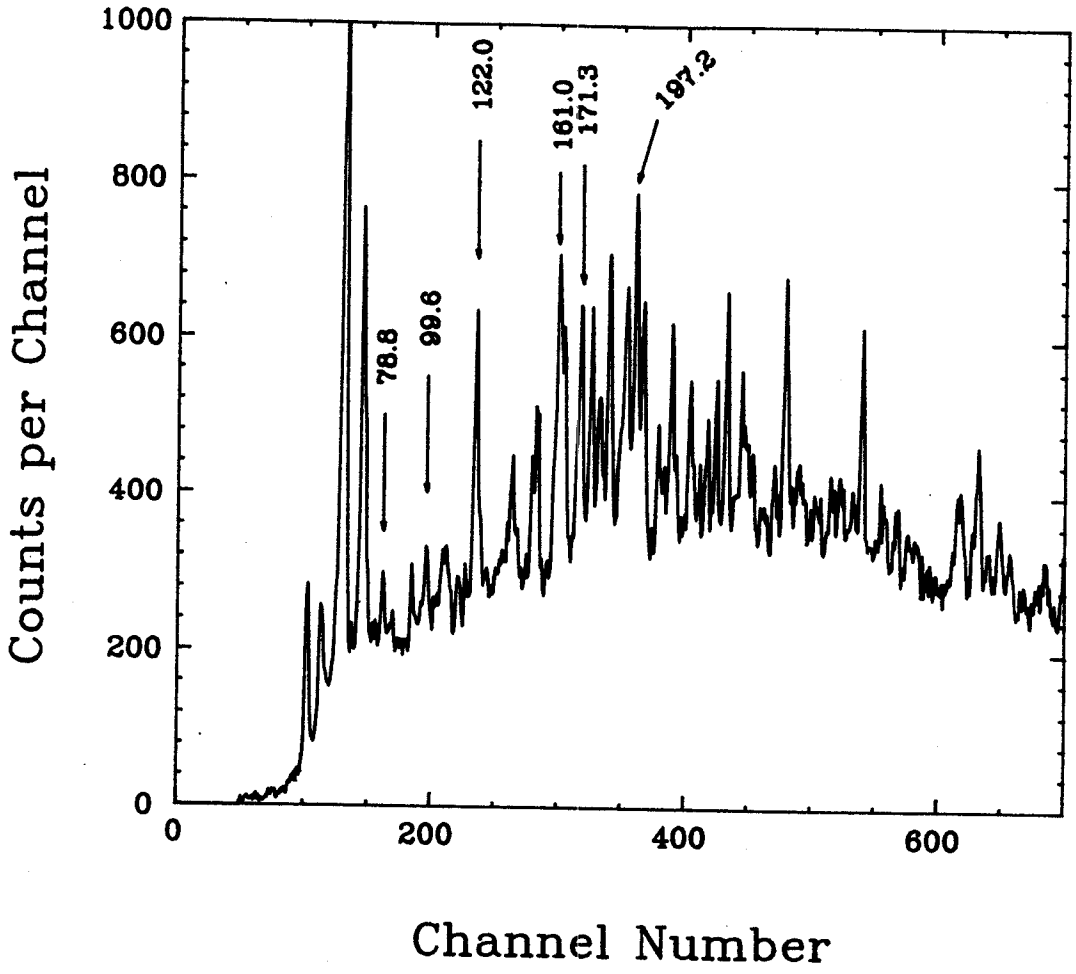

Figure V-10. Total prompt coincidence spectrum from the reaction $^{159}Tb(^{22}Ne,5n\gamma)^{176}Re$ at 113-MeV.

Comparing this spectrum with the one shown in Figure V-5, which was obtained without setting any condition in the TAC spectrum (i.e., a wide-open TAC gate), it is clear that the intensity of 78.8-keV Y-ray is significantly reduced in the former spectrum. This explained why this 78.8-keV transition appears only weakly in prompt coincidence with others. A total-delayed-coincidence spectrum was also obtained and shown in Figure V-11. The intensity of 78.8-keV transition is enhanced over that in the integral coincidence spectrum (Figure V-5). A list of the relative intensity of this transition in various coincidence spectra is given in Table V-2, where the 171.3-keV Y-ray was used as normalization. Data in Table V-2 convince us that the 78.8-keV is a delayed transition.

The half-life of the 78.8-keV Y-ray was determined by the method described in section 2.1, with the resulting TAC spectrum prompt portion subtracted. This is shown in Figure V-12. The statistics are too poor to give an accurate half-life from this spectrum, but a rough half-life is extracted to be 25 ± 10 ns.

Those transitions that have been identified in Section 2.2 were analyzed by the late coincidence method in order to learn whether they are related to the 78.8-keV delayed transition. The 78.8-keV transition has shown up in all the late coincidence spectra gated by these known transitions. This fact suggests that all the known transitions so far are delayed by the 78.8-keV transition. The sum of the gated spectra for two groups is shown in Figures V-13 and V-14. But, no linking transition can be assigned.

There are two other transitions, at 99.6 and 122.0 keV, that are also enhanced in total-delayed-coincidence spectrum (Figure V-11), and

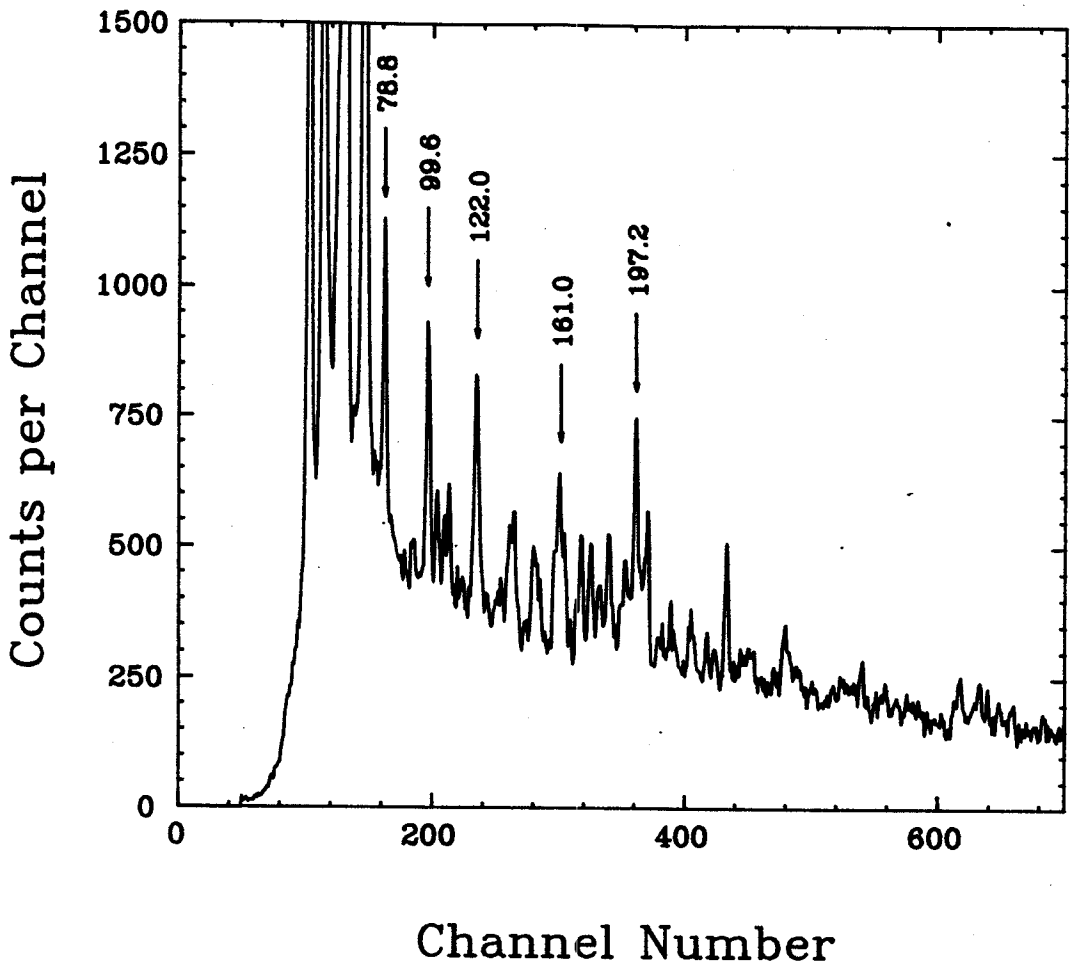

Figure V-11. Total-delayed-coincidence spectrum from the reaction $^{159}Tb(^{22}Ne,5nγ)^{176}Re$ with a beam energy of 113 MeV.

Table V-2. Relative intensities of 78.8-, 99.6-, and 122.0-keV γ-rays in the various coincidence spectra.

	Relative Intensity		
	78.8 keV	99.6 keV	122.0 keV
Singles	4.3	1.8	1.5
Total coincidence	1.4	1.3	1.5
Prompt coincidence	0.30	0.49	1.1
Delayed coincidence	3.6	2.5	2.6

* The uncertainty is ±10%.

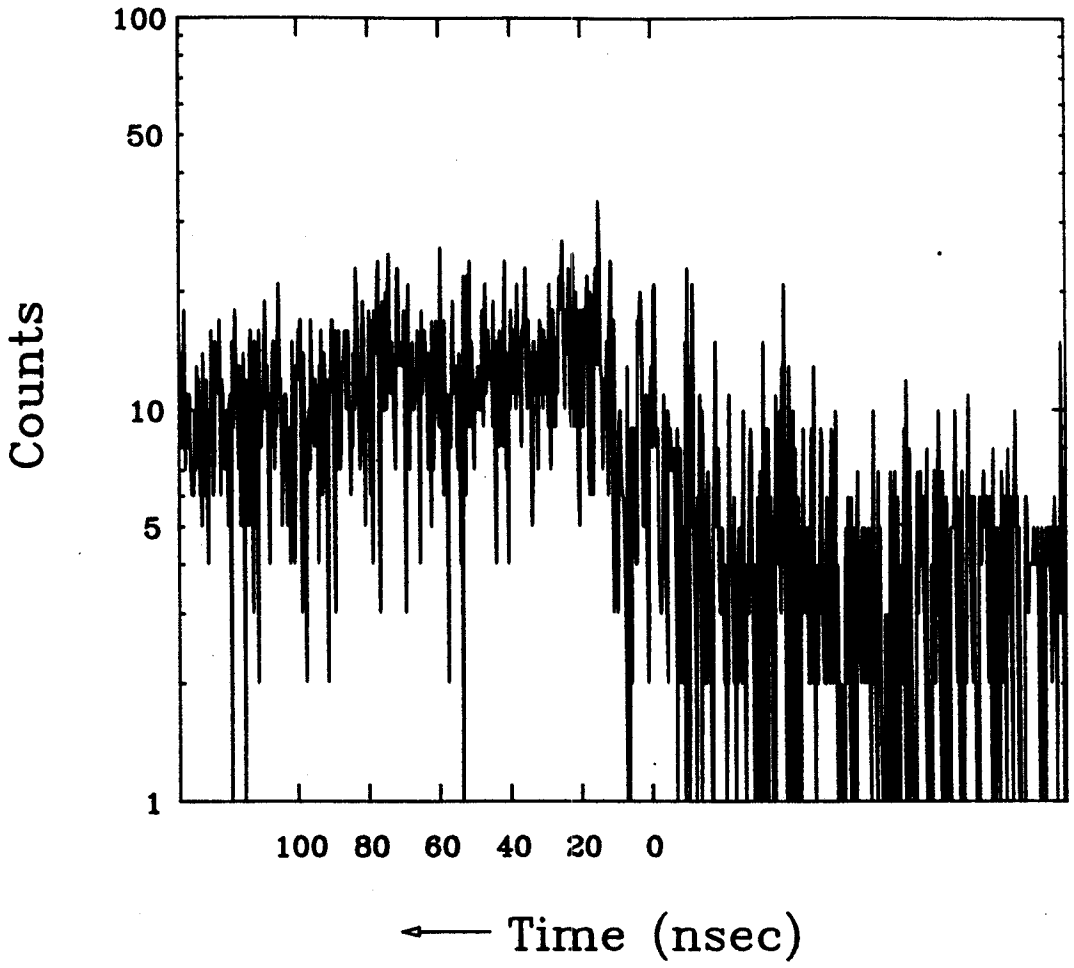

Figure V-12. TAC spectrum gated by 78.8-keV Y-ray from the reaction $^{159}Tb(^{22}Ne,5nY)^{176}Re$ at a beam energy of 113 MeV.

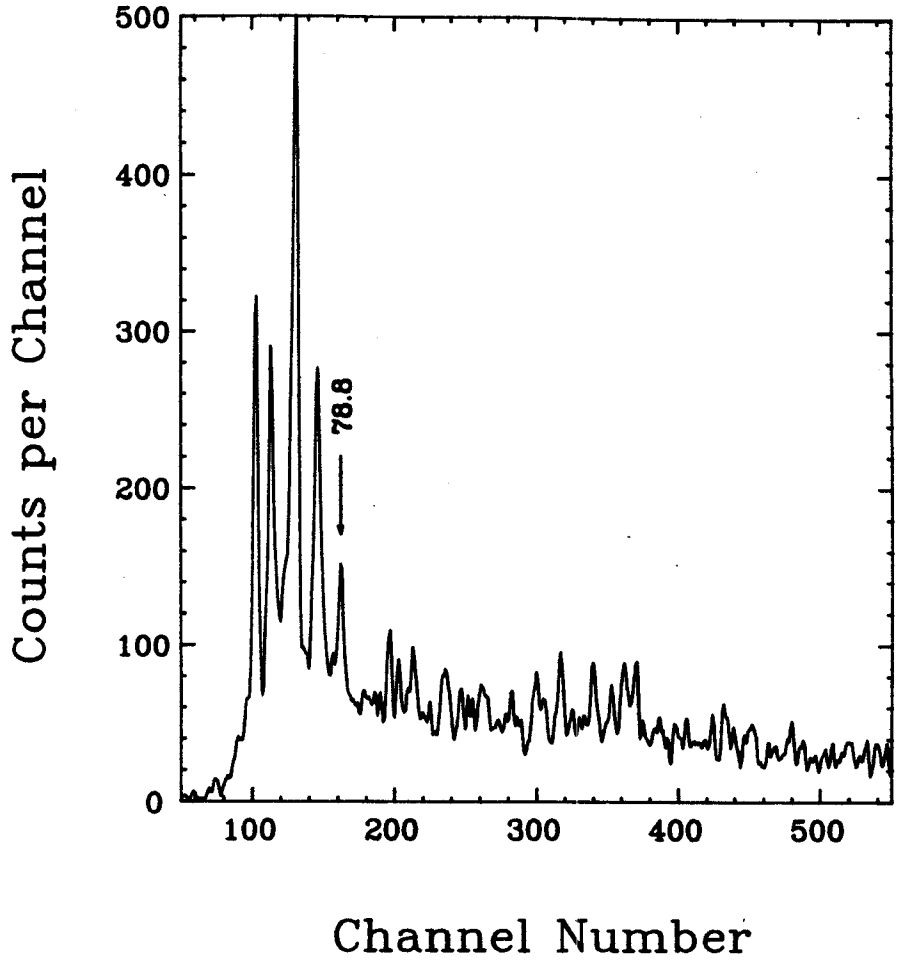

Figure V-13. Sum of four gated-delayed-coincidence spectra of the 171.3-, 267.7-, 359.0-, and 441.9-keV transitions.

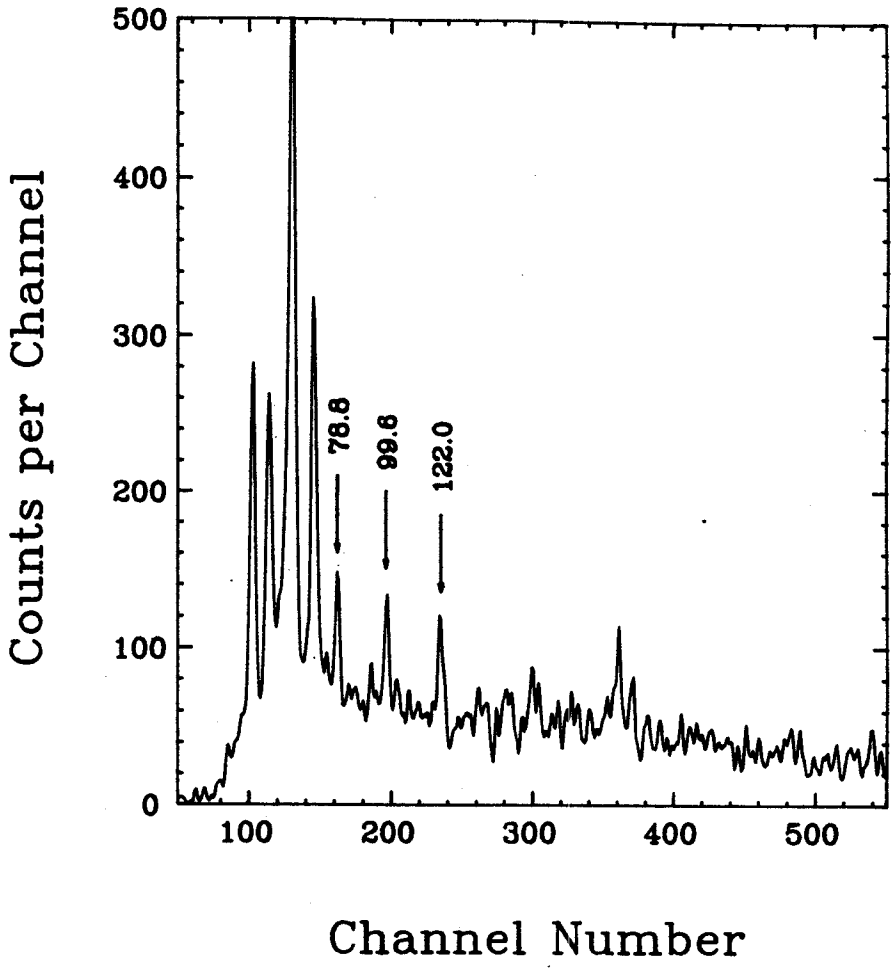

Figure V-14. Sum of four gated-delayed-coincidence spectra of the 161.0-, 197.2-, 222.7-, and 252.3-keV transitions.

their relative intensities have also been listed in Table V-2. Notice that especially the 99.6-keV transition becomes very weak in the total prompt coincidence spectrum.

Both the 99.6- and 122.0-keV transitions show up in the 161.0-, 197.2-, 223.7-, and 252.3-keV sum-gated late-coincidence spectrum (Figure V-14). Therefore, we have to check what comes earlier or later than the 99.6- and 122.0-keV Y-rays. These late and early coincidence spectra are compared with prompt gated-coincidence spectra in Figures V-15 and V-16, respectively, for 99.6 keV and 122.0 keV. The situation is very complicated here, because both the 99.6- and 122.0-keV Y-rays are contaminated by background (in addition, the 122.0-keV Y-ray is also contaminated by ^{177}Re). Moreover, both of them have been found in coincidence with the same group of transitions. The contaminations prevent us from drawing any conclusions, and the low statistics dot not allow us to do any advance analysis such as doubly-gated studies.

However, one more thing we can try is to set a narrower TAC prompt gate on the 99.6-, 122.0-keV, and related transitions, for example at 197.2 keV. If a transition is a delayed one, it will disappear much more quickly than a prompt transition as the TAC prompt gate gets narrower. These results are shown in Figures V-17, V-18, and V-19. The relative intensity of the 99.6-keV Y-ray becomes much weaker in the upper part of Figure V-19, whereas, that of the 122.0-keV Y-ray remains nearly unchanged. This suggests that the 99.6-keV transition comes later than the 197.2-keV but the 122.0-keV transition does not. The same sort of conclusion can be made from Figure V-18, viz., that the 99.6-keV transition is delayed respect to the 122.0-keV transition. And from Figure V-17 it can be seen that the 122.0-, 161.0-, and 197.2-keV

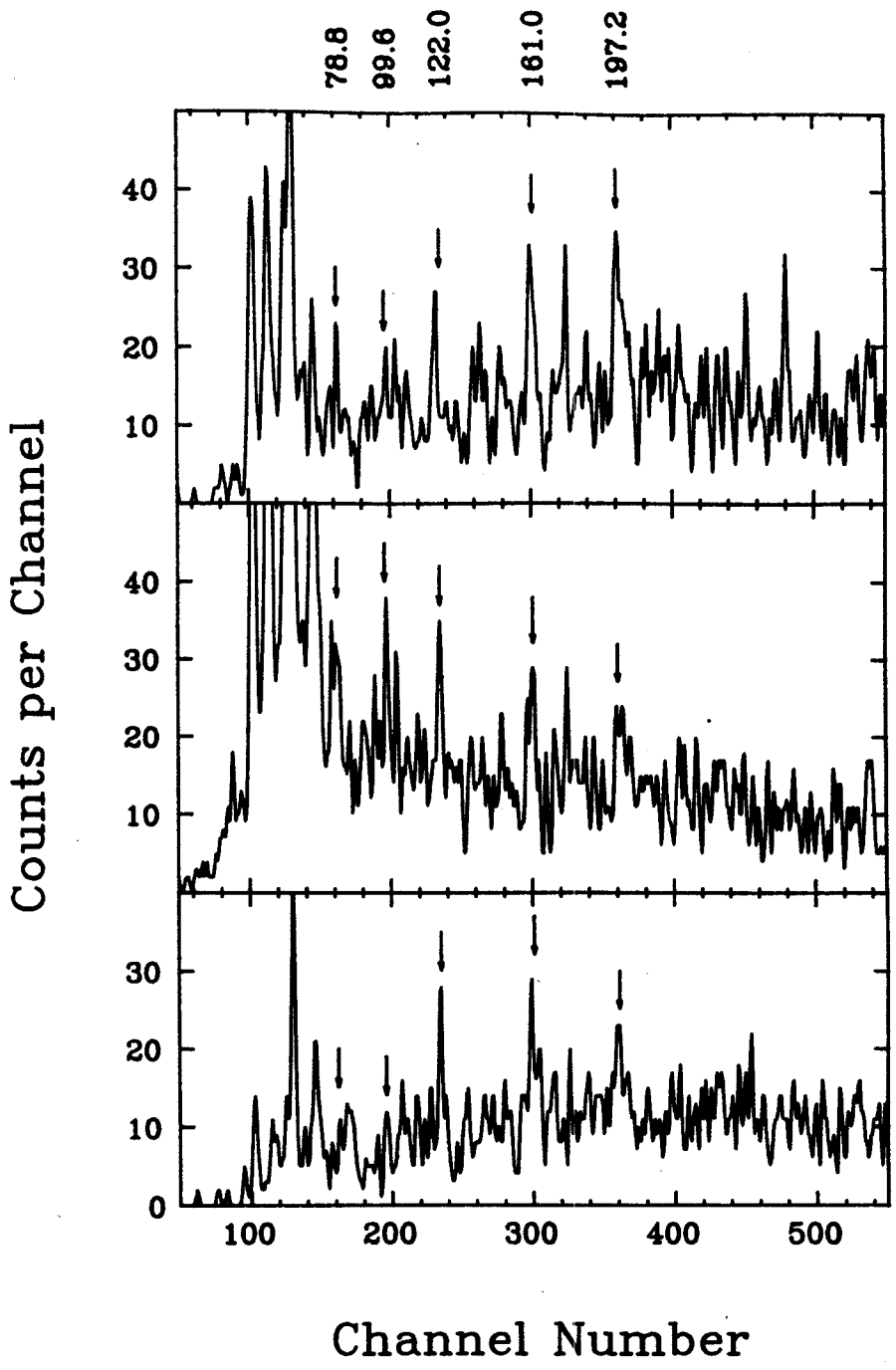

Figure V-15. Three 99.6-keV gated-coincidence spectra. Top: early. Middle: late. Bottom: prompt.

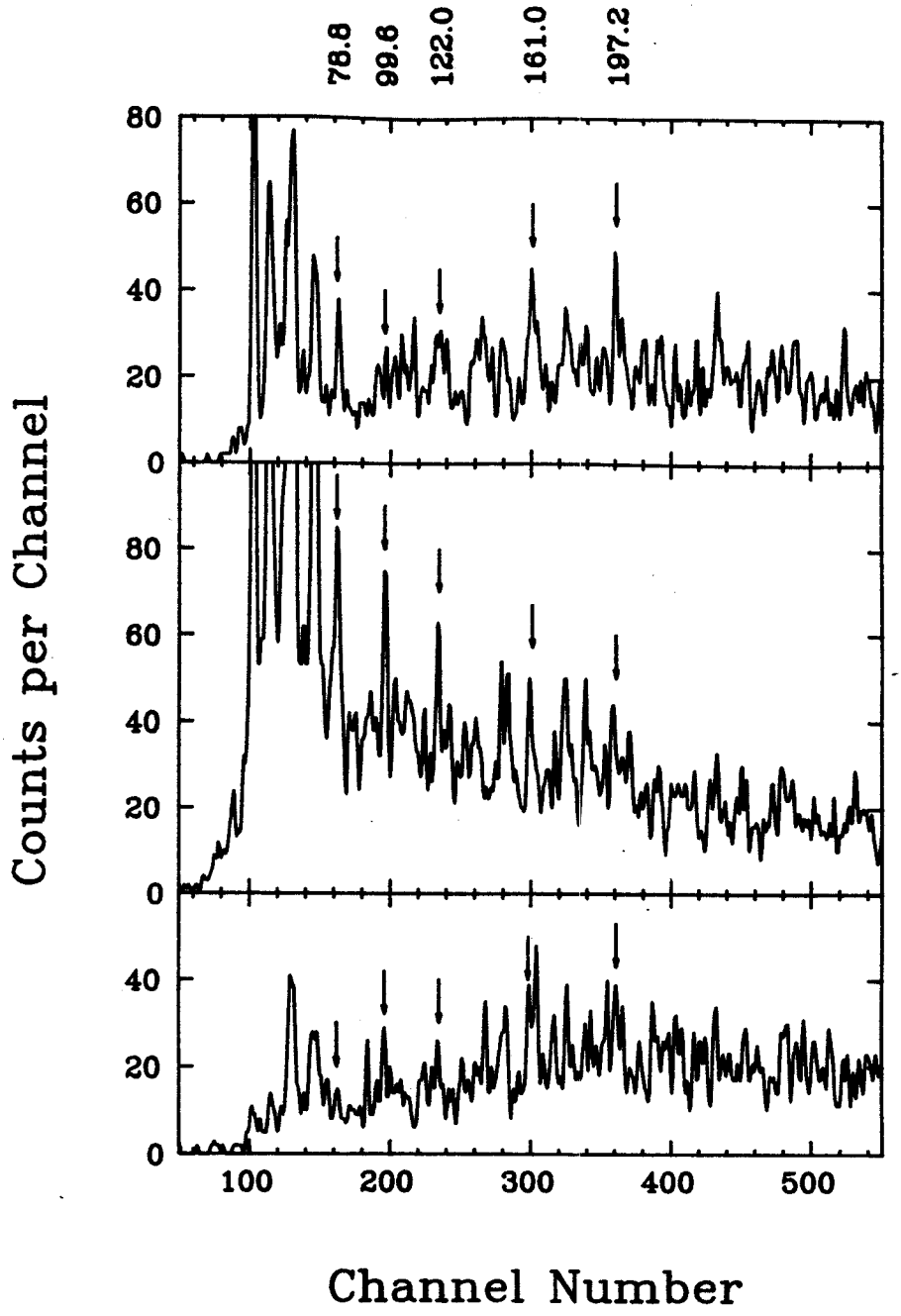

Figure V-16. Three 122.0-keV gated-coincidence spectra. Top: early. Middle: late. Bottom: prompt.

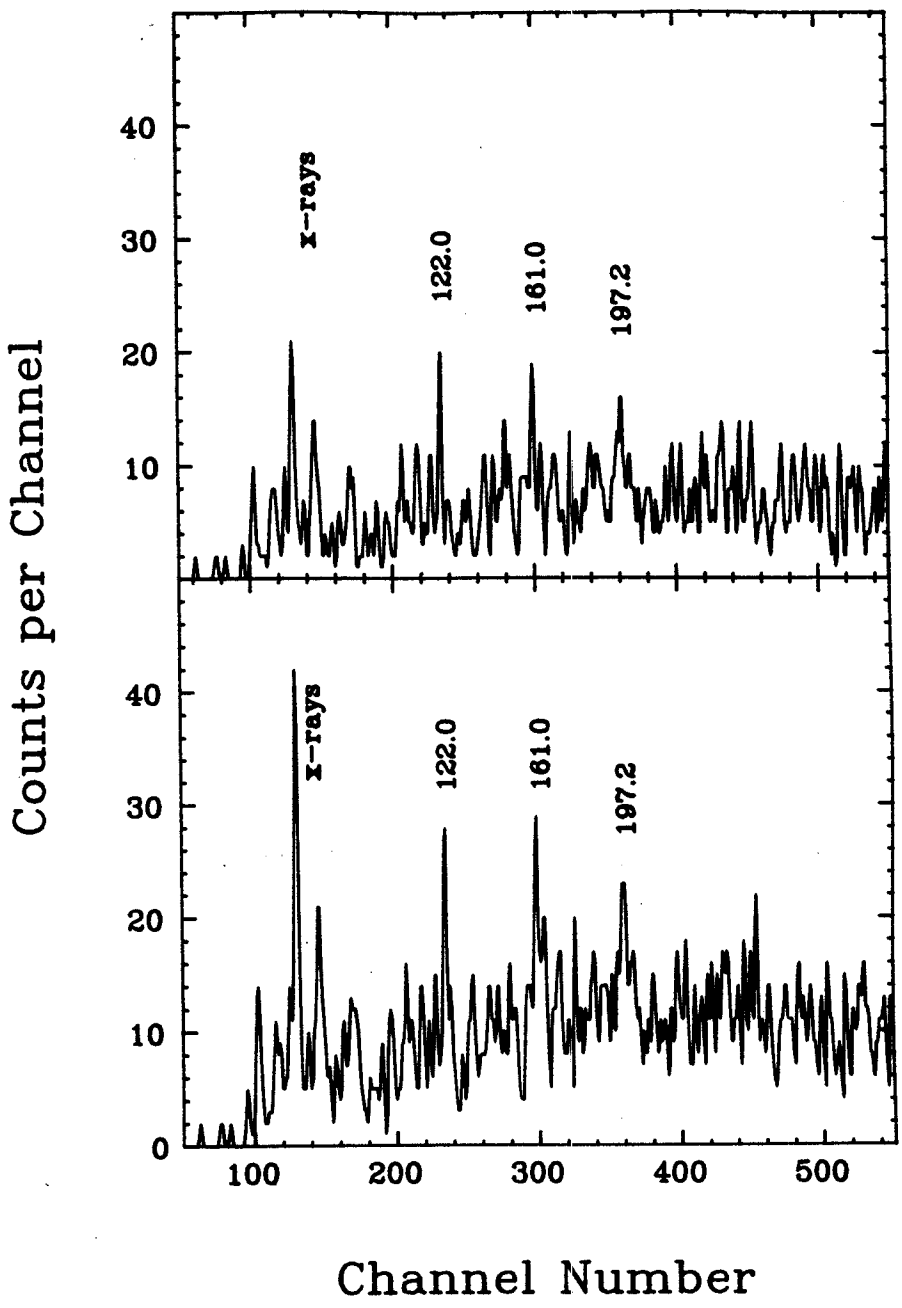

Figure V-17. Two 99.6-keV gated-coincidence spectra. Top: narrower TAC gate. Bottom: wider TAC gate.

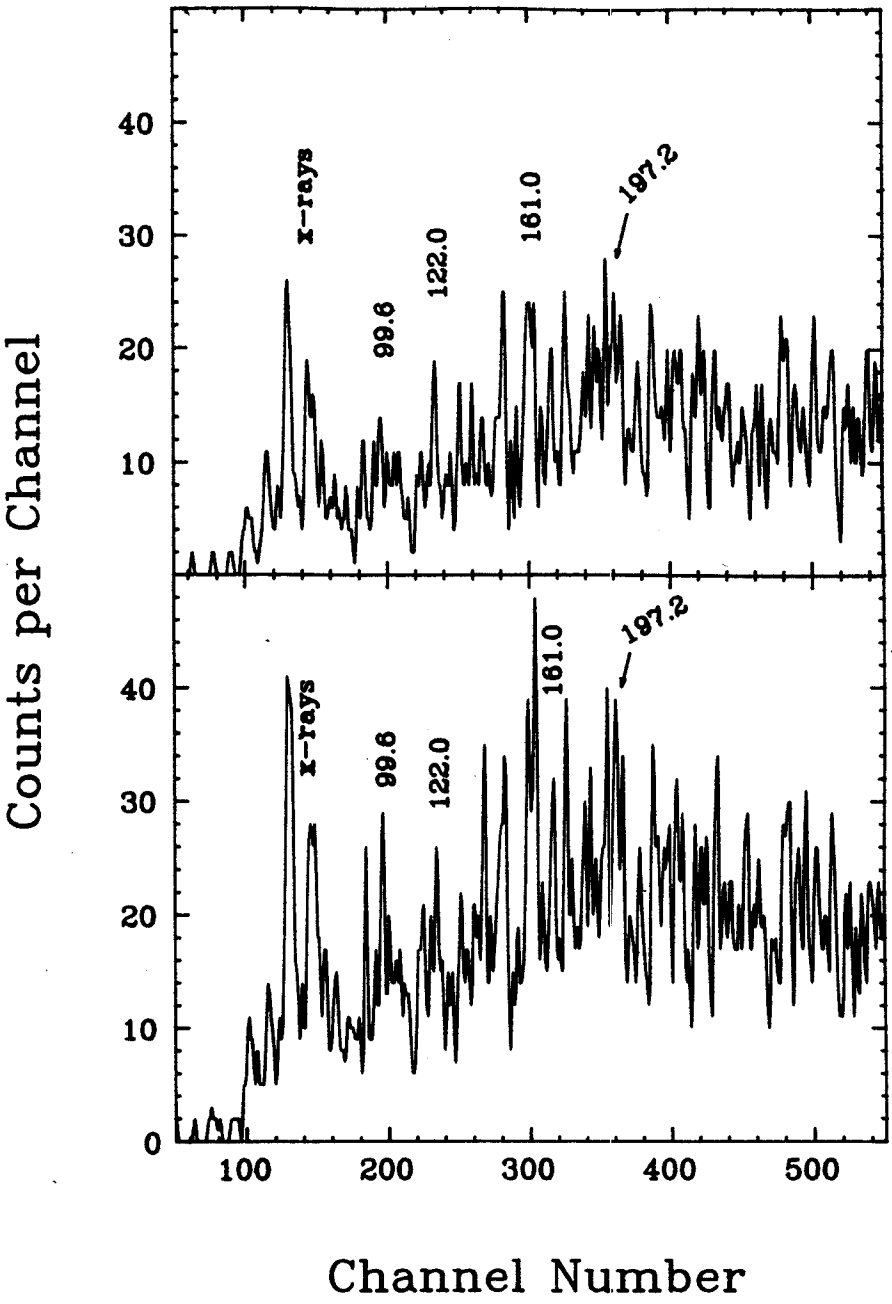

Figure V-18. Two 122.0-keV gated-coincidence spectra. Top: narrower TAC gate. Bottom: wider TAC gate.

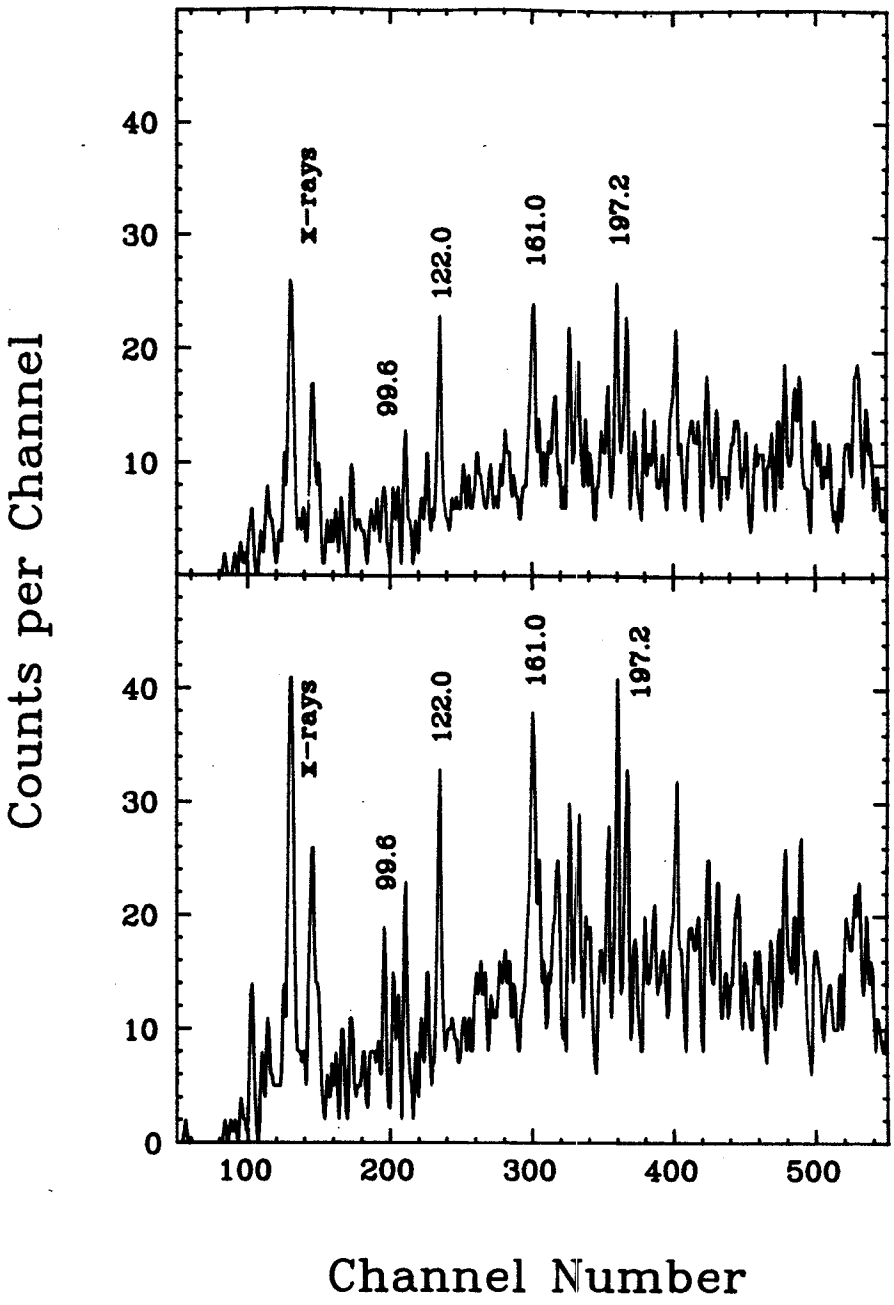

Figure V-19. Two 197.2-keV gated-coincidence spectra. Top: narrower TAC gate. Bottom: wider TAC gate.

transitions keep the same intensity relations, whether the TAC prompt gate is narrow or not. Unfortunately, a quantitative analysis cannot be made. But, it is still safe to conclude that this 99.6-keV transition is a delayed one, and it is the same one that has been found in coincidence with transitions of energies 122.0, 161.0, 197.2 keV, etc. The half-life, 21±7 ns, was extracted from the gated TAC spectrum, which is shown in Figure V-20.

2.4 Results From the Low Energy Photon Spectrometer (LEPS)

The function of the LEPS in the set-up was to resolve low energy γ-rays that could not be resolved by intrinsic Ge detectors. But our LEPS did not retain particularly good resolution anymore. It is down to 1.8-keV FWHM for 80.99-keV ^{133}Ba line. Also, the bulky size of the NaI(Tl) annulus prevented LEPS from being placed closer to the target and limited its solid angle. This, plus the fact that the LEPS has low efficiency, resulted in the LEPS collecting few events. The consequence was that no new transition could be clearly identified in the LEPS total coincidence spectrum, which is shown in Figure V-21.

No surprising results come out when we set energy gates on the LEPS and looked what was in coincidence in one of the Ge spectra. We also tried to set gates in the reverse way. A combination gate on either 171.3, 267.7, 359.0, or 441.9 keV was set on Ge detector, and we record the events from the LEPS. A peak with energy 85 keV, marked by an arrow, seems to be enhanced in the gated spectrum in Figure V-22 when compared with Figure V-21. We must not draw any conclusions, of course, by this weak evidence along, but it might indicate something we have missed in Ge detectors. The same kind of energy gate has also been set

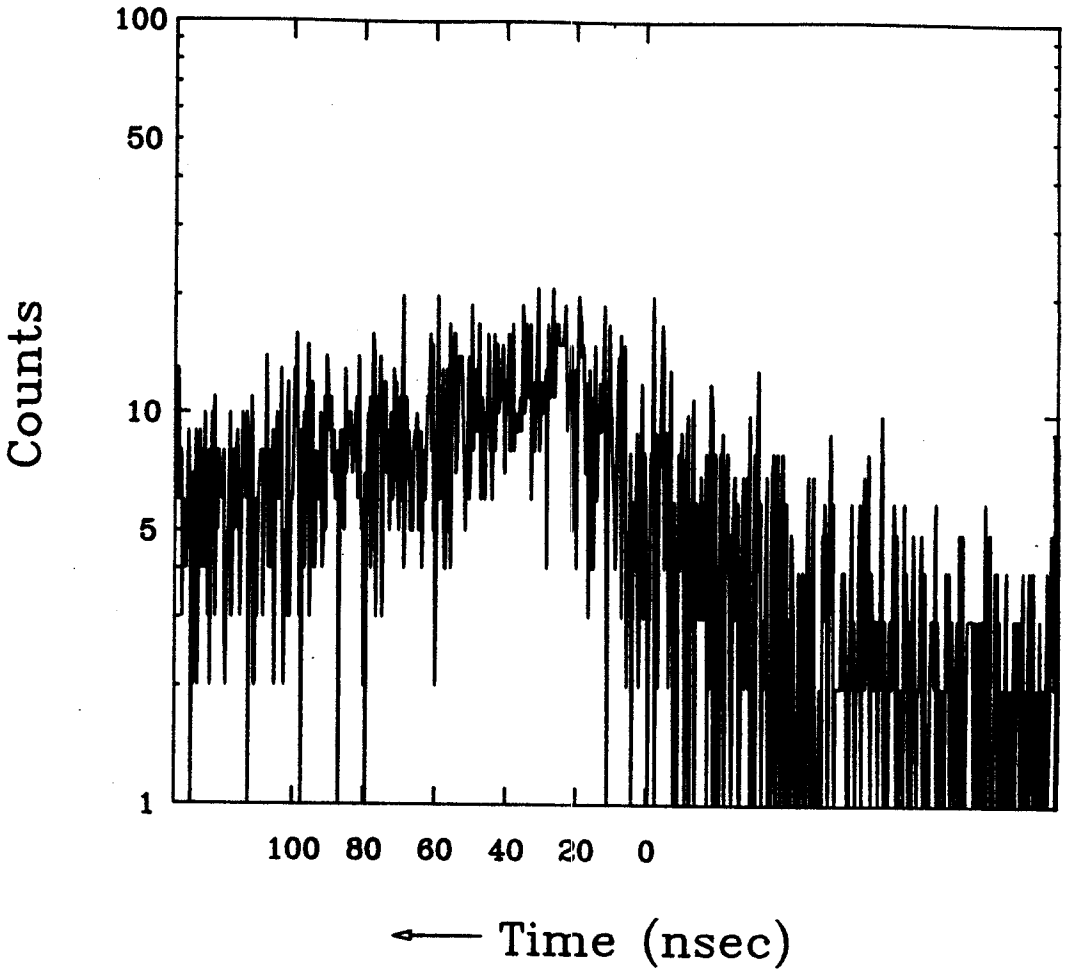

Figure V-20. TAC spectrum gated by the 99.6-keV Y-ray from the reaction, $^{159}Tb(^{22}Ne,5nY)^{176}Re$, at an energy of 113 MeV.

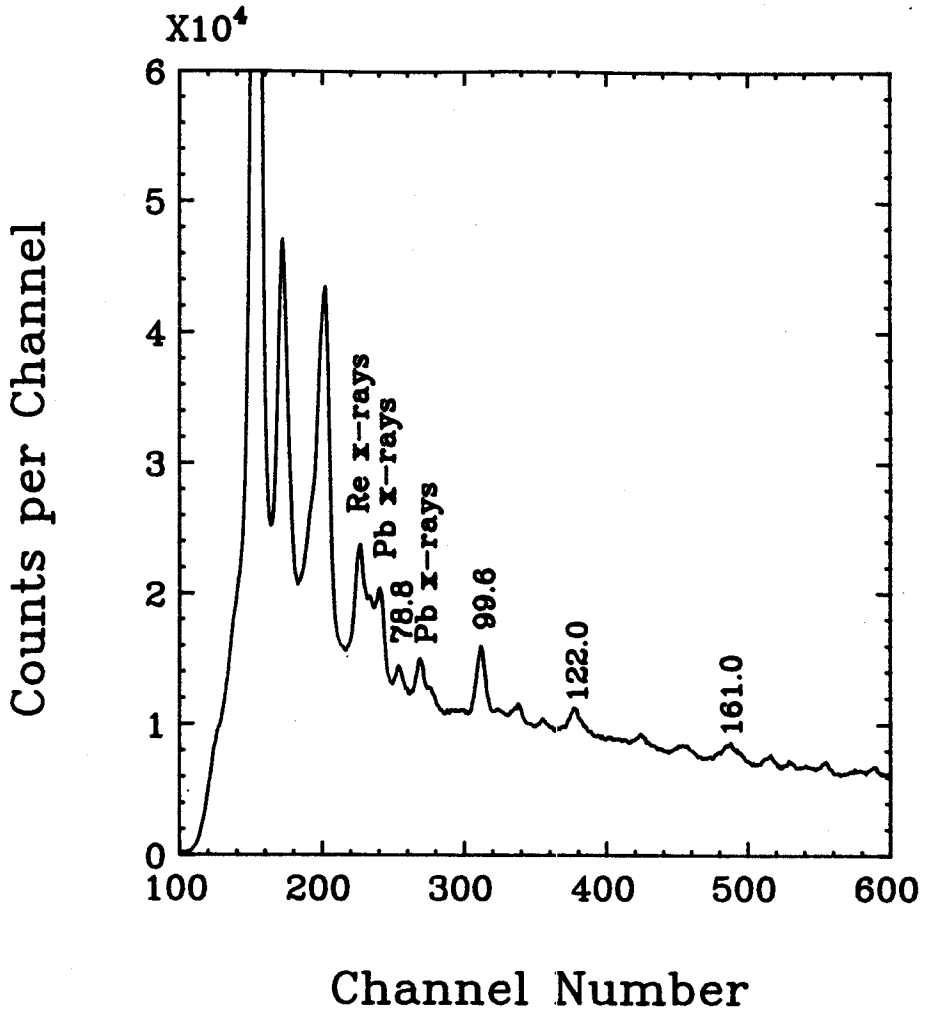

Figure V-21. Integral LEPS coincidence spectrum from the reaction $^{159}Tb(^{22}Ne,5n\gamma)^{176}Re$ at a beam energy of 113 MeV.

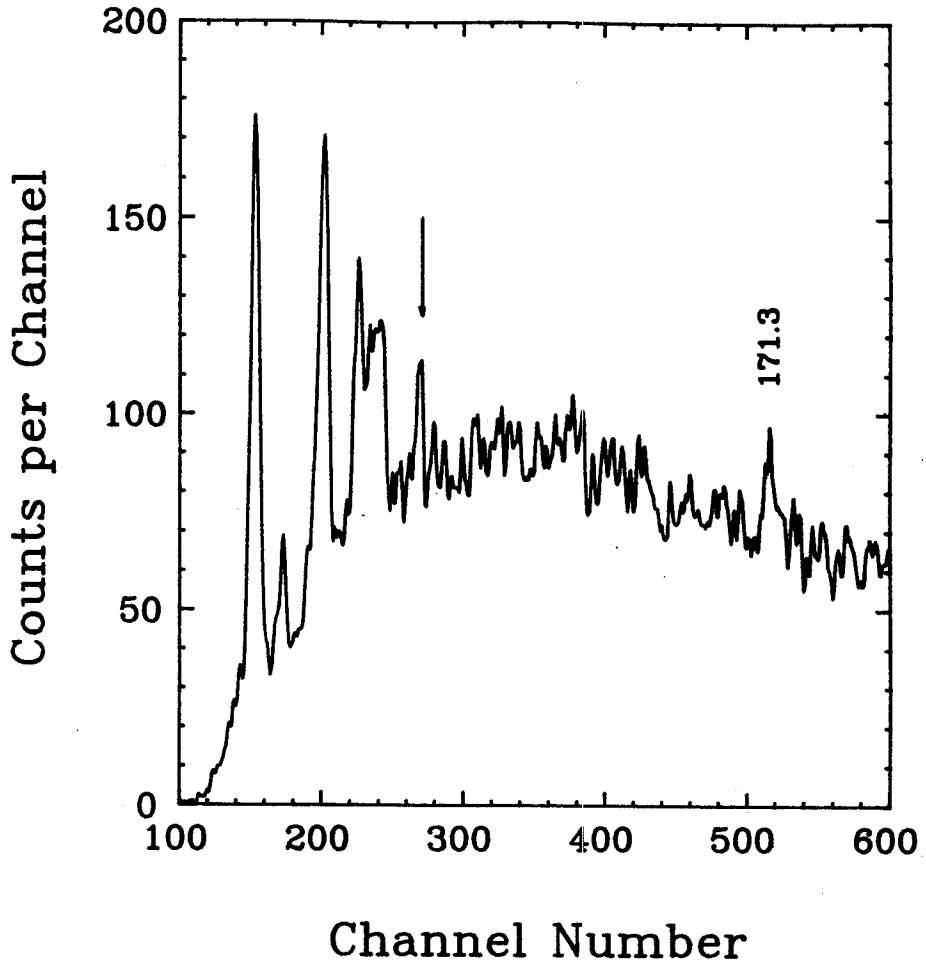

Figure V-22. Gated LEPS coincidence spectrum by a combination of the 171.3-, 267.7-, 359.0-, and 441.9-keV transitions.

on transitions at 99.6, 122.0, 161.0, or 197.2 keV. Nothing interesting was found in this gated spectrum, shown in Figure V-23, but one bump might be the transition claimed by Santos et al. [Sa89]. This will be discussed again in later section.

2.5 Multiplicity Filter

The multiplicity filter, composed of seven 7.6×7.6-cm NaI(Tl) detectors covered only a small portion of 4π. Thus, many valid signals escaped. The capability of this filter and the fact that the data were already in low statistics, made it difficult to set any requirement on the multiplicity filter. Therefore, this part of the analysis did not provide us any valuable information.

3. Analysis of the Continuum Spectrum

We analyzed the continuum Y-ray spectrum for evidence of large deformation. The coincidence events were sorted into a two-dimensional matrix. The matrix was unfolded and uncorrelated Y-rays subtracted by the method of Andersen et al. [An79]. Figure V-24 shows three cuts perpendicular to the diagonal in the symmetrized E_{γ_1}-E_{γ_2} matrix. These cuts correspond to energies of 400, 904, and 1120 keV. The dynamic moment of inertia, $\mathcal{J}^{(2)}$, was deduced from the width of the valley by Equation III-2, yielding values of 36, 53, and 67 $\hbar^2$ MeV^{-1}, respectively, for the 400-, 904-, and 1120-keV regions. These values are smaller than that for a superdeformed band (85 $\hbar^2$ MeV^{-1} for ^{152}Dy). Also, since we did not see a clear valley developed along the E_{γ_1}=E_{γ_2} diagonal line, like what was observed for the superdeformed band [Ny84],

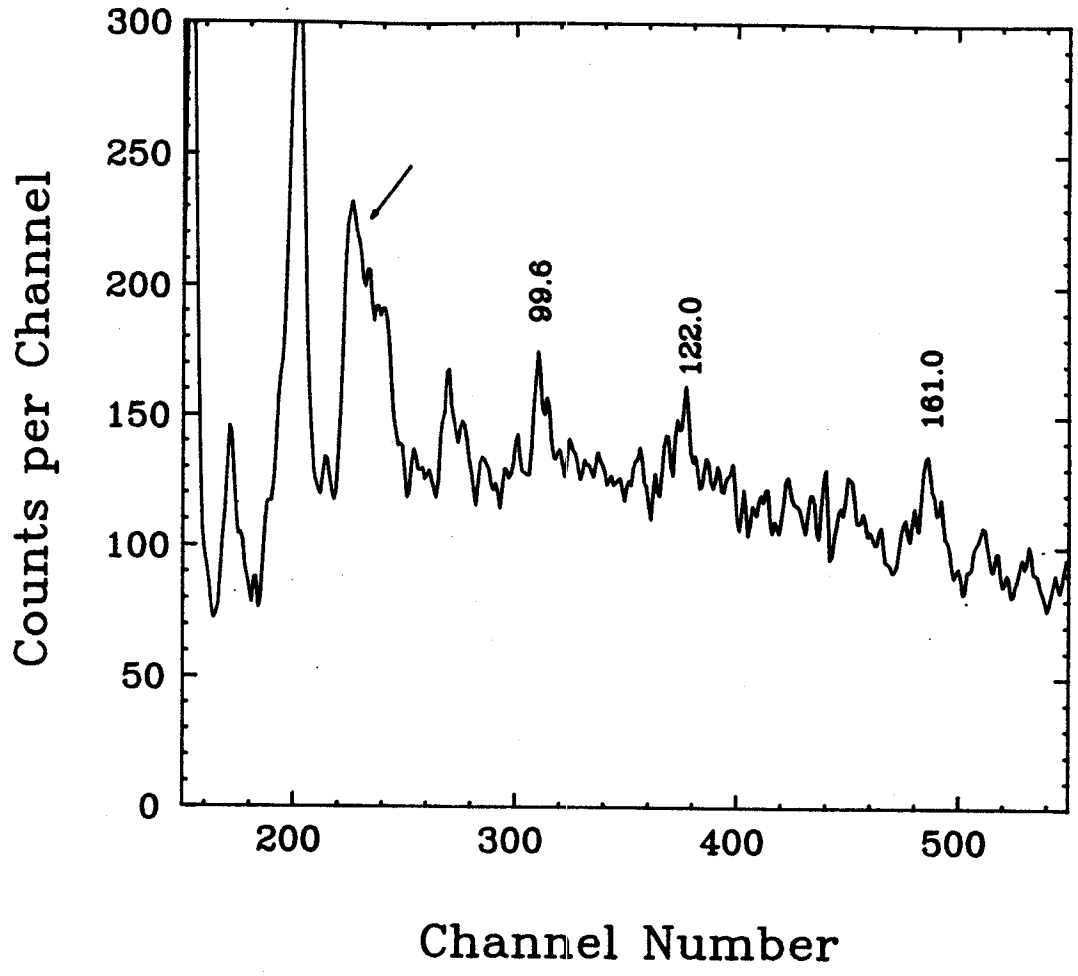

Figure V-23. Gated LEPS coincidence spectrum by a combination of the 99.6-, 122.0-, 161.0-, 197.2-, 222.7-, and 252.3-keV transitions.

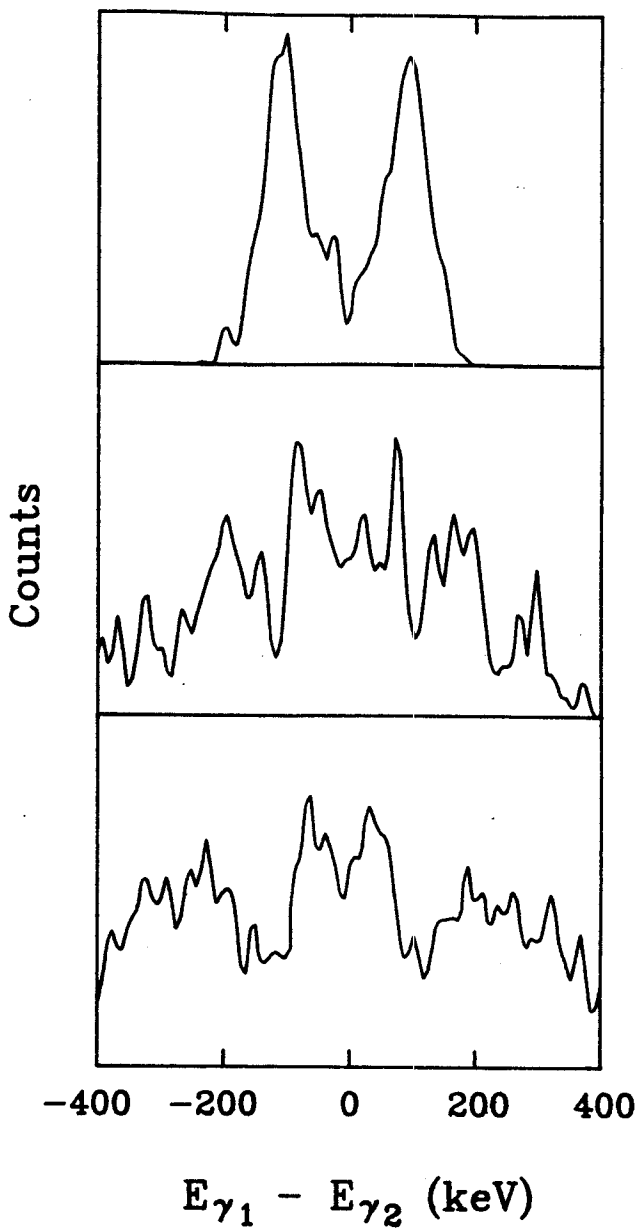

Figure V-24. Cuts perpendicular to the diagonal in the symmetrized E_{γ_1}-E_{γ_2} matrix from the reaction, $^{159}Tb(^{22}Ne,5n\gamma)^{176}Re$. Top: 400-keV region. Middle: 904-keV region. Bottom: 1120-keV region.

this may not be the indication of superdeformed bands.

B. RESULTS OF $^{165}Ho(^{16}O,5nY)^{176}Re$ REACTION

1. Excitation Functions

Excitation function experiments were conducted, taking the advantage of SUNY Stony Brook LINAC, injected by a FM tandem Van de Graaff accelerator. Beam energies were varied in the range from 122.8 to 72.78 MeV. Some of the singles spectra at various energies are compared in Figure V-25. As some of the important transitions are labeled, it can be seen that the production cross-section of ^{177}Re was dominant at all energies. This came about because of the very thick target used, for the beam eventually got degraded inside the target. Thus, not only the nuclei that can be produced under that certain beam energy will appear in a reaction slice, but also any other nuclei that can be produced below that beam energy. This made the excitation function experiments a little difficult to analyze and make choosing an optimum beam energy for producing ^{176}Re difficult. Thus, after consulting the CASCADE calculation (the result is shown in Figure V-26), we chose to run our Y-Y coincidence experiment with a 96.9-MeV ^{16}O beam, because, all else being equal, higher beam energy at least can excite the interesting nucleus to higher spin.

2. Y-Y Coincidence Results

A total coincidence spectrum is shown in Figure V-27, with the ^{176}Re transitions labeled. As expected, transitions from ^{177}Re (not

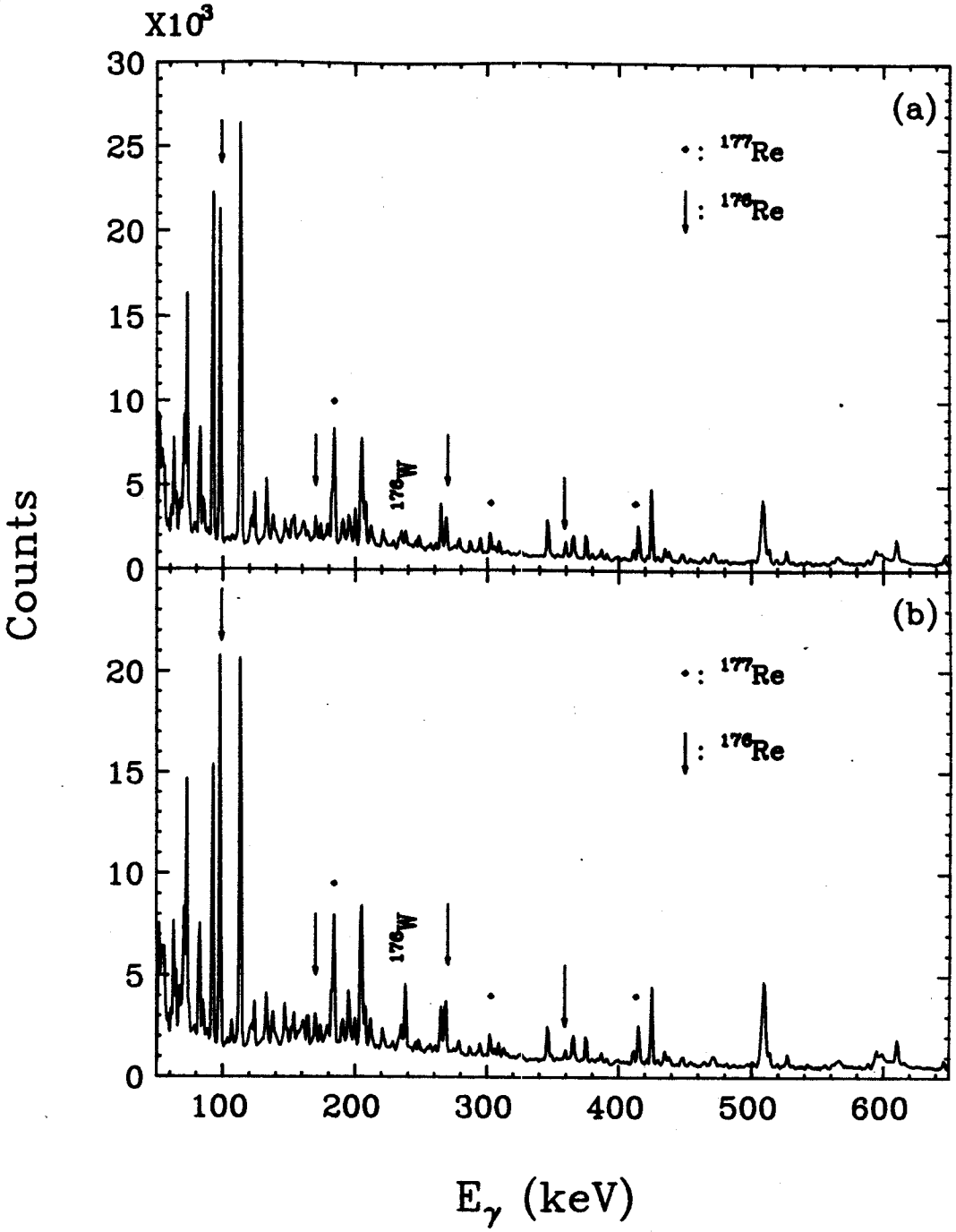

Figure V-25. Singles spectra of excitation-energy experiments from the reaction, ^{165}Ho(^{16}O,nγ). (a) 86.3-MeV. (b) 92.9-MeV.

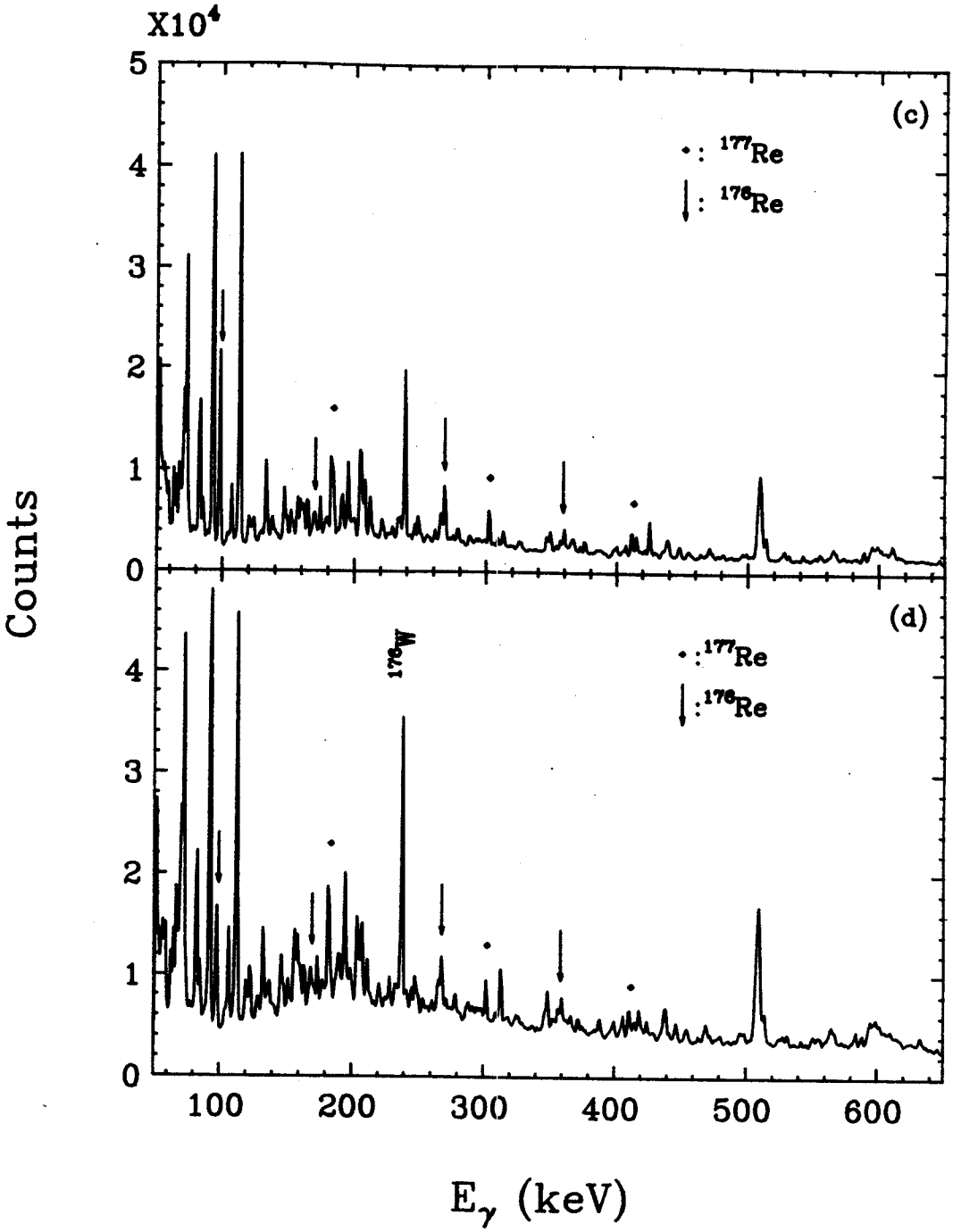

Figure V-25. (cont'd.). (c) 101.1-MeV. (d) 115.3-MeV.

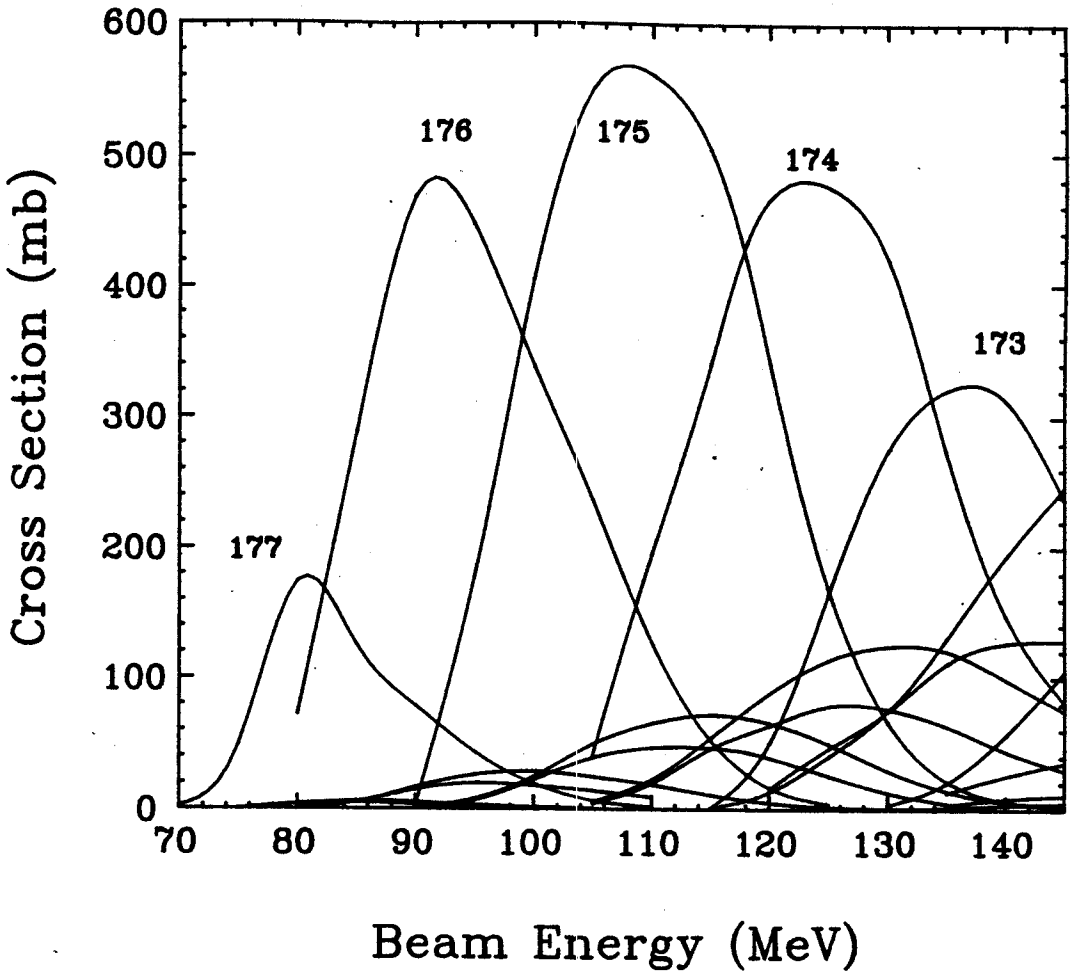

Figure V-26. Cross-sections versus beam energies calculated by program CASCADE, for the reaction of ^{16}O beam on a ^{165}Ho target.

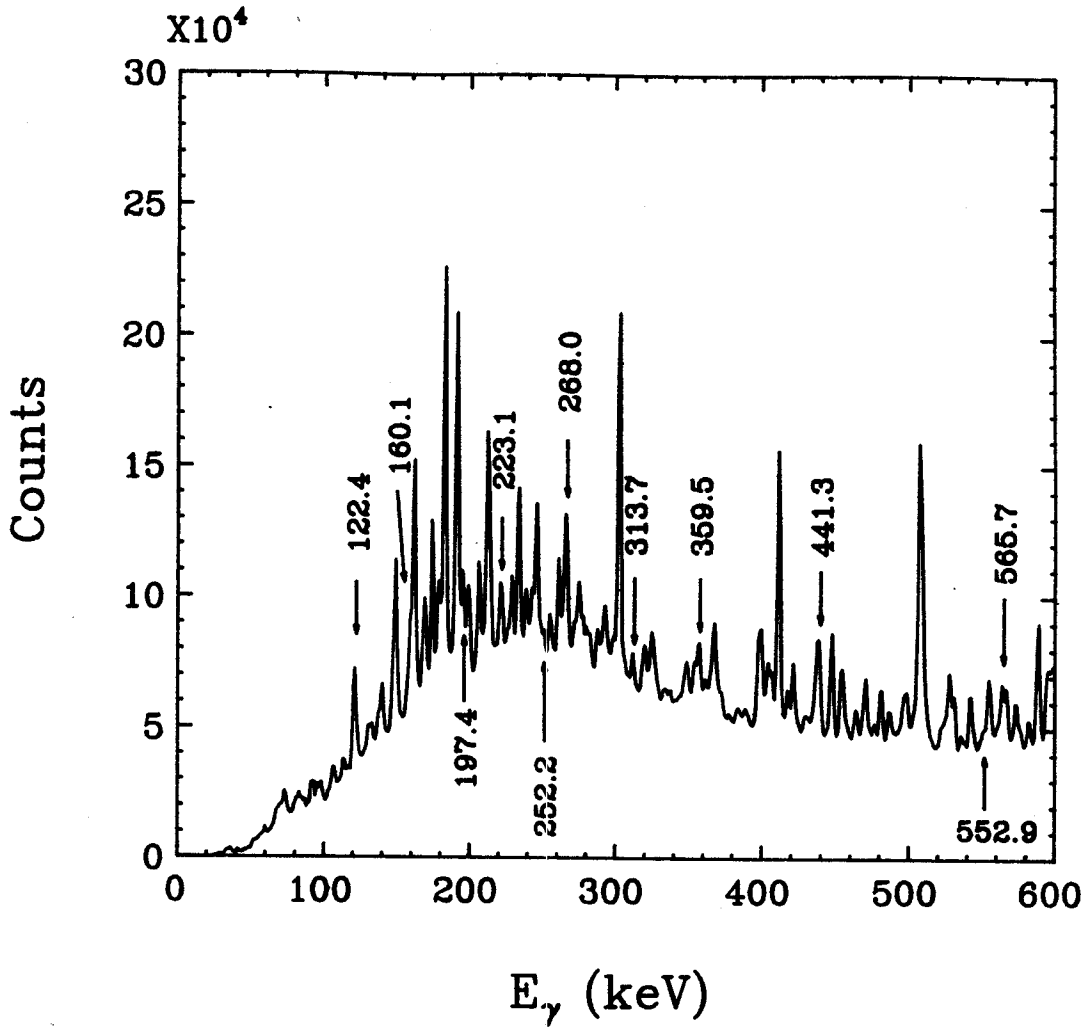

Figure V-27. Total coincidence spectrum from the ^{165}Ho(^{16}O,nY) reaction at a beam energy of 96.9 MeV.

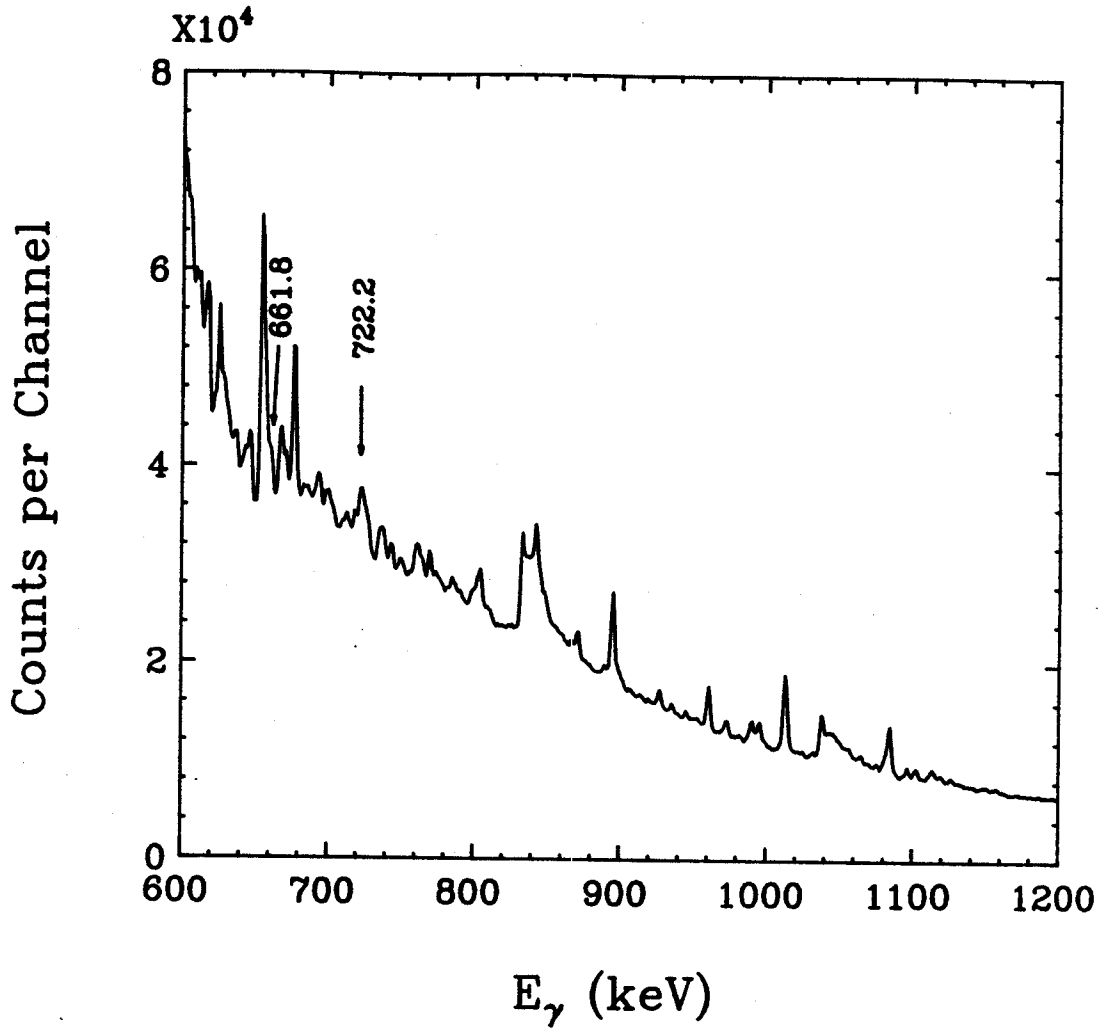

Figure V-27. (cont'd.).

labeled in Figure V-27) are much stronger than those from ^{176}Re. This is too bad, but fifty times of events have been collected, so some new transitions should be able to be extracted from this experiment.

2.1 Analysis of Side Product -- ^{177}Re

Again, a careful analysis has been done for transitions that belong to ^{177}Re. Almost all the transitions that have been reported before can be confirmed by our data, except for some minor disagreements. In addition, a few new transitions can be assigned to ^{177}Re.

We observed the K=1/2 decoupled band up to spin I=45/2 as Yang et al. [Ya89], but a discrepancy appears for two transition in the band. Two gated-coincidence spectra are displayed in Figure V-28, and a sum of six gated-coincidence spectra in Figure V-29. Especially note that transitions at 656.0 and 659.0 keV are an unresolved doublet in the Y-Y coincidence spectrum (Figure V-27), whereas they are revealed in the gated spectrum in Figure V-28. Our data show that the energy of 37/2 → 33/2 transition is 677.7 keV instead of 687.4 keV; 723.9 keV for 49/2 → 45/2 instead of 729.0 keV as reported before. Two more transitions, at 805.1 and 895.9 keV, are also related to the K=1/2 band, and are believed to be the next two intraband transitions based on intensities and spacings of those established transitions. This K=1/2 band now is extended to spin I=57/2.

Of course, it is not exciting that we confirm the data that have been reported before. However, this assures us that our analysis and interpretation are correct.

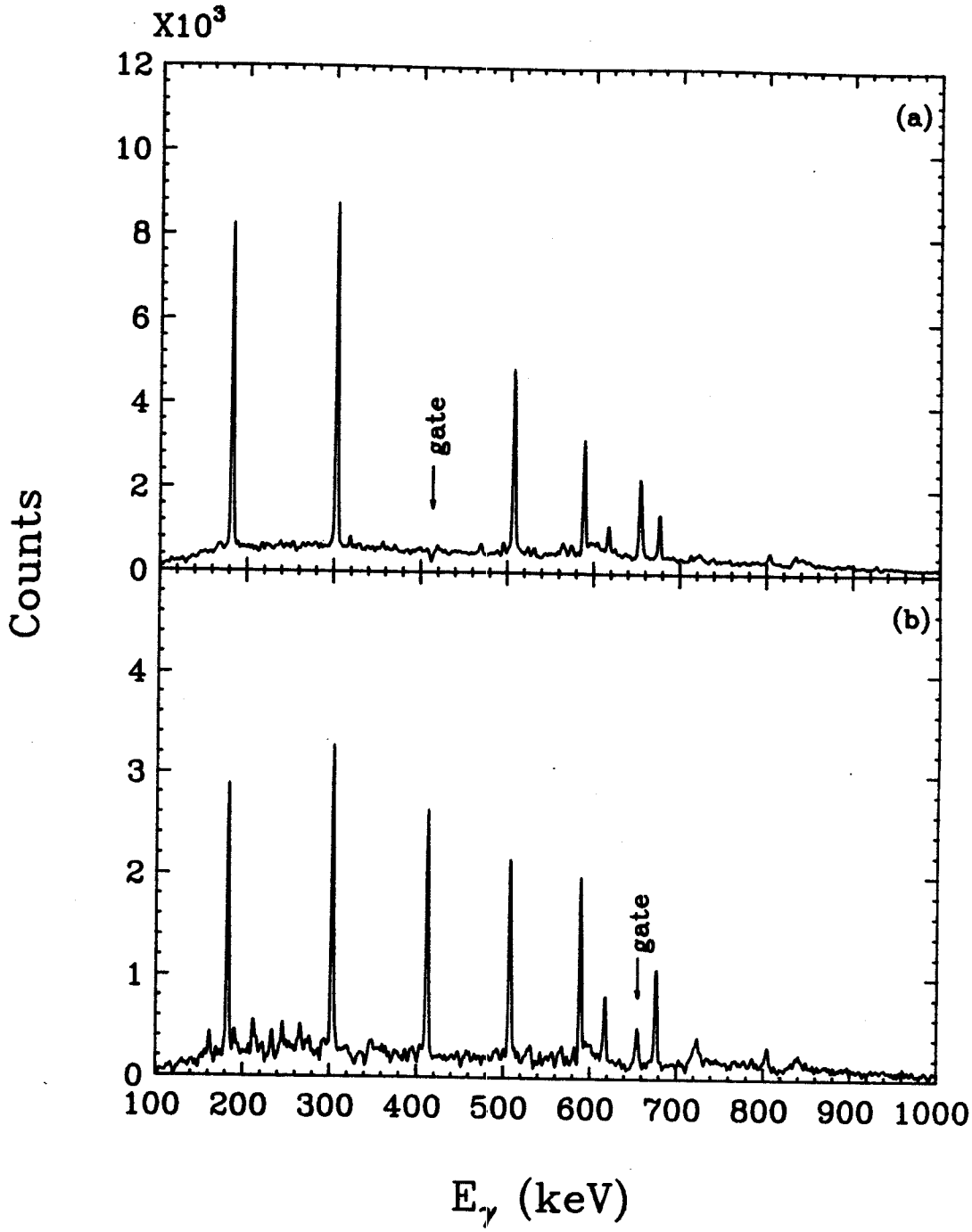

Figure V-28. Selected gated-coincidence spectra from the transitions of the K=1/2 band of ^{177}Re. (a) 413.7-keV gate. (b) 656.0-keV gate.

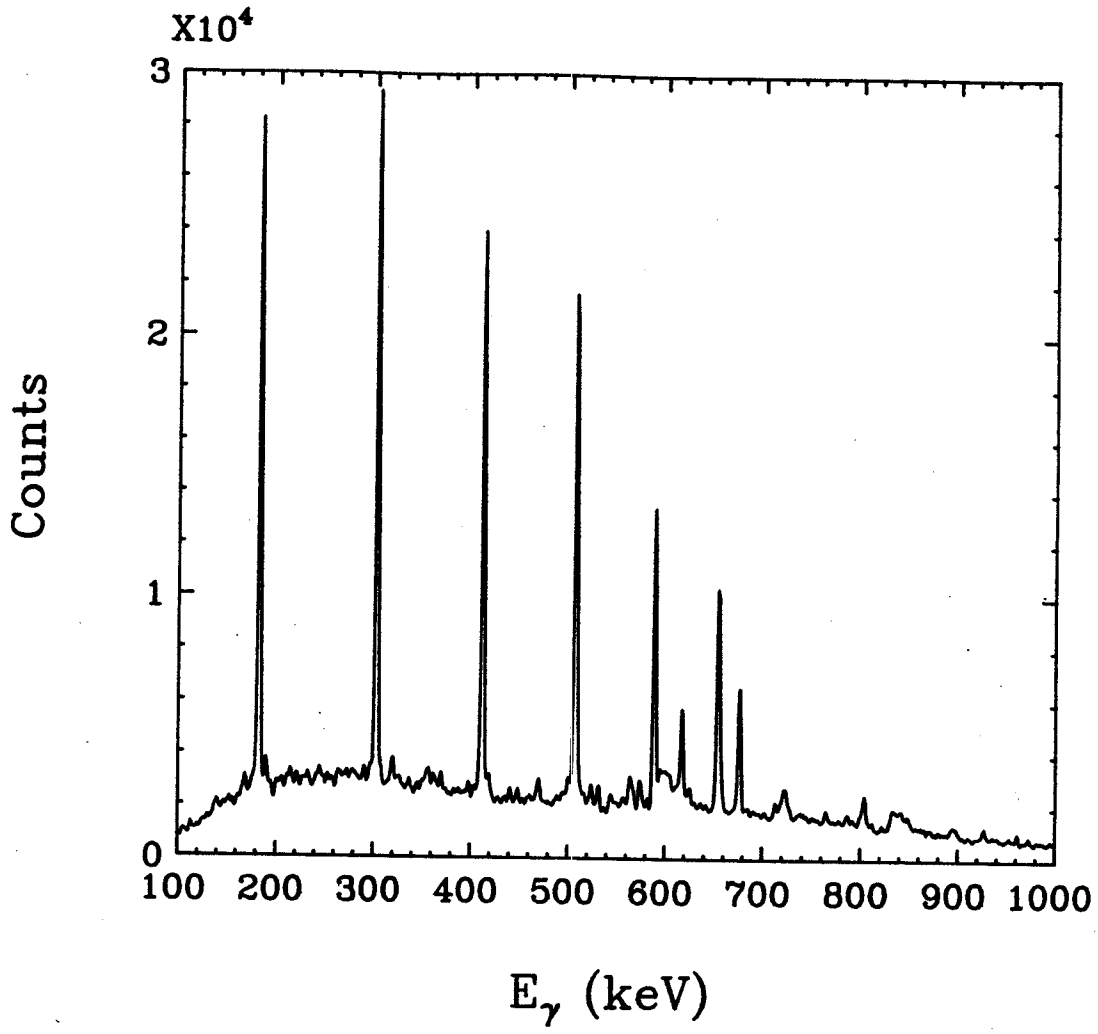

Figure V-29. Sum of several gated-coincidence spectra on the transitions from the K=1/2 band of ^{177}Re.

2.2 Analysis of ^{176}Re Data

By taking a quick look of the Y-Y coincidence spectra, we did see some high-energy transitions that we could not see before. But we saw no new transitions in the low-energy area. Energy gates of all the known transitions from previous experiments have been set on the two-dimensional array and produced gated-coincidence spectra. Background has been subtracted from these spectra, adopting the method described in section A.2.1. The energies of the Y-rays were determined from the Y-Y coincidence spectrum in general. But when a transition appeared as part of a multiplet, its energy was derived from gated-coincidence spectra.

The group of transitions at 171.4, 268.0, 359.5 keV, etc., in coincidence with one another, can be confirmed, as can be seen from the gated-coincidence spectra shown in Figure V-30. Only the 171.4-keV gated spectrum is clean, where the intensities of the coincident transitions change smoothly. Four new transitions, at 552.9, 596.5, 601.0, and 661.8 keV, can be picked up from these gated spectra. And they can been seen better in the sum of gated spectra of the 171.4-, 268.0-, 359.5-, 441.3-, and 565.7-keV transitions shown in Figure V-31. The 722.2-keV transition stands out cleanly, too, and could very well be the next transition. Unfortunately, the gated spectrum on 722.2 keV is contaminated by the 723.9-keV transition from ^{177}Re, so we were unable to confirm it with the reverse gate.

We suspected there might be a transition between the 441.3- and 565.7-keV transitions with an energy very close to 511 keV. The requirement on the multiplicity filter was set to be three as mentioned before. Consequently, most of the garbage transitions, for example

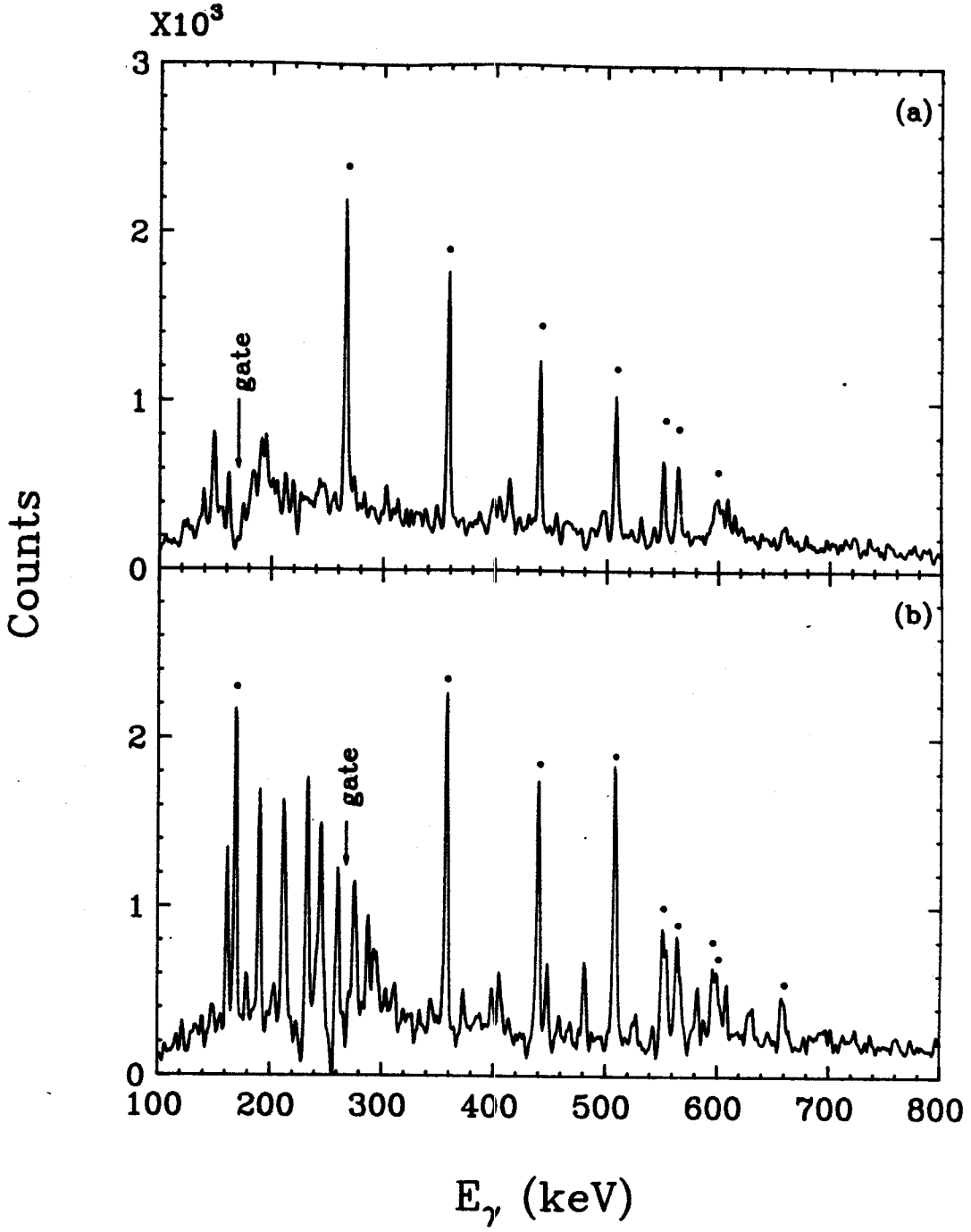

Figure V-30. Selected gated-coincidence spectra from the 171.4-keV transition group. (a) 171.4-keV gate. (b) 268.0-keV gate.

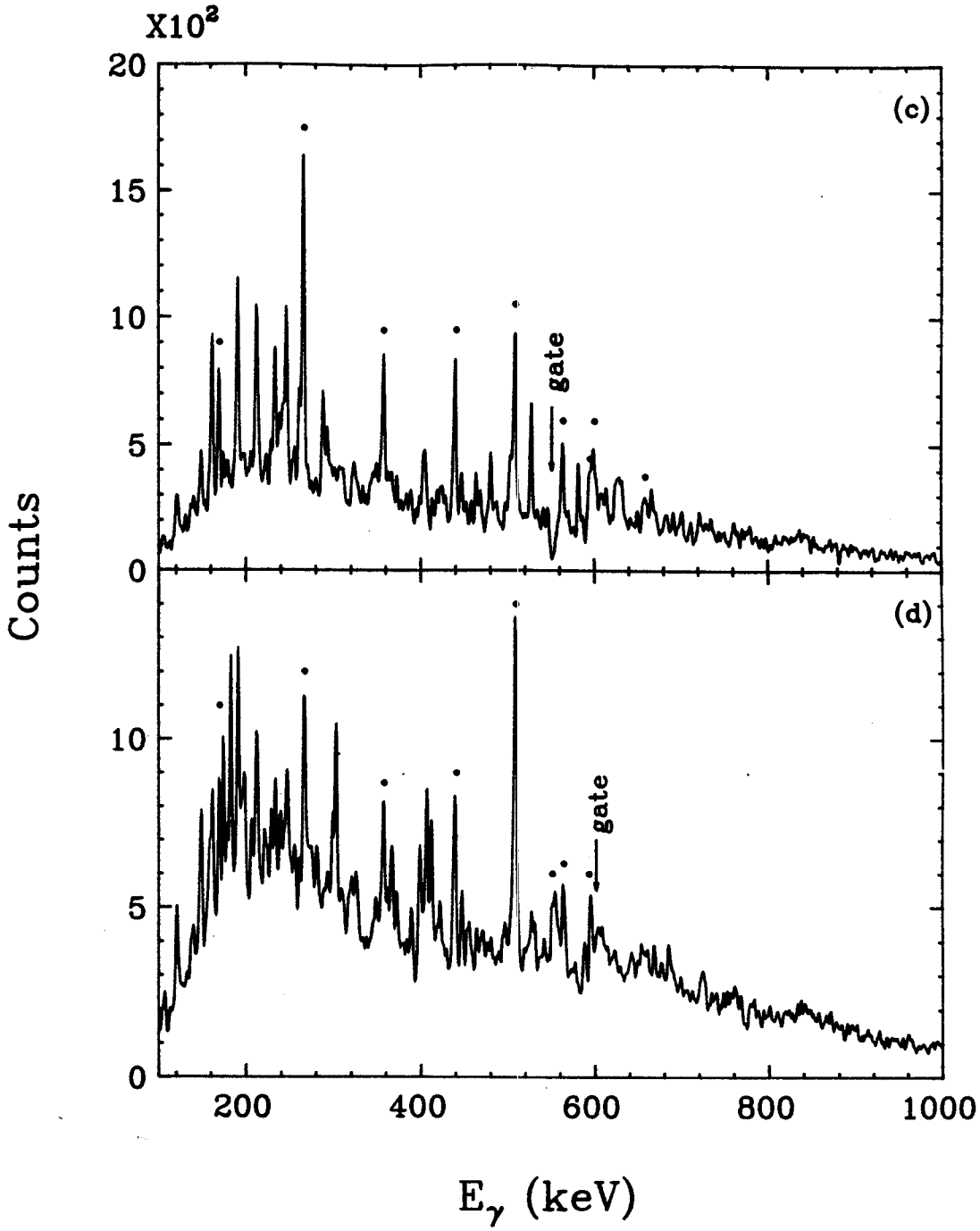

Figure V-30. (cont'd.). (c) 552.9-keV gate. (d) 601.0-keV gate.

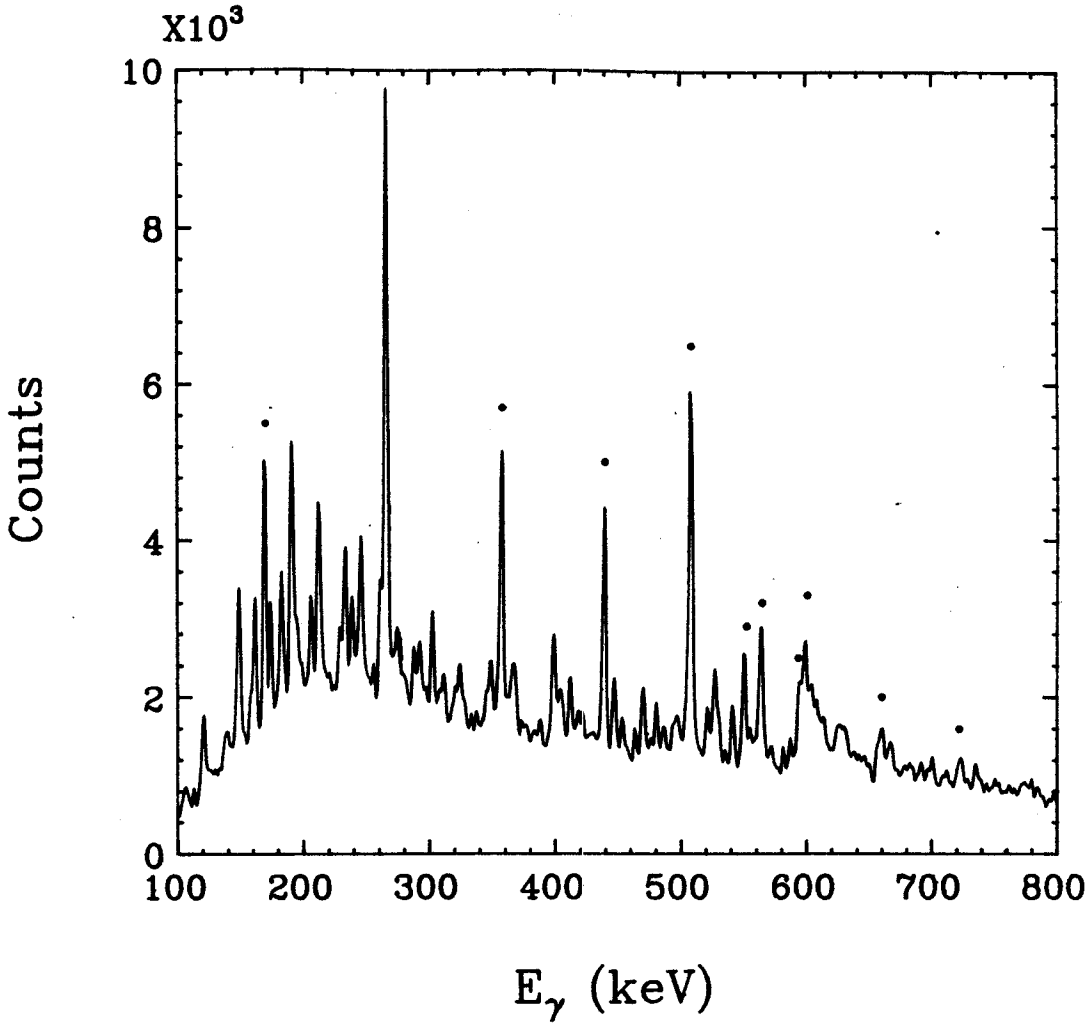

Figure V-31. Sum of the gated-coincidence spectra from transitions belonging to the 171.4-keV group.

x-rays, Coulomb excitation lines, and electron-positron annihilation peaks, should be eliminated. But, there is still a very strong peak near 511 keV. This tells us that it is a real peak. Figure V-32 gives the 511-keV gated-coincidence spectrum. Although this transition is a multiplet (509.7-keV Y-ray in the K=1/2 band in ^{177}Re, and a 511.0-keV cross-over transition from the K=9/2 band), it is not difficult to see transitions at 171.4, 268.0, 359.5 keV, etc., as pointed out by the arrows. From the sum gated-coincidence spectrum (Figure V-31), the part that belongs to ^{176}Re has energy 509.9 keV. This value can also be obtained in all the singly-gated spectrum (Figure V-31).

The other group of transitions, constituted of the 99.6-, 122.4-, 161.1-, 197.4-, and 223.1-keV Y-rays, was also analyzed. These transitions are severely contaminated by the neighboring odd-mass ^{177}Re. Some of the gated-coincidence spectra are shown in Figure V-33. The coincidence relations can be firmly proved in spite of the contamination. The 252.2- and 275.0-keV transitions, which can hardly be seen in the previous experiment, show up much more clearly, and their energies can be determined quite precisely. In addition, three more transitions, at 294.2, 313.7, and 326.7 keV, seem also to be in coincidence with the transitions mentioned above. In a sum gated-coincidence spectrum (Figure V-34) consisting of the 161.1-, 197.4-, 223.1-, and 252.2-keV, which have less interference from ^{177}Re, we do confirm that the 294.2-, 313.7-, and 326.7-keV transitions belong to this group.

Doubly-gated coincidence analysis can also be performed since there were five Ge detectors. Two out of the five Ge detectors were gated by known transitions, allowing us to look at what appeared in the remaining

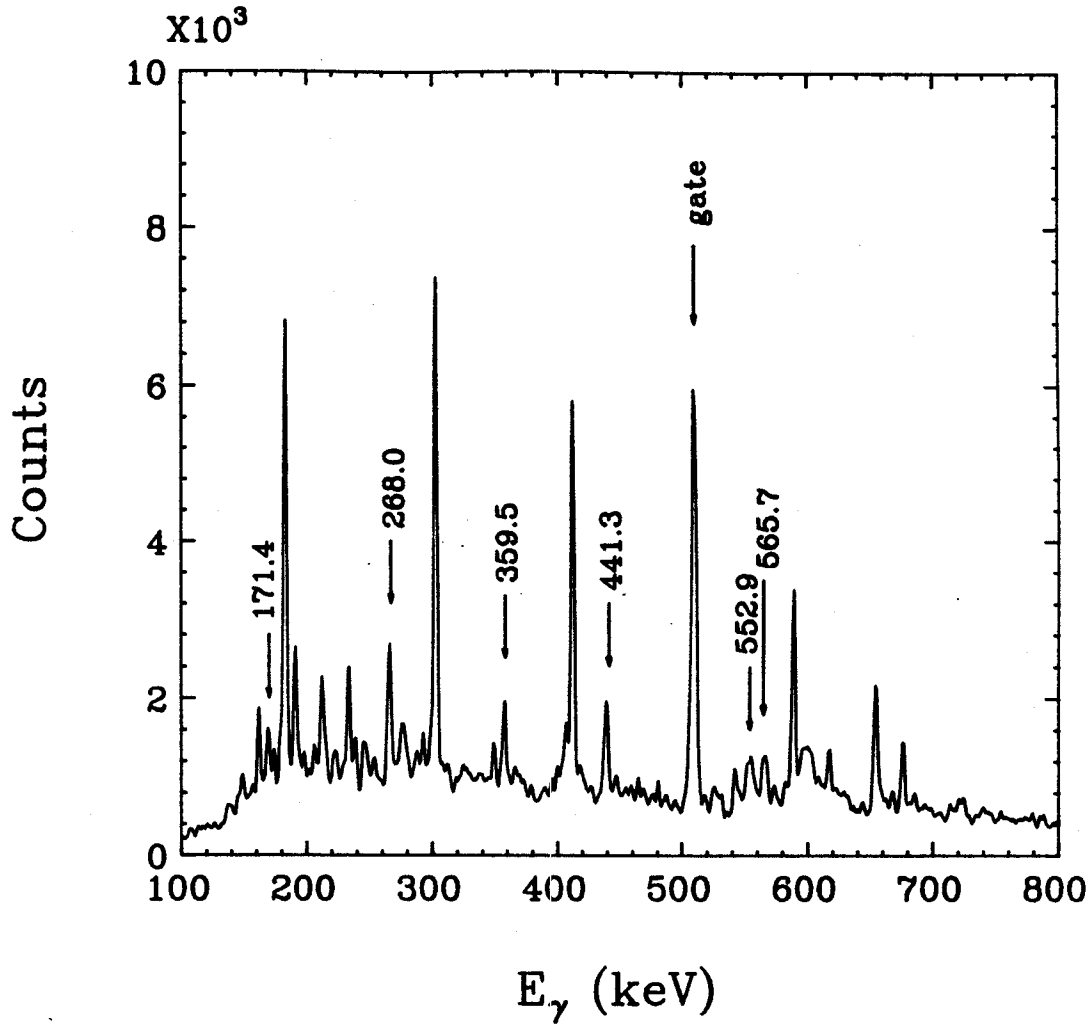

Figure V-32. Gated-coincidence spectrum in the complex 511-keV peak .

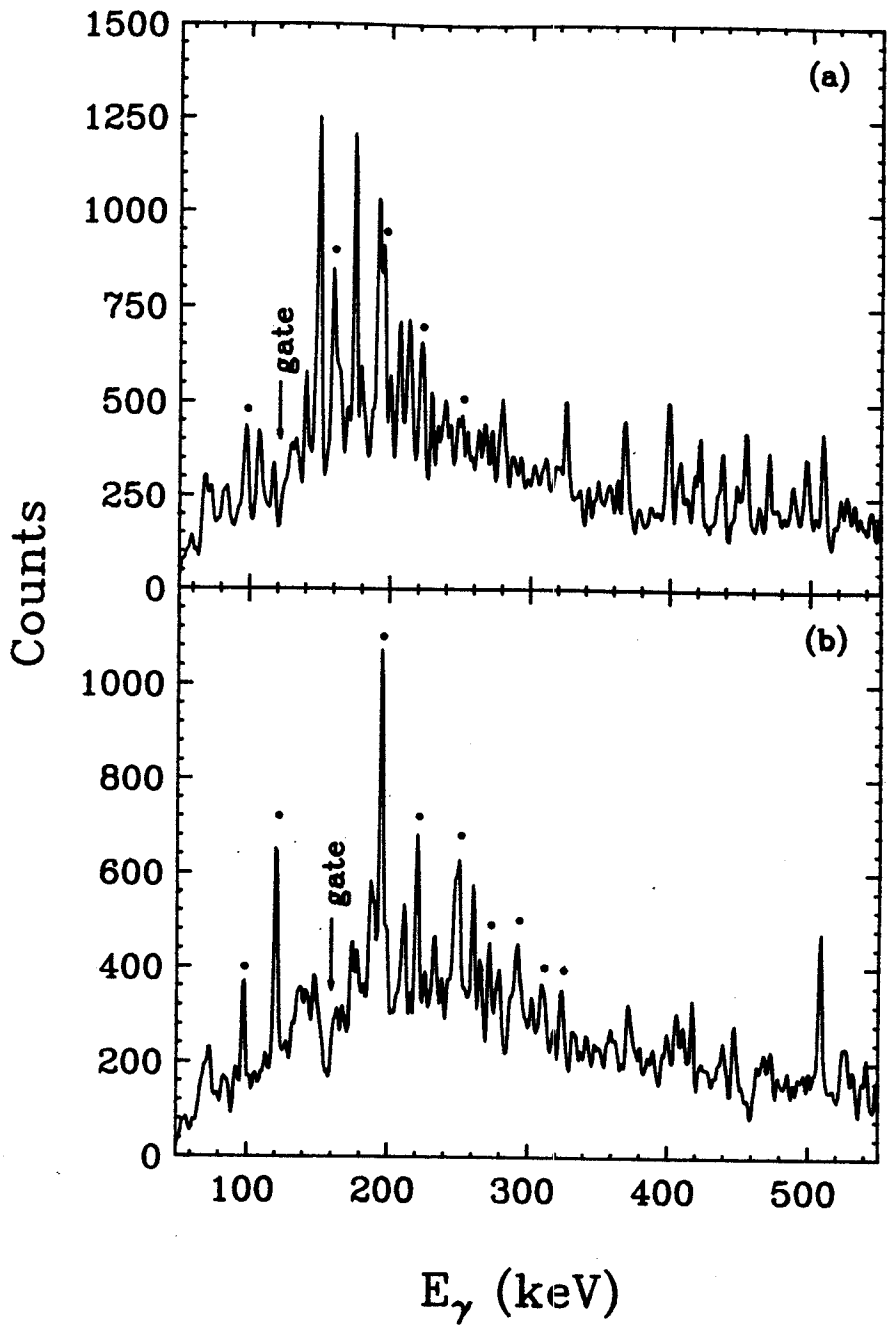

Figure V-33. Selected gated-coincidence spectra on transitions from the 99.6-keV group. (a) 122.4-keV gate. (b) 161.1-keV gate.

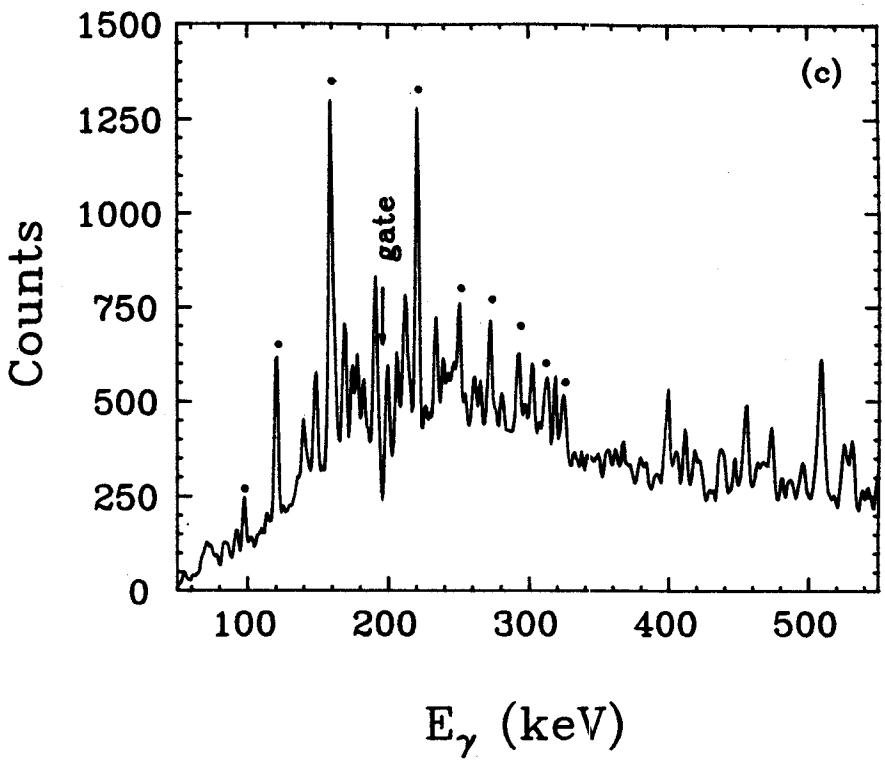

Figure V-33. (cont'd.). (c) 197.4-keV gate.

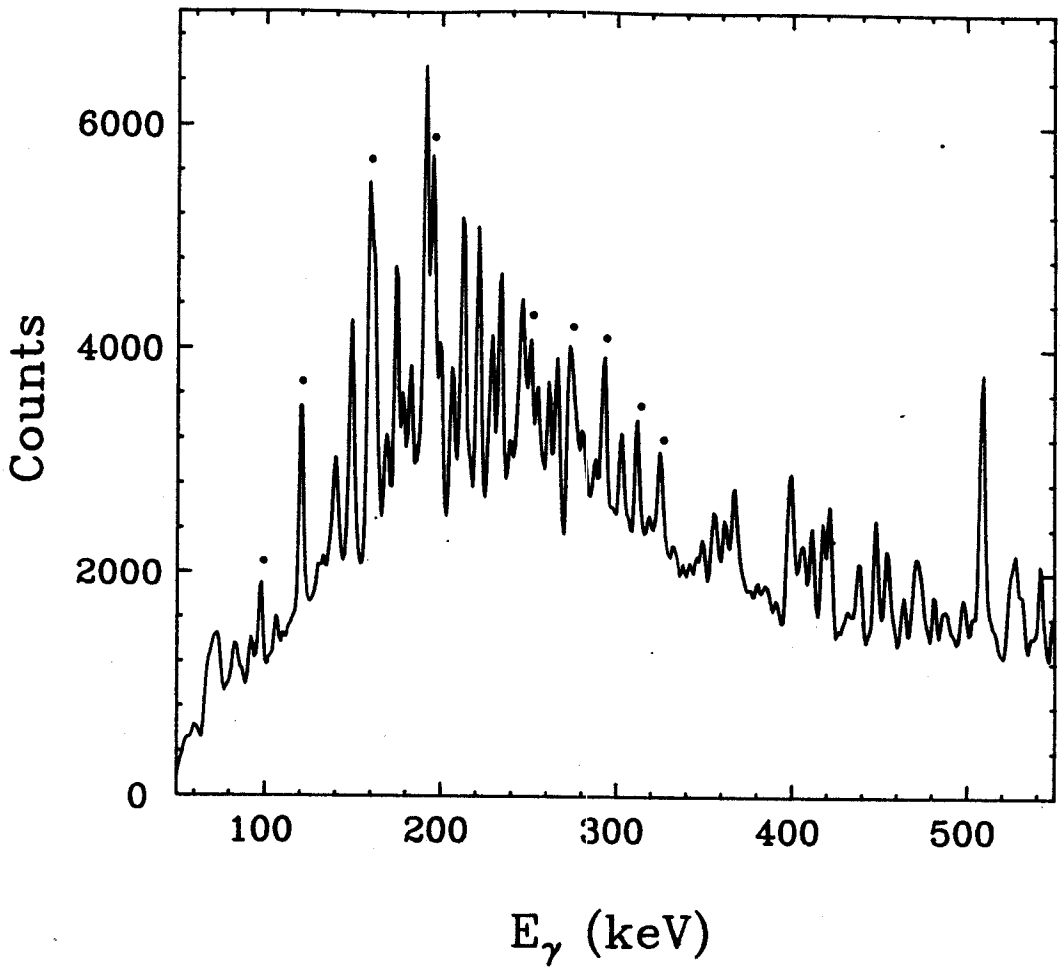

Figure V-34. Sum of four gated-coincidence spectra from the 99.6-keV transition group.

three detectors. The contamination from other stuffs should be reduced by doing this. This kind of analysis has been done for both groups of transitions. Of course statistics are much less in the doubly-gated coincidence spectrum. Therefore, only spectra with gates set on all the possible combinations of pairs of each group are given in Figures V-35 and V-36. From these spectra, we confirm all the coincidence relations among Y-rays once again. Especially, notice the much wider peak near 600 keV, which is a combination of 596.5- and 601.0-keV Y-rays.

The gated-coincidence spectra of each of the two groups are free of transitions from the other group. In other words, no linking transition connecting these two groups can be identified.

3. Angular Correlations

The standard method for obtaining average directional correlation intensity ratios [Kr73] is to set gates on a known quadrupole transition [Pa89], then compare the intensities of transitions collected at 90° with that at non-90°. If the transition is a quadrupole, the intensity ratio is usually ≥ 1.0, whereas it is ≤ 0.7 for a dipole transition. The 171.4-keV transition was chosen to be the gating transition, because it is a rather clean transition. The results are listed in Table V-3, where the 565.7-keV Y-ray was used as normalization. All the intensity ratios are larger than one, and 268.0-, 359.5-, 441.3-, 509.9-, 565.7-, and 552.9-keV are all quadrupole transitions. For the other group, 197.4-keV transition was the gating transition and 99.6-keV transition was used as normalization. The results are also listed in Table V-3. Here, the intensity ratios are smaller than 0.7, except for 122.4 and 161.1 keV. E2 transitions always mix with M1 transitions and make the

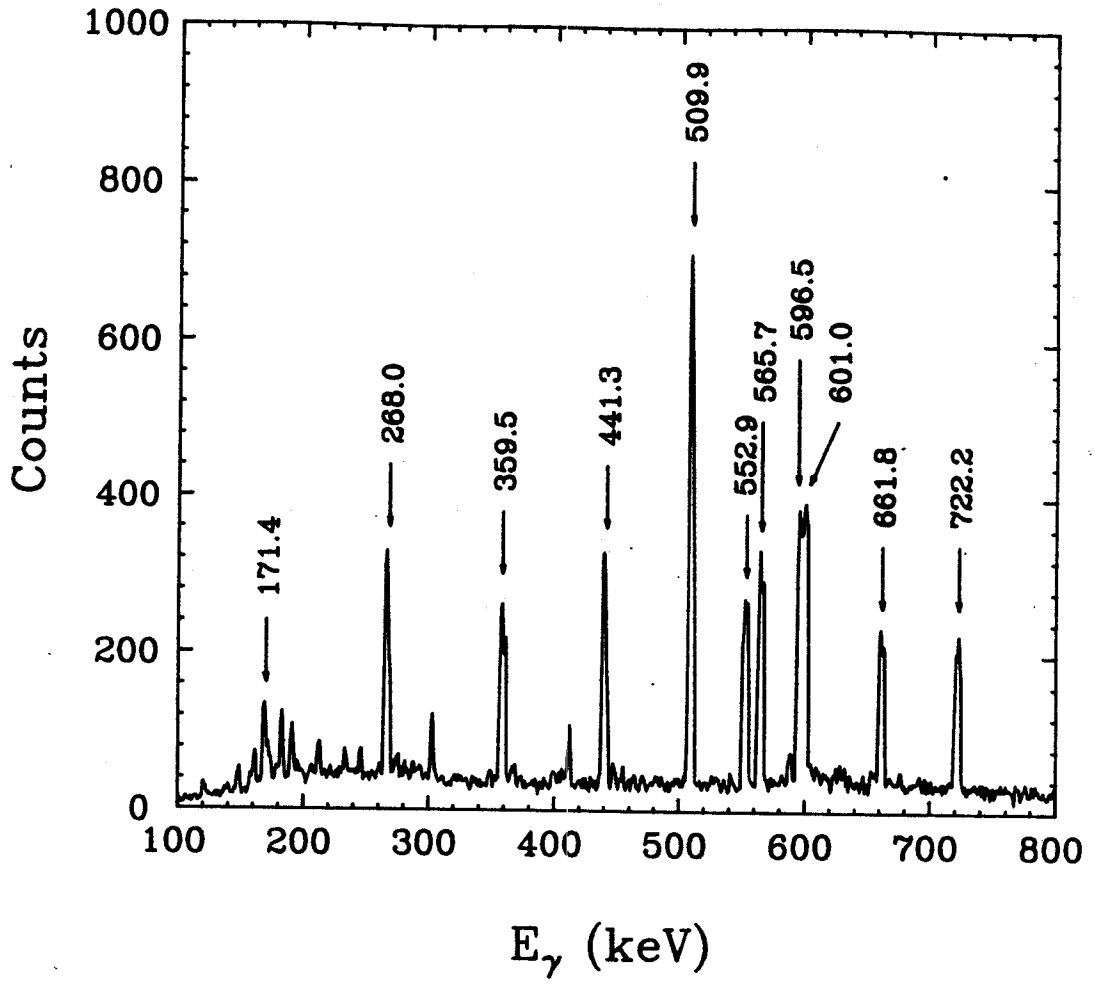

Figure V-35. Sum doubly-gated coincidence spectrum on the 171.4-keV group.

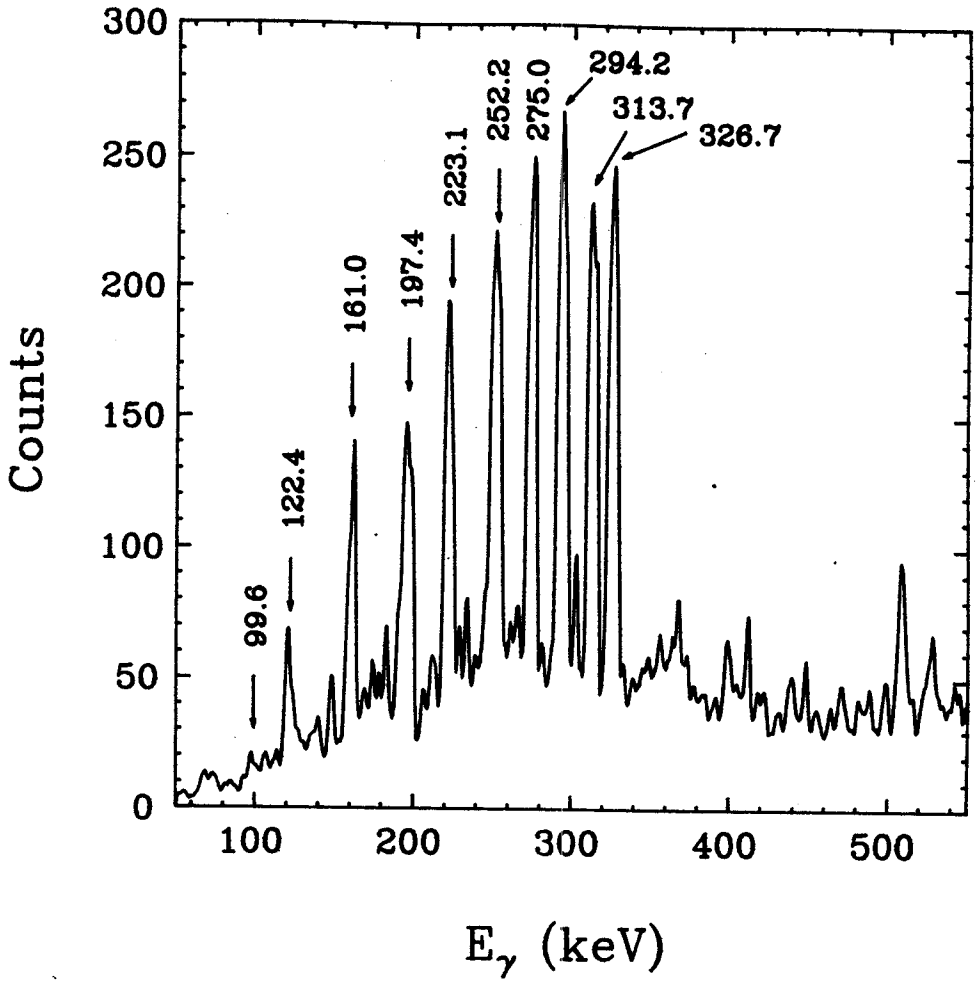

Figure V-36. Sum doubly-gated coincidence spectrum on the 99.6-keV group.

Table V-3. Relative Intensities and Intensity Ratios of Some Y-rays of the Angular-Correlation Array Gated by (A) the 171.4-keV and (B) the 197.4-keV Transition.

	E_γ (keV)	Relative Intensity		
		Horizontal	Vertical	Ratio
(A)	268.0	3.59	3.46	1.04
	359.5	2.93	2.55	1.15
	441.3	2.04	1.93	1.06
	509.9	2.11	1.79	1.18
	552.9	0.953	0.894	1.07
(B)	122.4	2.26	2.80	0.805
	161.1	5.27	7.02	0.751
	223.1	3.64	6.53	0.557
	252.2	1.99	3.94	0.505
	275.0	1.30	3.28	0.397
	294.2	1.26	3.18	0.398
	313.7	0.782	1.98	0.394
	326.7	0.665	1.70	0.390

[1] The uncertainty is ±10%.

ratios larger than those for pure M1 transitions. Therefore, these transitions are mainly M1 with small portion of E2.

4. The Continuum Spectrum

The continuum spectrum of this experiment was analyzed using the same method as described in Section A.3. Figure V-37 shows cuts obtained for the 800- and 870-keV regions. Values of $\mathcal{J}^{(2)}$, the dynamic moment of inertia, were 58.8 and 76.9 $\hbar^2$ MeV^{-1}, respectively. The latter value already approaches the value for a superdeformed band. However, we could not obtain nice cuts showing the ridges beyond 1000 keV.

C. DISCUSSIONS AND CONCLUSIONS

1. Level Scheme

The two sets of transitions that are strongly coincident within the groups are summarized in Table V-4 with their energies, intensities (I_γ, corrected for detector efficiency), and total transition intensities (I_t, corrected for assigned multipolarity). The intensities are from sum-gated coincidence spectra and were normalized to a selected transition of each group (171.4 and 122.4 keV, respectively, for group A and B). It is not very meaningful to extract intensities, because some of the transitions in group A are not only in coincidence in ^{176}Re, but also in coincidence in ^{177}Re; thus, their intensities arise from both nuclei. However, this table is most important for those transitions with energies above 550 keV. They are not contaminated, and their

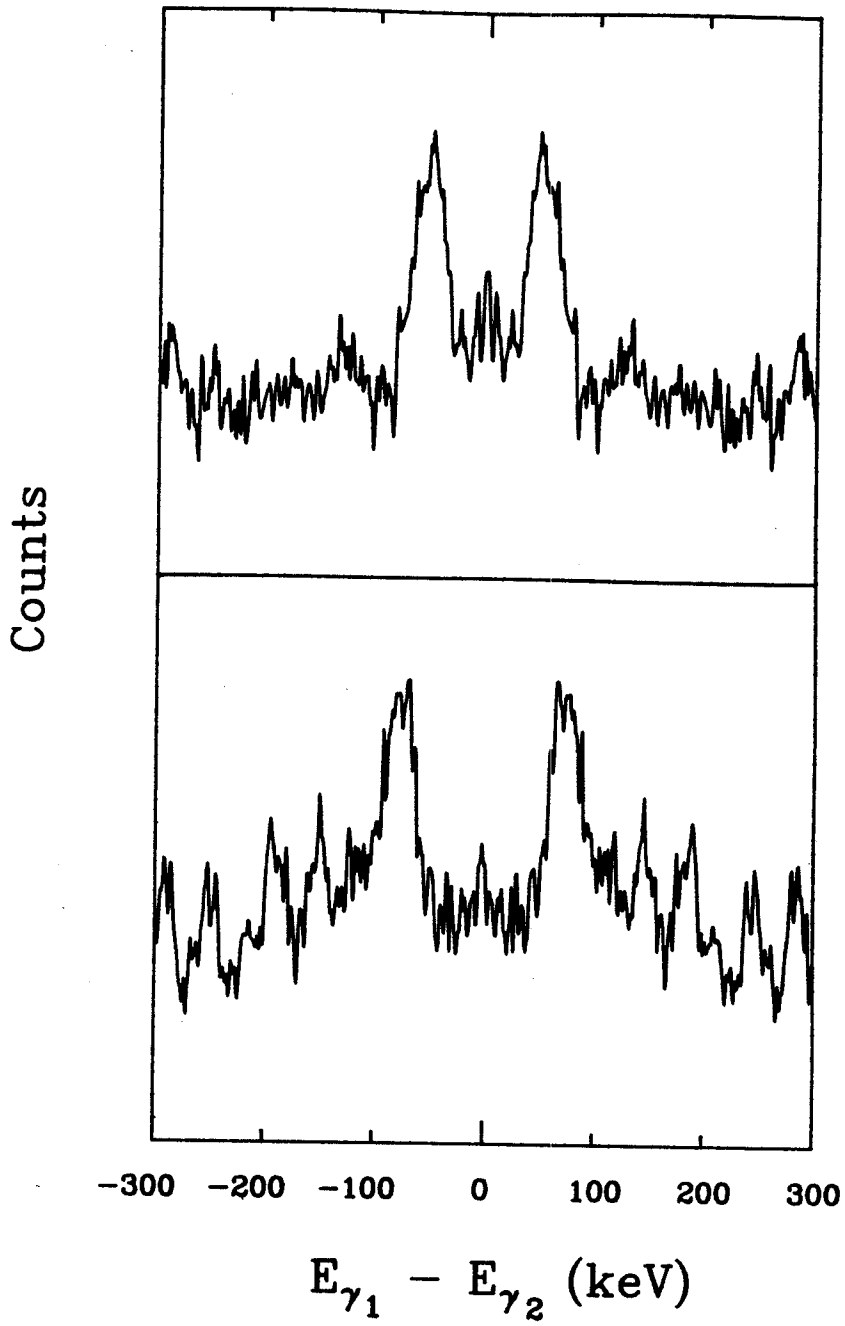

Figure V-37. Cuts perpendicular to the diagonal in the symmetrized E_{γ_1} - E_{γ_2} matrix from the $^{165}Ho(^{16}O,5n\gamma)^{176}Re$ reaction. Top: 800-keV region. Bottom: 870-keV region.

Table V-4. γ-ray Energies, Intensities, and Total Transition Intensities from the Reaction $^{165}Ho(^{16}O,5n\gamma)^{176}Re$.

(A)

E_γ (keV)	I_γ	I_t	Multipolarity
171.4	100	≡100	E2
268.0	172(9)[1]	122	E2
359.5	172(9)[1]	114	E2
441.3	163(8)	106	E2
509.9	266(13)[1]	167	E2
565.7	95(8)	59	E2
601.0(0.8)	89(9)	56	E2
552.9	76(6)	48	E2
596.5(0.8)	66(7)	41	E2
661.8(0.6)	55(4)	35	E2

* The uncertainty in energy is ±0.2 keV unless otherwise indicated.
[1] These transitions are contaminated by ^{177}Re, and the contaminant transitions are in coincidence with each other.

Table V-4. (cont'd.).

(B)	E_γ (keV)	I_γ	I_t	Multipolarity
	99.6	42(2)	65	M1
	122.4	100	≡100	M1
	161.1(0.5)	146(15)[3]	87	M1
	197.4	142(15)[2]	63	M1
	223.1	133(10)	51	M1
	252.2	118(18)	41	M1
	275.0(0.5)	118(21)[3]	38	M1
	294.2(0.5)	124(25)[3]	39	M1
	313.7	87(9)	26	M1
	326.7	77(8)	23	M1

[2] Unresolved multiplets in spectrum.
[3] Contaminated by neighboring nuclei.

orders within the bands strongly depend on their intensities. We propose the level scheme as in Figure V-38.

2. The 171.4-keV Band

The spacings of this band are too large for typical $\Delta I=1$ M1 intraband transitions for well-deformed nuclei in this region. Comparing these spacings with neighboring nuclei, they appear like the $\Delta I=2$ E2 transitions of the ground-state band of even-even W [Dr78] or Os [Dr82] nuclei or the K=1/2 decoupled band of the odd-mass Re nuclei [Ne76,Ya83]. Indeed, several other odd-odd nuclei in this mass region show similar characteristics, and this kind of rotational band is called a doubly-decoupled band, as was discussed in Chapter III. Checking the low-lying single-particle orbits of the neighboring odd-proton Re and odd-neutron W and Os nuclei, we find that both odd-proton and odd-neutron $\Omega=1/2$ orbits (proton 1/2[541] from $h_{9/2}$ and neutron 1/2[521] from $p_{3/2}$) lie very low in excitation energy. Therefore, it is very possible that they couple together in ^{176}Re. We thus believe these transitions must be the components of $\Delta I=2$ E2 transitions of a doubly-decoupled band. Santos et al. [Sa89], who also studied ^{176}Re at about the same time as we did, have also assigned this as a doubly-decoupled band. However, they observed only up through the 509.9-keV transition. They measured the internal conversion coefficients for these lower-lying transitions and adopted E2 multipolarity for all of them. Another proof comes from the directional-correlation intensity ratios listed in Table V-3, where we assumed the 171.4-keV transition was a quadrupole transition.

As stated in Chapter III, the spin of the lowest state of the

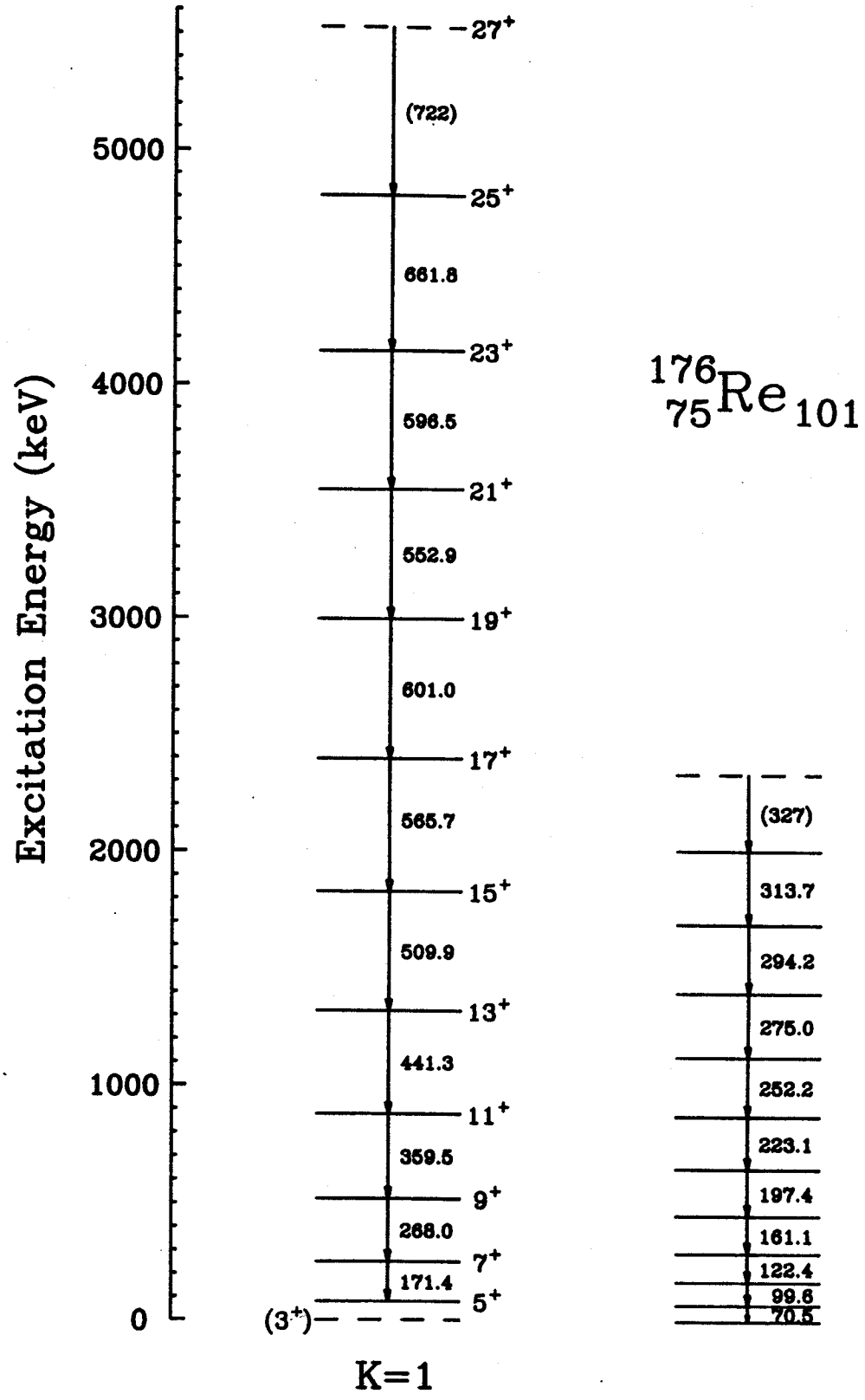

Figure V-38. Partial level scheme of ^{176}Re.

doubly-decoupled bands seems to be correlated with the spin of the lowest state of the K=1/2 decoupled band of the neighboring odd-proton nuclei. 3^+ is believed to be the spin of the lowest state of ^{176}Re based on this hypothesis. Therefore, we need to determine whether the lowest energy transition, 171.4 keV, is the 5 → 3 transition or not. A characteristic of doubly-decoupled bands is that their spacings are similar to those of the ground-state band of the even-even core and those of the K=1/2 decoupled band of the neighboring odd-mass nucleus [St76,Kr86a,Kr87a]. We thus compare the doubly-decoupled band of ^{176}Re with its counterpart in ^{174}W and ^{177}Re in Figure V-39. (We should compare it with ^{175}Re , but since that is unknown, we take ^{177}Re and include ^{176}W as well.) Similarities can be found in ^{172}Ta [Kr88a] and $^{182-186}$Ir [Kr85,Kr86a]. It is apparent that 171.4 keV is too large for a 5 → 3 transition but is suitable for a 7 → 5 transition. Comparison with other doubly-decoupled bands suggests that it is a 7 → 5 transition. Actually, a simple way to solve this question is to use the fact that the moment of inertia of an odd-odd nucleus is larger than that of the neighboring odd-mass nucleus. Then we can use Equation II-1 and get a feeling for the spin of the level from which the 171.4-keV γ-ray originates.

Then, why did neither we or Santos et al. observe the 5 → 3 transition? Could it be that 5^+ is the spin of the lowest state of the ^{176}Re doubly-decoupled band? The energy of the 5 → 3 transition of the ^{172}Ta and ^{174}Ta doubly-decoupled bands is around 80 keV. The internal-conversion coefficient for a 75-keV E2 transition is 15.2 and for a 82-keV transition is 9.55 [Rö78b]! Thus, we could not have observed such a transition. In the gated LEPS spectrum (Figure V-22), a peak seems to

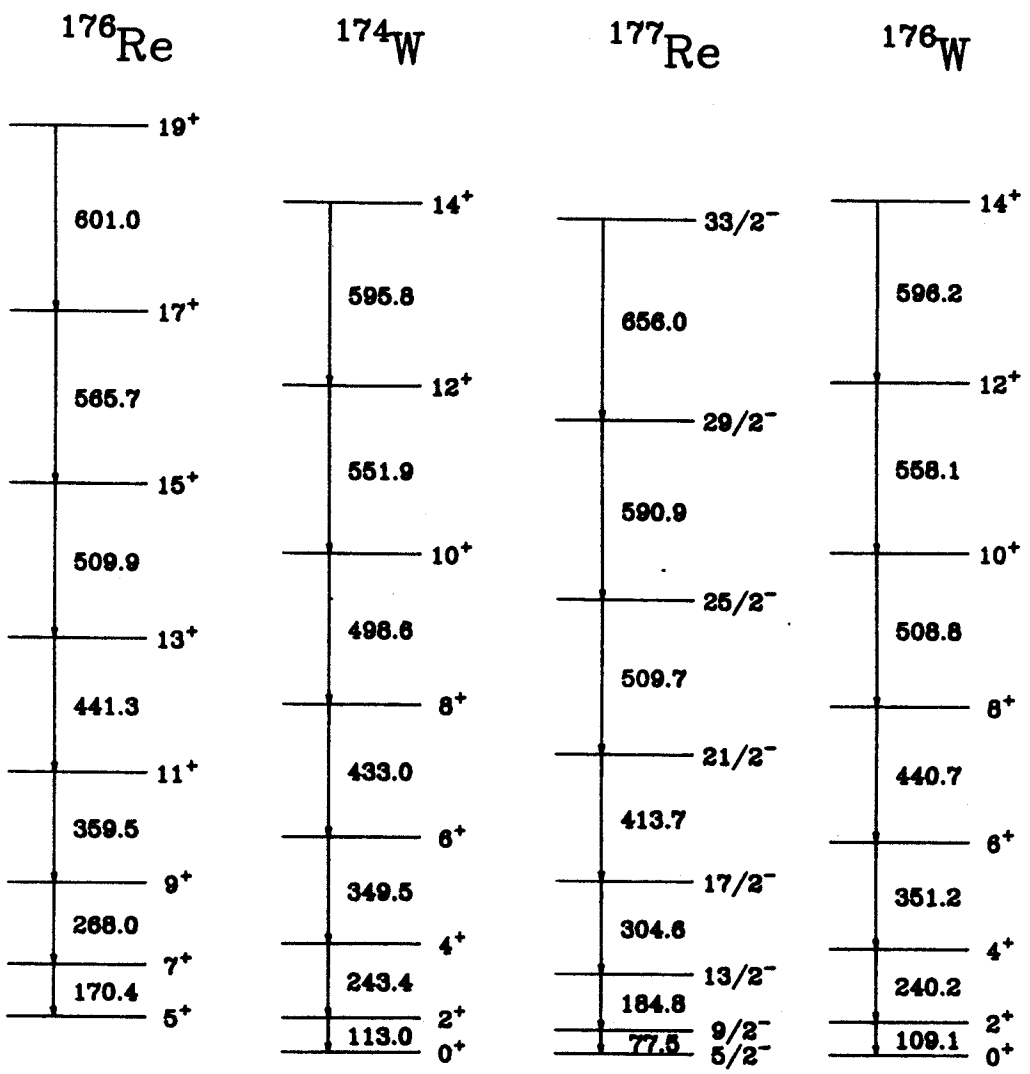

Figure V-39. Comparison the first few transitions of the doubly-decoupled band of ^{176}Re, with those of the K=1/2 band of odd-mass ^{177}Re and of the ground-state band of even-even W isotopes.

be enhanced when compared with the total coincidence LEPS spectrum (Figure V-21). Its energy is about 85 keV. This could be a candidate for the 5 → 3 transition we were looking for. However, this is such weak evidence that we can not make any definite assignments. It certainly needs careful study to find out whether there is a 5 → 3 transition for ^{176}Re, and, if so, what its energy is.

In conclusion, we have observed eleven transitions from the doubly-decoupled band and observed spins up to I=27. The band has positive parity, as both the available proton and neutron Ω=1/2 orbits have negative parities. The spacings of the first few transitions do increase smoothly, but become irregular at I=21. This indicates backbending. We thus plot I_x versus hω (rotational frequency, $\approx E_\gamma/2$) in Figure V-40, and this produces a typical backbending curve. In order to make it more obvious, we also plot the alignment i_x versus hω in Figure V-41, along with that of nearby even-even W isotopes [Dr78] and of ^{177}Re [Ya83]. i_x was calculated by the Harris formula (Equation III-4), and J_0 and J_1 were derived by least-squares fitting of the first few data points. $J_0 = 38.2\ \hbar^2\ \text{MeV}^{-1}$ and $J_1 = 86.2\ \hbar^4\ \text{MeV}^{-3}$ were obtained.

The crossing frequency in the ^{176}Re band is very close to that in ^{174}W and even might be slightly lower. The $i_{13/2}$ neutrons are typical of backbending for this mass region. The doubly-decoupled band does not occupy $i_{13/2}$ neutron orbits, so it does not block the available orbits for backbending [Ri81]. The odd-neutron in ^{176}Re weakens the pairing correlations [Di83,Ga82]; thus, it makes the backbending a little easier than in the even-even core nucleus. On the other hand, the odd-proton drives the nucleus to larger deformation [Be88,Ga88] and makes the backbending more difficult. These two factors seem to cancel each other

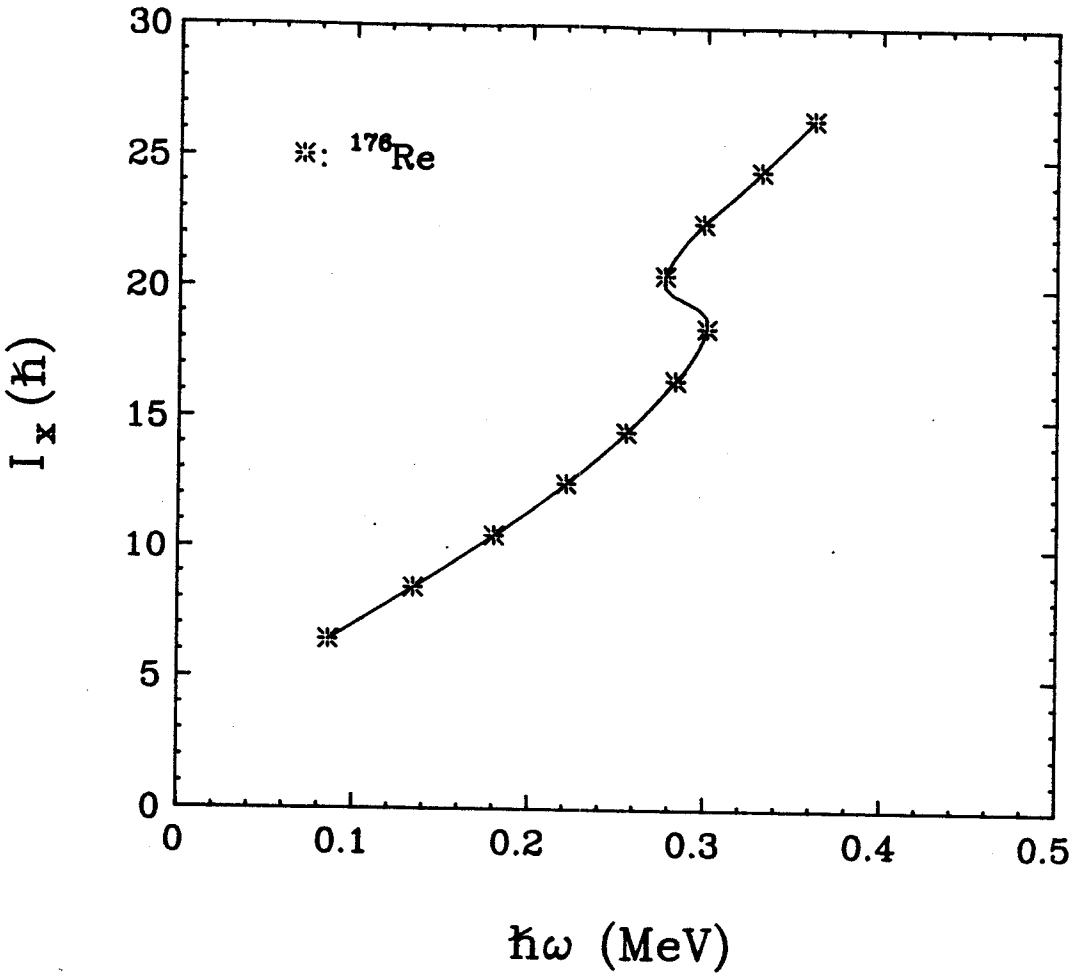

Figure V-40. Plot of I_x versus $\hbar\omega$ of the 171.4-keV band of ^{176}Re.

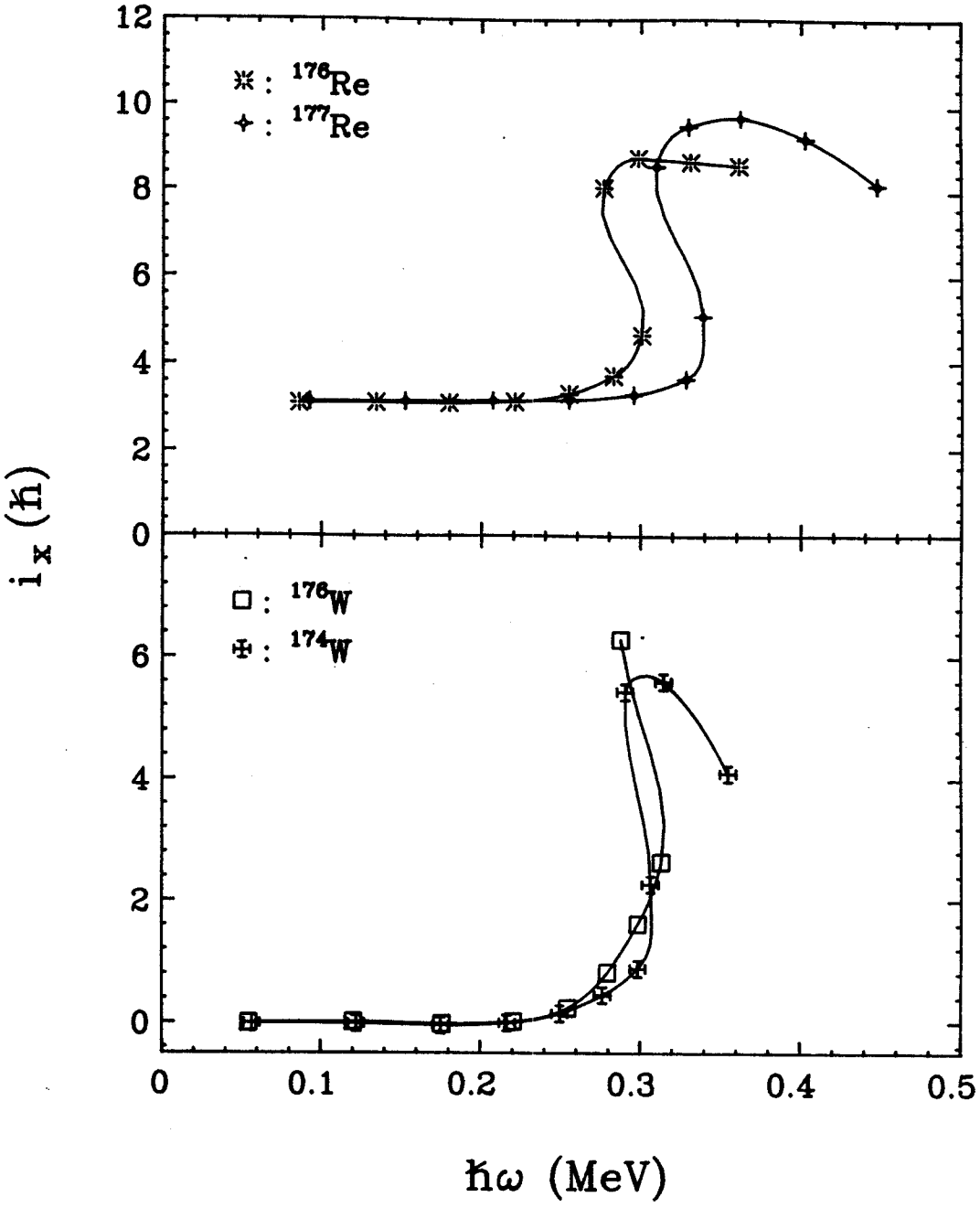

Figure V-41. Plot of alignment (i_x) versus rotational frequency ($\hbar\omega$) of ^{176}Re, ^{177}Re, ^{174}W, and ^{176}W.

out, resulting in nearly the same crossing frequency as in ^{174}W. Conversely, the odd-proton band in ^{177}Re backbends at higher frequency because it does not have the odd-neutron to compensate the deformation change driven by the odd-proton. Studies [Ja88a,Ka78,La86,Ra86] have shown that $h_{9/2}$ protons align themselves almost simultaneously with $i_{13/2}$ neutrons for the backbending in many nuclei in this mass region. However, this would not occur for ^{176}Re, because the $h_{9/2}$ proton orbits have been blocked, and, if the protons were responsible for backbending, it would occur at higher frequency then that for the even-even core nucleus. A cranked-shell model calculation of ^{176}Re [Xu89] predicts that the crossing frequency for $i_{13/2}$ neutrons is 0.33 MeV and for $h_{9/2}$ protons is 0.48 MeV. These results also support the conclusion that alignment of a pair of $i_{13/2}$ neutrons causes backbending in the doubly-decoupled band of ^{176}Re.

3. The 99.6-keV Group

The spacings of γ transitions of this group increase regularly and are comparable to ΔI=1 intraband transitions in nearby nuclei. The intensity ratios from the angular-correlation experiment reveal that these transitions are most likely M1 transitions mixed with a small amount of E2. Therefore, we suggest this group of γ transitions forms a "normal" rotational band. We observed neither cross-over transitions nor any connection between this band and the 171.4-keV band. Therefore, spin cannot be assigned uniquely.

This band was also reported by Santos et al. [Sa89], and we agree on the energies of the transitions commonly identified. However, Santos et al. observed a 70.5-keV transition, which also appeared to be in

coincidence with the 99.6-keV transition, etc., and was placed as the first transition in the band. The Ge spectrum at that energy region in our ^{22}Ne beam experiment was entirely blocked by x-rays, so no Y-ray could be resolved. We have looked for this 70.5-keV transition in the LEPS spectrum, and we might see it as a slight bump (Figure V-23). Based on the spectra of Santos et al., we believe this transition is in coincidence with others, but how they defined a coincidence event is not clear. This transition was not clearly seen in the experiments with ^{16}O beam, either. An energy gate was set on where the peak is supposed to be, but no conclusions can be drawn from this gated-coincidence spectrum.

We think the 99.6-keV transition is delayed, as discussed before. Santos et al. [Sa89] did not perform delay analysis, nor can we confirm its being delayed by doing delay analysis of the data from SUNY Stony Brook because of the limitation of that set-up. This 99.6-keV Y-ray was quite strong in the singles spectrum from our excitation-function experiments but weak in the total-coincidence spectrum. However, comparing the singles spectrum (see Figure V-25) with the coincidence spectrum (Figure V-27), we find a severe cut-off below roughly 150 keV in the coincidence spectrum. The intensity of the 99.6-keV transition (Table V-4) is less than that of the 161.1- or 194.4-keV transition, even after correcting for internal conversion. This might be a sign that the 99.6-keV Y-ray is indeed delayed, but we are not sure how much the cut-off affects the collection of data from this transition.

Santos et al. [Sa89] have discussed a possible configuration for this band. They think it is a rather compressed band, based on the first two transitions (70.5- and 99.6-keV), and this reflects the

coupling of a odd-particle having a large decoupling constant. Table V-5 lists the low-lying single-particle orbits [Sa89] from nearby odd-mass nuclei, along with their excitation energies. The excitation energies of proton orbits come from ^{177}Re, while those of neutron orbits are taken from an average of ^{175}W [Wa78] and ^{177}Os [Dr83]. Two orbits show such characteristics, $\pi 1/2^-[541]$ and $\nu 7/2^+[633]$. Coupling of the former with $\nu 5/2^-[512]$ is not a favored choice, because the spin of such a band is too low for receiving such large population in high-spin reactions. Thus, the only candidates left are couplings of the latter with $\pi 5/2^+[402]$ or $\pi 9/2^-[514]$. Santos et al. favored the $\pi 5/2^+[402]$ coupling because a similar band was found in ^{180}Re. Their arguments, based on the structure of the band and systematics, probably are the best one can do under such circumstances. Although this band would have a rather high excitation energy (≈300 keV from Table V-5), its high K value and involvement of the highly-decoupled neutron orbit would compensate for the energy factor.

The discussions of Santos et al. are based on the fact that the 70.5- and 99.6-keV transitions belong to the same band as the 122.2-keV and other transitions. However, our studies indicated that the 99.6-keV transition is delayed. If this is indeed true, the configuration assigned by Santos et al. would not be appropriate, because then the 70.5- and 99.6-keV transitions cannot belong to the same band as the 122.4-keV transition. Now this band looks rather regular, neither compressed nor staggered. Therefore, the configuration should not involve orbits such as $\pi 1/2^-[541]$ and $\nu 7/2^+[633]$, and possible configuration are couplings of $\pi 5/2^+[402]$ or $\pi 9/2^-[514]$ with $\nu 5/2^-[512]$ or $\nu 1/2^-[521]$. We plot the predictions of IBFFA calculations, which

Table V-5. Zeroth-Order Estimates of the Energies (in keV) of the States in ^{176}Re from Couplings of the Nilsson Orbits in the Neighboring Odd-Mass Nuclei. Only Triplet Couplings Are Listed.

	$1/2^-[541\downarrow]$	$5/2^+[402\uparrow]$	$9/2^-[514\uparrow]$
	0.0	0.085	≈0.04
$1/2^-[521\downarrow]$	3^+	2^-	4^+
0.0	0.0	0.085	≈0.04
$5/2^-[512\uparrow]$	2^+	5^-	7^+
0.128	0.128	0.213	≈0.168
$7/2^+[633\uparrow]$	3^-	6^+	8^-
0.268	0.268	0.353	≈0.308

will be discussed in details in Chapter VI, of all the states from Table V-5 in Figure V-42, along with 122.4-keV and other experimental transitions in the band. As expected, bands numbered 5, 6, 7, and 8, those involving coupling of $\pi 1/2^-[541]$ or $\nu 7/2^+[633]$, are either compressed or staggered (or even invert the level orders); thus, they can be excluded. None of the remaining four calculated bands gives such good agreement with experimental data that we can definitely assign it to be the correct configuration. However, bands 1 and 4 ($K^\pi = 2^-$ and 7^+) seem to give somewhat better spacings than the others.

If the spacings of a rotational band follow Equation II-2, then in the $(E_I - E_{I-1})/2I$ versus $2I^2$, a straight line could be obtained. However, Coriolis effects will distort the regular spacings and zigzag the straight line [S184]. In Figure V-43, the four IBFFA-calculated bands and the experimental energies are plotted in this manner, assuming each of the four possible K values. It is apparent that lines for $K^\pi = 4^+$ and 2^- bands are much zigzagged and the experimental points resemble those of the 5^- and 7^+ bands. This evidence supports the fact that the 122.4-keV and higher transitions form a rather regular band with $K = 5^-$ or 7^+ likely to be correct value.

The IBFFA calculations can also give predictions of B(E2) and B(M1) values. However, this kind of calculation has not proven to be very accurate for odd-odd nuclei (because of lack of experimental data to calibrate and test the model), so we will not discuss this further. We therefore conclude, based on energy spacings and band structure, that 7 is a better spin assignment for the band-head of the band having the first transition at 122.4 keV. Further, we prefer 7^+ also because it is predicted to have lower excitation energy, and its higher spin is more

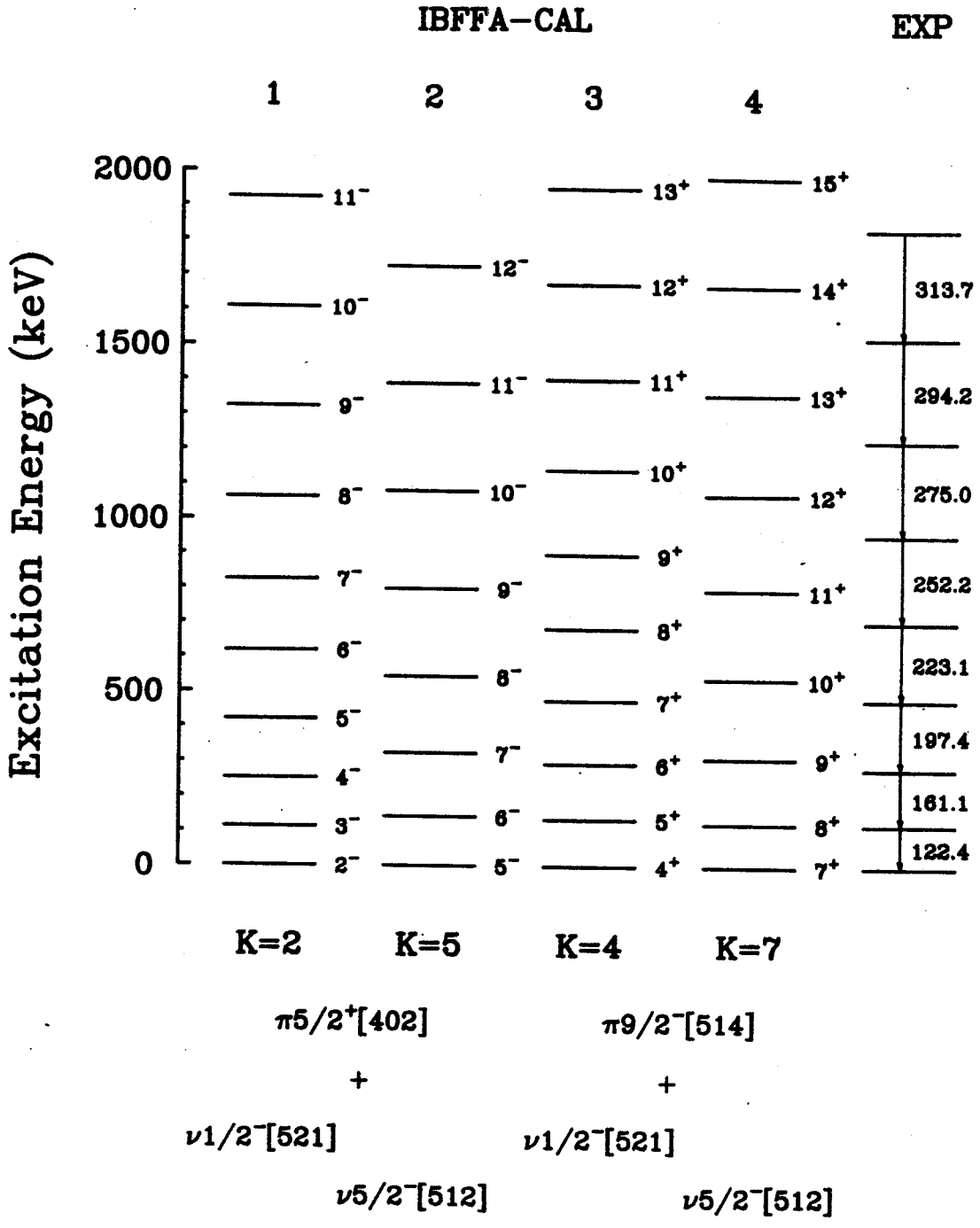

Figure V-42. IBFFA-calculated excitation energies for states in odd-odd ^{176}Re compared with the 122.4-keV band from experiment.

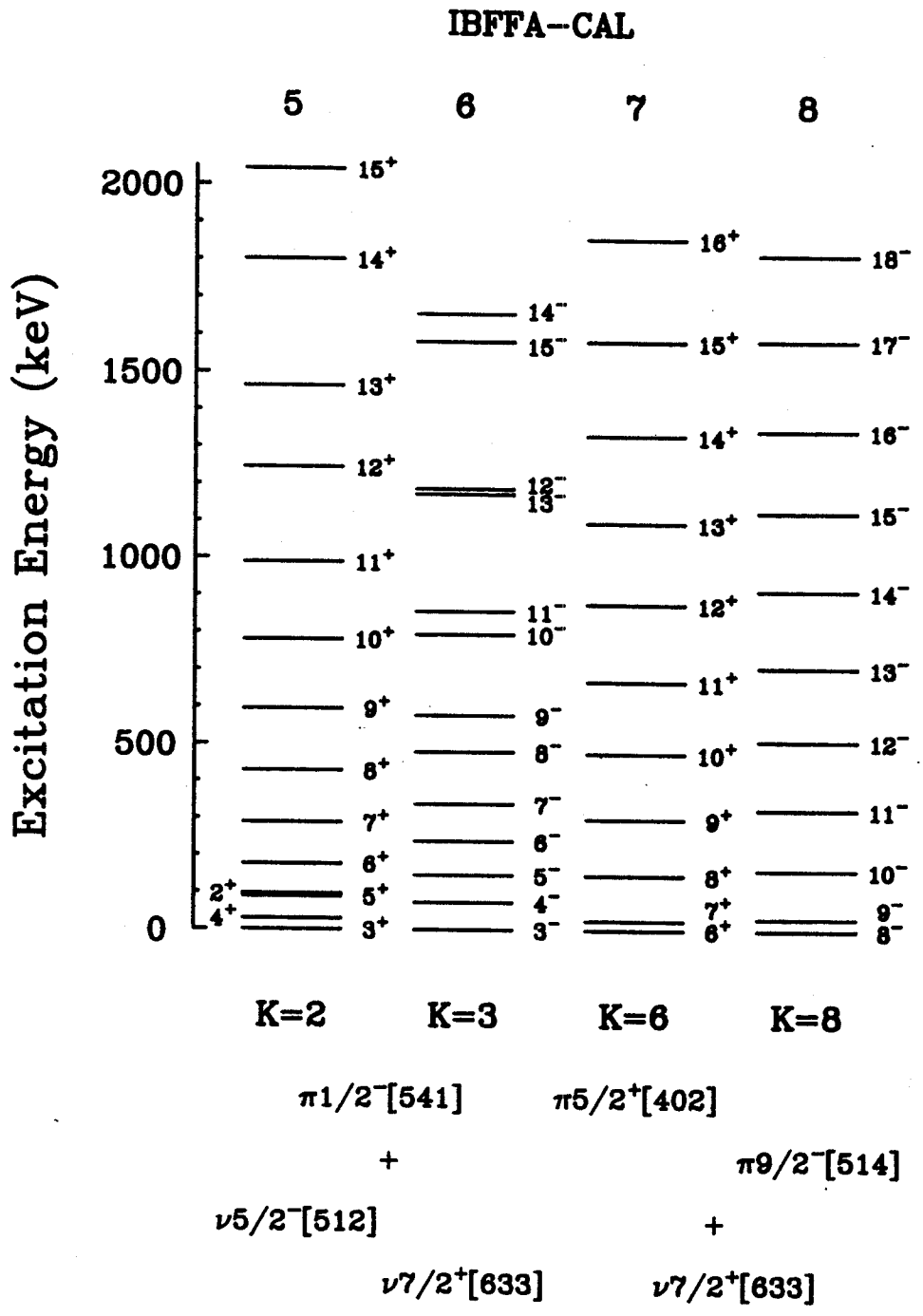

Figure V-42. (cont'd.).

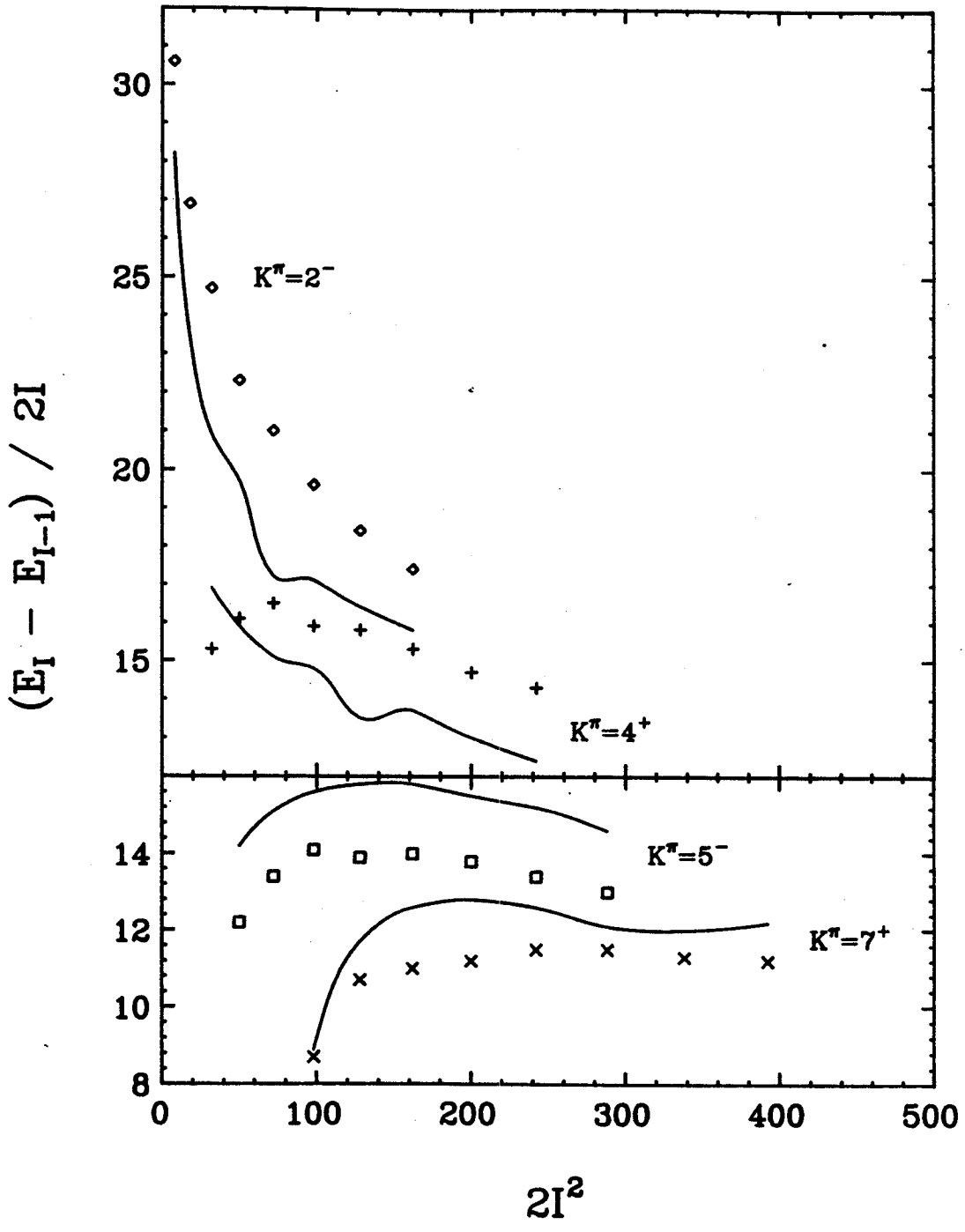

Figure V-43. The IBFFA-calculated bands (curves) and experimental data (symbols) are plotted in the manner of a trumpet plot to emphasize distortions in the spacings.

likely to receive large population from our reactions.

4. The 78.8-keV Transition

In the excitation-function experiments conducted at SUNY Stony Brook, we observed a small 78.8-keV peak. [Recall that in the $^{159}Tb(^{22}Ne,5n\gamma)^{176}Re$ experiment part of the strong 78.8-keV peak came from target Coulomb excitation.] And no 78.8-keV transition was found in the γ-γ total-coincidence spectrum. The same limitations affecting the detection of the 99.6-keV γ-ray also affect this transition. Santos et al. [Sa89] did not mention this transition. (There is a peak having an energy of about 79 keV in the singles spectrum, but they assigned it to a transition from ^{177}Re decay.)

If this 78.8-keV γ-ray is real and the 171.4-keV state does decay through by this transition, then the level which this transition decays to must be the ground state or lie very close to it. The spin of the ground state of ^{176}Re was tentatively assigned 3^+ from studies of its decay to ^{176}W [Ho76]. The only likely candidate for a 3^+ state is $\pi 1/2^-[541] \times \nu 1/2^-[521]$, but this is the configuration of the doubly-decoupled band and could not do for the level here. However, the three proton orbits in Table V-5 lie very closely together in ^{177}Re, and their order could be inverted by the proton-neutron residual interactions in the odd-odd nucleus. Besides, the order of these orbits is unknown in ^{175}Re, so the predictions of excitation energies could very well be different from those listed in Table V-5. The spin 3 assigned to the ground state of ^{176}Re was based on the fact that it decays to both 4^+ and 2^+ states of ^{176}W and on systematics of adjacent odd-mass nuclei

[Hr75]. This is a very shaky assignment when the odd-particle states are not well understood.

5. The other 197.4-keV Transition

There are two 197.4-keV transitions in the experiment conducted at NSCL MSU. One is found in coincidence with the 122.4-keV group, and the other with the 315.1- and 420.5-keV γ-rays. The spacings of these three transitions are similar to that of the doubly-decoupled bands, and we thought this might be another doubly-decoupled band or the unfavored signature of the band (with even-spin). However, such a situation was not seen in the spectra collected at SUNY Stony Brook. Therefore, we suspect the 197.4-, 315.1-, and 420.5-keV γ-rays come from a neighboring nucleus. In reviewing the total-coincidence spectrum, we found that γ-rays of ^{176}Re were stronger than those of ^{177}Re in the experiments using the ^{22}Ne beam. This means that the beam energy lies most likely towards the lower-mass side of the excitation function, so some ^{175}Re might be produced. On the other hand, in the ^{16}O beam experiments, because of the ≈51.7 mg/cm^2 thick target, the beam eventually got stopped inside the target (the stopping range for a 96-MeV beam is 43.3 mg/cm^2), and was able to produce large amounts of ^{177}Re. This can be seen in the spectra, where transitions from ^{177}Re were the strongest ones. More important, the intensities of these three transitions became quite strong at higher beam energies (for example, 115- to 130-MeV). Therefore, we prefer that the 197.4-, 315.1-, and 420.5-keV γ-rays are transitions from the K=1/2 decoupled band of ^{175}Re. Indeed, the spacings of the K=1/2 bands of odd-mass Re isotopes increase with

decreasing mass number, and the three transitions here can fit into the trend very well.

D. SUMMARY

From the results of our $^{159}Tb(^{22}Ne,nY)$ and $^{165}Ho(^{16}O,nY)$ reactions and the results of Santos et al. [Sa89], two rotational bands have been confirmed for odd-odd ^{176}Re. One of the two bands is the doubly-decoupled band, such a band having been found for a series of odd-odd nuclei in the mass region 172-186. The band is established up to spin 27, but the lowest level of the band is not clear. The observation of this band supports the mechanism [Sl84] of heavy-ion compound-nucleus reactions forming particle states highly-aligned with rotation, with the subsequent Y-ray cascades feeding down through similar states.

The other band is a rather normal rotational band with $\Delta I=1$ intraband transitions. There are a few possible configurations for this band. However, to narrow down the choice, one needs to confirm whether or not the 99.6-keV transition is a delayed transition. The status of the 78.8-keV transition is also questionable; also, the spin of the ground state.

We have analyzed the continuum spectra from both experiments. None of the experiments showed us a clear valley along the diagonal line above 1 MeV for an extensive range, say 0.5 MeV, in the symmetrized E_{γ_1} - E_{γ_2} matrix. Although at some energies, the dynamic moment of inertia is comparable to that of a superdeformed band, the absence of a well-

established valley prevents us from drawing firm conclusions. Nevertheless, it is clear that the nucleus becomes much more deformed as excitation energy goes up.

Both reactions we used are suitable for producing ^{176}Re, if the right beam energy and thickness of the target are chosen. In future experiment will be important to lower the threshold in order to see low energy Y-rays and resolve those Y-rays from contaminations such as x-rays. It will also be necessary to obtain half-life information and perform delay analysis, since meta-stable states are quite common in this mass region. Of course, statistics are very important for observing weak high-spin transitions. To resolve the problem of so many similar transitions in neighboring nuclei, some methods for filtering the interesting nucleus from others, such as collecting three-fold coincidence data or perform doubly-gated coincidence analysis will be essential.

CHAPTER VI

THE INTERACTING-BOSON MODEL

A. INTRODUCTION

The interacting-boson approximation (IBA) model was introduced by Arima and Iachello [Ar75b] in 1975. They added monopole s-bosons in addition to the quadrupole d-bosons. The boson number is conserved in the IBA model, which makes different from other boson models. Also, a boson can be regarded as a collective pair of nucleons [Ar77]. The IBA model describes only phenomena which are based on the same collective degrees of freedom [Sc88]. This limitation is the result of a truncated basis set. For low-lying states this is sufficient; however, more complicated phenomena such as backbending can only be described in the IBA framework using an extended model space [Ge80,Ha83].

The IBA model [Ar76a,Ar76b,Ar78,Ar79,Sc79a,Ca78,Ta83] has proven to be able to give a rather accurate description of the properties of low-lying collective states in even-even nuclei. Likewise, its extension to odd-mass nuclei, the interacting-boson-fermion approximation (IBFA) model [Ia79,Sc82b,Sc84a,Sc85a,Sc85b], is able to reproduce a large variety of properties in phenomenological calculations. In this chapter we shall examine the extension of the model to odd-odd nuclei, where we call it the interacting-boson-fermion-fermion approximation (IBFFA) model.

Odd-odd nuclei have been calculated before in the framework of the IBA model. The earliest calculations were done using supersymmetries [Ba81,Hu84] and were applied to nuclei in the Pt-Au region. With the use of these symmetries it becomes possible to treat rather complicated systems in a very simple manner. The disadvantage of such methods is that they assume the Hamiltonian of the system exhibits specific

symmetries. In realistic cases such symmetries are present in only relatively few nuclei. The large majority of nuclei do not lend themselves to such treatment; hence, a full numerical treatment has to be done. Paar et al. [Pa87] and Blasi et al. [Bl] have performed calculations of this sort. However, in order to keep the calculations tractable, they had to limit themselves to only the unique-parity orbits. Similarly, calculations of two-quasiparticle states in even-even nuclei [Ba81,Br84,Fa83,Ge80,Lo86] within the IBA framework have been limited to unique-parity orbits. In our present work we present calculations for odd-odd nuclei where there is no restriction to unique-parity orbits. These calculations were made possible by the particular, very efficient model-space truncation scheme used.

We selected the present odd-odd isotopes of Re because of our long-standing interest in these nuclides and because reasonably well-understood experimental data exist for some of the odd-odd isotopes and for many nearby odd-mass nuclides.

In Sec. B we present a short outline of the IBA model and its applications to the even-even Os isotopes. These will serve as the cores to which the odd particles are coupled in the subsequent calculations for the odd-mass nuclides and odd-odd Re isotopes. In Sec. C we discuss the case of the coupling of a single odd particle to the core, the IBFA model. There we present our results for the odd-mass Re and Os isotopes. These calculations serve to determine the parameters that govern the coupling of the odd proton and odd neutron to the even-even Os cores. In Sec. D we cover the actual calculations for the five odd-odd Re isotopes, including an outline of the IBFFA model used and

some details of the calculations. Finally, in Sec. E we summarize our results and make comparisons with experimental data.

B. THE EVEN-EVEN $^{176-186}_{76}$Os CORES

1. Excitation Energies

To described the structure of an odd-mass or an odd-odd nucleus in the IBA model, first a description of the appropriate even-even core should be obtained. Only the valence nucleons are important when counting the number of bosons [Sc80]. However, if the shell is more than half filled, then the number of hole-pairs should be considered. Since in the $^{180-184}_{75}$Re nuclei both the protons and the neutrons are past the middle of the 50-82 and 82-126 major shells, respectively, the $^{A+2}_{76}$Os nuclei constitute the even-even cores. The bosons are hole-like, and therefore only the degrees of freedom of holes should be coupled to the system of bosons. On the other hand, $^{176,178}_{76}$Os nuclei are the even-even cores for ^{176,178}Re, and now the neutron bosons are particle-like. In Table VI-1, we list the even-even cores, the number of particles (outside the closed shell) or number of holes (toward the next closed shell), total number of bosons considered, and the odd-mass and odd-odd nucleus that will be calculated later using the particular core.

In the odd-odd nuclei we will be interested exclusively in states below 2 MeV in excitation energy. Only the structures of the lowest-lying states in the even-even core will enter into the calculations for these odd-odd states. Since these are predominantly symmetric in the proton-neutron degree of freedom, a description in terms of the IBA-1

Table VI-1. Even-Even Os Cores, Their Number of Particles or Holes, Boson Number, and Related Odd-Mass and Odd-Odd Nuclei Associated with the Cores.

Even-even core	$^{186}_{76}Os$	$^{184}_{76}Os$	$^{182}_{76}Os$	$^{178}_{76}Os$	$^{176}_{76}Os$
Number of neutrons				20	18
or holes	16	18	20		
Number of proton holes	6	6	6	6	6
Total number of bosons	11	12	13	13	12
odd-proton nucleus	$^{185}_{75}Re$	$^{183}_{75}Re$	$^{181}_{75}Re$	$^{177}_{75}Re$	$^{175}_{75}Re$
odd-neutron nucleus	$^{185}_{76}Os$	$^{183}_{76}Os$	$^{181}_{76}Os$	$^{179}_{76}Os$	$^{177}_{76}Os$
odd-odd nucleus	$^{184}_{75}Re$	$^{182}_{75}Re$	$^{180}_{75}Re$	$^{178}_{75}Re$	$^{176}_{75}Re$

model [Sc80], where no explicit distinction is made between proton and neutron excitations, is sufficient. The IBA-1 Hamiltonian in general can be written as

$$H = n_d\varepsilon_d + \kappa''P\cdot P + \kappa'L\cdot L + \kappa Q\cdot Q. \qquad \text{(VI-1)}$$

Here n_d is the number of d-wave bosons at an energy ε_d, P•P represents pairing interactions between bosons, L•L is the "dipole" or angular-momentum interaction, and Q•Q is the quadrupole interaction. The Hamiltonian can be diagonalized numerically, so the IBA model is able to give detailed descriptions of many different nuclei not only the three limiting cases (an anharmonic vibrator [Ar76b], an axial rotor [Ar78], and a γ-unstable rotor [Ar79]), but anywhere in between the three limits. For our calculations a simplified Hamiltonian for an axial rotor was used, which corresponds to $\kappa''=0$. Specifically,

$$L = \sqrt{10}\,(d^\dagger\tilde{d})^{(1)} \qquad \text{(VI-2)}$$

and

$$Q = (s^\dagger\tilde{d} + d^\dagger s)^{(2)} + \chi(d^\dagger\tilde{d})^{(2)}\ . \qquad \text{(VI-3)}$$

The constants, κ, κ', and χ are determined empirically. The program which does the calculation is PHINT [Sc84b]. The set of parameters we used for our calculations, adjusted so as not only to obtain a good overall agreement in the excitation-energy spectra, but also retain consistently varying trends, are list in Table VI-2. $^{186\text{-}194}$Os [Ca78]

Table VI-2. IBA Parameters for the Even-Even Os Core Nuclei.

A		176	178	180	182	184	186
N		100	102	104	106	108	110
ϵ_d	(MeV)	0.54	0.53	0.52	0.50	0.47	0.44
κ'	(MeV)	0.0000	0.0015	0.0025	0.0000	0.0005	0.0015
κ	(MeV)	-0.0140	-0.0150	-0.0160	-0.0200	-0.0235	-0.0245
χ		-1.163	-0.929	-0.760	-0.537	-0.581	-0.514
χ_T		-0.276	-0.263	-0.249	-0.236	-0.212	-0.195
e_B	(eb)	0.136	0.138	0.140	0.142	0.144	0.147

have been calculated before. However, those isotopes have higher mass numbers and are closer to the O(6) limit (an anharmonic vibrator), which corresponds to $\kappa=0$. Thus, their calculations were performed in a perturbed O(6) scheme. Chiang et al. [Ch88a] also calculated $^{180-188}$Os but they used the general Hamiltonian, so their parameters are somewhat different from ours.

The calculated energies are compared with experimental energies in Figure VI-1. Although ^{180}Os was not used for later calculations, we still calculated it in order to maintain smoothly varying parameters through all the Os isotopes. All six isotopes show a well-developed ground-state rotational band, and some of them have ß- or γ-vibrational bands. Our calculations reproduce the general features of these spectra, although they overestimate the staggering in the γ-vibrational bands. However, since these vibrational bands lie at at least several hundred keV above the ground state, they are not crucial for later calculations.

2. Electromagnetic Properties

Since at a later stage we shall calculate electromagnetic properties for the odd-odd nuclei, we need to determine the boson effective charge and the d-boson g factor by reproducing the relevant quantities in the even-even core nuclei.

The operator used in the calculation of quadrupole properties is

$$T^{(E2)} = e_B[(s^\dagger\tilde{d} + d^\dagger\tilde{s})^{(2)} + \chi_T(d^\dagger\tilde{d})^{(2)}] , \qquad \text{(VI-4)}$$

where e_B is the boson effective charge. In the E2 operator the boson

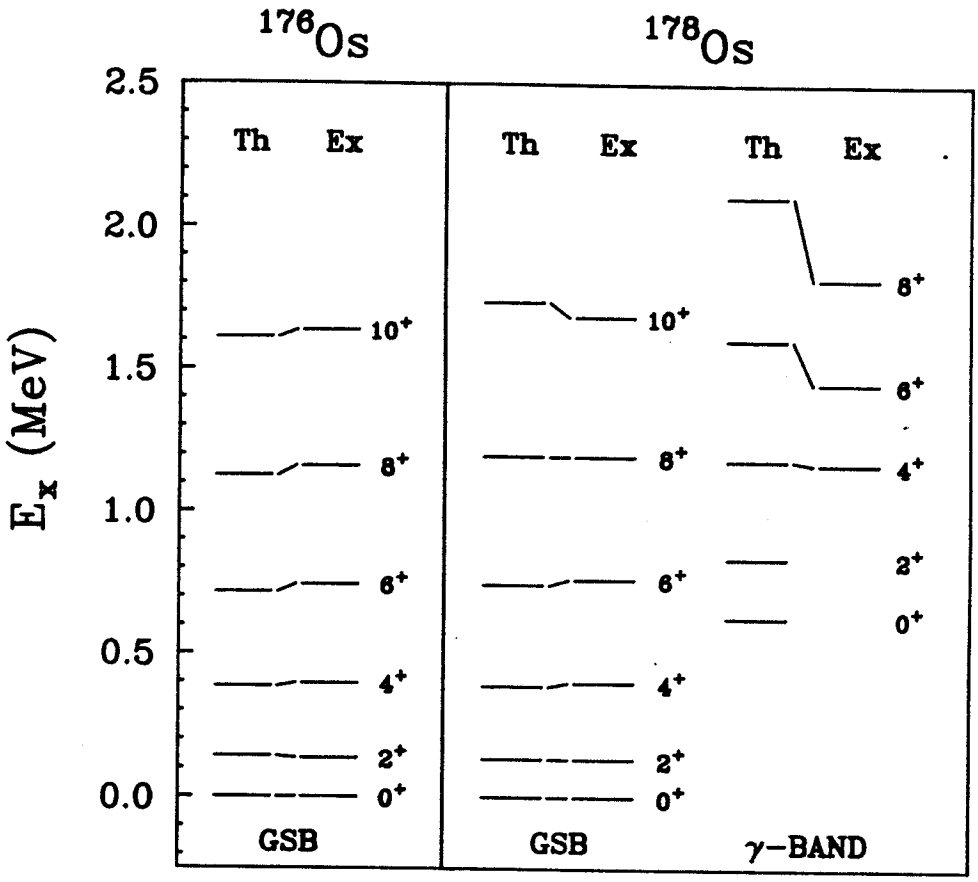

Figure VI-1. IBA-calculated excitation energy spectra for the even-even Os core isotopes compared with experimental data.

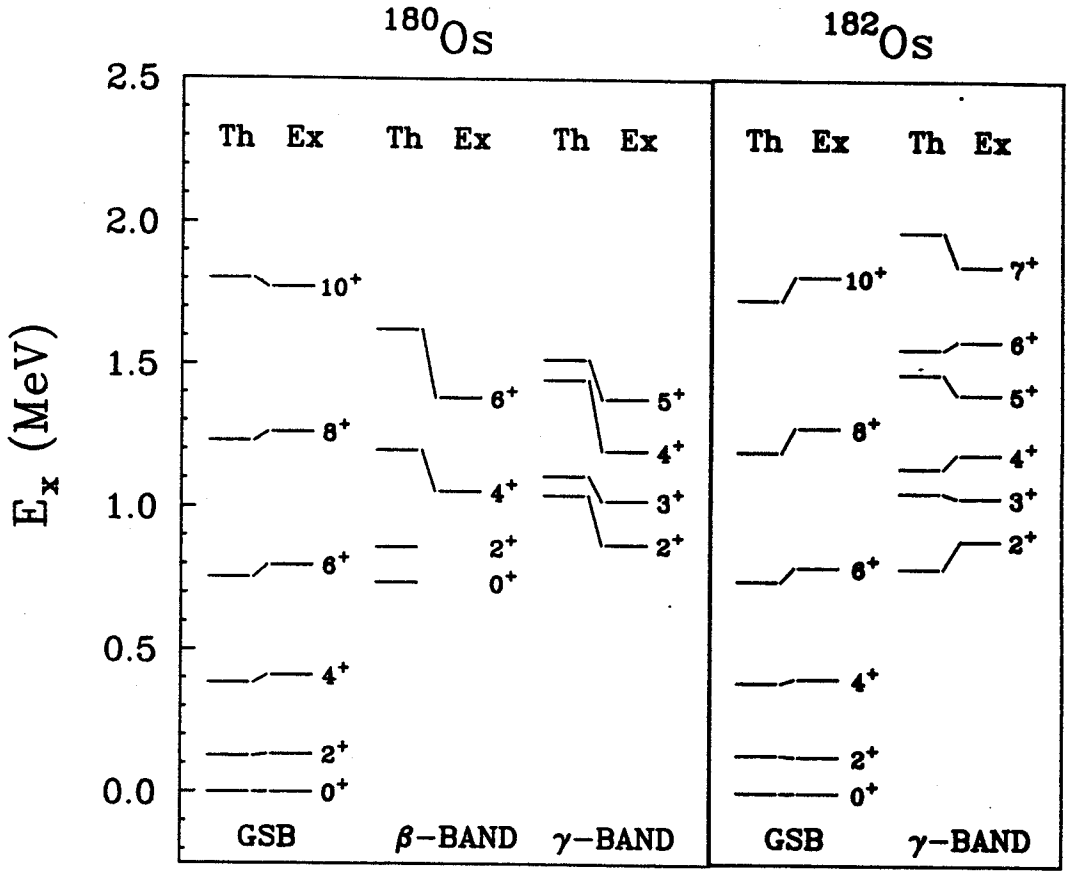

Figure VI-1. (cont'd.).

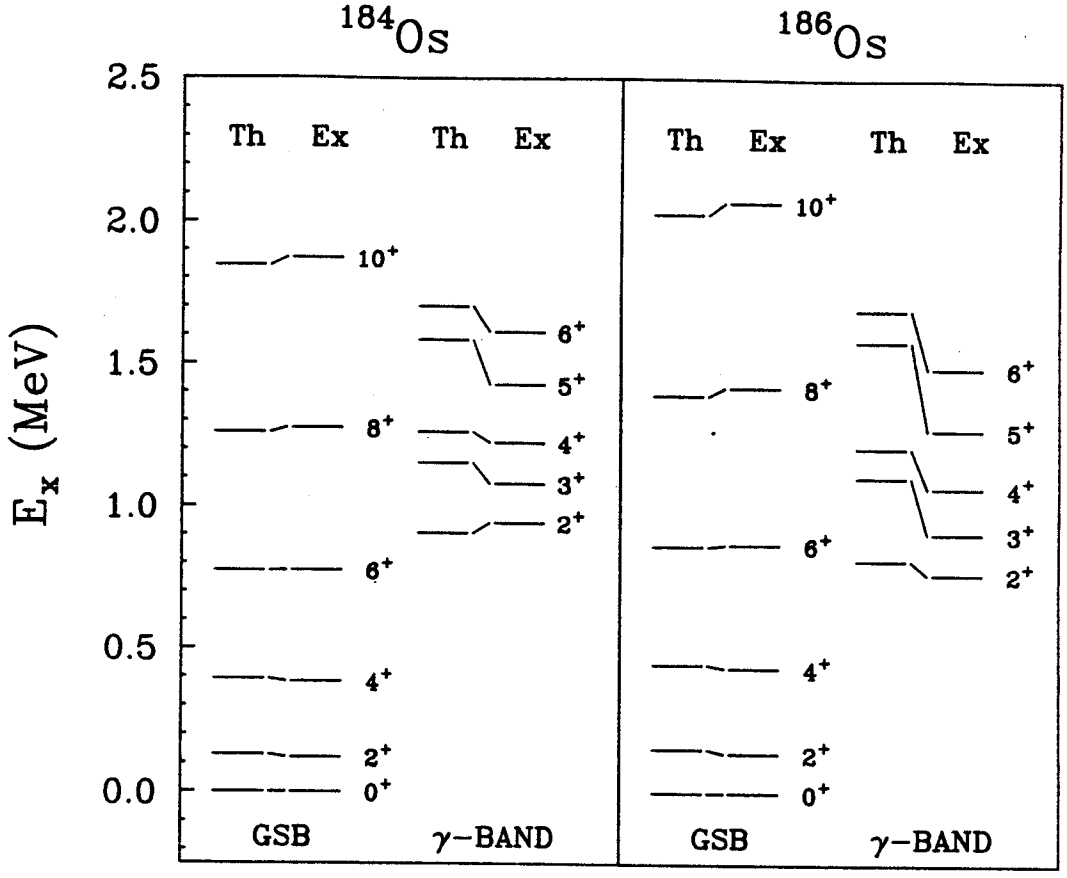

Figure VI-1. (cont'd.).

effective charge and the parameter χ_T were adjusted for $^{182-186}$Os so as to obtain the best overall agreement with the experimental B(E2) values. Purely systematic values were chosen for $^{176-180}$Os because of lack of experimental data.

Some calculated and experimental [Mi71,Ch72,La72,Wa72,Ho77,Ru77, Ra87] B(E2) values for important transitions in the even-even Os isotopes are shown in Figure VI-2, and electric quadrupole moments are shown in Figure VI-3. We used the experimental B(E2) values for the $0_1^+ \rightarrow 2_1^+$ and $0_1^+ \rightarrow 2_2^+$ transitions (the $2_1^+ \rightarrow 2_2^+$ transition was not used because of the possibility of M1 admixture; note that the agreements are less good for this transition) and varied the values for e_B and χ_T in order to get the best fit. (It has been checked for ^{186}Os that other known B(E2) values are also reproduced.)

The M1 operator can be written as

$$T^{(M1)} = g_d\sqrt{10}\,(d^\dagger\tilde{d})^{(1)}\,, \qquad \text{(VI-5)}$$

where g_d is the d-boson g factor. By comparing Equation VI-5 with Equation VI-2, it can be seen that the M1 operator is proportional to the total angular-momentum operator L in the boson space. This operator thus does not induce M1 transitions but only magnetic moments. For even-even medium-heavy nuclei this is realistic, since B(M1) values are indeed very small compared with the magnetic moments. From the value of the known g factors of the 2_1^+ states we deduce that g_d=0.25 nm for the d-boson g factor [Le82].

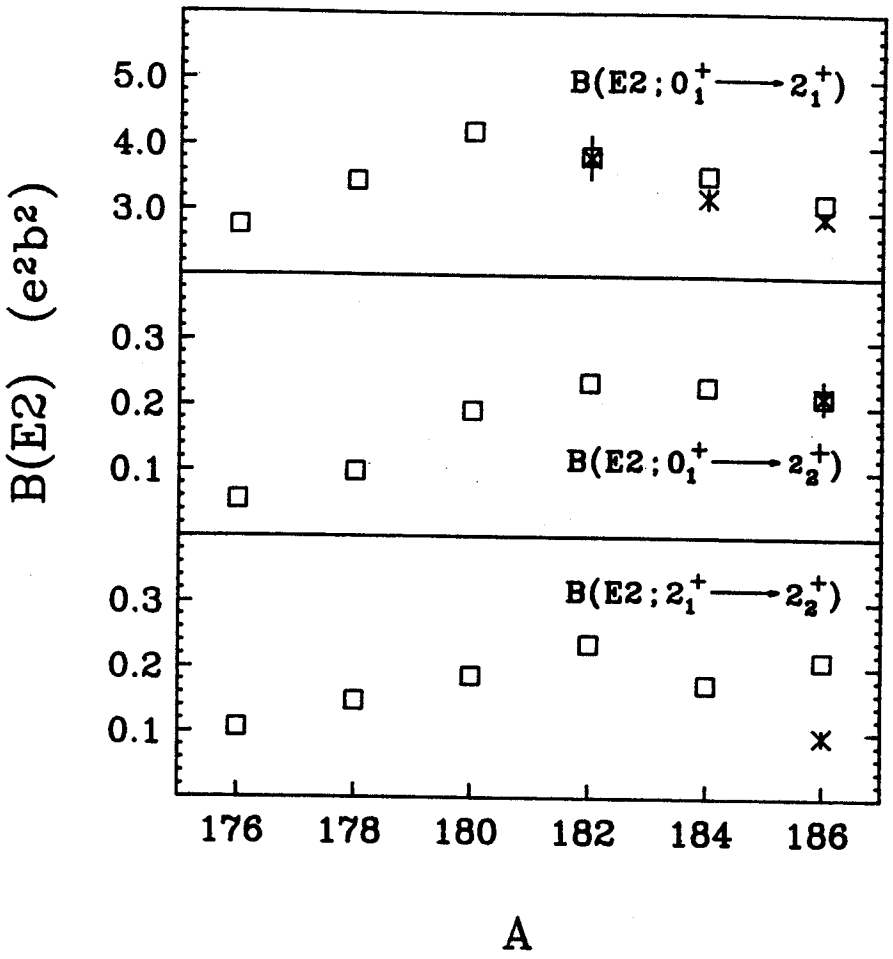

Figure VI-2. IBA-calculated B(E2) values for the even-even Os core isotopes compared with experimental values. The squares are the calculated values; the crosses (with error bars) are the experimental values.

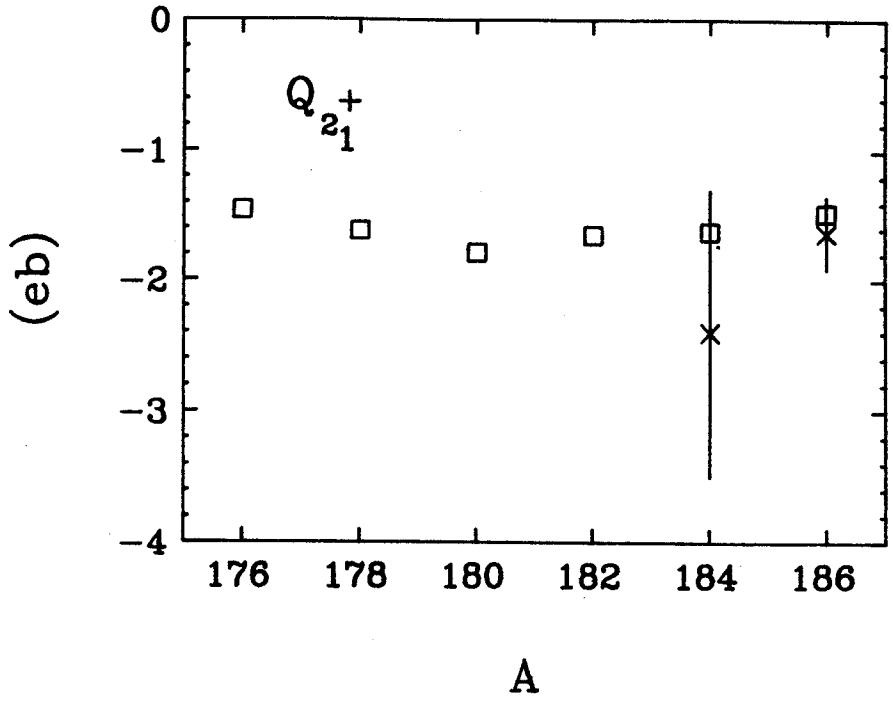

Figure VI-3. IBA-calculated Q values for the 2_1^+ state in the even-even Os core isotopes compared with experimental values. The squares are the calculated values; the crosses (with error bars) are the experimental values.

C. THE ODD-MASS NUCLEI

1. Short Discussion of Theory

Odd-mass nuclei are described in the framework of the IBA model by coupling the degrees of freedom of a single odd particle to the system of s and d bosons that describes the even-even core nucleus. The general Hamiltonian for such a system can be written as [Sc82b,Sc84, Sc85a,Sc85b]

$$H_{IBFA} = H_{IBA} + H_F + V_{BF} , \qquad \text{(VI-6)}$$

where H_{IBA} is the usual s-d boson Hamiltonian as given by Equation VI-1, H_F is the fermion Hamiltonian, and V_{BF} is the boson-fermion coupling interaction. Since only a single odd particle is coupled to the bosons, H_F contains only one-body terms and it can be expressed by the creation (or annihilation) operator for an odd particle, using single quasi-particle energies. Most of the interesting physics goes into the structure of the boson-fermion interaction, which contains three components [Sc82b, Sc84,Sc85a,Sc85b,Ch88b]. The first component represents the direct component of the quadrupole interaction between the odd particle and the bosons. Because of the two-particle nature of the bosons, bringing the Pauli exclusion principle into play, there is also an exchange component. The last component, the monopole force, can result from a variety of causes, in particular, from the blocking of certain degrees of freedom by the odd particle. In practical calculations the strength of the third component is such that it has only a minor influence on the structure of the spectrum. In the actual

calculations, by using the program ODDA [Sc85c], BFQ, BFE, and BFA are the parameters that determine the magnitude of the three components in V_{BF}. In addition, V_{BF} is related to the occupation probabilities of the single-particle orbits.

2. $^{175-185}$Re: Odd-Proton Couplings

2.1 Excitation Energies

The $^{A}_{75}$Re isotopes are described in the IBFA model by coupling the degrees of freedom of a single proton hole to an $^{A+1}_{76}$Os core. The calculations were performed separately for positive- and negative-parity states. In the description of negative-parity states, in addition to the $h_{11/2}$ unique-parity orbit in the Z=50-82 shell, we also included the $h_{9/2}$ orbit from the next major shell because states originating from it have been observed experimentally. Since we included the $h_{9/2}$ state in the basis set, for consistency we included all positive-parity orbits ($g_{7/2}$, $d_{5/2}$, $d_{3/2}$, and $s_{1/2}$) in the Z=50-82 shell, even though the last two have rather high single-particle energies and contribute very little to the wave functions.

In the calculation of negative-parity states, all parameters describing the boson-fermion interaction, including occupation probabilities, were adjusted so as to yield a best agreement with the experimental excitation energies. The only constraint on the parameters was that they vary smoothly and systematically from isotope to isotope. The same principle was followed for calculating positive-parity states, except that the occupation probabilities were calculated via the BCS formalism. The single-particle energies used in the BCS calculations are listed in Table VI-3. These values were extrapolated from the

Table VI-3. Single-Particle Energies for Odd-Mass Re Positive-Parity States.

	$g_{7/2}$	$d_{5/2}$	$d_{3/2}$	$s_{1/2}$
^{175}Re	0.000 MeV	1.525	2.449	2.497
^{177}Re	0.000	1.445	2.469	2.495
^{179}Re	0.000	1.365	2.489	2.493
^{181}Re	0.000	1.285	2.509	2.491
^{183}Re	0.000	1.202	2.522	2.489
^{185}Re	0.000	1.125	2.555	2.487

experimental single-particle energies of nuclei having closed-shell configurations. To improve the fit, in some instances they were varied, but by no more than 200 keV. The complete sets of parameters used in the calculations are listed for negative-parity states in Table VI-4 and for positive-parity states in Table VI-5. Note that the occupation probabilities are such that all particles in the Z=50-82 valence shell are accounted for.

The Re isotopes lie in the well-deformed region, and their excitation-energy spectra clearly show features of rotational bands. All the isotopes in which we are interested, except ^{175}Re which we know nothing about, have similar spectra. $K^{\pi}=5/2^{+}$ is the ground-state rotational band for $^{181-185}$Re, $9/2^{-}$ is the second lowest-lying band, and a $K^{\pi}=1/2^{-}$ band comes down in energy with decreasing mass number. This last band originates from the spherical $h_{9/2}$ state from the next major shell. For ^{177,179}Re these three bands all appear, but their excitation energies have not been established; only that they are excepted to lie very closely together. A point to note is that the spacing between the $5/2^{-}$ and the $9/2^{-}$ members of the $K^{\pi}=1/2^{-}$ band is uncertain because the transition energy is too low for the Y-rays to have been observed. These energies were determined from Coriolis-coupling calculations and systematics by Leigh et al. [Le72] for ^{177,179}Re and by Singh et al. [Si74] for ^{181,183}Re.

We show a comparison between calculated and experimental [Ar75a,Br88,El81b,Fi84,Fi87,Le72,Ne76,Si74,Ya83] excitation energies for the negative-parity states in Figure VI-4. The $K^{\pi}=9/2^{-}$ rotational band has a large $h_{11/2}$ single-particle component, the only negative-parity orbit in the Z=50-82 shell. The other band, $1/2^{-}$, has a large $h_{9/2}$

Table VI-4. IBFA Parameters for Odd-Mass Re Negative-Parity States.

	^{175}Re	^{177}Re	^{179}Re	^{181}Re	^{183}Re	^{185}Re
BFE	1.28	1.36	1.38	1.40	1.48	1.68
BFQ	1.25	1.02	0.839	0.736	0.627	0.510
BFM	-0.10	-0.10	-0.10	-0.10	-0.10	-0.10
X	-1.20	-1.2	-1.20	-1.20	-1.20	-1.20
v^2 $h_{11/2}$	0.58	0.59	0.60	0.62	0.65	0.68
v^2 $h_{9/2}$	0.05	0.05	0.05	0.05	0.05	0.05
E(MeV) $h_{9/2}$	5.200	4.500	3.900	3.125	2.35	2.036

Table VI-5. IBFA Parameters for Odd-Mass Re Positive-Parity States.

	^{175}Re	^{177}Re	^{179}Re	^{181}Re	^{183}Re	^{185}Re
BFE	0.295	0.418	0.585	0.730	0.875	1.013
BFQ	0.751	0.661	0.581	0.496	0.380	0.363
BFM	0.05	0.00	0.00	0.00	-0.10	-0.10
X	-1.20	-1.20	-1.20	-1.20	-1.20	-1.20
v^2 $g_{7/2}$	0.974	0.974	0.972	0.970	0.968	0.966
v^2 $d_{5/2}$	0.919	0.918	0.915	0.914	0.913	0.912
v^2 $d_{3/2}$	0.722	0.723	0.672	0.623	0.574	0.512
v^2 $s_{1/2}$	0.705	0.713	0.671	0.631	0.590	0.545

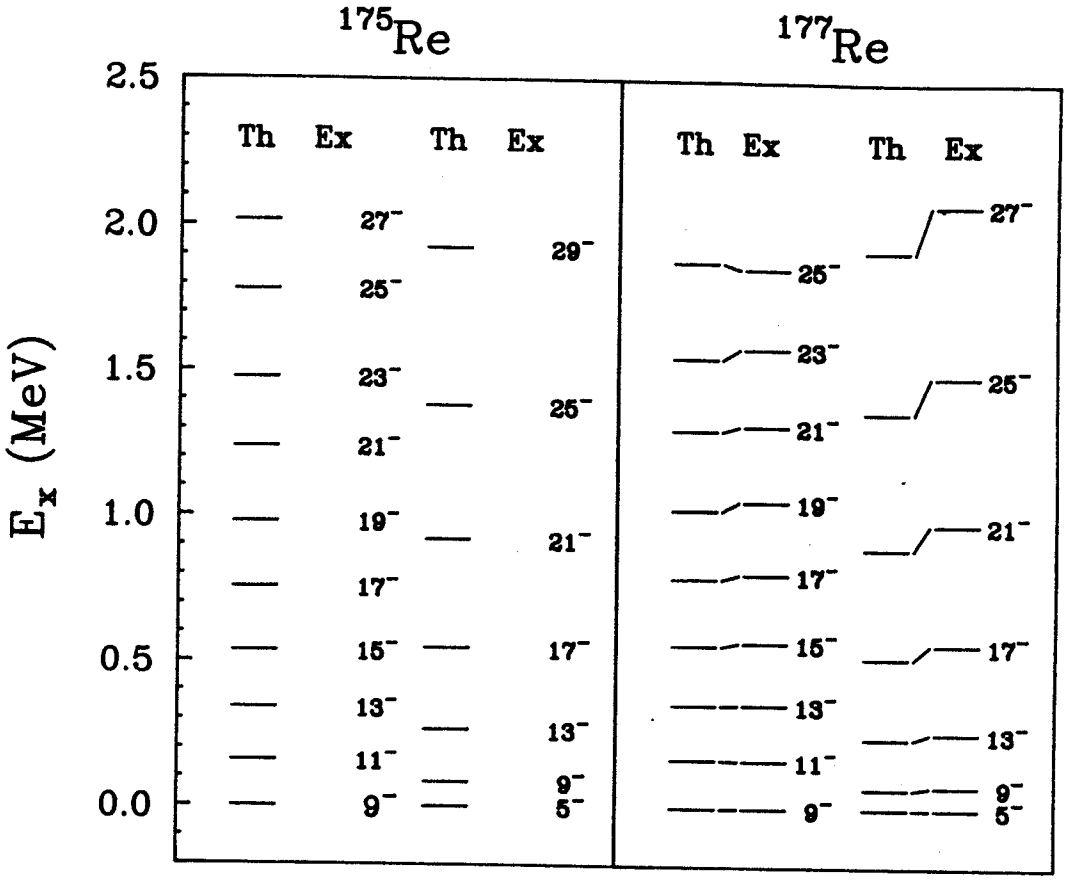

Figure VI-4. IBFA-calculated excitation energies for negative-parity states in the odd-mass Re isotopes compared with experimental data. States are labeled with 2J.

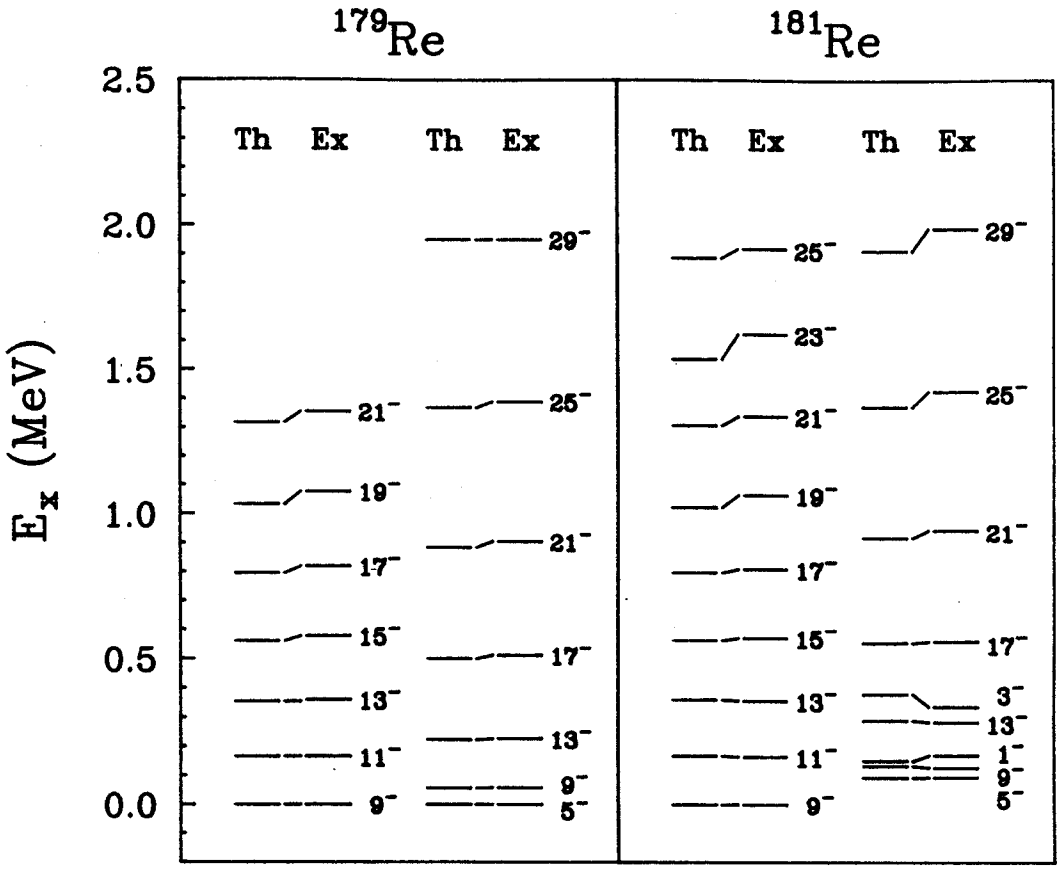

Figure VI-4. (cont'd.).

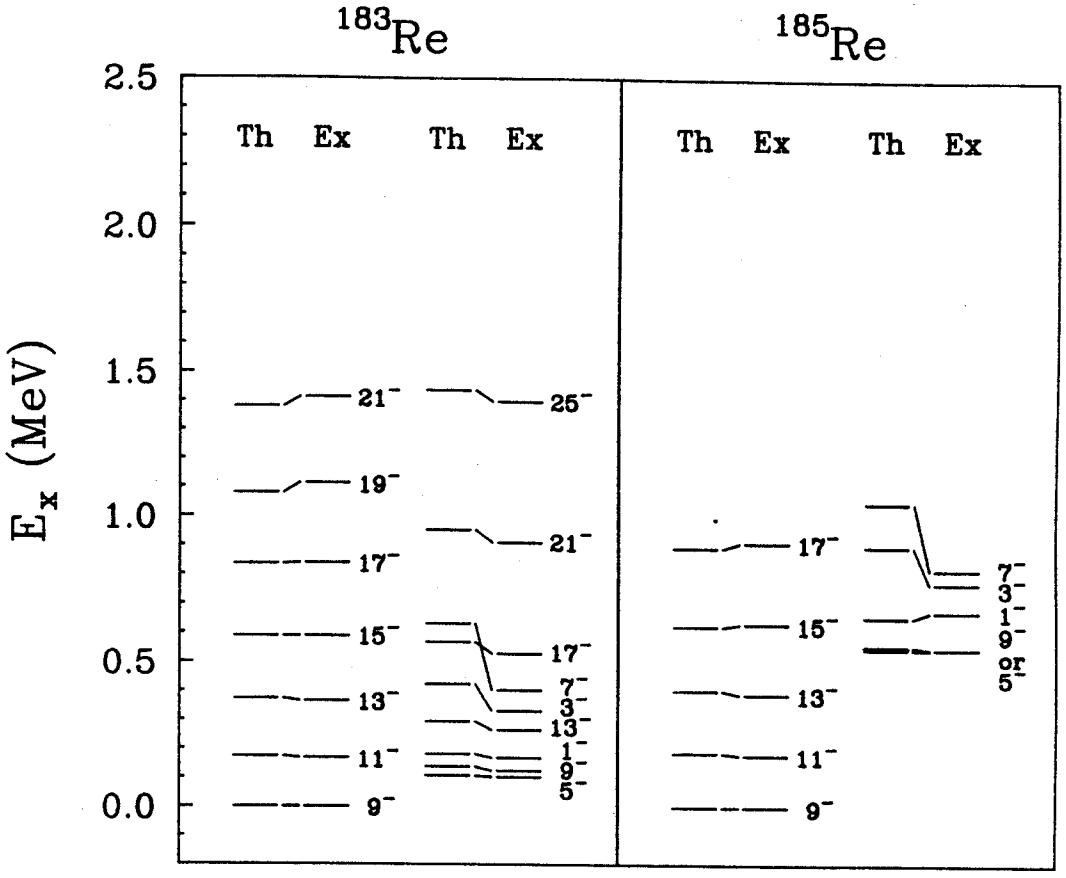

Figure VI-4. (cont'd.).

component coming from the next major shell. Although this band is not too well defined in ^{185}Re, we show it for consistency. Also, since no states have been identified, the parameters for ^{175}Re come purely from extrapolation of those from the other five Re isotopes. Our calculations reproduce the rotational features of these two bands quite well, including the strong decoupling in the $1/2^-$ band. Members of the negative signature branch of this band were fit somewhat better than members of the positive branch. It may be necessary to include more single-particle orbits from the next major shell, e.g., $f_{7/2}$, in order to improve the fits to this $1/2^-$ band. However, this would make the calculation considerably more complicated, which we wanted to avoid. It should be noted that in our calculations we did not employ a Coriolis force attenuation. Had we included this as a free parameter, as is often done in calculations for odd-mass nuclei, we would certainly have been able to improve our fits.

Results for the positive-parity states are shown in Figure VI-5. Since, in general, the boson number we dealt with is around 13, we usually truncated it by one or two in order to make the calculations more feasible, especially for calculations like these, where four orbits have been involved. Fits are very good for the $5/2^+$ bands and reasonable for the other bands. The excitation energies for the band heads could probably be improved by varying the single-particle energies in the calculations, but we chose not to do that so long as an overall reasonable fit could be achieved. Other positive-parity bands in the three heavier Re isotopes either have higher excitation energies or are not well known experimentally, so we do not consider them further in this investigation; also, no other states are known for the lighter

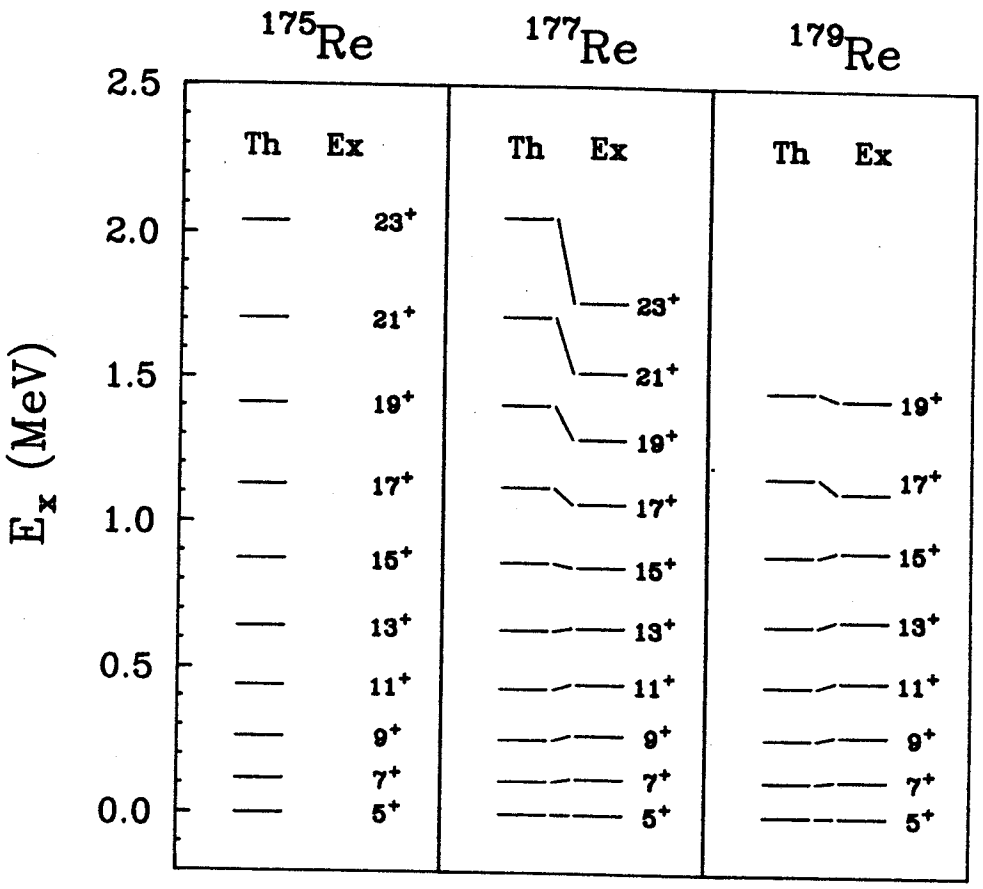

Figure VI-5. IBFA-calculated excitation energies for positive-parity states in the odd-mass Re isotopes compared with experimental data. States are labeled with 2J.

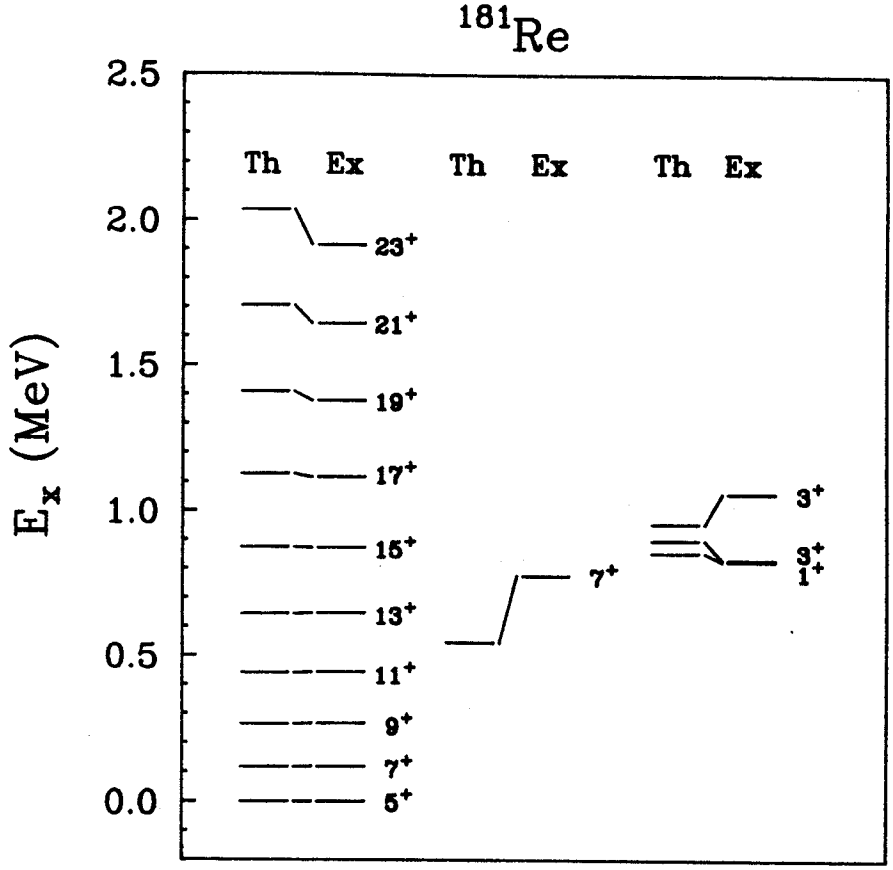

Figure VI-5. (cont'd.).

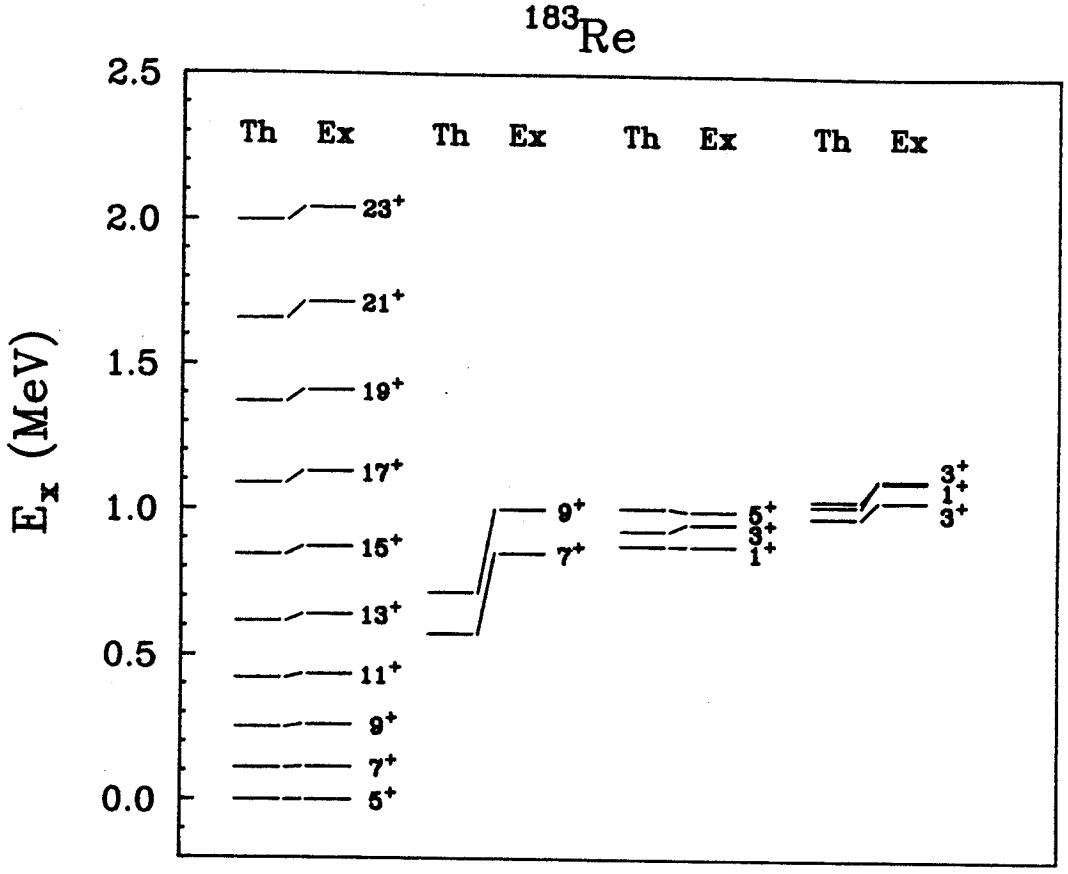

Figure VI-5. (cont'd.).

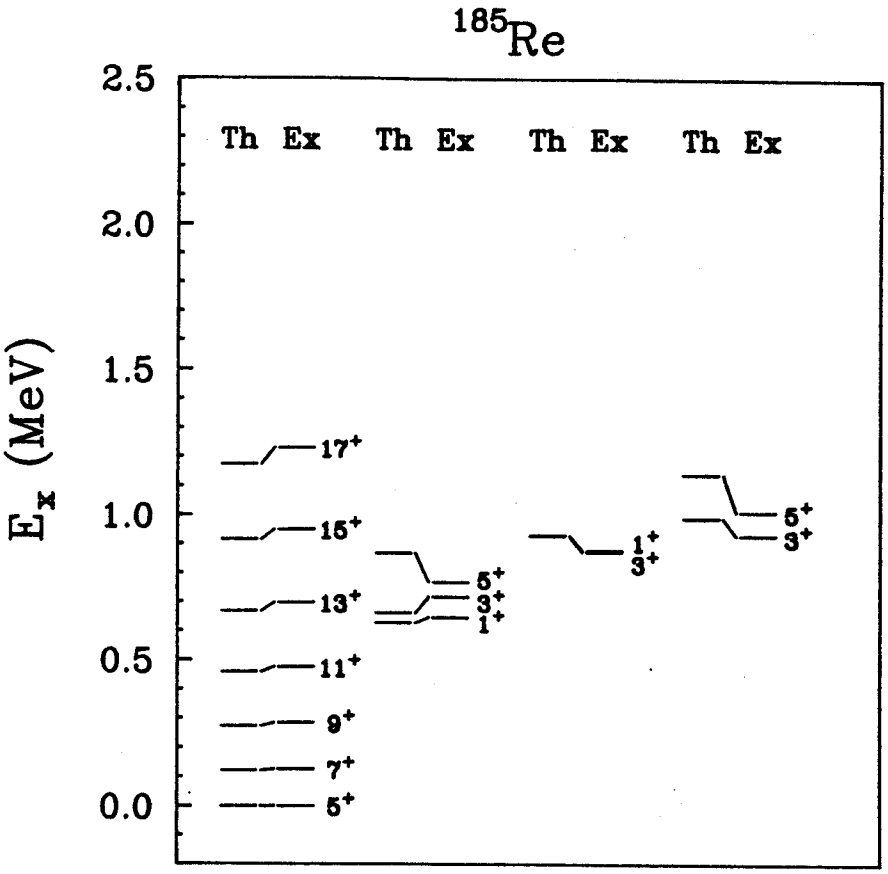

Figure VI-5. (cont'd.).

isotopes.

2.2 B(E2) Values and Quadrupole Moments

In the IBFA model the E2 transition operator [Sc84,Sc85a,Sc85b] contains contributions from both the bosons and the odd Fermion:

$$T^{(E2)} = e_B Q_B + e_F Q_F \qquad \text{(VI-7)}$$

Here Q_B is the same as Q defined in Equation VI-4, while

$$Q_F = \sum_{jj'} Q_{jj'} (a_j^\dagger \tilde{a}_{j'})^{(2)} \quad . \qquad \text{(VI-8)}$$

We used the e_B values given in Section B.2 for the Os cores; also, $e_F = e_B$ [Sc82b].

Some selected B(E2) values for crossover and stopover transitions between lower-lying members of the more well-defined bands are shown in Figure VI-6. The contributions from the odd fermion appear to be rather small for these transitions, as can be seen from the fact that the curves for the six isotopes can almost be superimposed. The quadrupole moments of some low-lying band heads are shown in Figure VI-7. Unfortunately, the experimental data are relatively few [Bi67,Bü81,Er81, Ha81,Oh87,Sp80], making it difficult to obtain quantitative tests of the values. However, data do exist [Bi67] for the

$$5/2^+7/2[402\uparrow] \rightarrow 5/2^+5/2[402\uparrow]$$

and

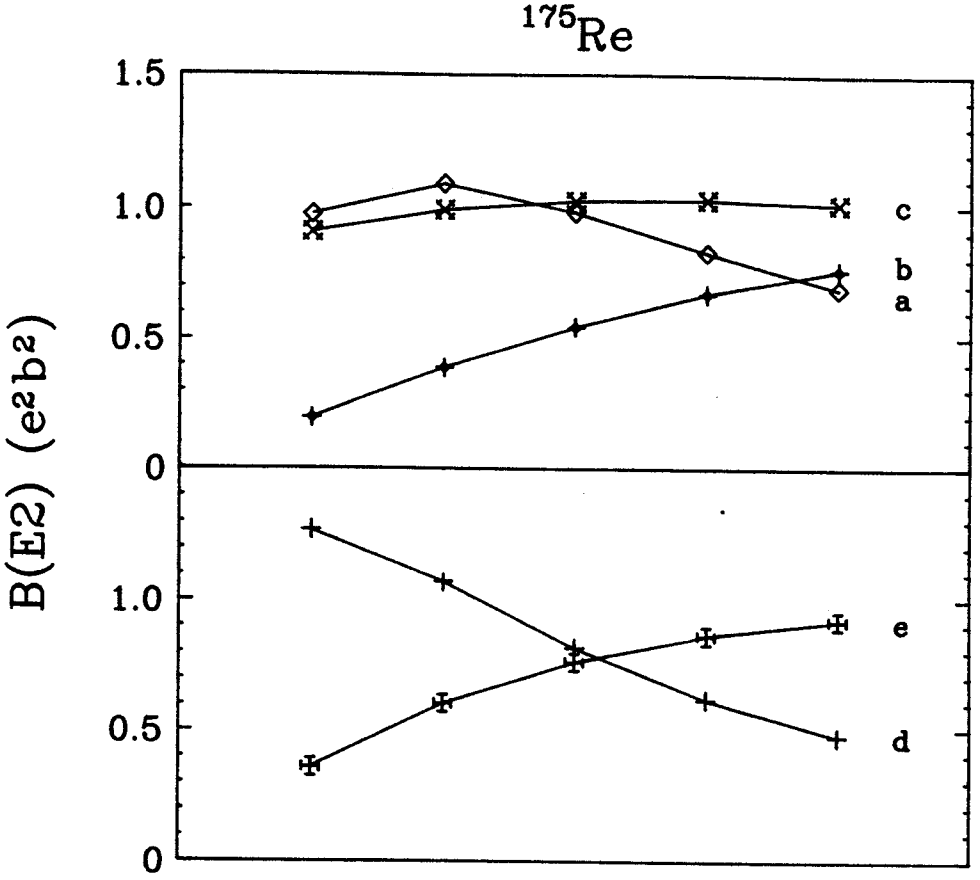

Figure VI-6. IBFA-calculated B(E2) values for the first five crossover and stopover transitions in low-lying bands in the odd-mass Re isotopes. Within each figure the curves represent transitions in bands as follows: a, $9/2^-$ stopover; b, $9/2^-$ crossover; c, $1/2^-$ crossover; d, $5/2^+$ stopover; e, $5/2^+$ crossover. The left-most point represents the lowest transition of its kind in that band, with the successively higher transitions following in order.

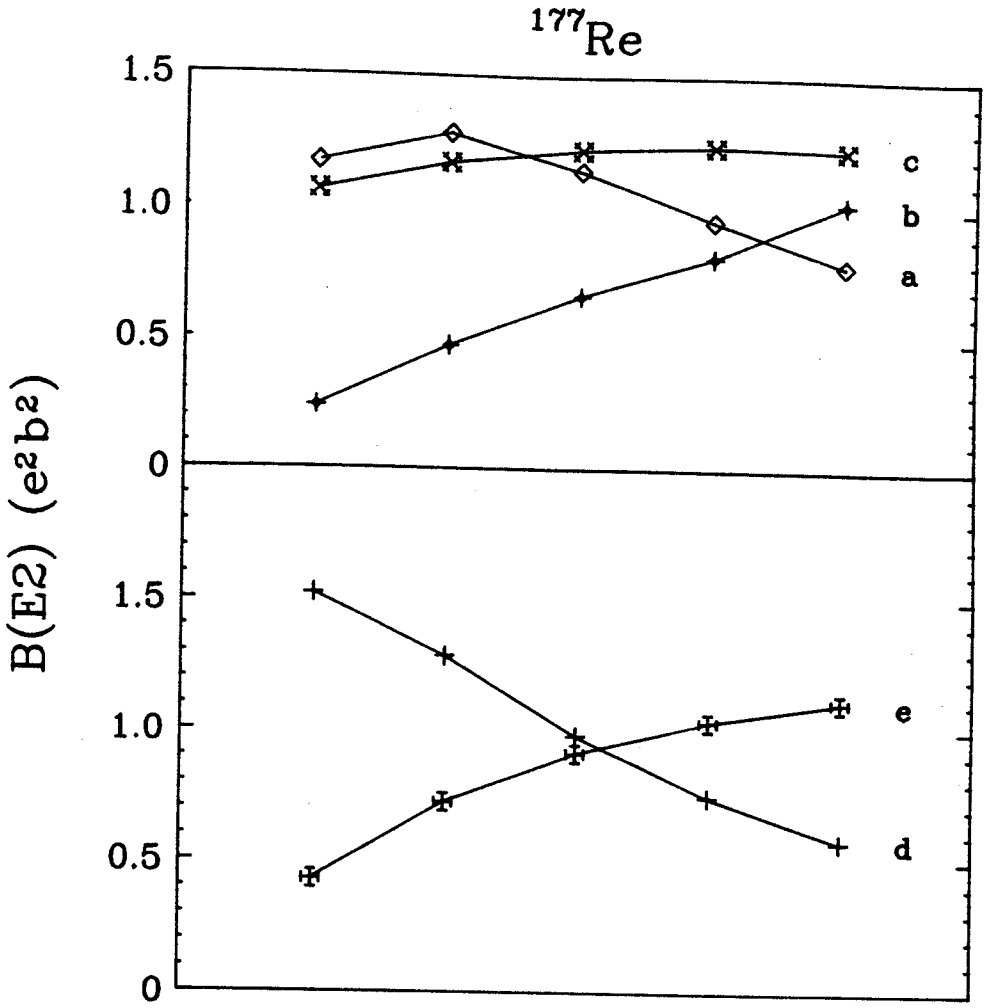

Figure VI-6. (cont'd.).

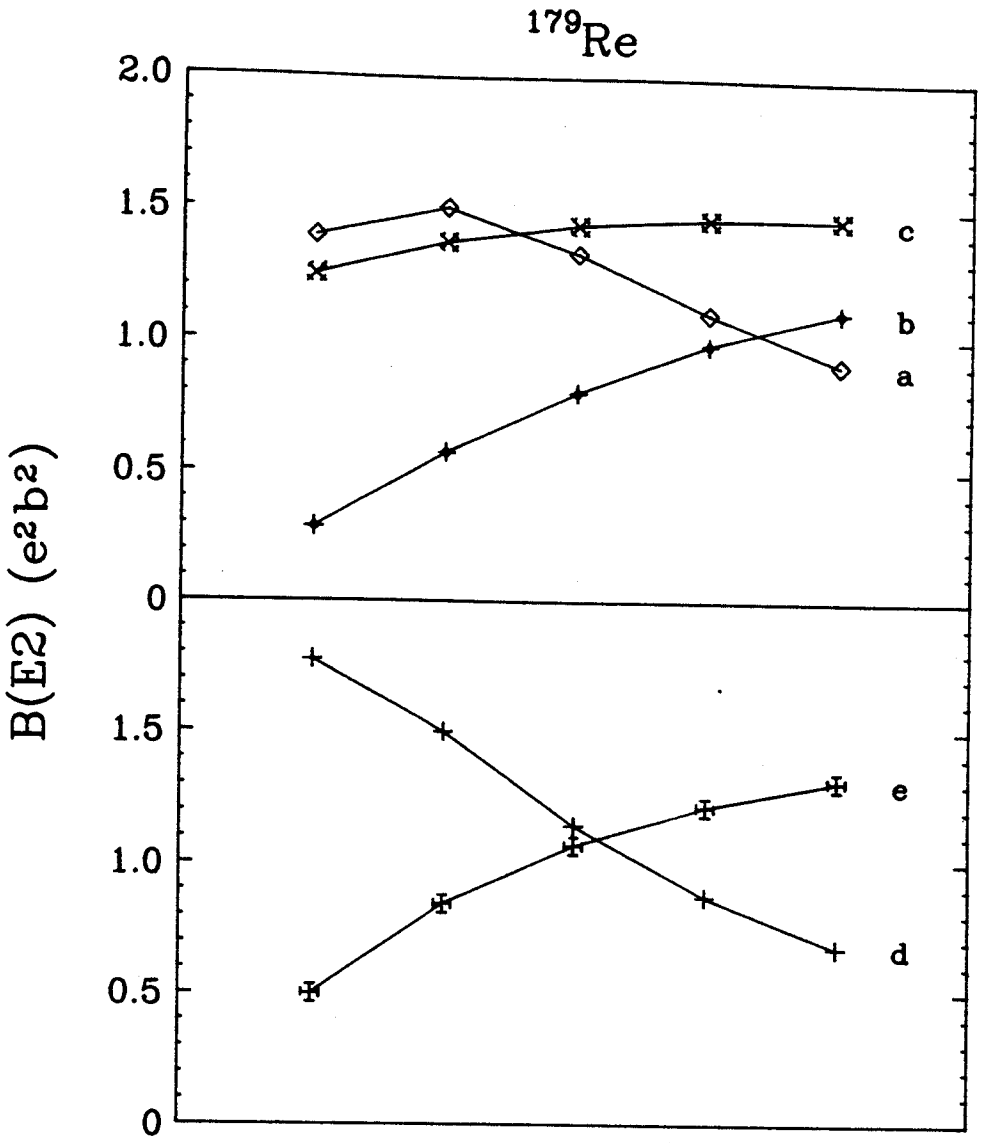

Figure VI-6. (cont'd.).

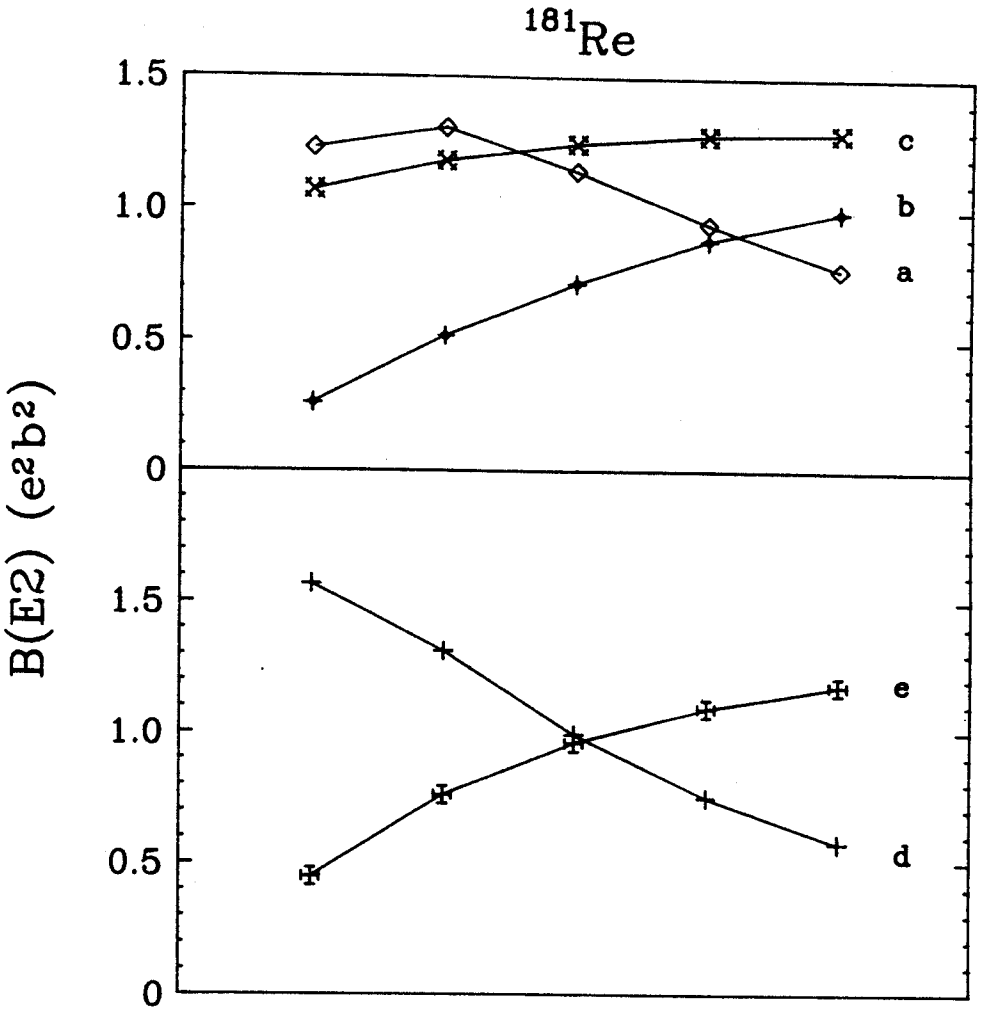

Figure VI-6. (cont'd.).

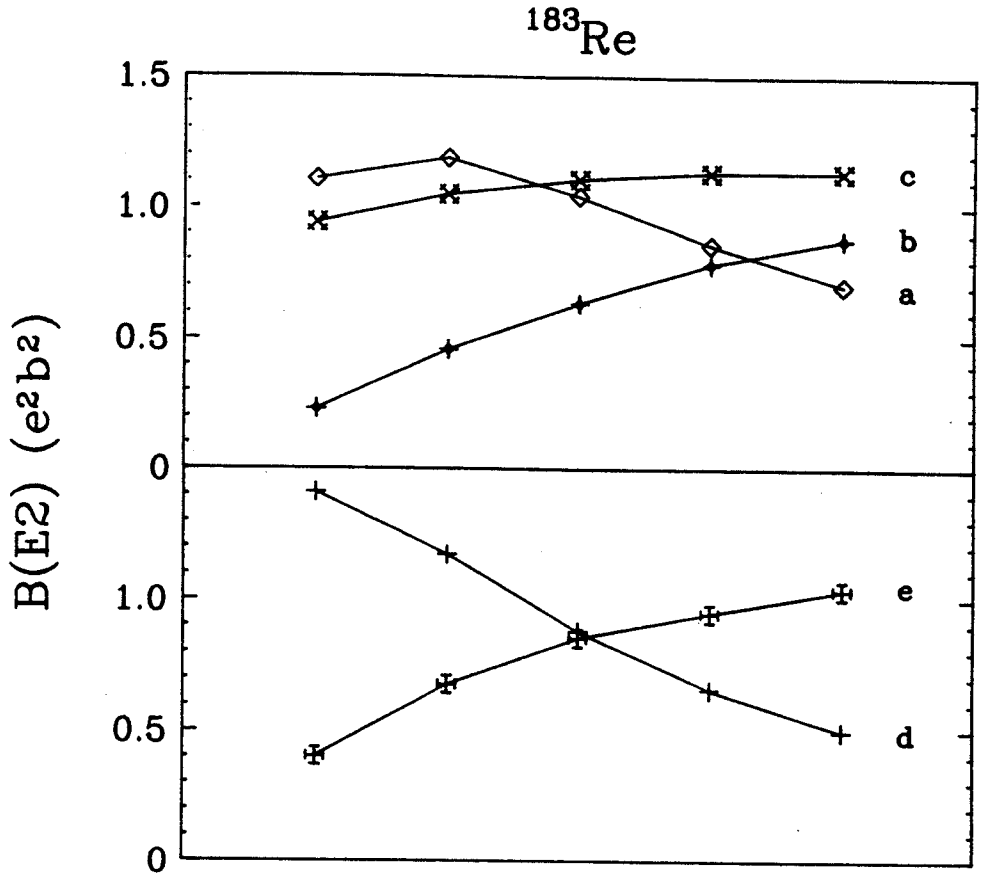

Figure VI-6. (cont'd.).

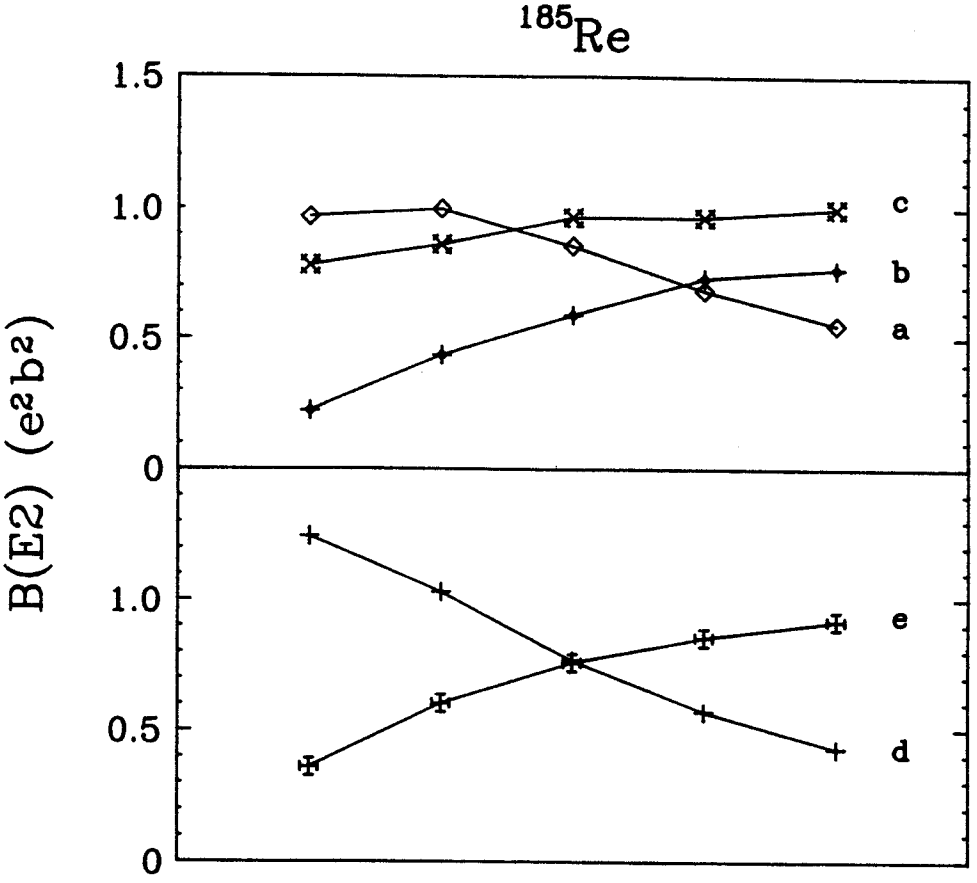

Figure VI-6. (cont'd.).

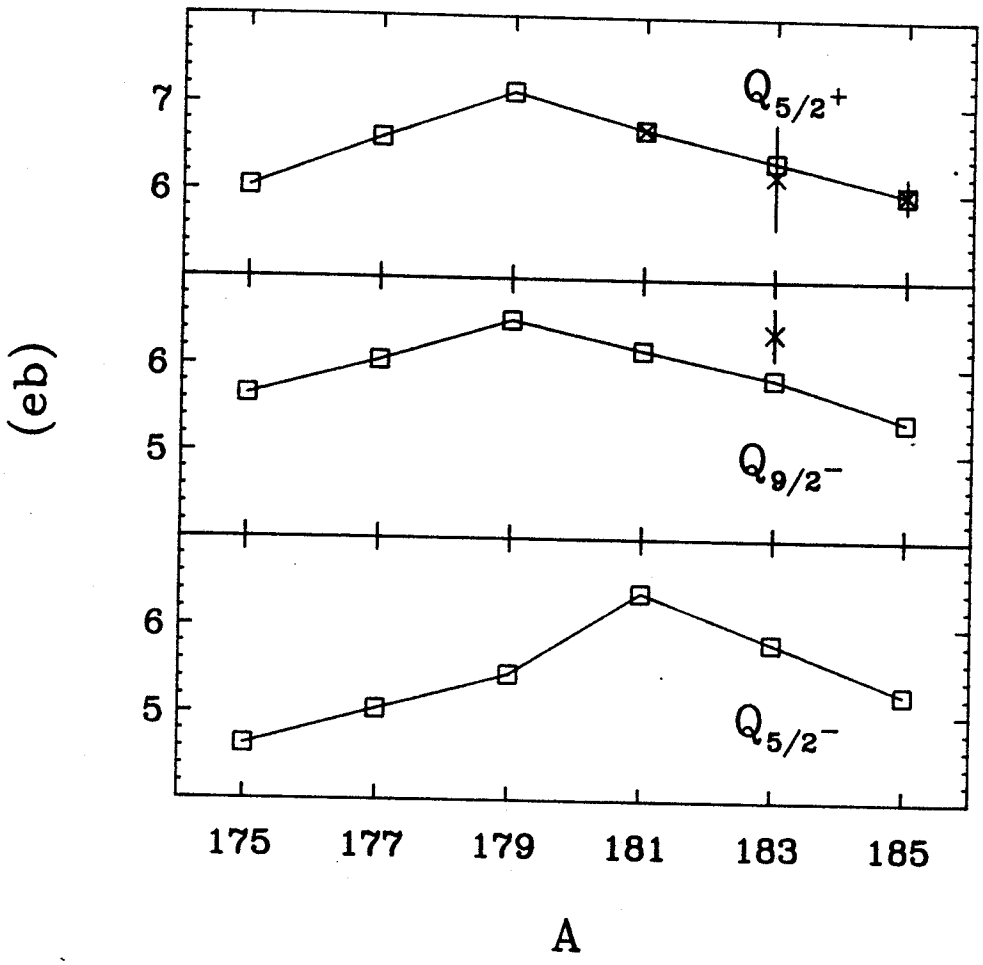

Figure VI-7. IBFA-calculated Q values for selected band-head states in the odd-mass Re isotopes compared with experimental data. The squares are the calculated values; the crosses (with error bars) are the experimental values.

$5/2^+9/2[402\uparrow] \rightarrow 5/2^+5/2[402\uparrow]$

transitions in ^{185}Re. The respective experimental (calculated) B(E2) values are 1.0 (1.24) and 0.31 (0.36) eb.

2.3 Magnetic Moments and B(M1) Values

Contrary to the case of the electric quadrupole properties, the magnetic properties of odd-mass nuclei depend strongly on the properties of the odd particle, so they should provide a good test of the wave functions. For our M1 operator [Sc84,Ch88b] we used

$$T^{(M1)} = \sqrt{3/4\pi}\left[g_d\sqrt{10}(d^\dagger\tilde{d})^{(1)} - \sum_{jj'} g_{jj'}\sqrt{j(j+1)(2j+1)/3}\,(a_j^\dagger\tilde{a}_{j'})^{(1)}\right], \qquad \text{(VI-9)}$$

where g_d is the boson g factor and $g_{jj'}$ is the odd-particle g factor, which can be written as a linear combination of g_l and g_s [Sc84,sc85b]. We extracted the boson g factor from the magnetic moment of the 2_1^+ states in the even-even Os cores [Le82], obtaining a value of g_d=0.25 nm. Following the procedure used for similar calculations in the Eu isotopes [Sc82b], we quenched the value of g_s by a factor of 0.7 from the single-particle estimate down to 4.0 nm.

Some selected magnetic moments are shown in Figure VI-8. It can be seen that they are determined essentially by the fermion part of the operator, Equation VI-9. Some calculated B(M1) values are shown in Figure VI-9. Unfortunately, no experimental data exist at this time to

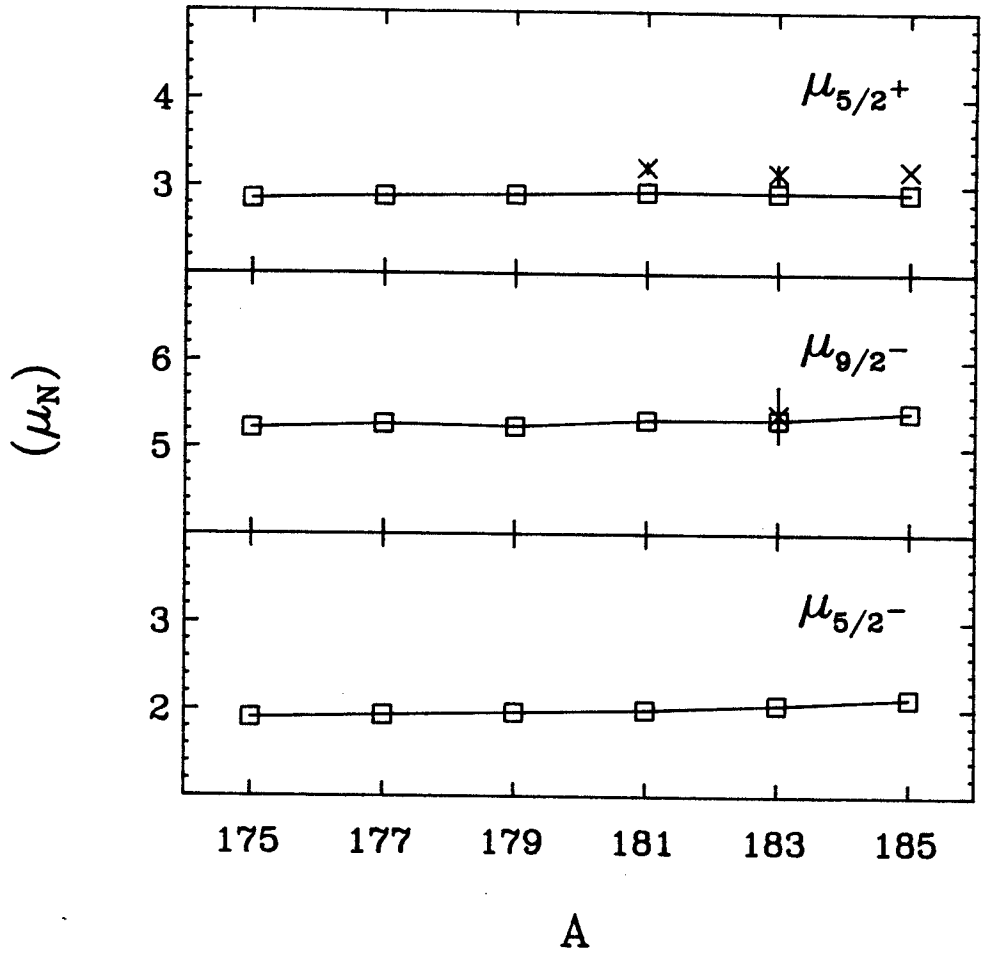

Figure VI-8. IBFA-calculated μ values for selected band-head states in the odd-mass Re isotopes compared with experimental data. The squares are the calculated values; the crosses (with error bars) are the experimental values.

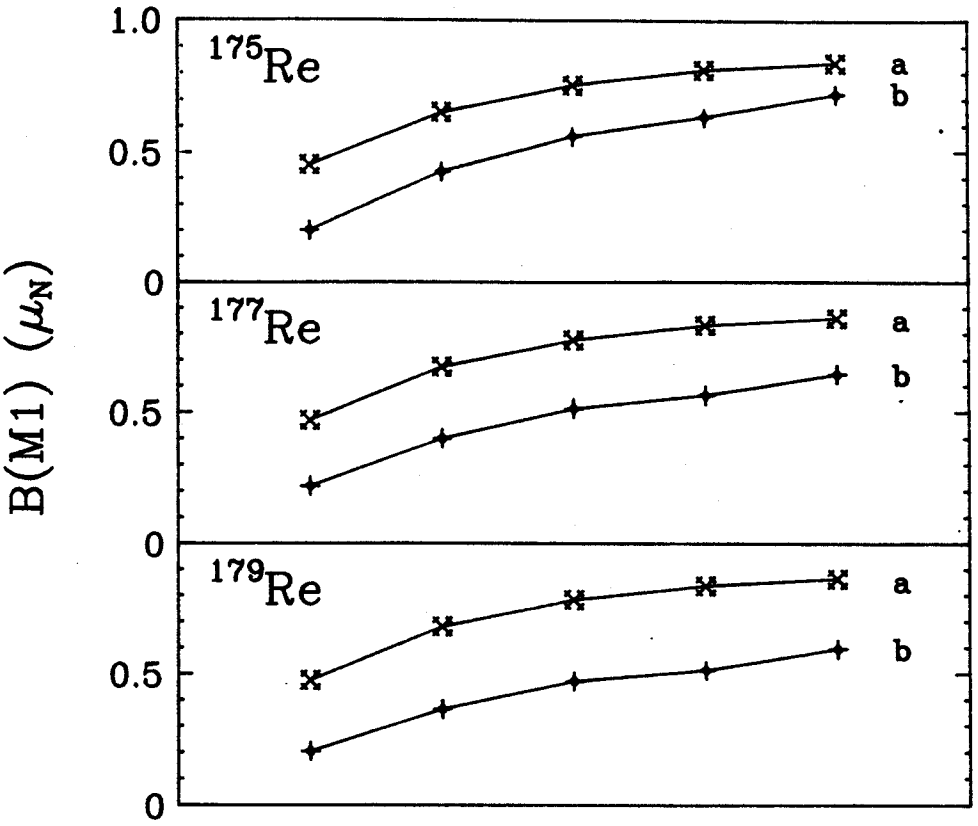

Figure VI-9. IBFA-calculated B(M1) values for selected transitions between low-lying band members in the odd-mass Re isotopes. The curves correspond to the following bands: a, $5/2^+$ band; b, $9/2^-$ band. Transitions between the lowest members of a band lie on the left, between members increasing systematically toward the right.

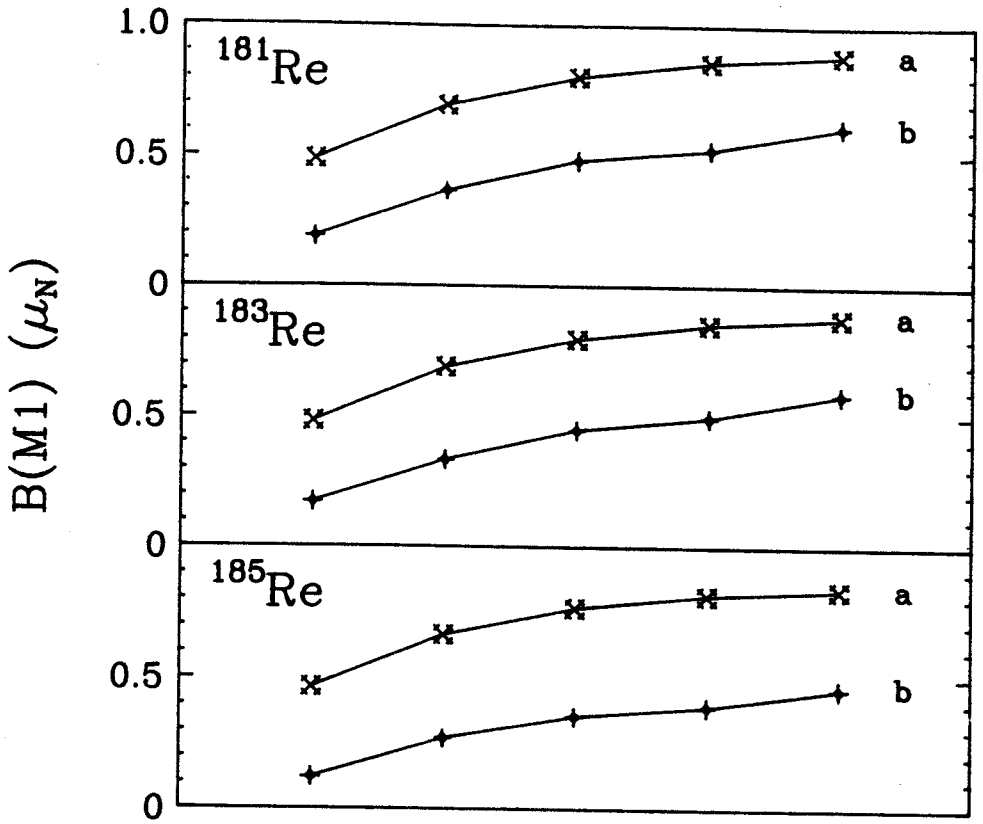

Figure VI-9. (cont'd.).

test the predictions.

3. $^{177-185}$Os: Odd-Neutron Couplings

3.1 Excitation Energies

The odd-mass $_{76}$Os isotopes are described in the IBFA model by coupling the degrees of freedom of a single neutron hole (for $^{181-185}$Os) or a single neutron particle (for ^{177,179}Os) to an appropriate Os core. In general, the same procedure was followed as in the calculations for the odd-mass Re isotopes. Again, all the single-particle orbits ($f_{7/2}$, $h_{9/2}$, $p_{3/2}$, $f_{5/2}$, and $p_{1/2}$) in this region, the N=82-126 shell, were included. This made the calculations rather time consuming, so no detailed fit to the experimental excitation energies was attempted. The single-particle energies were obtained as in the Re case. For simplicity, we tried to keep these values constant; however, if no satisfactory results could be obtained with the initial values, they were modified (by no more than 300 keV) in order to obtain better agreement with experiment. The list of single-particle energies used is given in Table VI-6. The complete sets of parameters used in the calculations are listed for positive-parity states in Table VI-7 and for negative-parity states in Table VI-8.

For the odd-mass Os isotopes having N=101-109, the $i_{13/2}$ orbit is the only positive-parity orbit entering the calculations. We show the results of the calculations for positive-parity states and compare them with experimental values [Be72,Br88,Dr83,El81b,Fi84,Fi87,La75,La78] in Figure VI-10.

As expected for high-j (low-Ω) orbits, Coriolis coupling is strong for states originating from the $i_{13/2}$ state. Thus, there is a

Table VI-6. Single-Particle Energies for Odd-Mass Os Negative-Parity States.

	$f_{7/2}$	$h_{9/2}$	$p_{3/2}$	$f_{5/2}$	$p_{1/2}$
^{177}Os	0.000 MeV	0.360	1.800	1.820	2.120
^{179}Os	0.000	0.430	1.750	1.860	2.170
^{181}Os	0.000	0.460	1.700	1.880	2.220
^{183}Os	0.000	0.510	1.605	1.928	2.273
^{185}Os	0.000	0.560	1.505	1.978	2.323

Table VI-7. IBFA Parameters for Odd-Mass Os Positive-Parity States.

	$^{177}_{Os}$	$^{179}_{Os}$	$^{181}_{Os}$	$^{183}_{Os}$	$^{185}_{Os}$
BFE	2.760	2.450	2.430	2.021	2.010
BFQ	0.380	0.441	0.486	0.468	0.307
BFM	-0.10	-0.10	-0.10	-0.10	-0.10
χ	-1.00	-1.00	-1.00	-1.00	-1.00
$v^2_{i_{13/}}$	0.300	0.350	0.375	0.600	0.780

Table VI-8. IBFA Parameters for Odd-Mass Os Negative-Parity States.

	^{177}Os	^{179}Os	^{181}Os	^{183}Os	^{185}Os
BFE	0.941	0.809	0.732	0.800	1.100
BFQ	0.180	0.228	0.286	0.190	0.120
BFM	-0.10	-0.10	-0.10	-0.10	-0.10
X	-1.00	-1.00	-1.00	-1.00	-1.00
v^2 $f_{7/2}$	0.801	0.846	0.884	0.863	0.854
v^2 $h_{9/2}$	0.683	0.734	0.798	0.740	0.703
v^2 $p_{3/2}$	0.139	0.190	0.277	0.260	0.276
v^2 $f_{5/2}$	0.135	0.166	0.219	0.172	0.151
v^2 $p_{1/2}$	0.0965	0.115	0.143	0.114	0.102

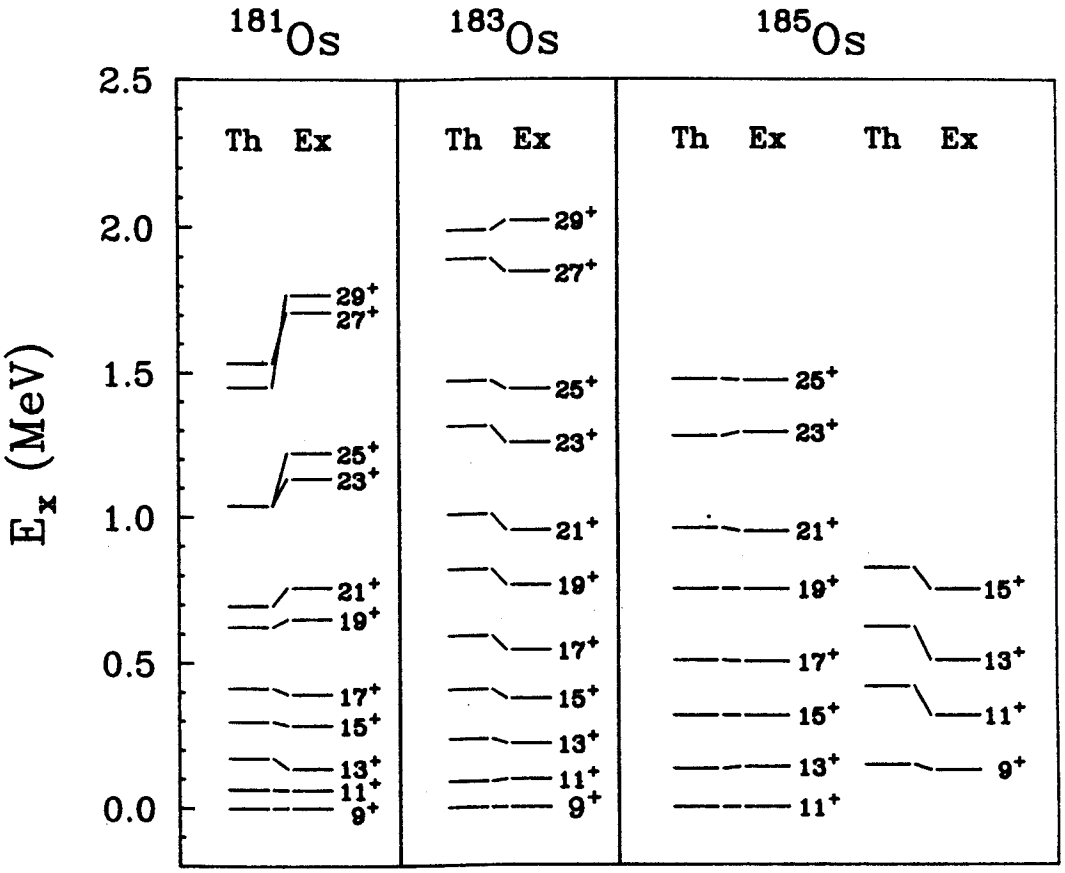

Figure VI-10. IBFA-calculated excitation energies for positive-parity states in the odd-mass Os isotopes compared with experimental data. The states are labeled with 2J.

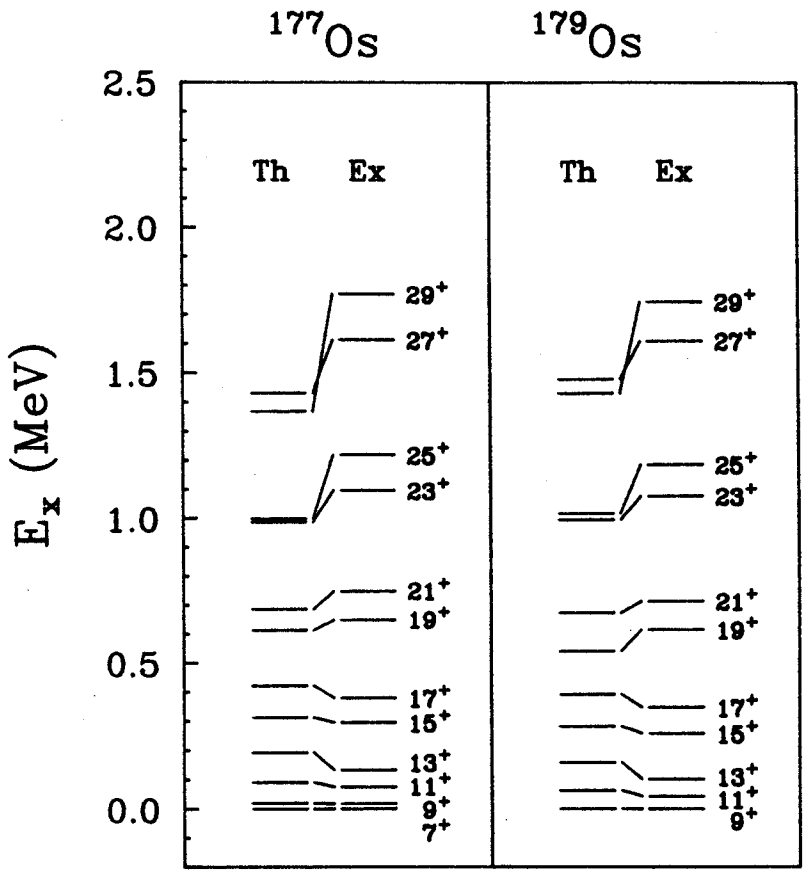

Figure VI-10. (cont'd.).

considerable amount of staggering for the positive-parity bands. The three lower mass isotopes, $^{177-181}$Os, show greater Coriolis coupling than the higher mass ones, as seen from the spacings of the first few transitions of the bands. These spacings (18.3 and 43.7 keV for the first transitions, respectively, for ^{177}Os and ^{179}Os) are too small for a band with K=7/2 or 9/2. Moreover, in ^{181}Os the band has been reported [Ne76,Fi84] as being a mixed $i_{13/2}$ band, namely, the Nilsson states $9/2^+[624]$ and $7/2^+[633]$ combined. In our calculations, we find inversion of order between members with opposite signature. This situation does appear in experimental data but at higher spin values than predicted. This fact suggests that the Coriolis force is overestimated in our calculations. However, notice that there is no free parameter controlling the Coriolis force; it arises naturally in the IBFA model [Sc87]. Nevertheless, our calculations do reproduce the features of these positive-parity bands reasonably well.

Results for negative-parity states are compared with experiments in Figure VI-11. A similar K=1/2 band, though not built on the same Nilsson state, exists in all the five Os isotopes. Both signature members have been observed from in-beam γ-ray experiments only for ^{177}Os [Dr83] and ^{185}Os [El81b]; for the other isotopes, only a few states of positive signature are known, mostly from decay studies [La75,La78]. In Figure VI-11 we show both signature members, and we have pretty good agreement with experiment data for ^{177}Os and ^{185}Os. This and the fact that there is no inverting of orders at low spin members as in the odd-mass Re cases suggest that the Coriolis coupling is not so large as in Re isotopes. Therefore, we think that for all five Os isotopes, the members having positive signature do not shift to higher energies

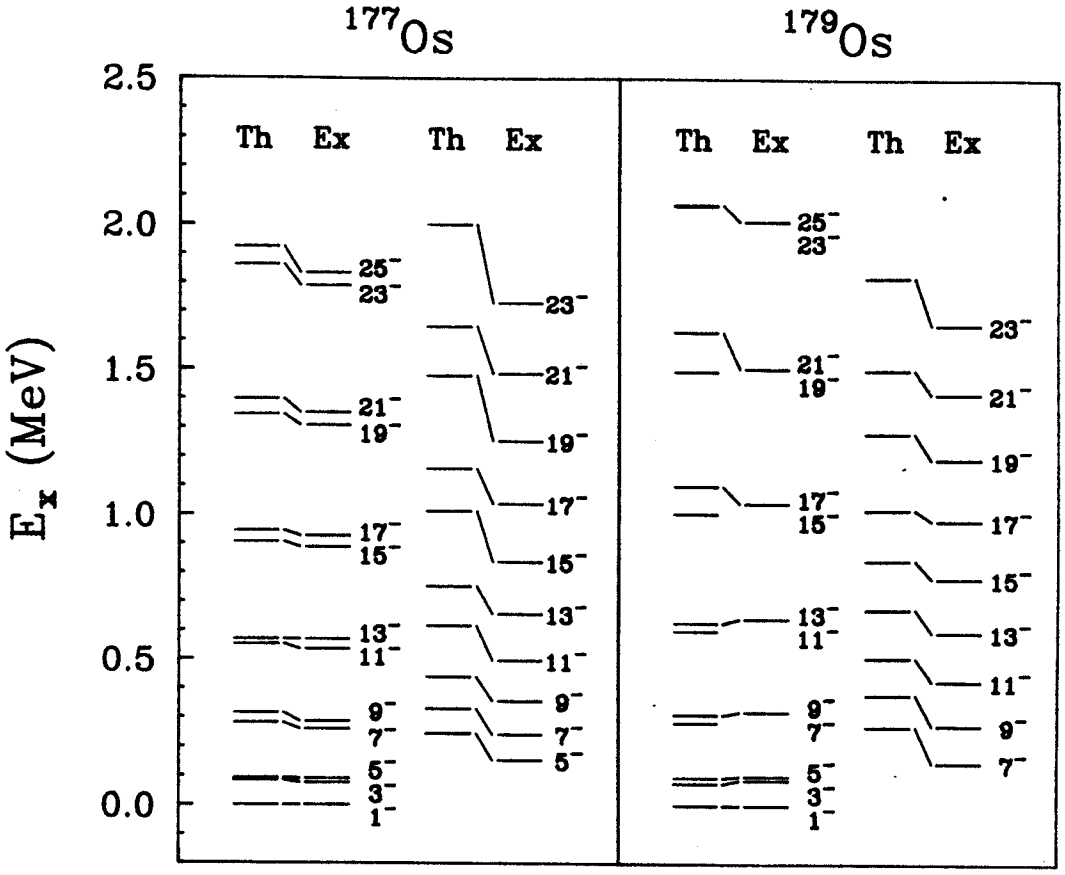

Figure VI-11. IBFA-calculated excitation energies for negative-parity states in the odd-mass Os isotopes compared with experimental data. The states are labeled with 2J.

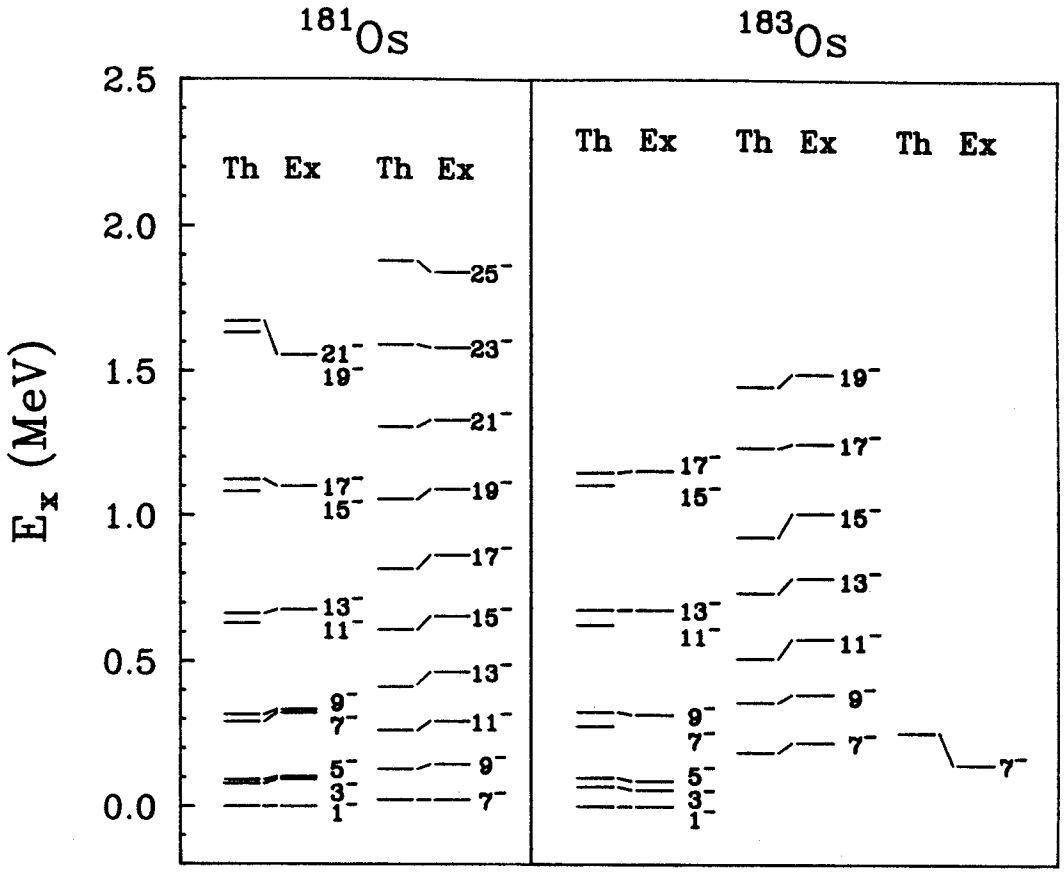

Figure VI-11. (cont'd.).

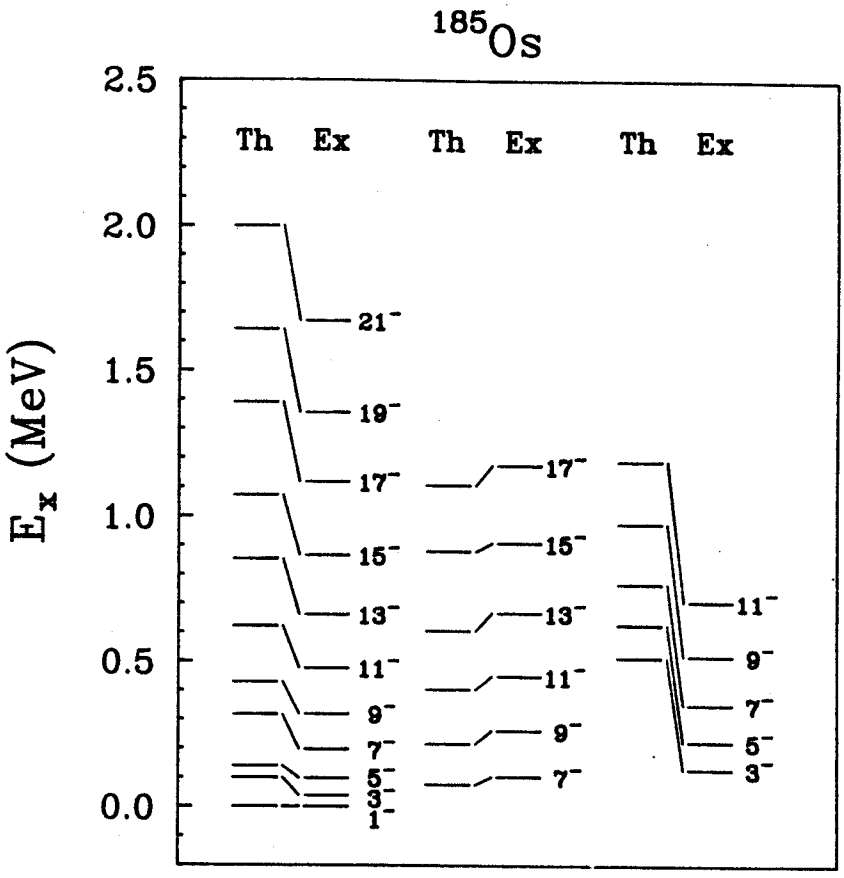

Figure VI-11. (cont'd.).

respect to those having negative signature.

The relative positions of the two band heads in ^{181}Os are not known experimentally. It was suggested [Ne76] from systematics that the ground state is $7/2^-$, with the $1/2^-$ state lying at very low excitation energy. Because of this ambiguity, we did not try to force the $7/2^-$ to be the ground state in our calculations but rather sought an overall good fit to these two close-lying bands. We actually obtained a $1/2^-$ ground state, with the $7/2^-$ band starting at 21.6 keV.

Spin assignments for the $7/2^-$ band in ^{185}Os are uncertain [El81b], which made any precise determination of parameters for this nucleus rather difficult. We thus chose a set of parameters that gave the best agreement with the experimental results for all five isotopes in a systematic way, under the assumption that the spin assignments were correct. This was done instead of forcing a best fit to individual sets of levels.

3.2 Electromagnetic Properties

The electromagnetic properties of the odd-mass Os isotopes were calculated in the same manner as for the odd-mass Re isotopes, except that e_P=0, g_l=0, and g_s=-2.7 nm. There are relatively few experimental data [Ha80,Li73,Oh87] available for comparison, and the structures of these Os isotopes are not unique Thus, only some selected values of B(E2) are shown in Figure VI-12, and calculated B(M1) values for ^{179}Os and ^{181}Os, which have the same rotational bands, are shown in Figure VI-13. Quadrupole moments of some low-lying band heads are listed in Table VI-9; selected values of magnetic moments are listed in Table VI-10. Experimental data for the odd-mass Os isotopes are very scarce, making

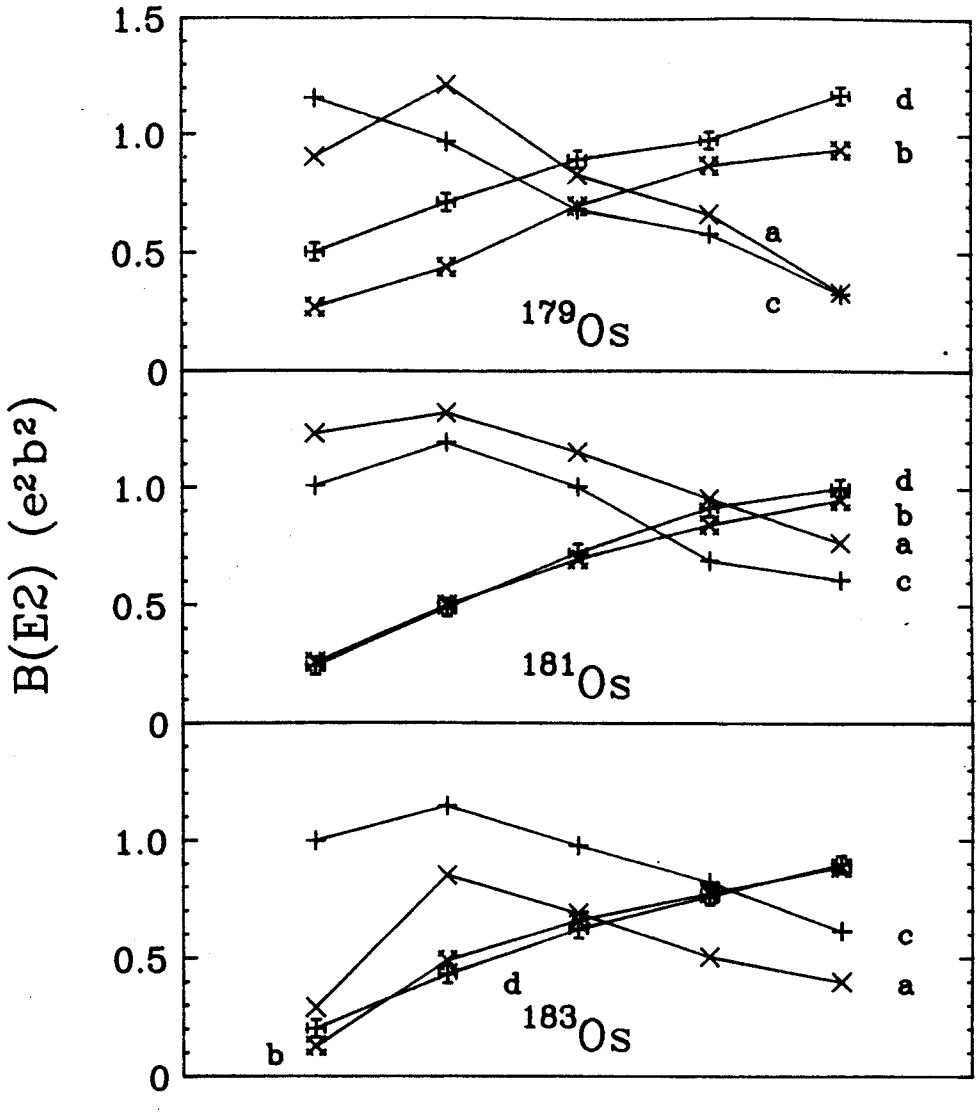

Figure VI-12. IBFA-calculated B(E2) values for selected stopover and crossover transitions in low-lying bands in the odd-mass Os isotopes. Within each figure the curves represent transitions in bands as follows: a, $7/2^-$ stopover; b, $7/2^-$ crossover; c, $9/2^+$ stopover; d, $9/2^+$ crossover; e, $1/2^-$ stopover; f, $1/2^-$ crossover. The transitions between the lowest members of a band are on the left, with the successively higher transitions following in order.

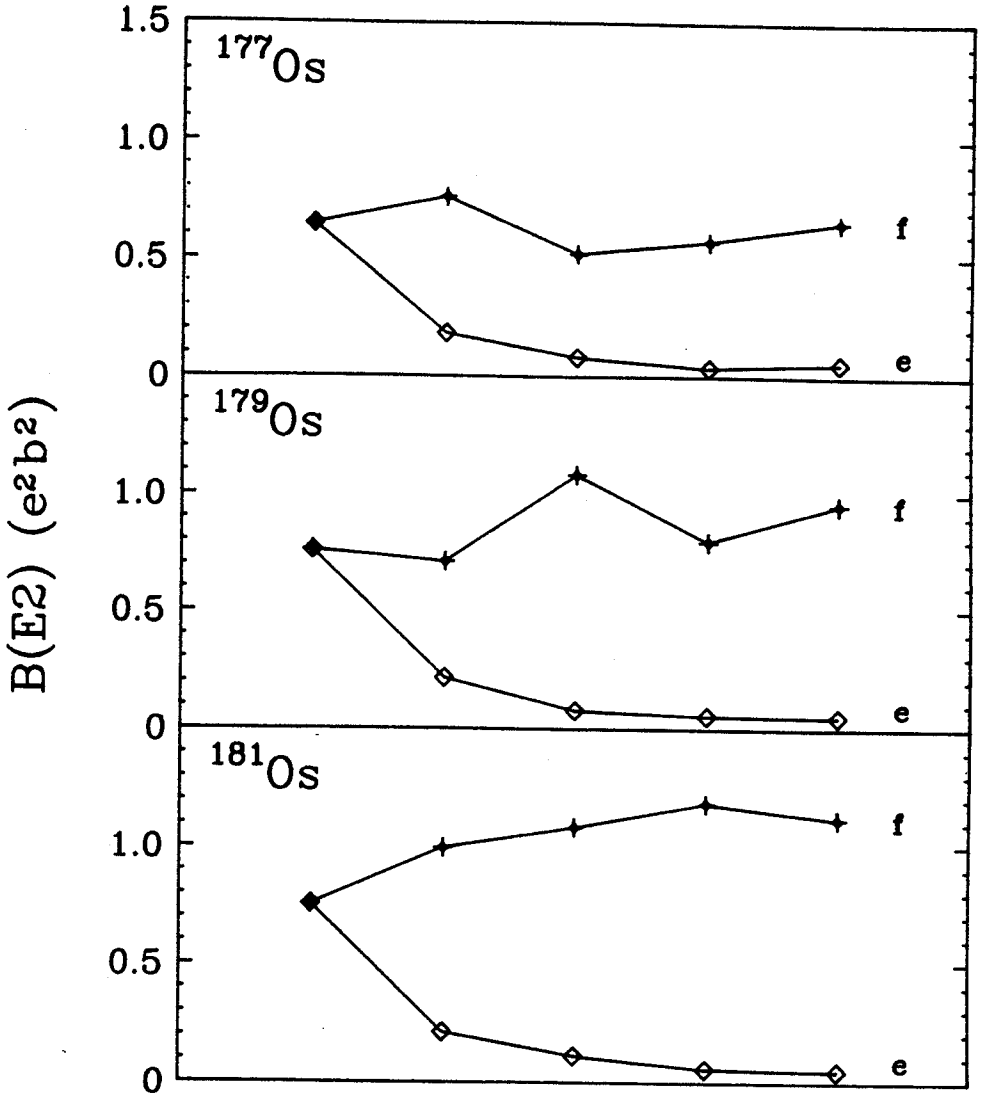

Figure VI-12. (cont'd.).

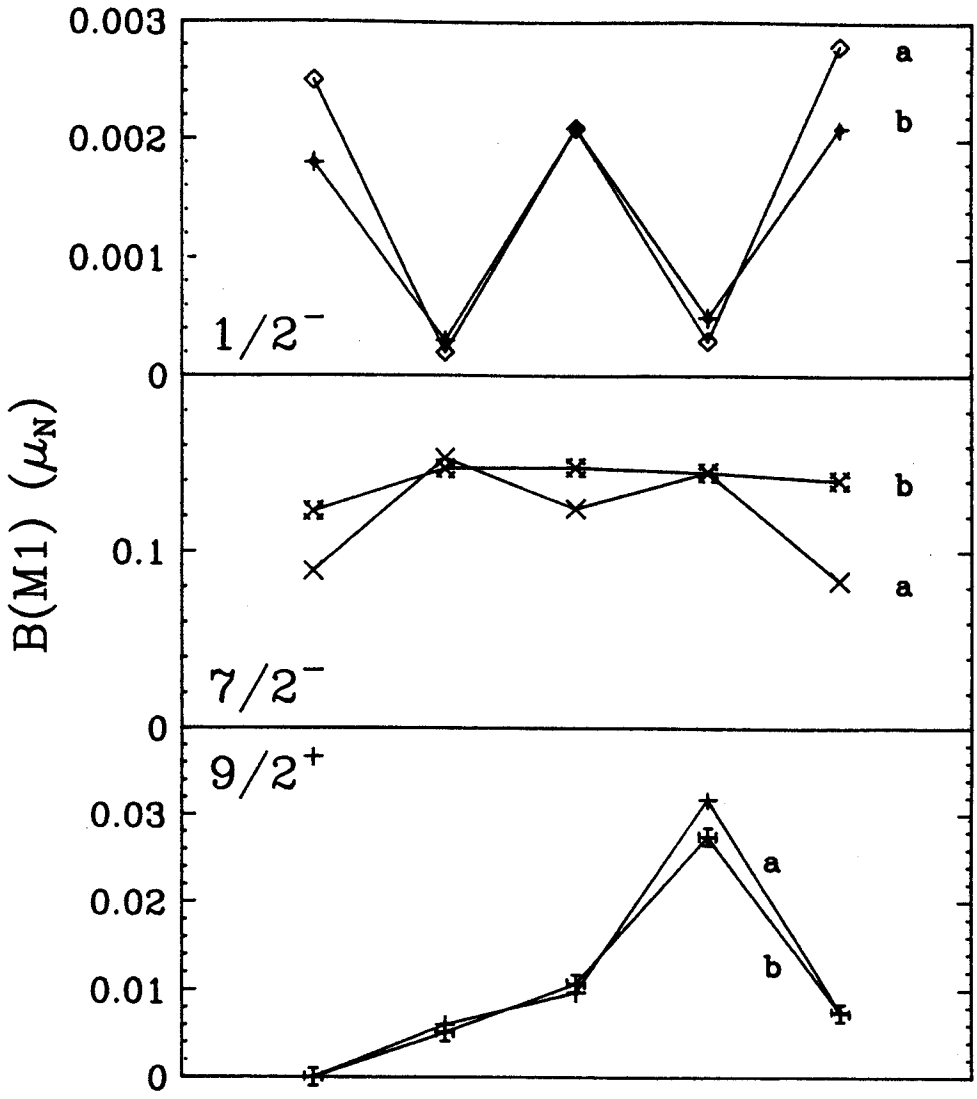

Figure VI-13. IBFA-calculated B(M1) values for selected transitions in low-lying bands in the odd-mass Os isotopes. Curve a represents ^{179}Os; curve b represents ^{181}Os. Transitions between the lowest members of a band lie on the left, between members increasing systematically toward the right.

Table VI-9. IBFA-Calculated Q Values (eb) for Selected Band-Head States in the Odd-Mass Os Isotopes. Known Experimental Values Are in Parentheses.

K^{π}	^{177}Os	^{179}Os	^{181}Os	^{183}Os	^{185}Os
$1/2^-(f_{5/2})$				5.8283	5.4241
$1/2^-(p_{3/2})$	5.6966	6.1641	6.1199		
$7/2^-(f_{7/2})$		3.2025	6.3729	5.5201	
$7/2^-(h_{9/2})$					5.3400
$9/2^+(i_{13/2})$		4.9536	5.3244	5.2882	4.9425
				(5.72±0.50)	

Table VI-10. IBFA-Calculated μ (nm) values for Selected Band-Head States in the Odd-Mass Os Isotopes. Known Experimental Values Are in Parentheses.

K^{π}	^{177}Os	^{179}Os	^{181}Os	^{183}Os	^{185}Os
$1/2^-(f_{5/2})$				0.1433	0.2033
$1/2^-(p_{3/2})$	0.1096	0.1433	0.0908		
$7/2^-(f_{7/2})$		0.4700	0.7429	0.8391	
$7/2^-(h_{9/2})$					0.7147
$9/2^+(i_{13/2})$		1.2251	1.2297	1.0045	0.9975
				(0.800±0.019)	

meaningful comparisons difficult.

Interference effects are much more important for the Os isotopes than they were for the Re isotopes, particularly where $1/2^-$ states are involved. For example, compare the curves for B(M1) values in the $1/2^-$ band shown in Figure VI-13 -- constructive and destructive interference effects are very apparent. Less immediately striking, but perhaps of more significance, are similar effects in the curves for B(E2) values shown in Figure VI-12. There the interference effects are sufficient to add appreciably to the normally-dominant core contributions. This presents a decided contrast to the very smooth behavior for the B(E2) values for the Re isotopes shown in Figure VI-6.

D. THE ODD-ODD NUCLEI: $^{176-184}$Re

1. Excitation Energies

The Hamiltonian for deformed odd-odd nuclei can be written as follows [Ch88b,Sc88]:

$$H = H_{IBA} + H_{p,F} + H_{n,F} + H_{p,BF} + H_{n,BF} + V_{pn} \qquad \text{(VI-10)}$$

The first five terms are determined from the previous even-even and odd-mass calculations. The last term is the residual interaction between the odd-proton and the odd-neutron, which takes the form,

$$V_{pn} = V_q Q_p \cdot Q_n + V_s \sigma_p \cdot \sigma_n \, . \qquad \text{(VI-11)}$$

The structure of these nuclei is dominated by the features of each of the two odd particles that are coupled to the core. Equation VI-11 here represents only the residual interaction between the odd particles. It plays a relatively minor role, because its dominant component is a quadrupole-quadrupole force, and most of the quadrupole neutron-proton interaction is already taken into account via the particle-boson interaction in the first five terms of Equation VI-10. The effect of the residual interaction to enhance these correlations is thus small, as is confirmed by numerical calculations. Therefore, we simply use $V_q=0$ for our calculations.

The above arguments, however, are not valid for the odd-tensor components. Of special interest is the proton-neutron spin-spin interaction, the last term in Equation VI-11. The expectation value of σ for bosons is small, because of their large quadrupole collectivity. Since this interaction is not taken into account in the particle-boson interactions, we retain it in the residual interaction. Its effect is well known, introducing a triplet-singlet splitting of the order of 100 keV or less. In our calculations we chose the strength of V_s to be -0.02 MeV, constant for all orbits and isotopes. This reproduces reasonably well the triplet-singlet splitting observed near closed shells.

In order to make numerical calculations feasible, we have truncated the full two-quasiparticle basis space. In the calculation of ^{182}Re, for example, we first calculated ^{183}Re in the full basis of one proton hole in all possible orbits coupled to the complete core. From this calculation only the 15 lowest states for each spin and parity were retained and used for coupling the odd neutron hole, ^{183}Os. The

coupling of the first particle is in a complete basis; truncation is made only in coupling of the second particle. We can also do the calculation in reverse order, i.e., first couple the odd neutron to the even-even core and then coupled the odd proton to the truncated basis. The effect of the basis truncation can thus be investigated by comparing the results of two complementary coupling schemes. We have verified that for the present calculation this change of the coupling order reproduces almost identical energies for the first 5 levels of each spin, and reproduces the energies to within 20 keV for higher levels. We have also checked the effect of decreasing the number of levels entering for basis of the second-coupling from 15 to 12 for each spin. This changed the energies of interest by less than 10 keV.

1.1 ^{182}Re

Experimental data are most complete for ^{182}Re [S184], where four rotational bands plus a few other states have been characterized in considerable detail. The 7^+ ground state and the 2^+ state are the triplet and singlet couplings of the $\pi 5/2^+[402\uparrow]$ (originating from the $d_{5/2}$ spherical state) and the $\nu 9/2^+[624\uparrow]$ (from the $i_{13/2}$ spherical state) orbits. The excitation energy of the 2^+ state is unknown; because of the long half-life for a M5 γ-transition between these states, each decays independently by β^+/ε. The IBFFA calculation predicted the 2^+ state to lie at 38.6 keV, but we plot the two halves of the energy spectrum in Figure VI-14 separately, one with 7^+, the other with 2^+ as the base. The results agree well with experimental data, except for the 4^- band. The reason for this discrepancy lies in the fact that in the calculation there is a close-lying 5^- band, which is

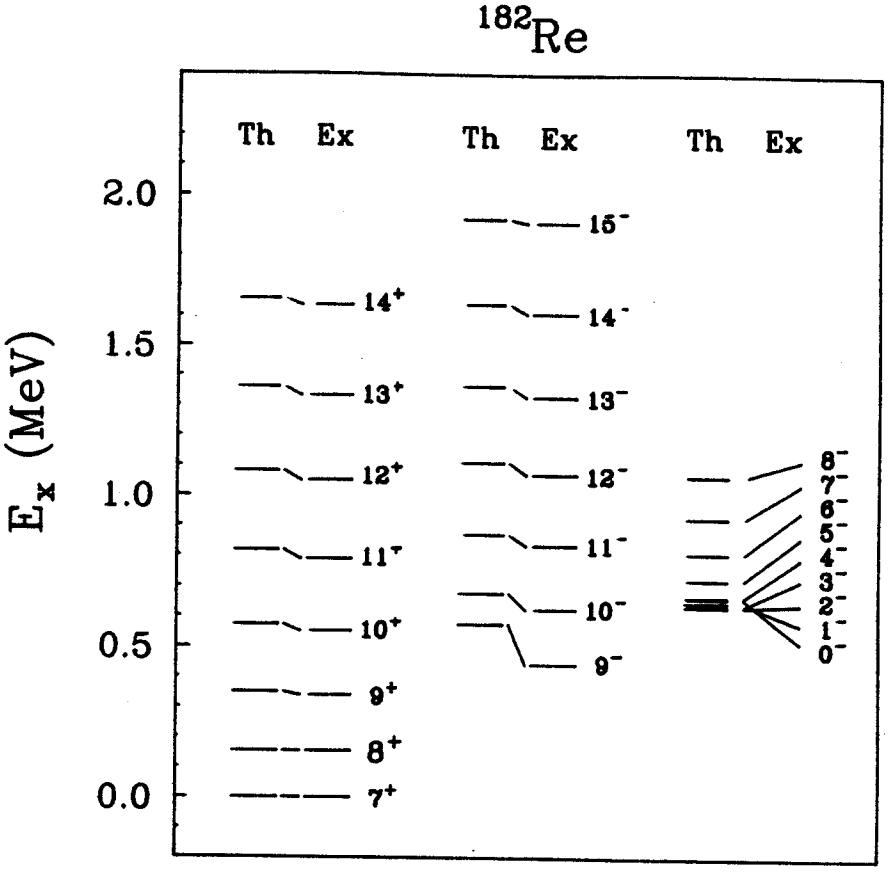

Figure VI-14. IBFFA-calculated excitation energies for states in odd-odd ^{182}Re compared with experimental data.

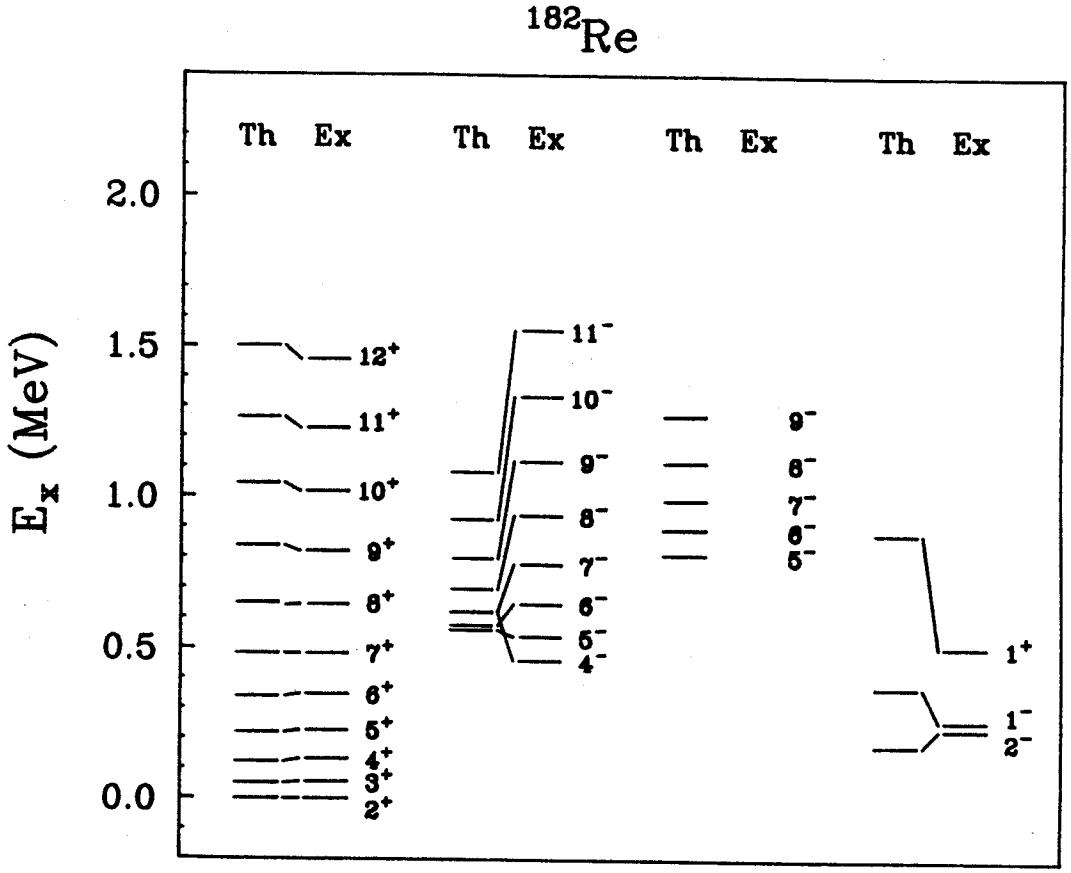

Figure VI-14. (cont'd.).

the singlet coupling with respect to the 4^- band. Both the odd-proton (the $K^\pi=1/2^-$ in ^{183}Re) and the odd-neutron ($K^\pi=9/2^+$ in ^{183}Os) components which constitute the odd-odd states here have large Coriolis couplings. Because of the Coriolis force, which is not attenuated in the present calculations, these two bands mix strongly, with the result that the lowest member of the $K^\pi=4^-$ band is a 5^- state.

In Figure VI-14, we also show a predicted $K^\pi=0^-$ and a $K^\pi=5^-$ band, which are the singlet couplings respective to the $K^\pi=9^-$ and the $K^\pi=4^-$ bands. We obtain quite reasonable values for the triplet-singlet splittings for the bands shown, although this is not always true for some higher-lying bands.

1.2 ^{180}Re

Only the results of ^{180}Re from our calculations are shown in Figure VI-15, because the assignments are considerably less certain for this nucleus. The calculations predict that there are quite a few relatively low-lying, low-spin bands. Indeed this is what one would expect from coupling the available single-particle orbits from the odd-mass neighbors. Rotational bands of ^{180}Re have been studied by two groups, however, there is discrepancy between their results. Lieder et al. [Li85,Ve85] observed at least six rotational bands. The K values [Ve85] of the bands were assigned on the basis of M1/E2 mixing ratios, with an uncertainty, $\Delta K=\pm 1$. Most of the bands in their results are low-spin bands and they are compatible with some of the bands predicted by IBFFA calculations. However, the uncertainty in the K assignment forbids a meaningful comparison.

Kreiner et al. [Kr87b] also studied ^{180}Re. Four rotational bands

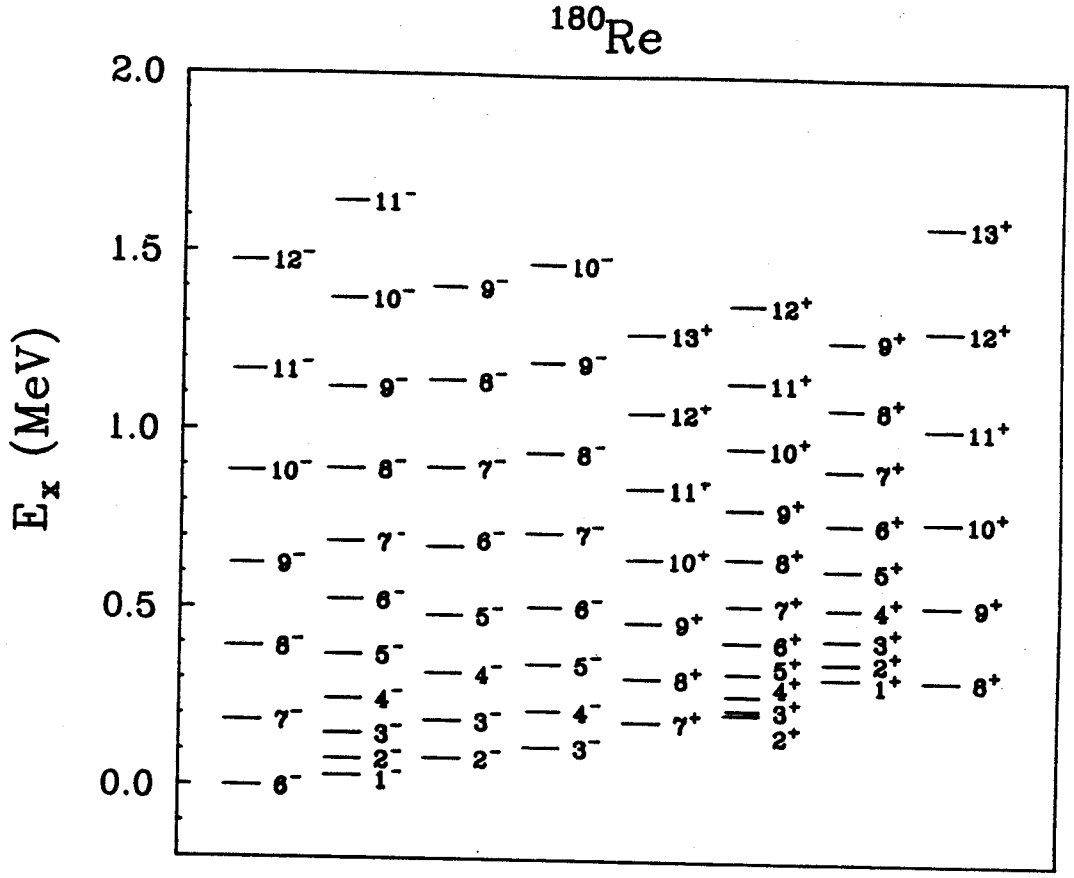

Figure VI-15. IBFFA-calculated excitation energies for states in odd-odd ^{180}Re. The bands come in pairs, with the triplet coupling on the left and the singlet coupling on the right.

were observed, and three of them are coincide with the results of Lieder et al., but with different spin assignments. Kreiner's results did not show any connection with the ground state, and the proposed spin assignments are based on a 5^+ "effective" ground state. The assignment of this effective ground state is not mentioned, and the only 5^+ state that can be formed by coupling the available odd-mass states observed in the nearby odd-mass nuclei (see Table III of [Kr87b]) will have an excitation energy of a few hundreds of keV. Therefore, these spin assignments are questionable. However, if we accept their assignments for the band configuration, the energy spacings from our calculations do correspond to their results. The comparisons are listed in Table VI-11. The calculations predict the spacings of $K^\pi=8^+$ band very well. Whereas, the spacings of $k^\pi=7^+$ and 5^+ bands are smaller than experimental results, because the Coriolis forces in these bands are overestimated. We do not agree on the neutron orbit Kreiner et al. assigned for the $K^\pi=8^-$ band. We think it should be the $\nu 9/2^+[624]$, the same as in $K^\pi=7^+$ band. Also, in our calculations the first level of this band has spin 9. If they did misassign the K for this band, the experimental data and the calculated values become much closer.

Overall speaking, the results of Lieder et al., seem to be, in general, much compatible with our calculations. However, no conclusions should be drawn before definite spin assignments for the band-head are made.

1.3 ^{184}Re

A number of rotational bands have been observed in ^{184}Re, but only the ground state 3^- and an 8^+ band having its band head at 188 keV have

Table VI-11. IBFFA Calculated Energy Spacings for ^{180}Re Compared with Experimental Data.

$K^{\pi}=8^{+}$	$\pi 9/2^{-}[514]\times\nu 7/2^{-}[514]$	
	EXP	IBFFA-CAL
$9^{+} \rightarrow 8^{+}$	228.7	210.8
$10^{+} \rightarrow 9^{+}$	246.0	236.5
$11^{+} \rightarrow 10^{+}$	261.4	260.2
$12^{+} \rightarrow 11^{+}$	275.4	277.0

$K^{\pi}=7^{+}$	$\pi 5/2^{+}[402]\times\nu 9/2^{+}[624]$	
	EXP	IBFFA-CAL
$8^{+} \rightarrow 7^{+}$	149.5	123.5
$9^{+} \rightarrow 8^{+}$	182.1	157.0
$10^{+} \rightarrow 9^{+}$	220.5	178.6

Table VI-12. (cont'd.).

$K^{\pi}=5^{+}$	$\pi 1/2^{-}[541]\times\nu 1/2^{-}[521]$	
	EXP	IBFFA-CAL
$7^{+} \rightarrow 5^{+}$	191.1	142.5
$9^{+} \rightarrow 7^{+}$	297.8	248.0
$11^{+} \rightarrow 9^{+}$	386.4	354.2
$13^{+} \rightarrow 11^{+}$	465.6	451.1

$K^{\pi}=8^{-}$	$\pi 9/2^{-}[514]\times\nu 7/2^{+}[633]$	
	EXP	IBFFA-CAL
$9^{-} \rightarrow 8^{-}$	134.3	---
$10^{-} \rightarrow 9^{-}$	176.4	119.6
$11^{-} \rightarrow 10^{-}$	210.1	165.4
$12^{-} \rightarrow 11^{-}$	237.2	191.4
$13^{-} \rightarrow 12^{-}$	261.0	199.0
$14^{-} \rightarrow 13^{-}$	282.5	216.3

been given definite assignments [Ma77]. A comparison of our results with these experimental data is shown in Figure VI-16. Our calculations indicate the two bands mentioned above, plus tentatively assigned 1^- and 2^- bands starting at 56 and 74 keV, respectively. The spacings within the bands is reproduced quite well, but there are minor problems with the positions of the band heads themselves. In particular, note that we calculated the 2^- band head to lie below 3^- band head, whereas the reverse is observed. The most probable interpretation for these states is that they are the triplet and singlet couplings of a $\pi 5/2^+[402\uparrow]$ and a $\nu 1/2^-[510\uparrow]$ Nilsson state, so the triplet would appear to lie lower in energy than the singlet. However, there is considerable mixing of the $1/2^-$ neutron states in the odd-mass Os isotopes, and our calculations would indicate large contributions from $1/2^-[521\downarrow]$ and $1/2^-[501\downarrow]$ states, so the question of triplet versus singlet couplings becomes a bit obscure.

1.4 The Doubly-Decoupled Bands of ^{176,178,180}Re

Both ^{176}Re and ^{178}Re have been studied by Santos et al. [Sa89], and ^{176}Re also by us. However, none of the studies was able to give solid spin assignments, except for the well-known doubly-decoupled band. Therefore, for these two nuclei we will only discuss the doubly-decoupled bands, along with the similar band in ^{180}Re. Figure VI-17 shows the comparisons of our calculations with experimental data. Although 3^+ is predicted to be the level with the lowest excitation energies for all the three doubly-decoupled band, no $5 \rightarrow 3$ transition has ever been observed. In Figure VI-17, we thus used the values from calculations in both cases for easy comparison.

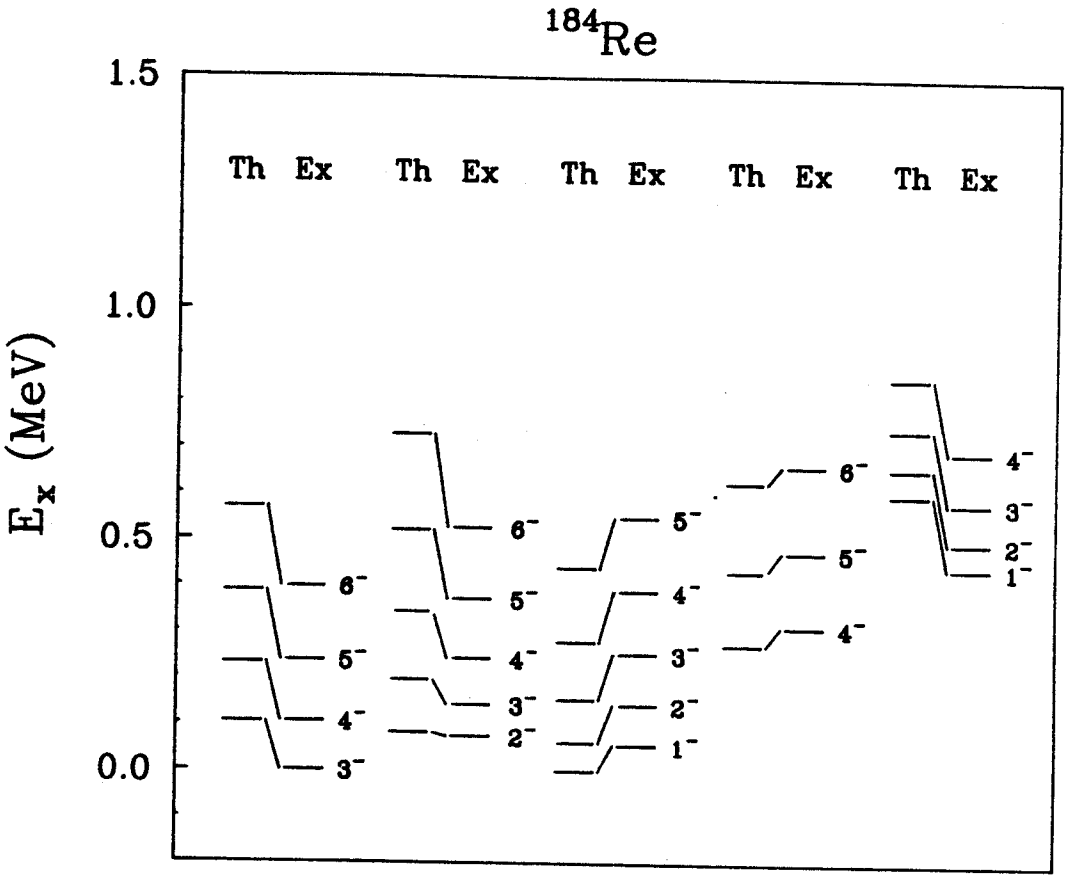

Figure VI-16. IBFFA-calculated excitation energies for states in odd-odd ^{184}Re compared with experimental data. The bands are plotted in pairs, with the triplet coupling on the left, the singlet coupling on the right of each pair.

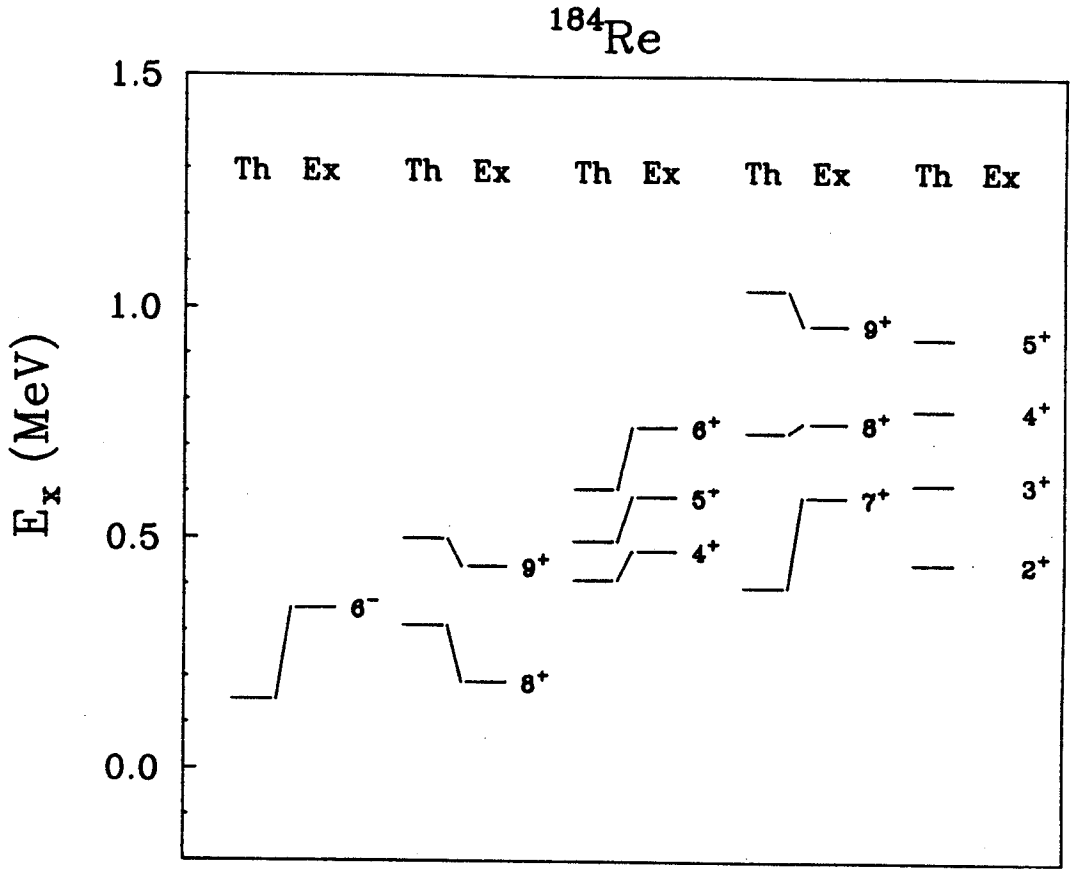

Figure VI-16. (cont'd.).

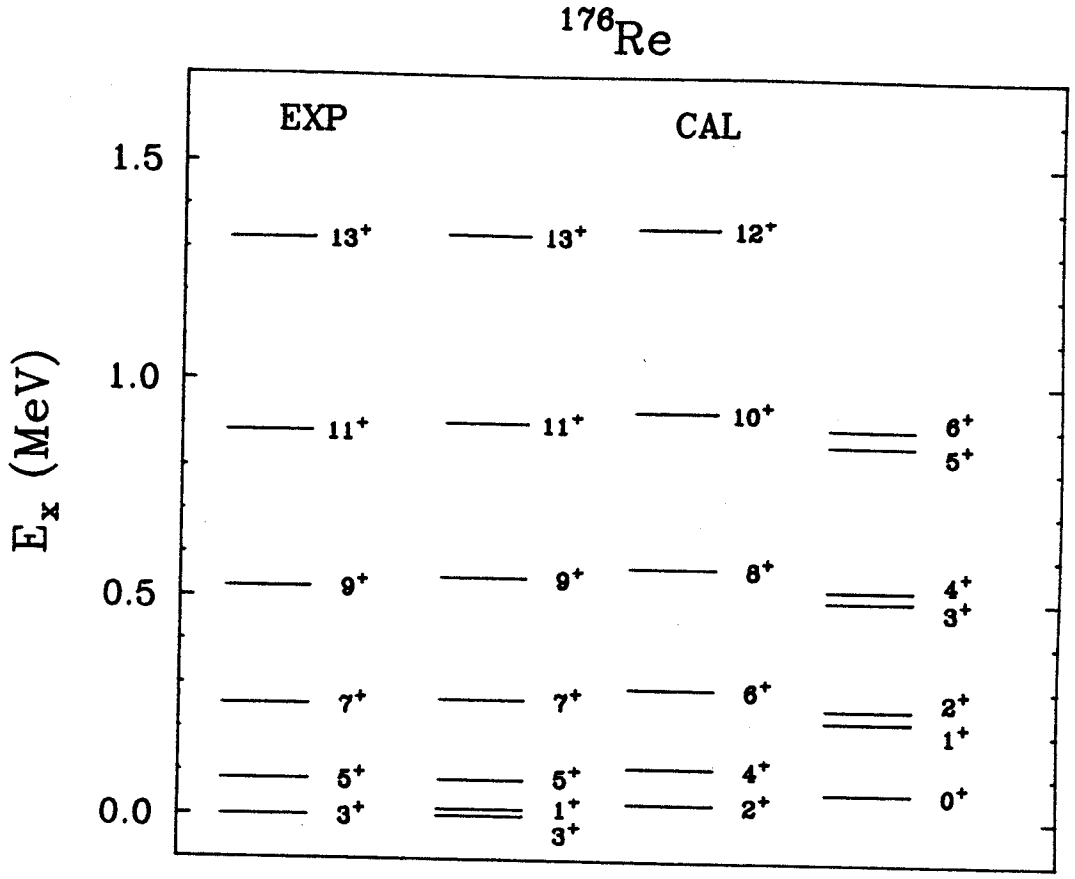

Figure VI-17. IBFFA-calculated doubly-decoupled bands of ^{176}Re, ^{178}Re, and ^{180}Re compared with experimental data.

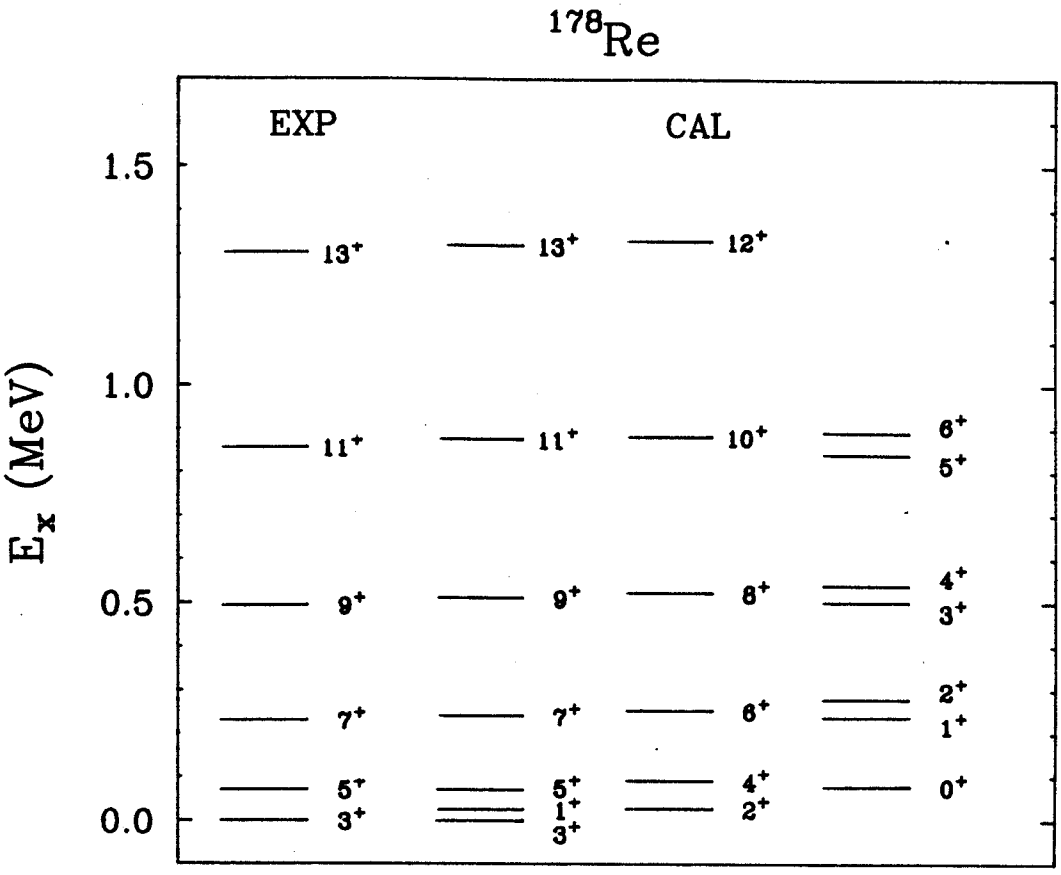

Figure VI-17. (cont'd.).

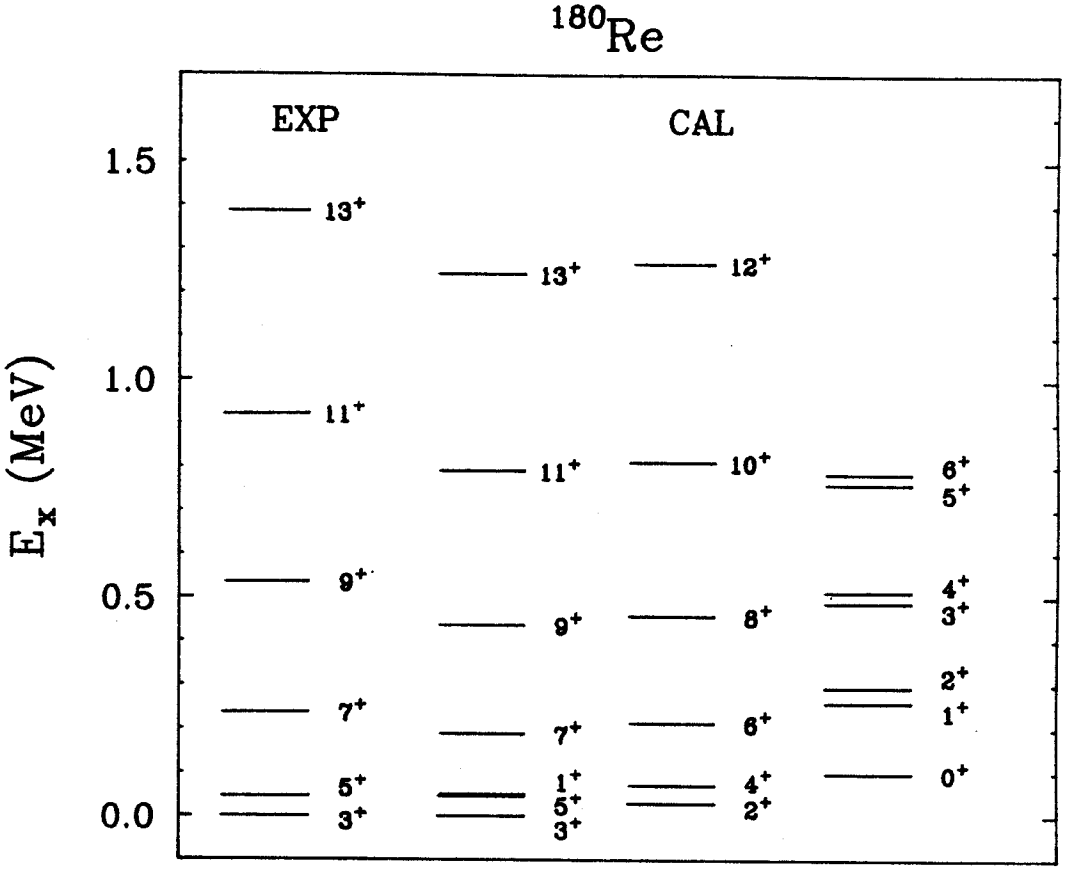

Figure VI-17. (cont'd.).

In Figure VI-17, we not only show the observed favored members, but also the predicted unfavored members with even spin. Furthermore, the singlet coupling of the 1/2-1/2 orbits, which produces a K=0 band, is displayed at the very right side. There is pretty good correspondence for all the three nuclei. This is especially surprising for ^{176}Re, for the odd-proton nucleus ^{175}Re in the calculation for ^{176}Re is totally unknown, so the parameters in IBFA calculations were decided purely based on systematics.

The energies of 5 → 3 transitions are predicted to be 82.9, 71.0, and 45.7 keV, respectively, for ^{176}Re, ^{178}Re, and ^{180}Re. If we believe that the IBFFA calculations can predict the first transition as well as other transitions, then the fact that the first transition was not observed can be explained by the large internal conversion coefficients for these E2 transitions. However, since the IBFFA calculations are simply the coupling of the odd-mass nuclei, ambiguities in the existence (or the magnitude of the energy) of the 9/2 → 5/2 transition, counterpart of the 5 → 3 transition in odd-proton nucleus, may very much affect the prediction of this 5 → 3 transition in odd-odd nucleus.

2. Quadrupole Properties

Quadrupole transitions in medium-heavy nuclei are in general of the order of several hundreds of single-particle units. In the calculation of strong, collective transitions, therefore, the contributions from the odd proton and odd neutron are unimportant. We thus limited the E2 operator to that defined in Equation VI-4, with the boson effective charge e_B the same as enters into the description of E2 properties in the even-even core and the two related odd-mass nuclei. The comparison

of the quadrupole moments for odd-odd Re isotopes is made in Table VI-12, and B(E2) values of the first few transitions of the rotational bands in ^{182}Re are shown in Figure VI-18. The predictions of the quadrupole moments agree reasonably well with experiments.

3. Magnetic Dipole Properties

Contrary to quadrupole transitions, M1 transitions are at most a few single-particle units in strength. The single-particle part of the operator, as given in Equation VI-9, thus plays the same important role as it did in the odd-mass nuclei, with the d-boson g factor equal to the g factor for the 2_1^+ states in the even-even core, g_s quenched by a factor of 0.7, and g_l taken equal to their free values. Some magnetic moments are listed in Table VI-13, and B(M1) values are shown in Figure VI-19.

D. CONCLUSIONS

Although only the simplified Hamiltonian for an axial rotor was used, the IBA model once again proved its ability to give very accurate predictions of the excitation energy spectra, as well as the electromagnetic properties for even-even Os isotopes with mass 176-186.

The Os cores were coupled with a single particle or hole in the subsequent IBFA calculations, and, in general, the calculations produce satisfactory results for odd-mass Re and Os isotopes. We dealt with quite strong Coriolis coupling in these Re and Os isotopes and found that the IBFA calculations usually overestimate the Coriolis force.

Table VI-12. Quadrupole Moments for Odd-Odd Re Isotopes.

Isotope	J^{π}	Q_{IBA} (eb)	Q_{Exp} (eb)
^{180}Re	6^-	6.50	---
	1^-	6.45	---
^{182}Re	7^+	5.66	6.1±0.3
	2^+	5.40	>6.3±0.2
^{184}Re	3^-	5.06	7.1±0.3
	8^+	4.83	---

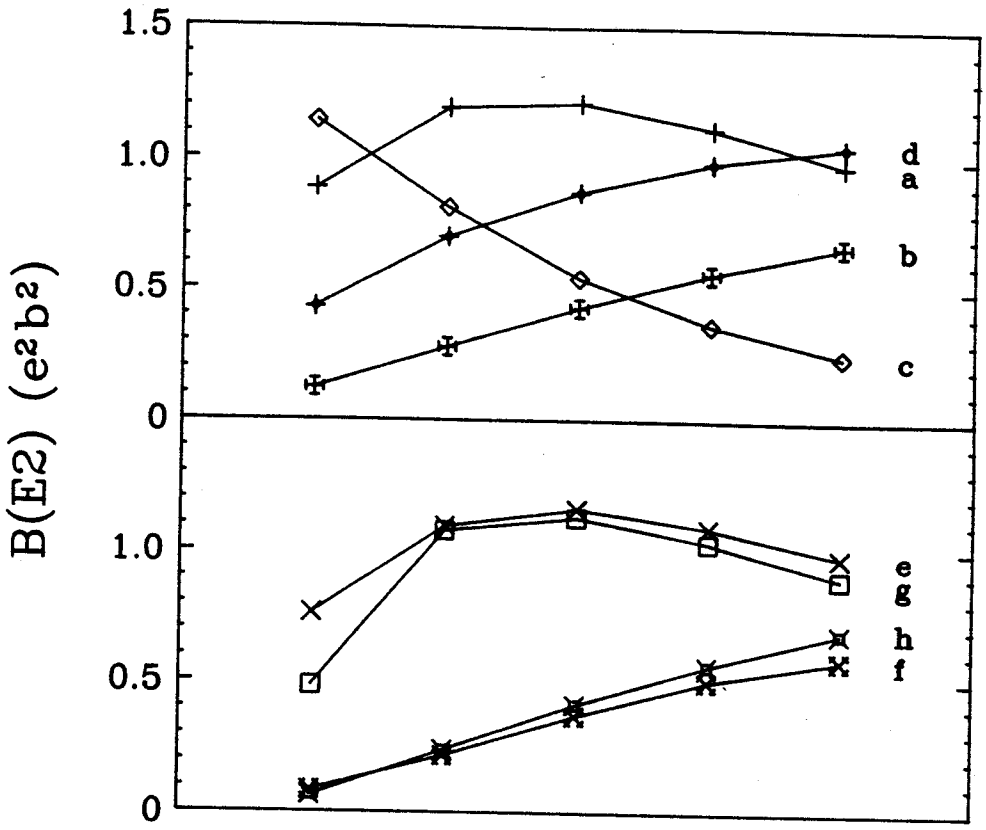

Figure VI-18. IBFFA-calculated B(E2) values for selected crossover and stopover transitions between members of low-lying bands in the odd-odd ^{182}Re. The curves correspond to transitions in bands as follows: a, 7^+ stopover; b, 7^+ crossover; c, 2^+ stopover; d, 2^+ crossover; e, 9^- stopover; f, 9^- crossover; g, 4^- stopover; h, 4^- crossover. Transitions between the lowest members of a band lie at the left, with transitions between systematically increasing members more toward the right.

Table VI-13. Magnetic Moments for Odd-Odd Re Isotopes.

Isotope	J^{π}	μ_{IBA} (nm)	μ_{Exp} (nm)
^{180}Re	6^-	2.41	---
	1^-	2.35	---
^{182}Re	7^+	2.33	2.76±0.17
	2^+	3.28	3.16±0.22
^{184}Re	3^-	3.19	2.50±0.19
	8^+	2.09	2.89±0.13

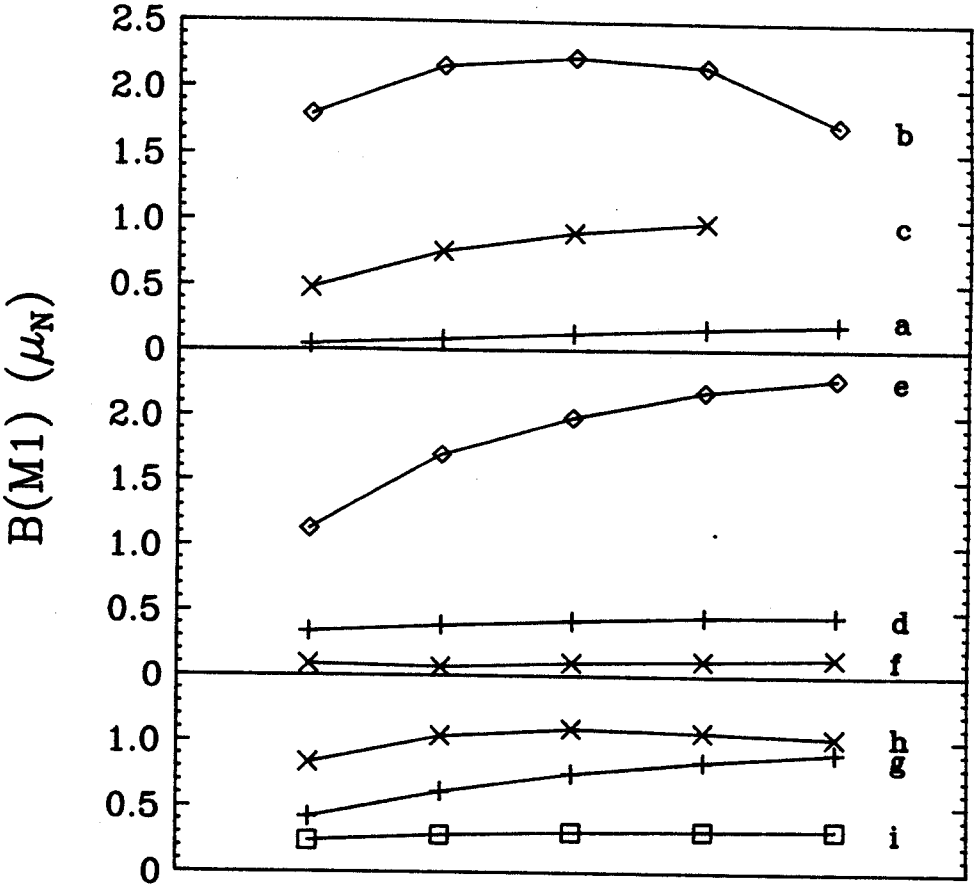

Figure VI-19. IBFFA-calculated B(M1) values for selected transitions among low-lying band members in the odd-odd Re isotopes. The curves represent transitions in bands as follows. ^{180}Re: a, 6^-; b, 1^-; c, 2^-. ^{182}Re: d, 7^+; e, 2^+; f, 9^-. ^{184}Re: g, 3^-; h, 1^-; i, 8^+. Transitions between the lowest members of bands lie at the left, with transitions between systematically increasing members toward the right.

However, taking into account that this Coriolis force arises naturally in the IBFA model and there is no parameter whatsoever to control its magnitude, we feel the results are more than satisfactory. Furthermore, even though now and then the spacings within the band cannot be reproduced too well, the IBFA calculations do successfully reproduce the general feature of the nucleus.

We required the parameters in the IBFA calculations to change smoothly from isotope to isotope. Among the odd-mass Re isotopes, this restriction is justified in $^{177-185}$Re, because they show very similar excitation energy spectra. We have also learned from ^{175}Re that using parameters determined solely by systematics also produced a reasonable picture of the levels. The excitation energy spectra of odd-mass Os isotopes are much more varied, but this did not affect the results of calculations. In addition, in order to save computing time, we even further truncate the boson number down by 1 or 2 unit, and never try to make a splendid fit.

These calculations of odd-odd Re isotopes are the first complete calculation of their kind - we calculated both positive- and negative-parity states and included all the available single-particle orbits. No additional parameters were introduced in the IBFFA calculations except for the proton-neutron spin-spin interaction, which is set to be a constant for all the orbits and isotopes.

The IBFFA model is able to give an accurate description of states in the odd-odd Re nuclei, as can be seen from the comparisons with experimental data. These odd-odd nuclei constitute a very stringent test of the model, because odd-odd nuclei do not provide the same sort of smoothly varying systematics as do other types of nuclei.

Usually pretty good spacings within the bands can be obtained in IBFFA calculations, from comparison with the two most completely studied odd-odd ^{182}Re and ^{184}Re. However, poorer spacings were obtained for a few bands, especially the $K^{\pi}=4^{-}$ band of ^{182}Re. The couplings for the 4^{-} band are $\pi 1/2^{-}[541\uparrow]$ and $\nu 9/2^{+}[624\uparrow]$. Both have strong Coriolis force, and thus the fits were relatively poor in the IBFA calculations. Errors accumulate from previous IBA and IBFA calculations are going to IBFFA calculations: any difficulties in describing the even-even cores and, particularly, the odd-mass states are compounded in the odd-odd systems. However, if good fits for the even-even cores and odd-mass nuclei can be obtained, then good spacings in the odd-odd nuclei are likely. This can also be seen in the $1/2^{-}$ bands in the odd-mass Os isotopes, where the fits are in general the poorest among the odd-mass states. Correspondingly, relatively poor fits were obtained for odd-odd bands involving these $1/2^{-}$ neutrons, such as inverting the triplet and singlet couplings for the 3^{-} and 2^{-} bands in ^{184}Re.

There is problem in predicting the positions of the band heads. This is the result of inadequate fitting of the positions of odd-mass band-heads, but it also points out the difficulty in using constant V_q for the proton-neutron residual interaction (V_{pn}) in the IBFFA Hamiltonian. The other component in V_{pn}, the spin-spin interaction, seems to be the reason why some of the triplet couplings lie higher than the singlet couplings. To free V_q and V_s, allowing them to vary over a reasonable range, will certainly improve the fits of the odd-odd nuclei. However, this will destroy the simplicity of the IBFFA model. Indeed, the model has already shown its power for predicting the energy spectra and electromagnetic properties for the odd-odd nucleus [Ch88b,Sc89], and

it seems a shame to improve the model by making the calculations much more complicated.

LIST OF REFERENCES

A

[An79] O. Andersen, J.D. Garrett, G.B. Hagemann, B. Herskind, D.L. Hillis, and L.L. Riedinger, Phys. Rev. Lett. **43**, 687 (1979).

[Ar75a] A. Artna-Cohen, Nucl. Data Sheets **16**, 267 (1975).

[Ar75b] A. Arima and F. Iachello, Phys. Rev. Lett. **35**, 1069 (1975).

[Ar76a] A. Arima and F. Iachello, Phys. Rev. C **14**, 761 (1976).

[Ar76b] A. Arima and F. Iachello, Ann. Phys. (N.Y.)**99**, 253 (1976).

[Ar77] A. Arima, T. Otsuka, F. Iachello, and I. Talmi, Phys. Lett. **66B**, 205 (1977).

[Ar78] A. Arima and F. Iachello, Ann. Phys. (N.Y.)**111**, 201 (1978).

[Ar79] A. Arima and F. Iachello, Ann. Phys. (N.Y.)**123**, 468 (1979).

B

[Ba81] A.B. Balantekin, I. Bars, and F. Iachello, Phys. Rev. C **47**, 19 (1981).

[Be72] F.M. Bernthal, J.S. Boyno, C.L. Dors, T.L. Khoo, and R.A. Warner, MSU Cyclotron Laboratory Annual Report for 1972-73, p.72; C.L. Dors, F.M. Bernthal, and R.A. Warner, ibid.,p.74.

[Be79a] F.A. Beck, E. Bozek, T. Byrski, C. Gehringer, J.C. Merdinger, Y. Schutz, J. Styczen, and J.P. Vivien, Phys. Rev. Lett. **42**, 492 (1979).

[Be79b] R. Bengtsson and S. Frauendorf, Nucl. Phys. **A327**, 139 (1979).

[Be80] R. Bengtsson, Proceesings of the International Conference on Nuclear Behavior at High Angular Momentum, Strasbourh, Suppl. J. de Phys. **C10**, 84 (1980).

[Be81] R. Bengtsson and J.C. Waddington, Phys. Rev. C **24**, 2367 (1981).

[Be87a] C.W. Beausang, L. Hildingsson, E.S. Paul, W.F. Pier, Jr., N. Xu, and D.B. Fossan, Phys. Rev. C **36**, 1810 (1987).

[Be87b] E.M. Beck, F.S. Stephens, J.C. Bacelar, M.A. Deleplanque, R.M. Diamond, J.E. Draper, C. Duyar, and R.J. McDonald, Phys. Rev. Lett. **58**, 2182 (1987).

[Be87c] E.M. Beck, R.J. McDonald, A.O. Macchiavelli, J.C. Bacelar, M.A. Deleplanque, R.M. Diamond, J.E. Draper, and F.S. Stephens, Phys. Lett. **195B**, 531 (1987).

[Be88] R. Bengtsson, Proceedings of the International Conference on Contemporary Topics in Nuclear Structure Physics, Cocoyoc, Mexico, 1988, p.317.

[Bi67] K.M. Bisgard and E. Veje, Nucl. Phys. **A103**, 51 (1967).

[Bo75] A. Bohr and B.R. Mottelson, Nuclear Structure, Vol II, W.A. Benjamin, Inc., 1975.

[Bo76] J.P. Boisson, R. Piepenbring, and W. Ogle, Phys. Reports **26C**, 99 (1976).

[Br84] S. Brandt, B. Paar, and D. Vretenar, Z. Phys. A **319**, 355 (1984).

[Br88] E. Browne, Nucl. Data Sheets **55**, 483 (1988).

[Bü81] S. Büttgenbach, R. Dicke, G. Gölz, and F. Träber, Z. Phys. A **302**, 281 (1981).

C

[Ca78] R.R. Casten and J.A. Cizewski, Nucl. Phys. **A309**, 477 (1978).

[Ch72] A. Christy and O. Häusser, Nucl. Data Tables **A11**, 281 (1972).

[Ch88a] H.C. Chiang, S.T. Hsieh, and T.T.S. Kuo, Phys. Rev. C **38**, 2453 (1988).

[Ch88b] W.-T. Chou, Wm.C. McHarris, and O. Scholten, Phys. Rev. C **37**, 2834 (1988).

D

[Da86] J. Davidson, M. Davidson, M. Debray, G. Falcone, D. Hojman, A.J. Kreiner, I. Mayans, C. Polmar, and D. Santos, Z. Phys. A **324**, 363 (1986).

[De80] M.A. Deleplanque, F.S. Stephens, O. Anderson, C. Ellegaard, J.D. Garrett, B. Herskind, D. Fossan, M. Neiman, C. Roulet, D.C. Hillis, H. Kluge, R.M. Diamond, and R.S. Simon, Phys. Rev. Lett. **45**, 172 (1980).

[De88a] M.A. Delephanque, C.W. Beausang, J. Burde, R.M. Diamond, J.E. Draper, C. Duyar, A.O. Macchiavelli, R.J. McDonald, and F.S. Stephens, Phys. Rev. Lett. **60**, 1626 (1988).

[De88b] M.A. Delephanque, C.W. Beausang, J. Burde, R.M. Diamond, F.S. Stephens, R.J. McDonald, and J.E. Draper, preprint, LBL-25941, 1988.

[Di63] R.M. Diamond, B. Elbek, and F.S. Stephens, Nucl. Phys. **A43**, 560 (1963).

[Di80] R.M. Diamond and F.S. Stephens, Ann. Rev. Nucl. Part. Sci. **30**, 85 (1980).

[Di83] R.M. Diamond, Proceedings of the International Conference on Nuclear Physics With Heavy Ions, Stony Brook, NY, 1983, p.179.

[Di84] R.M. Diamond and F.S. Stephens, Nature **310**, 457 (1984).

[Dr78] G.D. Dracoulis, P.M Walker, and A. Johnston, J. Phys. G **4**, 713 (1978).

[Dr82] G.D. Dracoulis, C. Fahlander, and M.P. Fewell, Nucl. Phys. **A383**, 119 (1982).

[Dr83] G.D. Dracoulis, C. Fahlander, and A.P. Byrne, Nucl. Phys. **A401**, 490 (1983).

E

[El81a] N. Elias, R. Beraud, A. Charret, R. Duffait, M. Meyer, S. Andre, J. Genevey, S. Tedesco, J. Treherne, F. Beck, and T. Byrski, Nucl. Phys. **A351**, 142 (1981).

[El81b] Y.A. Ellis-Akovali, Nucl. Data Sheets **33**, 557 (1981).

[Em73] G.T. Emery, R. Hochel, P.J. Daly, and K.J. Hofstetter, Nucl. Phys. **A211**, 189 (1973).

[Er81] H. Ernst, E. Hagn, and E. Zech, Phys. Rev. C **23**, 1739 (1981).

F

[Fa78] A. Faessler and M. Ploszajczak, Phys. Lett. **76B**, 1 (1978).

[Fa83] A. Faessler, Nucl. Phys. **A396**, 291c (1983).

[Fi84] R.B. Firestone, Nucl. Data Sheets **43**, 289 (1984).

[Fi87] R.B. Firestone, Nucl. Data Sheets **52**, 715 (1987).

[Fl76] C. Flaum and D. Cline, Phys. Rev. C **14**, 1224 (1976).

[Fo85] C. Foin, S. Andre, D. Barneoud, J. Genevey, J.A. Pinston, and J. Salicio, Phys. Lett. **159B**, 5 (1985).

[Fr81a] S. Frauendorf, Phys. Scripta **24**, 349 (1981).

[Fr81b] G. Friedlander, J.W. Kennedy, E.S. Macias, and J. Miller, Nuclear and Radiochemistry, 3rd Edition (John Wiley & Sons, 1981).

G

[Ga58] C.J. Gallagher and S.A. Moszkowski, Phys. Rev. **111**, 1282 (1958).

[Ga80] J.D. Garrett and J.J. Gaardhoje, XIV Masurian Summer School on Nuclear Physics, Mikolajki, Poland, 1980.

[Ga81] J.D. Garrett, O. Andersen, J.J. Gaardhoje, G.B. Hagemann, B. Herskind, J. Kownacki, J.C. Lisle, L.L. Riedinger, W. Walus, N. Roy, S. Jönsson, H. Ryde, M. Guttormsen, and P.O. Tjom, Phys. Rev. Lett. **47**, 75 (1981).

[Ga82] J.D. Garrett, Proceedings of the Conference on High Angular Momentum Properties of Nuclei, Oak Ridge, Tennessee, 1982, p.17.

[Ga88] J.D. Garrett, J. Nyberg, C.H. Yu, J.M. Espino, and M.M. Godfrey, Proceedings of the International Conference on Contemporary Topics in Nuclear Structure Physics, Cocoyoc, Mexico, 1988, p.699.

[Ge80] A. Gelberg and A. Zemel, Phys. Rev. C **22**, 937 (1980).

[Gr73] E. Grosse, F.S. Stephens, and R.M. Diamond, Phys. Rev. Lett. **31**, 840 (1973).

[Gr74] E. Grosse, F.S. Stephens, and R.M. Diamond, Phys. Rev. Lett. **32**, 74 (1973).

H

[Ha65] S.M. Harris, Phys. Rev. **138**, B509 (1965).

[Ha75] B. Harmatz, D.J. Horen, and Y.A. Ellis, Phys. Rev. C **12**, 1083 (1975).

[Ha80] E. Hagn and E. Zech, Z. Phys. A **295**, 345 (1980).

[Ha81] E. Hagn and E.G. Eska, Nucl. Phys. **A 363**, 269 (1981).

[Ha83] H. Hanewinkel, W. Gast, U. Kaup, H. Harter, A. Dewald, A. Gelberg, R. Reinhardt, P. von Brentano, A. Zemel, C.E. Alonso, and J.M. Arias, Phys. Lett. **133B**, 9 (1983).

[Ha88] B. Haas, P. Taras, S. Flibotte, F. Banville, J. Gascon, S. Cournoyer, S. Monaro, N. Nadon, D. Prevost, D. Thibault, J.K. Johansson, D.M. Tucker, J.C. Waddington, H.R. Andrews, G.C. Ball, D. Horn, D.C. Radford, D. Ward, C.St. Pierre, and J. Dudek, Phys. Rev. Lett. **60**, 503 (1988).

[Hi86] L. Hildingsson, C.W. Beausang, D.B. Fossan, W.F. Piel,Jr., A.P. Byrne, and G.D. Dracoulis, Nucl. Instrum. Methods **A252**, 91 (1986).

[Ho73] R. Hochel, P.J. Daly, and K.J. Hofstetter, Nucl. Phys. **A211**, 165 (1973).

[Ho76] D.J. Horen and B. Harmatz, Nucl. Data Sheets **19**, 383 (1976).

[Ho77] M.V. Hoehn, E.B. Shera, Y. Yamazaki, and R.M. Steffen, Phys. Rev. Lett. **39**, 1313 (1977).

[Hu53] T. Huss and C. Zupancic, Mat. Fys. Medd. Dan. Vid. Selsk. 28: No1, 1953.

[Hu84] T. Hubsch and V. Paar, Z. Phys. A **319**, 355 (1984).

I

[Ia79] F. Iachello and O. Scholten, Phys. Rev. Lett. **43**, 679 (1979).

J

[Ja88a] V.P. Janzen, M.P. Carpenter, L.L. Riedinger, W. Schmitz, S. Pilotte, S. Monaro, D.D. Rajnauth, J.K. Johansson, D.G. Popescu, J.C. Waddington, Y.S. Chen, F. Dönau, and P.B. Semmes, Phys. Rev. Lett. **61**, 2073 (1988).

[Ja88b] R.V.F. Janssens, G.-E. Rathke, M.W. Drigert, I. Ahmad, K. Beard, R.R. Chasman, U. Garg, M. Hass, T.L. Khoo, H.-J. Körner, W.C. Ma, S. Pilotte, P. Taras, and F.L.H. Wolfs, Proceedings of the Conference on High-Spin Nuclear Structures and Novel Nuclear Shapes, Argonne National Laboratory, 1988, p.31.

[Jo71] A. Johnson, H. Ryde, and J. Sztarkier, Phys. Lett. **34B**, 605, (1971).

K

[Ka78] A.C. Kahler, L.L. Riedinger, N.R. Johnson, R.L. Robinson, E.F. Zganjar, A. Visvanathan, D.R. Zolnowski, M.B. Jughes, and T.T. Sugihara, Phys. Lett. **72B**, 443 (1978).

[Kr73] K.S. Krane, R.M. Steffen, and R.M. Wheeler, Nucl. Data Tables **A11**, 351 (1973).

[Kr84] A.J. Kreiner, D.E. Di Gregorio, A.J. Fendrik, J. Davidson, and M. Davidson, Phys. Rev. C **29**, 1572 (1984).

[Kr85] A.J. Kreiner, D.E. Di Gregorio, A.J. Fendrik, J. Davidson, and M. Davidson, Nucl. Phys. **A432**, 451 (1985).

[Kr86] A.J. Kreiner, P. Thieberger, and E.K. Warburton, Phys. Rev. C **34**, 1150 (1986).

[Kr87a] A.J. Kreiner and D. Hojman, Phys. Rev. C **36**, 2173 (1987).

[Kr87b] A.J. Kreiner, J. Davidson, M. Davidson, D. Abriola, C. Pomar, and P. Thieberger, Phys. Rev. C **36**, 2309 (1987).

[Kr88a] A.J. Kreiner, D. Hojman, J. Davidson, M. Davidson, M. Debray, G. Falcone, D. Santos, C.W. Beausang, D.B. Fossan, R. Ma, E.S. Paul, S. Shi, and N. Xu, Phys. Lett. **215B**, 629 (1988).

[Kr88b] A.J. Kreiner, J. Davidson, M. Davidson, P. Thieberger, E.K. Warburton, S. Andre, and J. Genevey, Nucl. Phys. **A489**, 525 (1988).

[Kr88c] A.J. Kreiner, Phys. Rev. C **38**, 2486 (1988).

L

[La72] S.A. Lane and J.X. Saladin, Phys. Rev. C **6**, 613 (1972).

[La75] I.M. Ladenbauer-Bellis, H. Bakhru, and P. Sen, Nucl. Phys. **A252**, 524 (1975).

[La78] I.M. Landenbauer-Bellis, P. Sen, and H. Bakhru, Can. J. Phys. **56**, 321 (1978).

[La81] A.J. Larabee and J.C. Waddington, Phys. Rev. C **24**, 2367 (1981).

[La86] A.J. Larabee, M.P. Carpenter, L.L. Riedinger, L.H. Courtney, J.C. Waddington, V.P. Janzen, W. Nazarewicz, J.-Y. Zhang, R. Bengtsson, and G.A. Leander, Phys. Lett. **169B**, 21 (1986).

[Le72] J.R. Leigh, J.O. Newton, L.A. Ellis, M.C. Evans, and M.J. Emmott, Nucl. Phys. **A183**, 177 (1972).

[Le77] I.Y. Lee, M.M. Aleonard, M.A. Delephanque, Y. El Masri, J.O. Newton, R.S. Simon, R.M. Diamond, and F.S. Stephens, Phys. Rev. Lett. **38**, 1454 (1977).

[Le82] R. Levy, N. Tsoupas, N.K.B. Shu, A. Lopez-Garcia, W. Andrejtscheff, and N. Benczer-Koller, Phys. Rev. C **25**, 293 (1982).

[Li73] Th. Lindblad, R. Bethoux, R.H. Price, and P. Kleinheinz, Nucl. Phys. **A217**, 459 (1973).

[Lo86] V. Lopac, S. Brandt, V. Paar, O.W.B. Schult, H. Seyfarth, and A.B. Balantekin, Z. Phys. A **323**, 491 (1986).

[Lu88] Y.-X. Luo, J.-Q. Zhong, D.J.G. Love, A. Kirwan, P.J. Bishop, M.J. Godfrey, I. Jenkins, P.J. Nolan, S.M. Mullins, and R. Wadsworth, Z. Phys. A **329**, 125 (1988).

M

[Ma81] H.J. Mang, Proceedings of the Nuclear Physics Workshop, I.C.T.P., Trieste, Miramare, Italy, 1981, p.149.

[Mc65] Wm.C. McHarris, Thesis, Univ. of California, Berkeley, 1965.

[Mc68] I.E. McCarthy, Introduction to Nuclear Theory (John Wiley & Sons, Inc., 1968).

[Mi71] W.T. Milner, F.K. McGowan, R.L. Robinson, P.H. Stelson, and R.O. Sayer, Nucl. Phys. **A177**, 1 (1971).

N

[Ne75] K. Neergard and V.V. Pashkevich, Phys. Lett. **57B**, 218 (1975).

[Ne76] A. Neskakis, R.M. Lieder, M. Müller-Veggian, H. Beuscher, W.E. Davidson, and C. Mayer-Böricke, Nucl. Phys. **A261**, 189 (1976).

[No85] P.J. Nolan, A. Kirwan, D.J.G. Love, A.H. Nelson, D.J. Unwin, and P.J. Twin, J. Phys. G **11**, L17 (1985).

[Ny84] B.M. Nyako, J.R. Cresswell, P.D. Forsyth, D. Howe, P.J. Nolan, M.A. Riley, J.F. Sharpey-Schafer, J. Simpson, N.J. Ward, and P.J. Twin, Phys. Rev. Lett. **52**, 507 (1984).

O

[Oh87] S. Ohya, K. Nishimura, and N. Mutsuro, Hyperfine Interaction **36**, 219 (1987).

P

[Pa87] V. Paar, Proceedings of International Symposium on Capture Gamma-Rays, Leuven, 1987 (unpublished).

[Pa89] E.S. Paul, D. Ahn, D.B. Fossan, Y. Liang, R. Ma, and N. Xu, Phys. Rev. C **39**, 153 (1989).

[Pi81] J.A. Pinston, R. Bengtsson, E. Monnand, F. Schussler, and D. Barneoud, Nucl. Phys. **A361**, 464 (1981).

[Pü77] F. Pühlhofer, Nucl. Phys. **A280**, 267 (1977).

R

[Ra50] J. Rainwater, Phys. Rev. **79**, 432 (1950).

[Ra80] I. Ragnarsson, T. Bengtsson, G. Leander, and S. Agerg. Nucl. Phys. **A347**, 287 (1980).

[Ra86] M.N. Rao, N.R. Johnson, F.K. McGowan, I.Y. Lee, C. Baktash, M. Oshima, J.W. McConnell, J.C. Wells, A. Larabee, L.L. Riedinger, R. Bengtsson, Z. Xing, Y.S. Chen, P.B. Semmes, and G.A. Leander, Phys. Rev. Lett. **57**, 667 (1986).

[Ra87] S. Raman, C.H. Malarkey, W.T. Milner, C.W. Nestor, Jr., and P.H. Stelson, At. Data and Nucl. Data Tables **36**, 1 (1987).

[Ri74] L.L. Riedinger, G.J. Smith, P.H. Stelson, E. Eichler, G.B. Hagemann, D.C. Hensley, N.R. Johnson, R.L. Robinson, and R.O. Sayer, Phys. Rev. Lett. **33**, 1346 (1974).

[Ri80a] L.L. Riedinger, Nucl. Phys. **A347**, 141 (1980).

[Ri80b] L.L. Riedinger, O. Anderson, S. Frauendorf, J.D. Garrett, J.J. Gaardhoje, G.B. Hagemann, B. Herskind, Y.V. Makovetzky, J.C. Waddington, M. Guttormsen, and P.O. Tjom, Phys. Rev. Lett. **44**, 568 (1980).

[Ri80c] L.L. Riedinger, W.K. Luk, D.R. Haenni, S.A. Hjorth, N.R. Johnson, I.Y. Lee, and R.L. Robinson, Proceedings of International Conference on Nuclear Physics, Berkeley, 1980, Vol 1, p.383.

[Ri81] L.L. Riedinger, Proceedings of the Nuclear Physics Workshop, I.C.T.P., Trieste, Miramare, Italy, 1981, p.131.

[Rö78a] F. Rösel, H.M. Fries, K. Alder, and H.C. Pauli, Atom. Data and Nucl. Data Tables **21**, 91 (1978).

[Rö78b] F. Rösel, H.M. Fries, K. Alder, and H.C. Pauli, Atom. Data and Nucl. Data Tables **21**, 292 (1978).

[Ru77] P. Russo, D. Cline, and J. Sprinkle, Bull. Am. Phys. Soc. **22**, 545 (1977).

[Rz88] T. Rzaca-Urban, W. Gast, G. Hebbinghaus, A. Krämer-Flecken, R.M. Lieder, H. Schnare, C. Senff, M. Thoms, W. Urban, G. de Angelis, P. Kleinheinz, W. Starzecki, J. Styczen, P. von Brentano, A. Dewald, J. Eberth, W. Lieberz, T. Mylaeus, A. v.d. Werth, H. Wolters, K.O. Zell, S. Hepner, H. Hübel, M. Murzel, H. Grawe, H. Kluge, K.H. Maier, R. Chapman, J.C. Lisle, J.N. Mo, J.D. Garrett, G. Sletten, and J. Bacelar, Proceedings of the Conference on High-Spin Nuclear Structure and Novel Nuclear Shapes, Argonne National Laboratory, 1988, p.46.

S

[Sa89] D. Santos, A.J. Kreiner, J. Davidson, M. Davidson, M. Debray, D. Hojman, and G. Falcone, Phys. Rev. C **39**, 902 (1989).

[Sc79] O. Scholten, F. Iachello, and A. Arima, Ann. Phys. (N.Y.)**115**, 325 (1979).

[Sc80] O. Scholten, Ph.D. thesis, University of Groningen, 1980.

[Sc82a] Y. Schutz, J.P. Vivien, F.A. Beck, T. Byrski, C. Gehringer, J.C. Merdinger, J. Dudek, W. Nazarewicz, and Z. Symanski, Phys. Rev. Lett. **48**, 1534 (1982).

[Sc82b] O. Scholten and N. Blasi, Nucl. Phys. **A380**, 509 (1982).

[Sc83] H.W. Schuh, Computer code PHAEDRUS, 1983.

[Sc84a] O. Scholten and T. Ozzello, Nucl Phys. **A424**, 221 (1984).

[Sc84b] O. Scholten, Program package PHINT, 1984.

[Sc85a] O. Scholten, in Contemporary Research Topics in Nuclear Physics, edited by D.H. Feng, M. Vallieres, M.W. Guidry, and L.L. Riedinger (Plenum, New York, 1985), p.503.

[Sc85b] O. Scholten, Prog. in Part. and Nucl. Phys. **14**, 189 (1985).

[Sc85c] O. Scholten, Program package ODDA (1985).

[Sc86] O. Scholten, Program package DODO (1986).

[Sc87] A. Arima, A. Gelberg, and O. Scholten, Phys. Lett. **185B**, 259 (1987).

[Sc88] O. Scholten, Lectrues presented at the International School "Recent Advances in Experimental Nuclear Physisc", Poiana Brasov, Rumenia, 1988.

[Se67] G.G. Seaman, E.M. Bernstein, and J.M. Palms, Phys. Rev. **161**, 1223 (1967).

[Se77] E. Segre, Nuclei and Particles, 2nd Edition (W.A. Benjamin, Inc., 1977).

[Sh83] B. Sherrill and J. Winfield, MSUCL report no. 499, 1983.

[Sh88] S. Shi, C.W. Beausang, D.B. Fossan, R. Ma, E.S. Paul, and N. Xu, Phys. Rev. C **37**, 1478 (1988).

[Si74] P.P. Singh, L.D. Medsker, G.T. Emery, L.A. Beach, and C.R. Gossett, Phys. Rev. C **10**, 656 (1974).

[Sl84] M.F. Slaughter, R.A. Warner, T.L. Khoo, W.H. Kelly, and Wm.C. McHarris, Phys. Rev. C **29**, 114 (1984).

[Sp80] R. Spanhoff, M.J. Canty, H. Postma, and G. Mennenga, Phys. Rev. C **21**, 361 (1980).

[St72] F.S. Stephens and R.S. Simon, Nucl. Phys. **A183**, 257 (1972).

[St75] F.S. Stephens, Rev. Mod. Phys. **47**, 43 (1975).

T

[Ta83] I. Talmi, in Short-Distance Phenomena in Nuclear Physics, edited by D.H. Boal and R.H. Woloshyn (Plenum, New York, 1983), p.311.

[Ta88] P. Taras, S. Flibotte, J. Gascon, B. Haas, S. Pilotte, D.C. Radford, D. Ward, H.R. Andrews, G.C. Ball, F. Banwille, S. Cournoyer, D. Horn, J.K. Johansson, S. Monaro, N. Nadon, D. Prevost, C. Pruneau, D. Thibault, D.M. Tucker, and J.C. Waddington, Phys. Rev. Lett. **61**, 1348 (1988).

[Tw86] P.J. Twin, B.M. Nyako, A.H. Nelson, J. Simpson, M.A. Bentley, H.W. Cranmer-Gordon, P.D. Forsyth, D. Howe, A.R. Mokhtar, J.D. Morrison, J.F. Sharpty-Schafer, and G. Sletten, Phys. Rev. Lett. **57**, 811 (1986).

V

[Vo83] M.J.A. de Voigt, J. Dudek, and Z. Szymanski, Rev. of Mod. Phys. **55**, 949 (1983).

W

[Wa72] F.E. Wagner, H. Spieler, D. Kucheida, P. Kienle, and R. Wappling, Z. Phys. A **254**, 112 (1972).

[Wa78] P.M. Walker, G.D. Dracoulis, A. Johnston, J.R. Leigh, M.G. Slocombe, and I.F. Wright, J. Phys. G **4**, 1655 (1978).

[Wa88] R. Wadsworth, A. Kirwan, D.J.G. Love, Y.-X. Luo, J.-Q. Zhong, P.J. Nolan, P.J. Bishop, M.J. Godfrey, R. Hughes, A.N. James, I. Jenkins, S.M. Mullins, J. Simpson, D.J. Thornley, and K.L. Ying, J. Phys. G **13**, L207 (1988).

X

[Xu89] N. Xu, private communation.

Y

[Ya83] C.X. Yang, J. Kownacki, J.D. Garrett, G.B. Hagemann, B. Herskind, J.C. Bacelar, J.R. Leslie, R. Chapman, J.C. Lisle, J.N. Mo, A. Simcock, J.C. Wilmott, W. Walus, L. Carlen, S. Jönsson, J. Lyttkens, H. Ryde, P.O. Tjom, and P.M Walker, Phys. Lett. **133B**, 39 (1983).

[Yo82] N. Yoshida, A. Arima, and T. Otsuka, Phys. Lett. **114B**, 86 (1982).